THE ROLES OF SMC5/6 IN MAMMALIAN GERM CELL GENOME MAINTENANCE

By
Grace H. Hwang

A dissertation submitted to Johns Hopkins University in conformity with the requirements for the degree of Doctor of Philosophy

Baltimore, MD

Submission date: February 26, 2018

ABSTRACT

The SMC5/6 complex is a member of the structural maintenance of chromosome (SMC) family, which includes cohesion and condensin. SMC5/6 has been implicated to have roles homologous recombination, restart of stalled replication forks, maintenance of ribosomal DNA (rDNA) and heterochromatin, telomerase-independent telomere elongation, and regulation of chromosome topology in the mitotic cell cycle. From research using yeast and worms, the SMC5/6 complex is required for proficient meiotic recombination and chromosome segregation. However, the details of how the complex accomplishes these meiotic functions are unknown. Furthermore, there is limited information on the genome maintenance role of SMC5/6 in mammals. This thesis focuses on determining how SMC5/6 complex regulates cell cycle progression and DNA repair in mammals. Using conditional mutant mice of *Smc5*, I explore the molecular function of SMC5/6 during germ cell progression in both sexes. I demonstrate that SMC5/6 is essential for the formation of bivalents that are capable of accurate segregation during meiosis I, and age-related meiotic aberrancies may be directly related to a gradual reduction in SMC5/6 protein levels. On the other hand, I show that SMC5/6 complex is not essential for pre-meiotic DNA replication and meiotic progression during mouse spermatogenesis. However, if DNA processing events are compromised, for example by exogenous sources of DNA damage, the SMC5/6 complex is required to ensure genome integrity. Taken together, this dissertation supports the sexual dimorphic roles of SMC5/6 in mammalian genome maintenance in germ cells.

Advisor: Philip Jordan, Ph.D.

Readers: Sabra Klein, Ph.D.
Michael Matunis, Ph.D.
Alan Meeker, Ph.D.
Scott Bailey, Ph.D.

Alternates: Daniela Drummond-Barbosa, Ph.D.
Diane Griffin, Ph.D.
Andrew Holland, Ph.D.

ACKNOWLEDGEMENTS

I am very fortunate to have had my PhD experience at Hopkins. Special thanks are given to all those who supported me throughout this journey. Without the people mentioned below, none of my accomplishments would have occurred.

Firstly, I thank my advisor Philip Jordan for taking me as his first graduate student and for allowing me to work on this project. His support, patience, and teachings were invaluable, and I would not be the scientist or person today without his guidance. Phil's passion for science and work ethic is something that I will always revere and respect.

Thank you to our collaborators Mary Ann Handel, Fengyun Sun, Marilyn O'Brien, John Eppig, Emma Verver, and Geert Hamer for their valuable input and analysis. I thank my thesis advisory committee members who helped shape this project: Sabra Klein, Michael Matunis, Scott Bailey, Alan Meeker, and Pierre Columbe. Thank you to Daniela Drummond-Barbosa, whose continued support after my ScM with her was instrumental for my next steps. I thank current and previous members of the Jordan lab, who have been colleagues, friends, and great sounding-boards: Stephen Wellard, Marina Pryzhkova, Hima Gaddipati, Jessica Hopkins, Ayobami Ward, Sakshi Khurana, and others.

Thank you to all my friends that I've made in Baltimore and also those back at home. I would especially like to thank Danielle Bouchard, Stephen Wellard, Lyle McPherson, and Edward Culbertson for always being supportive and genuinely fun people to hang around with. Also, without Kaitlin Johnson, I could not have gotten through this program. I am so grateful every day that she is in the same year as me and

that I had the privilege to gain a new best friend. Thank you to Heidi Martini-Stoica, and Jasper Yan who've always supported even from different states. A special thanks to Daria Anichkova for being my greatest and most sarcastic sister I could ever ask for, and for her parents, Marina and Dmitriy, for adopting me almost every Thanksgiving. I thank Jessica Harrington for not just being a loving friend, but a mentor who literally got me back up on my feet after almost every slump. I thank my aunt and uncle, Hangil and Chong Park for their assistance and for having the burden of being the only family members who understand what it is to be a scientist.

Lastly but not least, I thank my family, Mom, Dad, and Daniel, for their unwavering care, support, guidance and patience throughout the years. For always listening to me when I complain, cry, or even just talk about my life even when they don't quite understand. I would not be here without my family.

TABLE OF CONTENTS

LIST OF TABLES

LIST OF FIGURES

LIST OFABBREVIATIONS

ADB	Antibody dilution buffer
ALT	Alternative lengthening of telomeres
ATP	Adenosine triphosphate
BLM	Bloom syndrome helicase
BRC1	BRCT domain protein
BRCA	Breast cancer 1
BRCT	BRCA C-Terminal
CEN	Centromere
ChIP	Chromatin immunoprecipitation
cKO	Conditional knockout
CO	Crossover
DAPI	DNA
DAZL	Deleted in azoospermia-like
dHJ	Double holiday junction
DMC1	DNA meiotic recombinase 1
DSB	Double strand break
DSBR	Double strand break repair
dsDNA	Double strand DNA
FANCM	Fanconi anemia complementation group m
FBS	Fetal bovine serum
FLP	Flippase recombinase
FRT	Flippase recognition target
GVBD	Germinal vesicle breakdown
Gy	Gray unit
H4K20	Histone H4 dimethyl K20, trimethyl 20
HEPES	4-(2-hydroxyethyl)-1-piperazineethanesulfonic acid
HORMAD	HORMA domain containing protein
HR	Homologous recombination
IBMX	3-isobutyl-l-xanthine
IVF	In-vitro fertilization

JM	Joint molecules
KO	Knock-out
MAGE	Melanoma-associated antigen gene
MEF	Mouse embryonic fibroblasts
MEM	Minimal essential medium
mESC	Mouse embryonic stem cells
MI	Metphase I
MII	Metaphse II
MLH1	mutL homolog 1
MMS21	Methyl methaneSulfonate sensitivity (NSE2)
MPH1	Mutator phenotype 1
NSE	Non-SMC element
NSMCE	Non-SMC element
PBE	Polar body extrusion
PBS	Phosphate buffer saline
PCH	Pericentromeric heterochromatin region
PCNA	Proliferating cell nuclear antigen
PLK1	Polo-like kinase 1
RAD18	RAD18 E3 ubiquitin ligase
rDNA	Ribosomal DNA
SAC	Spindle assembly checkpoint
SC	Synaptonemal complex
SDS PAGE	Sodium dodecyl sulfate polyacrylamide gel
SDSA	Synthesis-dependent single-strand annealing
SEI	Single-end invasion
SGS1	Slow growth suppressor 1
SLF1/2	SMC5/6 complex localization factor 1/2
SMC	Structural maintenance of chromosome
SP-RING	Siz/pias ring
ssDNA	Single strand DNA
STA-PUT	Velocity Sedimentation Cell Separator

SUMO	Small ubiquitin-related modifier
SYCP	Synaptonemal complex protein
TAM	Tamoxifen
TOPII	Topoisomerase II
TUNEL	Terminal deoxynucleotidyl transferase dUTP nick end labeling
Y2H	Yeast two-hybrid
ZMM:	Sip1-4, Mlh1/3, Msh4/5
ZP	Zona pellucida
αTUB	α-Tubulin
γTUB	γ-Tubulin

CHAPTER I

BACKGROUND AND SIGNIFICANCE

This chapter is an updated version of a review article that appeared in Chromosoma [Verver, D. E., Hwang, G. H.*, Jordan, P. W. and Hamer, G. (2016). "Resolving complex chromosome structures during meiosis: versatile deployment of Smc5/6". Chromosoma. **125**, 15-27]. The published review was written in collaboration with Dr. Dideke Emma Verver and Dr. Geert Hamer at the University of Amsterdam. The purpose of this chapter is to give an up to date overview of what is known about SMC5/6 functions in mitotic and meiotic cells.*

The Smc5/6 complex, along with cohesin and condensin, is a member of the Structural Maintenance of Chromosome (SMC) family; large ring-like protein complexes that are essential for chromatin structure and function. Thanks to numerous studies of the mitotic cell cycle, Smc5/6 has been implicated to have roles in homologous recombination, restart of stalled replication forks, maintenance of rDNA and heterochromatin, telomerase-independent telomere elongation and regulation of chromosome topology.

The nature of these functions implies that the Smc5/6 complex also contributes to the profound chromatin changes, including meiotic recombination, that characterize meiosis. Only recently, studies in diverse model organisms have focused on the potential meiotic roles of the Smc5/6 complex. Indeed, Smc5/6 appears to be essential for meiotic recombination. However, due to both the complexity of the process of meiosis and the versatility of the Smc5/6 complex, many additional meiotic functions have been described.

In this chapter, includes a clear overview of the multiple functions found so far for the Smc5/6 complex in meiosis. Additionally, a comparison between meiotic functions

and known mitotic functions is given, in an attempt to find a common denominator and thereby create clarity in the field of Smc5/6 research.

Smc5/6 complex structure

The Smc5/6 complex is a member of the Structural Maintenance of Chromosome (SMC) family, along with cohesin and condensin. The Smc5/6 complex is proposed to have the characteristic ring-like structure of the SMC family in which each SMC complex is comprised of two SMC proteins forming a heterodimer, and multiple non-SMC elements (Reviewed in (Jeppsson et al., 2014b)). The Smc5/6 complex is comprised of Smc5, Smc6, and several non-SMC elements of which Nse1-4 are conserved from yeast (Hazbun et al., 2003, Duan et al., 2009, Zhao and Blobel, 2005a, Pebernard et al., 2006) **(Fig. 1.1A, B)** to mammals (Taylor et al., 2008, De Piccoli et al., 2009) **(Fig. 1.1C)**. When referring to the Smc5/6 complex genes or proteins in general we will use yeast nomenclature. When referring to a specific organism, or data obtained using a specific organism, we will use the specific nomenclature of that organism, e.g. NSMCE1 for the mammalian ortholog of Nse1. The SMC proteins have an extensive coiled-coil domain interrupted by a hinge domain that folds each SMC back on itself. The two globular C and N terminal ends are juxtaposed to form an ATP-binding and ATP-hydrolysis site **(Fig. 1.1D)**. To form a closed-ring structure the ATPase domains are bridged together by non-SMC elements, while the SMC proteins associate tightly through their hinge regions (Reviewed in (Jeppsson et al., 2014b)).

In vitro assays using purified fission yeast proteins have shown that Nse1 binds to Nse3, and both Nse1 and Nse3 bind to Nse4 (Palecek et al., 2006b, Pebernard et al.,

2008a). Nse1 contains a RING-finger domain, common to ubiquitin E3 ligases, (Fujioka et al., 2002, McDonald et al., 2003, Potts, 2009), and Nse3 contains a MAGE (melanoma-associated antigen gene) domain (Pebernard et al., 2004). It has been shown that human NSMCE3 enhances the E3 ubiquitin ligase of NSMCE1 *in vitro* (Doyle et al., 2010a). Nse2 (also referred to as Mms21) is bound to Smc5, contains a SP-RING domain (McDonald et al., 2003, Pebernard et al., 2004) and functions as an E3 small ubiquitin-related modifier (SUMO) ligase (Zhao and Blobel, 2005a, Potts and Yu, 2007b, Andrews et al., 2005a). Nse4 is a α-kleisin subunit which bridges the ATPase head domains of Smc5 and Smc6 (Palecek et al., 2006b). Nse5 and Nse6 are also Smc5/6 components in budding and fission yeast. In budding yeast, Nse5 and Nse6 associate with the hinge region **(Fig. 1.1A)** (Duan et al., 2009). In fission yeast, Nse5 and Nse6 associate with the head domains **(Fig. 1.1B)**, which may enhance the stability of the complex (Pebernard et al., 2006). Recently, SLF1 and SLF2, SMC5/6 recruitment factors, have been discovered in *Xenopus* and mammalian cells, and SLF2 is a distant ortholog of yeast NSE6 (Räschle et al., 2015).

Smc5/6 in mitotic cells

In somatic cells, the Smc5/6 complex is involved in several processes required to maintain genomic stability. Mechanistically, these processes involve regulation of specific factors required for homologous recombination (HR) pathways. All these processes, including DNA replication, HR mediated DNA double strand break (DSB)

repair, correct chromosome topology and, eventually, proper metaphase conformation, are also essential for successful meiosis.

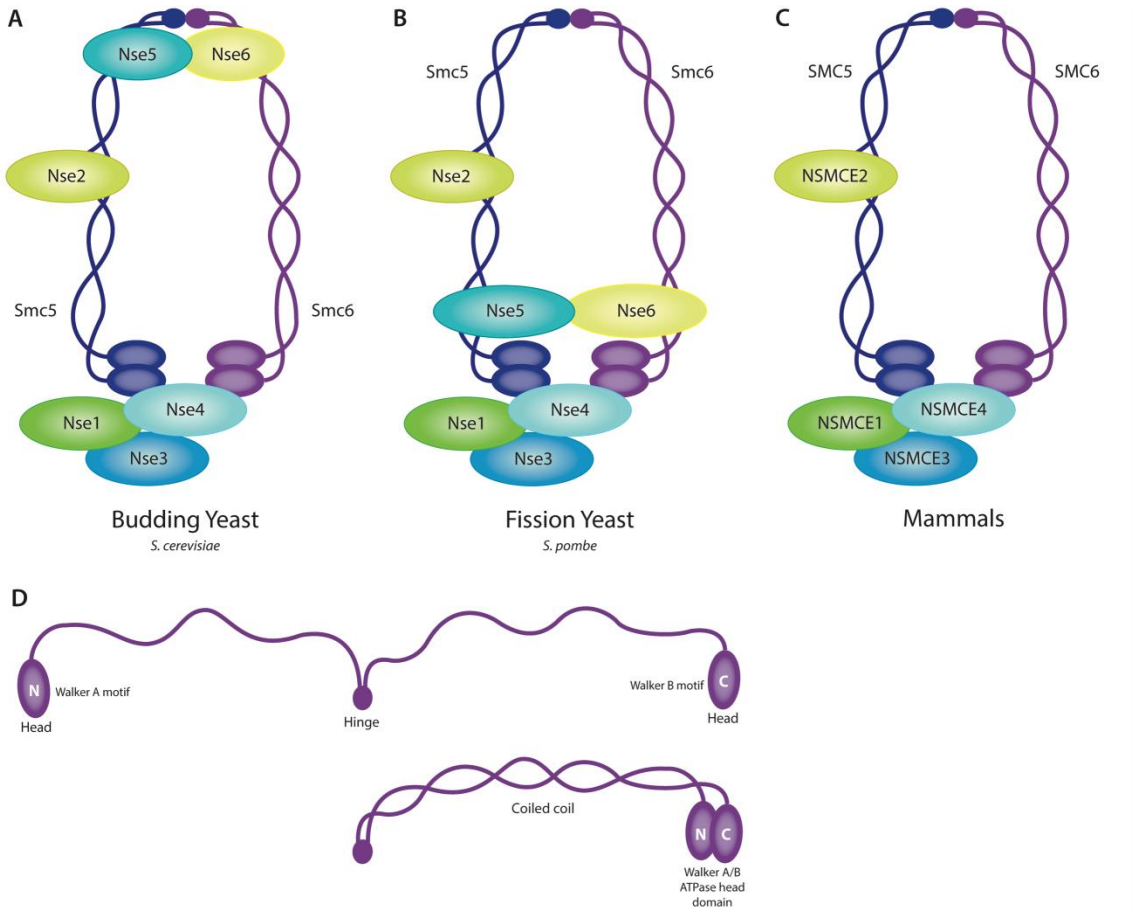

Figure 1.1 Structure and composition of Smc5/6 complex. Conserved from yeast to humans, Smc5 and Smc6 fold and interact at their central hinge domains. Through the coiled-coil stretch, the N- and C-termini are brought in close proximity creating an ATPase domain. The ring-like structure is closed by several non-SMC elements (Nse1, Nse3, and Nse4). In addition, the SUMO ligase Nse2 is bound to the coiled-coil region of Smc5. Nse5 and Nse6 are located at the hinge domain in budding yeast (**A**), at the ATPase domain in fission yeast (**B**). While Slf2, a distant ortholog of yeast, bonafide homologs of Nse5 and Nse6 have not been found yet in mammals (**C**). **(D)** Smc5 and Smc6 each contain an extensive coiled-coil domain that folds back on itself at a central hinge domain, juxtaposing the terminal head domains to form an ATP-binding and ATP-hydrolysis site

Smc5/6 and stalled replication forks

Smc5/6 is required for maintaining replication fork stability and the restart of stalled replication. In budding yeast, the absence of Nse2 SUMO ligase activity results in Rad51-dependent X-shaped HR intermediates or aberrant joint molecules (JMs) accumulating at stalled replication forks (Bermudez-Lopez et al., 2010, Branzei et al., 2006). The Smc5/6 complex functions with Sgs1, a homologue of the Bloom syndrome helicase (BLM), to inhibit the accumulation of these abnormal intermediates. It is possible that this function is conserved in humans, as hypomorphic mutations that lead to the loss of the NSMCE2 SP-RING domain result in delayed recovery from replication stress and a reduction in BLM foci (Payne et al., 2014a). These defects result in chromosome bridges and missegregation during the metaphase to anaphase transition. In budding yeast, Smc5/6 has been shown to interact and restrain the replication regression activity of Mph1 helicase, an ortholog of human FANCM, which is required for replication fork repair but can also lead to accumulation of JMs (Xue et al., 2014).

In fission yeast, similar JMs accumulate at the collapsed replication forks in *smc6* mutants, correlating with chromosome missegregation (Ampatzidou et al., 2006). Smc5/6 is required for the loading of Rpa and Rad52 onto stalled replication forks in order for the fork to maintain a recombination-competent conformation (Irmisch et al., 2009). Overexpression of Brc1, a BRCA C-terminal (BRCT) motif protein, rescues the replication-arresting defect of a Smc6 hypomorphic mutant (Lee et al., 2007, Sheedy et al., 2005, Verkade et al., 1999, Pebernard et al., 2006). Because this rescue is dependent on Brc1-mediated promotion of a post-replicative repair pathway and the function of structure-specific endonucleases Slx1/4 and Mus81/Eme1 that resolve the accumulated

JMs, Smc5/6 complex may be required to prevent the formation of replication stress-induced JMs and/or assist in their resolution.

Recently, SLF1 and SLF2, a distant ortholog of NSE6, was found to provide SMC5/6 a physical link to RAD18, an E3 ubiquitin ligase involved in post-replication DNA repair in vertebrate cells (Räschle et al., 2015). SLF2 is required to recruit SMC5/6 to damaged DNA, specifically interstrand crosslinks (ICL), to promote efficient repair of these lesions, and depletion of SLF1 or SLF2 leads to mitotic errors and sensitivity to exogenous DNA damage (Räschle et al., 2015).

Facilitating homologous recombination

Numerous studies using mammalian, plant, budding yeast and fission yeast cells have indicated that Smc5/6 functions in the homologous recombination pathway (Lehmann et al., 1995, Ampatzidou et al., 2006, McDonald et al., 2003, Pebernard et al., 2006, Cost and Cozzarelli, 2006, Mengiste et al., 1999, Torres-Rosell et al., 2005a, Torres-Rosell et al., 2005b, Watanabe et al., 2009, Stephan et al., 2011).

In budding yeast and human cells, Smc5/6 and cohesin are recruited to DSBs to promote repair via sister chromatid recombination (De Piccoli et al., 2006, Lindroos et al., 2006, Potts et al., 2006, Strom et al., 2004, Unal et al., 2004, Wu and Yu, 2012). Although Smc5/6 and cohesin complexes are recruited to DSBs independently, Nse2-mediated sumoylation of the α-kleisin subunit of cohesin, Scc1, is required to ensure proficient sister chromatid recombination (Wu and Yu, 2012, McAleenan et al., 2012). In

turn, sumoylation of Scc1 was shown to counteract the action of Wapl, a negative regulator of cohesin loading (Wu and Yu, 2012).

ChIP experiments in mouse B-cells showed that SMC5 co-localizes with RPA, the single strand binding protein involved in DNA replication and repair, and BRCA1, a protein involved in DSB repair, at early replication fragile sites (Barlow et al., 2013). These findings suggest that the SMC5/6 complex binds to ssDNA substrates created during HR and/or DNA replication.

Regulation of homologous recombination in repetitive sequences

In budding yeast, the ribosomal genes are organized into a single array of 100–200 identical repeats on chromosome XII that is compartmentalized into the chromatin region called nucleolus (Oakes et al., 2006). Due to the repetitive nature of the rDNA locus, HR-mediated DNA damage repair in this region can lead to illegitimate recombination events that result in JMs and unequal sister chromatid exchange (Eckert-Boulet and Lisby, 2009). In order to prevent such deleterious recombination events, DSBs occurring within rDNA are thought to be moved outside the nucleolus by a Smc5/6-dependent mechanism in order to be repaired (Torres-Rosell et al., 2005a, Torres-Rosell et al., 2007). However, the visible presence of DSBs in the nucleolus of Smc5/6 mutants could also be due to less efficient repair of these breaks without functional Smc5/6.

Similarly, in *Drosophila*, Smc5/6 is thought to be involved in the translocation of the damaged DNA within heterochromatin regions to adjacent euchromatic regions where

recombination can occur proficiently (Chiolo et al., 2011). Moreover, in heterochromatin, Smc5/6 suppresses HR until translocation of the DSB has occurred (Chiolo et al., 2011).

Mitotic metaphase

Smc6 location in mitotic metaphase cells has been studied multiple times, with varying outcomes. Some studies in mouse and human show that SMC6 is translocated away from the chromosomes during mitotic divisions (Verver et al., 2014a, Verver et al., 2013a, Taylor et al., 2001, Gallego-Paez et al., 2014), while other studies in budding yeast and mouse report Smc6 to be located at the centromeres of mitotic cells (Lindroos et al., 2006, Gomez et al., 2013, Yong-Gonzales et al., 2012).

The SMC5/6 complex is required for regulating topoisomerase IIα and condensin localization on replicated chromatids in human cells and mouse embryonic stem cells (mESCs) during mitosis, thereby ensuring correct chromosome morphology and segregation (Gallego-Paez et al., 2014, Pryzhkova and Jordan, 2016a). Topoisomerase II (TopoII) resolves DNA topological constraints by introducing transient DSBs that are needed to decatenate double stranded DNA to alleviate supercoiling (Nitiss, 2009). TopoII initiates the passage of an unbroken DNA strand through the DSB and then reseals the break (Nitiss, 2009). In addition, it has been shown that condensin aids in efficient TopoII chromosome condensation, sister chromatid decatenation and subsequent segregation in budding yeast (Leonard et al., 2015, Charbin et al., 2014). In budding yeast, Smc5/6 has recently been implicated in managing replication-induced topological stress (Carter and Sjogren, 2012, Jeppsson et al., 2014a) and induction of topological stress by TopoII inactivation correlates with increased frequency of Smc5/6 chromosomal

association sites (Jeppsson et al., 2014a, Kegel et al., 2011a). In fission yeast, TopoII and Smc5/6 are required for the timely removal of cohesins from the chromosome arms before metaphase (Tapia-Alveal et al., 2010). Retention of these cohesins would otherwise cause chromosome missegregation and subsequent mitotic catastrophe. This was further supported when overexpression of Separase, a protein that cleaves cohesin, was shown to rescue the lethality of TopoII and Smc5/6 mutants in fission yeast (Outwin et al., 2009). It was also found that *Smc5* depletion mESCS results in accumulation of cells in G2 and apoptosis—furthermore, the destabilization of SMC5/6 complex in mitotic mESCs results atypical localization of condensin on the chromosome arms and chromosome missegregation errors (Pryzhkova and Jordan, 2016a). Taken together, SMC5/6, condensin, and topoisomerase II seem to have interconnecting functions in mitotic cell cycle progression.

Meiosis

Meiosis is a specialized cell division during which one round of DNA replication is followed by two successive rounds of chromosome segregation. First, the homologous chromosomes, each consisting of one pair of sister chromatids held together by cohesin complexes, move to opposite poles (meiosis I). Second, the sister chromatids are segregated, resulting in the formation of four haploid cells (meiosis II). During prophase I, the homologous chromosomes align and, in most organisms, chromosome synapsis is achieved by formation of the synaptonemal complex (SC). Correct synapsis of the homologous chromosomes is required to facilitate meiotic recombination and the subsequent formation of meiotic crossovers. These meiotic crossovers, or chiasmata, introduce genetic variation among the resulting gametes. Additionally, together with

proper sister chromatid cohesion, they also ensure correct chromosome orientation and segregation during meiosis I (Reviewed in (Petronczki et al., 2003b)).

The molecular pathways required for DSB repair during meiosis have been studied in most detail in budding yeast (De Muyt et al., 2012, Zakharyevich et al., 2012). However, evidence indicates that these pathways are conserved (Berchowitz et al., 2007, Higgins et al., 2008, Holloway et al., 2008). The following paragraphs briefly summarize meiotic recombination, using budding yeast as an example **(Fig. 1.2)**. Meiotic recombination is initiated by Spo11-induced DSB formation, a 5-3' exonuclease that produces a 3' single-stranded DNA overhang at every break (Keeney et al., 1997). This 3' overhang is then coated by the Rad51/Dmc1 strand exchange proteins and invades the complementary sequence of the homologous chromosome **(Fig. 1.2B)**. DNA synthesis then starts from the invading end and proceeds beyond the DSB. This single-end invasion (SEI) is the precursor of all recombination pathways during meiosis (De Muyt et al., 2012, Zakharyevich et al., 2012).

Following SEI, most recombination events are processed via synthesis-dependent single-strand annealing (SDSA) **(Fig. 1.2B)**. During SDSA, the invading strand is thought to be displaced by the RecQ helicase BLM/Sgs1 (De Muyt et al., 2012, Jessop and Lichten, 2008, Jessop et al., 2006, Bennett et al., 1998, Oh et al., 2008). The displaced strand is then used as a synthesis template for the other damaged ssDNA end, and ligation results in the formation of a non-crossover.

The DSB repair mechanism in budding yeast that ensures reciprocal crossover formation is known as the ZMM (Zip1-4, Mlh1/3, Msh4/5) pathway. The ZMM pathway requires both SC components (Zip1-4 and Spo16), and the conserved mismatch repair

heterodimers MutSγ (Msh4-5) and MutLγ (Mlh1-3) (Borner et al., 2004, Lynn et al., 2007). At a ZMM designated recombination site the SEI is stabilized and the second end of the DSB is captured to form a double Holliday junction (dHJ). Interestingly, Sgs1 is required to stabilize the ZMM designated dHJs, which are resolved asymmetrically by Exo1-MutLγ to form COs, and eventually lead to chiasmata (Zakharyevich et al., 2012) **(Fig. 1.2C)**.

Timely organization of the different steps of meiotic DSB repair depends on tight regulation of the meiotic prophase I, which can be subdivided in four stages: leptonema, zygonema, pachynema and diplonema. During leptonema, the chromatin condenses and formation of axial elements between sister chromatids begin to form. Simultaneously, DSBs are induced by the endonuclease SPO11, triggering the meiotic DNA-damage response. During zygonema, homologous chromosomes begin to synapse, characterized by the formation of the SC, a proteinaceous structure which comprises axial proteins (now termed lateral elements) linked by central components. Single strand invasion occurs, followed by resection and DNA synthesis, resulting in recombination intermediates. Recombination events are neither randomly nor equally distributed throughout the genome, but are preferentially located at hotspots at which DSBs are more frequently formed (reviewed in (Keeney et al., 2014)). At pachynema, the homologous chromosomes are fully synapsed along their entire length. DSB repair via HR continues by the resolution of recombination intermediates into either a non-crossover or a crossover event. Only a minority of recombination intermediates are resolved as crossovers, but there are processes which ensure that at least one crossover is formed per homolog pair (reviewed in (Youds and Boulton, 2011)). Finally in diplonema, the

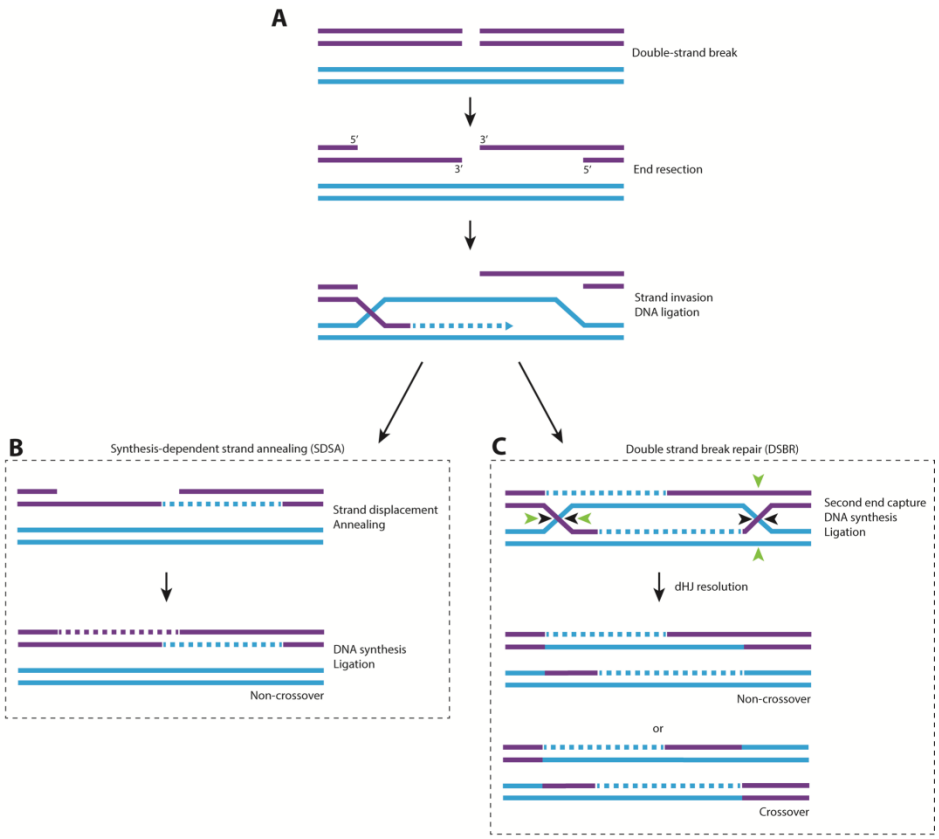

Figure 1.2. DNA double strand break repair by homologous recombination. (**A)** When a DNA double strand break (DSB) occurs, the DNA around the 5′ end is resected, creating a 3′ single-stranded DNA (ssDNA) overhang. This 3′ ssDNA overhang invades a homologous sequence, creating a D-loop. DNA is synthesized at the invading end using the undamaged template DNA strand. After this, further repair can be executed by synthesis-dependent strand annealing (SDSA) or double strand break repair (DSBR). (**B)** SDSA: The second DSB end will be annealed up to the ssDNA on the other break end, followed by gap-filling DNA synthesis and ligation. This will lead to a non-crossover event. (**C)** DSBR: The second DSB end can be captured to form a double Holliday Junction (HJ). The resulting recombination intermediate must be resolved by nicking the HJs. Depending on the nick sites, either parallel (*black arrows*) or anti-parallel (*green arrows)*, this will produce a non-crossover or a crossover event, respectively

synaptonemal complex gradually dissociates and most recombination intermediates are completely resolved. Importantly, crossovers remain as chiasmata in order to keep homologous chromosomes locally tethered and, together with proper chromosome cohesion, ensure bi-orientation and accurate segregation during meiosis I (reviewed in (Petronczki et al., 2003b)).

During the first meiotic division, homologous chromosomes, each containing two sister chromatids held together by cohesins, segregate to opposite poles. Bi-orientation of homologous chromosomes is crucial for their accurate segregation and misalignment may result in aneuploidy. The spindle assembly checkpoint (SAC) controls this bi-orientation by monitoring the tension that is generated when the homologous chromosomes are pulled to opposite directions and only allows subsequent chromosome segregation when all chromosomes are correctly orientated. The physical linkage that chiasmata provide achieves bi-orientation and inter-homolog tension. Failure to generate the chiasmata, e.g. due to absence of DSB induction, inadequate repair and lack of CO events, will lead to either a SAC induced metaphase I-arrest and apoptosis, or aberrant chromosome segregation and aneuploidy in the resulting gametes.

Localization of Smc5/6 in meiosis

Budding Yeast

Using immunofluorescence microscopy, Smc6 was observed to localize to the nucleolus in budding yeast at the entry into meiosis (Farmer et al., 2011, Lilienthal et al., 2013a). During meiotic progression, chromosome axes are formed and DSB repair is initiated. At this time, Smc5 and Smc6 localize as distinct foci along the chromosome

axes (Copsey et al., 2013a, Farmer et al., 2011, Lilienthal et al., 2013a, Xaver et al., 2013). Smc6 also frequently co-localizes side-by-side with Rad51 recombinase, indicating a potential function in the strand invasion step in HR repair (Copsey et al., 2013a, Xaver et al., 2013). The Smc6 localization along the axes becomes more abundant as synapsis occurs (Copsey et al., 2013a, Lilienthal et al., 2013a, Xaver et al., 2013). The formation of this punctate distribution does not depend on meiotic DSBs (Copsey et al., 2013a, Farmer et al., 2011). Contrasting data has been reported for the effect of cohesin mutation on Smc5/6 axis loading. It was observed by Lillienthal et al. that Smc6 binding to chromosomes is dependent on meiosis-specific cohesin subunit Rec8. Therefore, the Smc5/6 complex may be influenced by meiotic axis structure and/or the presence of sister chromatid cohesion. In contrast however, the localization of Smc5 was not affected by the absence of Rec8 (Copsey et al., 2013a). Although surprising, it is possible that Smc5 and Smc6 loading to chromosome axes is independent of one another, and Smc6 but not Smc5 requires cohesin. An alternative explanation is that differences in chromatin spreading techniques resulted in the contrasting observations. The localization of Smc5/6 during late prophase is still inconclusive. After late prophase, some studies reported Smc5 and Smc6 localization become more diffuse and are absent prior to metaphase I (Copsey et al., 2013a, Lilienthal et al., 2013a), while another study reported that Smc6 localized to the chromatin during both meiotic divisions, displaying dense clusters at the boundary between segregating chromatin masses (Xaver et al., 2013). These discrepancies may be due to sensitivity differences in chromatin spreading technique and epitope accessibility.

To assess chromatin localization of Smc5/6 in greater detail, genome-wide ChIP-on-chip localization studies were used (Copsey et al., 2013a, Xaver et al., 2013). These studies showed that Smc5 and Smc6 bind to many of the same chromosomal axis-associated sites as Rec8, including centromeres. In addition, Smc5/6 is enriched at DSB hotspots. However, this localization occurs independently of DSB formation, which supports the immunofluorescence microscopy data (Copsey et al., 2013a, Xaver et al., 2013). Finally, as observed in mitotic cells, Smc5/6 also binds to the rDNA, which remains unsynapsed during meiotic prophase I (Farmer et al., 2011, Lilienthal et al., 2013a, Xaver et al., 2013).

C. elegans

In *C. elegans*, SMC-6 localizes to the condensed chromatin of germ cells throughout meiosis (Bickel et al., 2010). SMC-6 becomes enriched on chromosomes during pachytene, which coincides with occurrence of DSB repair, complementing the localization pattern in budding yeast. SMC-6 remains on chromosome axes during diplotene and diakinesis in worms (Bickel et al., 2010).

Mouse, Human

The first indications of a possible role for SMC5/6 in mammalian meiotic progression were elevated levels of both SMC5 and SMC6 in the testis and localization in spermatocytes. (Taylor et al., 2001). It then took over 12 years before the role of SMC5/6 in mammalian meiosis was investigated in more depth revealing involvement at several

crucial and diverse steps during rodent and human spermatogenesis (Gomez et al., 2013, Verver et al., 2014a, Verver et al., 2013a). First, in mouse spermatocytes, SMC5, SMC6 and NSMCE1 were found to be located at pericentromeric heterochromatin (or so-called chromocenters): condensed repetitive sequences surrounding the centromeres (Gomez et al., 2013, Verver et al., 2013a). This localization already starts in differentiating spermatogonia, remains throughout all meiotic stages, including metaphase I and II, and disappears when the haploid spermatids start to elongate (Gomez et al., 2013, Verver et al., 2013a). Moreover, SMC5 and SMC6 were detected at the SC of synapsed homologous chromosomes from early zygonema until late diplonema in mouse spermatocytes (Gomez et al., 2013). This latter localization pattern was also reported for both SMC5 and SMC6 in human spermatocytes (Verver et al., 2014a). Finally, detection of SMC5, SMC6 and NSMCE1 at the XY-body during pachynema was observed in both mouse (Gomez et al., 2013, Taylor et al., 2001) and human spermatocytes (Verver et al., 2014a). However, it must be noted that in mouse spermatocytes, SMC5, SMC6 and NSMCE1 localize to the chromatin of the XY-body (Gomez et al., 2013), whereas in human spermatocytes the localization of SMC6 was limited to distinct foci located at the axial elements of the unsynapsed X and Y chromosomes (Verver et al., 2014a).

Functions of Smc5/6 in meiosis

Meiotic recombination

When meiotic recombination intermediates are not properly resolved to form either a non-crossover or crossover, aberrant joint molecules (JMs) can emerge. These JMs have the potential to block chromosome segregation if unresolved (Jessop and

Lichten, 2008, Copsey et al., 2013a, Xaver et al., 2013). Sgs1 limits the formation of these JM structures (De Muyt et al., 2012, Chen et al., 2010, Fabre et al., 2002, Sugawara et al., 2004, Jessop and Lichten, 2008). Several structure-selective nucleases, Mus81-Mms4, Slx1-Slx4, and Yen1, are involved in the resolution in these JMs (De Muyt et al., 2012, Zakharyevich et al., 2012, Matos et al., 2011). In budding yeast, the Smc5/6 complex antagonizes the formation of JMs via two mechanisms: (i) prevention of JMs by destabilizing SEI intermediates (Xaver et al., 2013) and (ii) facilitating JM resolution (Lilienthal et al., 2013a, Copsey et al., 2013a, Xaver et al., 2013). Like previously reported for the helicase BLM/Sgs1, the SUMO E3 ligase function of Nse2/Mms21 subunit is required to destabilize SEI intermediates (Xaver et al., 2013). This inhibition is needed to prevent the formation of inappropriate recombination intermediates. In the absence of Smc5/6, these inappropriate recombination intermediates develop into JMs that require the structure-selective resolvases Mus81-Mms4, Slx1-Slx4, and Yen1 to be processed (Zakharyevich et al., 2012). Of these resolvases, at least the ability of Mus81 to associate with, or be stabilized on, the meiotic chromosomes efficiently is dependent on Smc5/6 (Copsey et al., 2013a). Interestingly, while required to limit SEI stabilization, the SUMO E3 ligase function of Nse2/Mms21 is not required for Smc5/6 directed JM resolution (Xaver et al., 2013).

In fission yeast, meiotic recombination generates single Holliday junction (HJ) intermediates (Cromie et al., 2006, Davis and Smith, 2003, Hyppa and Smith, 2010, Keeney et al., 1997), which are eventually resolved by the Mus81-Eme1 complex (Cromie et al., 2006, Boddy et al., 2001, Osman et al., 2003). Based on genetic

experiments, the Smc5/6 complex subunits Nse5-Nse6 have a regulatory role in Mus81-Eme1 dependent HJ resolution (Wehrkamp-Richter et al., 2012b).

In *C. elegans* the SMC-5/6 complex is not required for chiasmata formation. However, mutation of *smc-5* or *smc-6* did result in chromosome fragmentation during meiosis I and an increased number of RAD-51 foci in the nucleus (Bickel et al., 2010). Interestingly, *mus-81, him-6* (a BLM ortholog) and *mus-81*, *xpf-1* double mutants display a similar phenotype to the *smc-5* or *smc-6* mutants (O'Neil et al., 2013). Because these genes are involved in two redundant HJ resolution pathways in *C. elegans* (Agostinho et al., 2013), the SMC-5/6 complex is likely to be involved in HJ resolution. Hence, the *C. elegans* SMC-5/6 complex may be playing similar JM antagonistic roles observed in budding yeast by hindering JM formation early and assisting JM resolution. However, *C. elegans* chromosomes are holocentric, and subsequent roles of SMC-5/6 in chromosome segregation may differ from other model organisms.

Preventing HR in heterochromatin

In budding yeast, Smc5/6 also binds to the rDNA, which remains unsynapsed during meiotic prophase I (Xaver et al., 2013, Farmer et al., 2011, Lilienthal et al., 2013a). Smc5/6 has been shown to have an anti-recombinogenic role at this repetitive DNA locus during vegetative growth (Torres-Rosell et al., 2007). Additionally, budding yeast Smc6 is strongly enriched in the pericentromeric regions during the mitotic G2 phase (Lindroos et al., 2006). Smc5/6 is essential for the timely separation of chromatids and the prevention of branched and entangled chromosome structures and subsequent

mitotic arrest (Lindroos et al., 2006). It is conceivable that Smc5/6 plays similar roles at the rDNA locus and pericentromeric regions during meiosis.

In mouse spermatocytes, SMC5, SMC6 and NSMCE1 localize at pericentromeric heterochromatin (Gomez et al., 2013, Verver et al., 2013a). As with rDNA, these regions are at high risk of aberrant recombination events when HR is enabled, leading to genomic instability (Goodarzi and Jeggo, 2012). An additional challenge specific to meiotic cells, is the endogenous induction of DSBs that are repaired by HR. Pericentromeric heterochromatin consists of densely packed repetitive sequences, and is therefore vulnerable to aberrant events such as the formation of intra-chromosomal recombination structures. As a result, meiotic recombination is generally suppressed around the centromeres (Lynn et al., 2004), via a mechanism yet to be elucidated. The role of Smc6 in preventing HR in these high-risk regions has already been established for yeast and *Drosophila* mitotic cells (Chiolo et al., 2011, Torres-Rosell et al., 2007). In line with these studies, pericentromeric heterochromatin of mouse prophase spermatocytes is simultaneously marked with SMC5, SMC6 and NSMCE1 (Gomez et al., 2013, Verver et al., 2013a) and deprived of recombination sites marked by RAD51 (Verver et al., 2013a). These findings suggest that also in mammalian germ cells, SMC5/6 might be responsible for preventing aberrant HR events in repetitive sequences. Interestingly, even though prevention of HR in heterochromatin might be a conserved function of SMC5/6, a similar localization was not found in human prophase spermatocytes (Verver et al., 2014a).

Centromere cohesion

During budding yeast meiosis, Smc5/6 regulates sister-chromatid cohesion at centromeres and is required for the timely removal of cohesin from chromosomal arms (Copsey et al., 2013a).

SMC6 is proximal to the centromeres during both meiotic metaphases in mouse (Gomez et al., 2013, Verver et al., 2013a) and human (Verver et al., 2014a). As well as during prophase I stages, SMC6 co-localizes at the centromeres with Topo IIα during metaphase I and II (Gomez et al., 2013). More specifically, in metaphase I and anaphase I, SMC6 was present as two foci proximal to the sister kinetochores, and only one signal near the kinetochores at metaphase II and anaphase II (Gomez et al., 2013). Additionally, in metaphase II spermatocytes, in which the centromeres are subjected to tension from opposite poles, SMC6 appeared as a strand connecting the sister kinetochores (Gomez et al., 2013). The finding that SMC6 co-localizes with Topo IIα, together with the fact that the strand of SMC6 joining sister kinetochores persists even after redistribution of Aurora-B, suggests that the SMC5/6 complex may regulate sister-chromatid centromere cohesion and dissolution of DNA catenates that form after DNA replication (Gomez et al., 2013). This role for SMC5/6 was further appointed when Topo IIα was inhibited by Etoposide, inducing lagging chromosomes during the second meiotic division. Both SMC6 and Topo IIα co-localized at stretched strands connecting these lagging chromatids at the site of the kinetochores (Gomez et al., 2013). Complementary data was acquired using budding yeast, where localization of Smc5 depends on meiotic DNA replication, and in the absence of TopoII, Smc5 localization is aberrant (Copsey et al., 2013a).

SC assembly/stability, homologous chromosome synapsis

Both in mouse and human spermatocytes, SMC5 and SMC6 were found to be located at the SC (Verver et al., 2014a, Gomez et al., 2013). Co-localization of mouse SMC6 with the SC central region proteins SYCP1 and TEX12 showed that SMC6 is restricted to synapsed chromosomes, leaving the un- or desynapsed axes including X and Y, unmarked (Gomez et al., 2013). Mammalian synapsis is characterized by the presence a central region that, besides SYCP1 (equivalent to Zip1 in budding yeast), also contains the central element proteins SYCE1-3 and TEX12 (Hamer et al., 2006, Hamer et al., 2008, Bolcun-Filas et al., 2007, Bolcun-Filas et al., 2009, Schramm et al., 2011). However, although dependent on SYCP1, loading of SMC6 to the mouse SC occurs independent of these central element proteins (Gomez et al., 2013). Additionally, mouse SMC5/6 localization is not dependent on meiosis-specific cohesin subunits REC8 and SMC1β (Gomez et al., 2013). The longitudinal localization pattern along the mammalian synapsed SC axes could suggest that localization of SMC5/6 is dictated by chromosome structure, as has been suggested in mitotic cells (Jeppsson et al., 2014b), or that the complex either facilitates SC assembly, chromosome synapsis or recruitment of other SC-associated proteins.

The XY body and unsynapsed chromosomes in pachytene spermatocytes

In males, due to a lack of homology, the X and Y chromosomes remain largely unsynapsed during the meiotic prophase I. During meiotic prophase, unsynapsed chromosomal regions are transcriptionally silenced by a process called meiotic silencing

of unsynapsed chromosomes (MSUC) (Ichijima et al., 2012). In the case of the X and Y chromosome, this silencing is called meiotic sex chromosome inactivation (MSCI), and is achieved by the formation of a so-called XY-body (or sex-body), marked by the presence of several DNA damage response proteins such as BRCA1, γ-H2AX and ATR (Ichijima et al., 2012). In male meiotic cells with extensive autosomal asynapsis, MSUC competes with MSCI for these proteins. The sex-chromosomes will then be inadequately silenced, which will result in a pachytene arrest (Burgoyne et al., 2009). In mouse spermatocytes, SMC5, SMC6 and NSMCE1 were found to cover the XY-body (Gomez et al., 2013). Because the XY-staining resembles that of γ-H2AX, it is proposed that the SMC5/6 complex might be facilitating MSCI at this site.

In human spermatocytes, SMC6 is present on the unsynapsed XY chromosomes in a more foci-like pattern (Verver et al., 2014a), suggesting a function in DSB-repair. Interestingly, it has been recently found that in the absence of synapsis, including the unsynapsed regions of the sex chromosomes, SPO11 will continue to make DSBs (Kauppi et al., 2013). In this light, the presence of SMC5/6 on the unsynapsed sex chromosomes might be required to repair these continuously induced DSBs. In addition to this observation, unsynapsed autosomes display both RAD51 and SMC6 foci (Verver et al., 2014a). Hence, it seems likely that human SMC5/6 plays a role in the repair of the continuously induced DSBs on unsynapsed meiotic chromosomes.

Discussion/concluding remarks

In recent years, assessment of Smc5/6 localization and analysis of Smc5/6 mutant phenotypes during meiosis has resulted in an abundance of data implying a number of

meiotic functions **(Table 1.1)**. In all models, and in line with its described functions during mitosis, Smc5/6 is involved in HR mediated repair and chromosome segregation, as depicted in **Fig. 1.3**. However, despite this common denominator, the meiotic functions of Smc5/6 seem astonishingly diverse.

Several studies in mammalian models have shown varying results when using antibodies against different epitopes of SMC6 simultaneously (Verver et al., 2014a, Gomez et al., 2013, Verver et al., 2013a). Since the technical variation within experiments was negligible, differences in localization pattern are most likely a reflection of varying conformations of the SMC6 protein or SMC5/6 complex as a whole, resulting in differing accessibility of these epitopes. Indeed, a study using budding yeast demonstrates that the Smc5/6 complex is physically remodeled in a ATP-dependent manner (Bermudez-Lopez et al., 2015). Even though future studies might unravel the role of conformation herein, another possibility is that Smc6 and/or Smc5 can act independently from the Smc5/6 complex, thereby showing differential localization patterns. When budding yeast proteins were purified separately, Smc5 and Smc6 were found to have some binding activity to ssDNA, independently of the presence of the other subunits (Roy and D'Amours, 2011, Roy et al., 2011). However, even though some studies support the complex-independent function of Smc5 and Smc6 (Laflamme et al., 2014, Roy et al., 2011, Vignard et al., 2011), most studies show that hypomorphic alleles and RNAi knockdown of Smc5 and Smc6 yield complementary phenotypes (e.g. (Gallego-Paez et al., 2014, Torres-Rosell et al., 2005b)). Moreover, fractionation experiments indicate that the majority of Smc5/6 components are in complex, and only a small fraction is present as isolated monomers (Torres-Rosell and Losada, 2011).

Table 1.1 Proposed functions of Smc5/6 in meiosis

	Meiotic Functions					
Organism	Response to DSBs	Meiotic recombination	Heterochromatin maintenance	Centromere cohesion	Homologous chromosome synapsis	Meiotic Sex Chromosome Inactivation
Budding Yeast *S. Cerevisiae*	- Co-localization of Smc6 side-by-side with Rad51 (Copsey et al. 2013; Xaver et al. 2013) - Smc5/6 enriched at DSB hotspots (Copsey et al. 2013; Xaver et al. 2013)	- Smc5/6 antagonizes the formation of joint molecules (Copsey et al. 2013; Lilienthal et al. 2013; Xaver et al. 2013) - Smc5/6 is required for regular localization of Mus81 (Copsey et al. 2013; Xaver et al. 2013)	- Localization of Smc5/6 to rDNA (Farmer et al. 2011; Lilienthal et al. 2013; Xaver et al. 2013). May have similar anti-recombinogenic role at rDNA as observed during vegetative growth (Torres-Rosell et al. 2007)	- Smc5/6 regulates centromere cohesion and required for timely removal of cohesin from chromosomal arms (Copsey et al. 2013)	- Localization of Smc5 and Smc6 along synapsed axes (Copsey et al. 2013; Lilienthal et al. 2013; Xaver et al. 2013)	
Fission Yeast *S. Pombe*	- Nse6 acts after the Rad51 and Dmc1 strand-exchange proteins (Wehrkamp-Richter et al. 2012)	- Regulatory role of Nse5-Nse6 in Mus81-Eme1 dependent Holliday junction resolution (Wehrkamp-Richter et al. 2012)				
Worm *C. Elegans*	- Enrichment of SMC-6 with the occurrence of DSB repair (Bickel et al. 2010) - Chromosome fragmentation and increased number of RAD-51 foci during MI in *smc-5* or *smc-6* (Bickel et al. 2010)	- Mutations *smc-5* or *smc-6* and double mutants *mus-81*, *him-6* and *mus81*, xpf-1 display similar phenotypes (Agostinho et al. 2013; O'Neil et al. 2013)			- Enrichment of SMC-5 and SMC-6 on chromosome axes during pachytene (Bickel et al. 2010)	
Mouse *M. Musculus*			- Localization of SMC5, SMC6 and NSMCE1 to pericentromeric heterochromatin (Gomez et al. 2013; Verver et al. 2013), which is simultaneously deprived of HR (Verver et al. 2013)	- Localization of SMC6 to centromeres (Gomez et al. 2013; Verver et al. 2013) - Co-localization of SMC6 with Topo IIα (Gomez et al. 2013)	- Localization of SMC5 and SMC6 on synapsed axes, co-localization with SYCP1 and TEX12 (Gomez et al. 2013)	- Localization of SMC5 and SMC6 to the XY body, similar pattern as γ-H2AX (Gomez et al. 2013; Verver et al. 2013)
Human *H. Sapiens*	- Localization of SMC6 foci to unsynapsed chromosomes, side by side to RAD51 foci (Verver et al. 2014)			- Localization of SMC6 to centromeres (Verver et al. 2014)	- Localization of SMC5 and SMC6 to synapsed axes (Verver et al. 2014)	- Localization of SMC6 foci to the X-Y chromosome axes (Verver et al. 2014)

Figure 1.3. Proposed functions of Smc5/6 in meiosis. (**A**) In budding and fission yeast, Smc5/6 is required for the resolution of meiotically induced joint molecules and correct segregation of homologous chromosomes. Without functional Smc5/6 recombination intermediates cannot be efficiently resolved, leading to the accumulation of inter-homolog, inter-sister, and multi-chromatid joint molecules and failure to segregate chromosomes properly. *Black spot* = centromere. (**B**) During mouse and human meiosis, SMC5/6 functions in a variety of processes. It is proposed to be involved in synaptonemal complex formation and/or stability, heterochromatin maintenance, and XY body silencing. Moreover, it may be required for repair of DSBs due to lack of synapsis and resolving meiotic recombination intermediates. Finally, SMC5/6 is involved in centromere cohesion during M-phase. *Purple* = SMC5/6 complex localization. *Gray filaments* = lateral elements of the synaptonemal complex. *Gray spot* = centromere. Note: depicted chromosomes represent (telocentric) mouse chromosomes

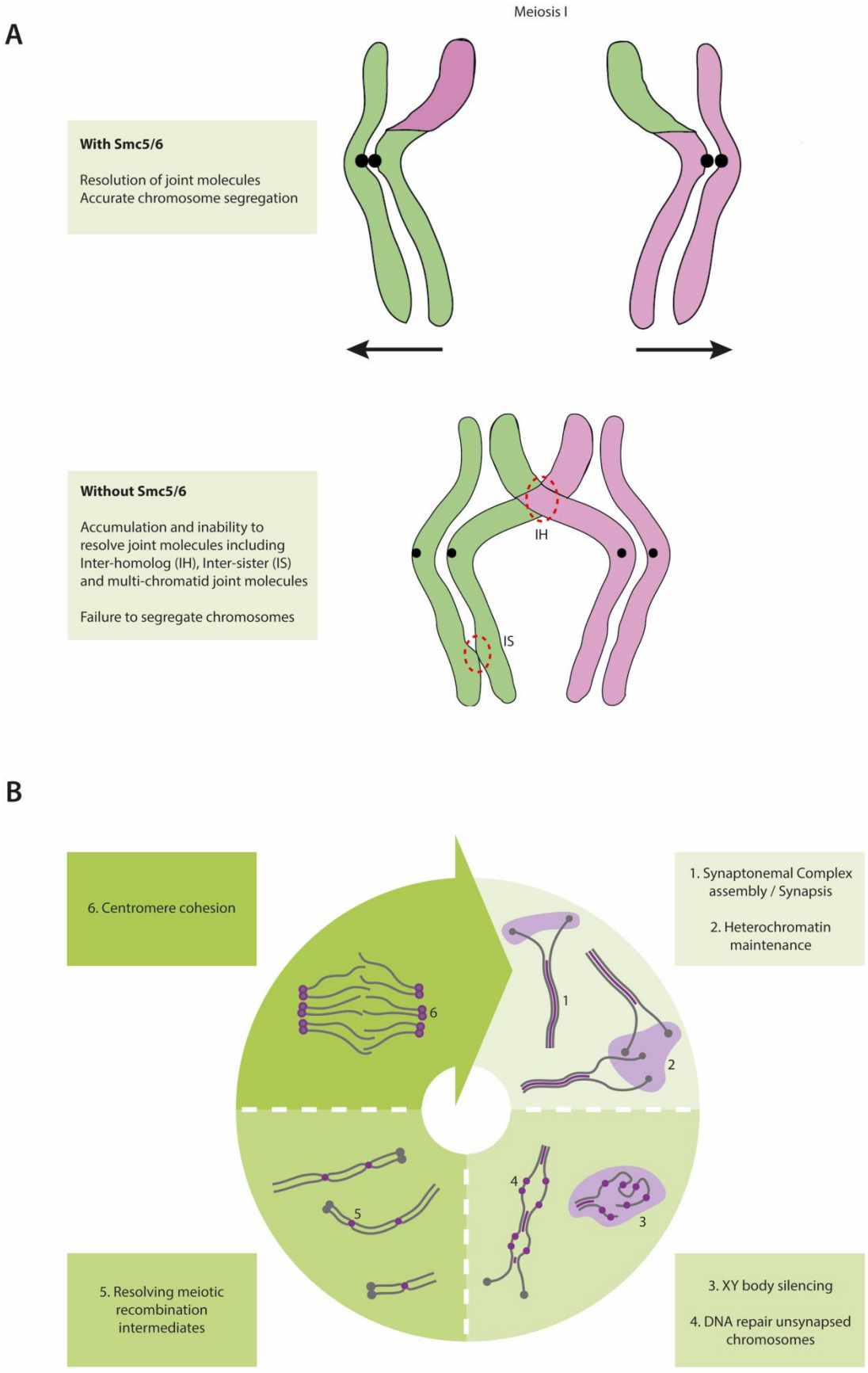
A
Meiosis I
With Smc5/6
Resolution of joint molecules
Accurate chromosome segregation
Without Smc5/6
Accumulation and inability to resolve joint molecules including Inter-homolog (IH), Inter-sister (IS) and multi-chromatid joint molecules
Failure to segregate chromosomes
IH
IS
B
6. Centromere cohesion
1. Synaptonemal Complex assembly / Synapsis
2. Heterochromatin maintenance
3. XY body silencing
4. DNA repair unsynapsed chromosomes
5. Resolving meiotic recombination intermediates
1
2
3
4
5
6

The diversity of mitotic and meiotic functions of Smc5/6 illustrates the versatility of this protein complex. Yet, the regions where Smc5/6 has been found to act are not random and its roles on rDNA, telomeres, DSBs, replication sites and collapsed replication forks all support the strong preference of Smc5 and Smc6 to capture ssDNA (Roy and D'Amours, 2011, Roy et al., 2011). The consequences of Smc5/6 binding to DNA seem to vary between the specific processes it is required for. During meiosis, the Smc5/6 complex can either link homologous chromosomes or may recruit other proteins to its site of action. Either way, both the fission and budding yeast Smc5/6 complex has been found to be crucial to resolve meiotic recombination intermediates (Xaver et al., 2013, Copsey et al., 2013a, Lilienthal et al., 2013a). Despite its seemingly diverse roles during different processes, resolving complex chromosome structures, which would otherwise cause cell cycle arrest or prevent chromosomes from being segregated, appears a major meiotic function of Smc5/6. However, how Smc5/6 is molecularly regulated during different meiotic processes, such as pre-meiotic S-phase, meiotic recombination and the meiotic M-phases, still needs further research. Creation and assessment of mammalian mutant models, together with the development of a comprehensive meiosis interactome for the SMC5/6 complex will further our comprehension of SMC5/6 functions. More knowledge on the meiotic functions of Smc5/6 may give insight in one of the biggest questions in biology: how are germ cells capable to passage their genome through essentially endless generations while maintaining sufficient genomic integrity.

Outline and Summary

The goal of this research is to investigate the functions of the SMC5/6 complex in germ cells during meiotic progression in mammals. As meiosis is a sexually dimorphic

process, my work is divided into two major sections: the roles of SMC5/6 in oogenesis and its roles in spermatogenesis. In Chapter II, I describe chromatin spread preparations for the analysis of mouse oocyte progression from prophase to metaphase II. These major techniques that I optimized in the lab allow for clear visualization of the dynamic localization patterns of chromatin-bound proteins and chromosome morphology of oocytes throughout mammalian oogenesis. In Chapter III, I present a published study that illuminates specific roles of SMC5/6 in mammalian oogenesis, using these major techniques. This study is the first to work towards elucidating the functions of SMC5/6 in mammalian oogenesis as many of the known functions of the complex have been discovered in the context of mitosis—specifically using yeast. Using conditional mutant mice of *Smc5*, I found that SMC5/6 may contribute to increased incidence of oocyte aneuploidy and infertility in aging females, a phenomenon observed in many mammals, including humans. In Chapter IV, I present a published study with additional unpublished data on the functions of SMC5/6 in spermatogenesis. Surprisingly, SMC5/6 is not required for male fertility and seems to be only required for exogenous DNA repair. This suggests that SMC5/6 has sexually dimorphic roles in mammalian germ cell progression and genome maintenance. In Chapter V, I discuss future directions for this research aiming to discover the interacting partners of the SMC5/6 complex. These experiments will further give insight in other functional roles of the complex in mammals. Finally, I will discuss the clinical relevance of SMC5/6 and its links to numerous diseases.

CHAPTER II

CHROMATIN SPREAD PREPARATIONS FOR THE ANALYSIS OF MOUSE OOCYTE PROGRESSION FROM PROPHASE TO METAPHASE

This chapter was published in Journal of Visualized Experiments [Hwang, G.H., Hopkins, J., Jordan, P.W.J. (2018)] accompanied by a video and is reproduced here with minor edits. The purpose of this chapter is to provide a detailed overview of the chromatin spread methods used to analyze mouse oogenesis.

Introduction

During spermatogenesis, large semi-synchronous waves of meiotic germ cells are rapidly and continuously replenished in the testis at the onset of puberty and throughout adulthood(Morelli and Cohen, 2005). In contrast to males, meiosis in females is initiated solely during fetal development. Following birth, oocytes remain arrested in a prolonged dictyate stage of prophase I with an intact germinal vesicle (GV; nuclear envelope) until puberty. At the onset of puberty, a subset of oocytes is cyclically selected to undergo growth and maturation, marking the initiation of meiotic resumption. Meiotic resumption in fully-grown oocytes is manifested by the disappearance of the GV in a process known as germinal vesicle breakdown (GVBD). The oocyte then undergoes chromosome condensation and segregation, followed by polar body extrusion. Oocytes become arrested upon progression to MII and are stimulated to complete the second and final meiotic division only after fertilization.

Female fertility is highly dependent on the success of meiotic prophase I progression. Key to this is formation of a physical linkage between homologous chromosomes known as the chiasmata, which is mediated by repair of induced DNA double strand breaks (DSBs) via crossover recombination (Keeney, 2008). This process occurs within the context of a dynamic protein-rich scaffold known as the synaptonemal

complex (SC) that forms between homologous chromosomes to facilitate their synapsis(Zickler and Kleckner, 2015). The SC is a zipper-like tripartite structure that consists of two parallel lateral elements connected by central region proteins that holds homologs together throughout ongoing DNA repair. Prior to synapsis, precursors of the lateral elements, called axial elements, form between sister chromatids. Synaptonemal complex proteins such as SYCP2 and SYCP3 form axial elements that colocalize to the sister-chromatid cohesion axes during early prophase. These later serve as binding sites for the transverse filament protein, SYCP1, which facilitates central element assembly and synapsis between aligned homologs(de Vries et al., 2005). In mouse oocytes, complete synapsis is indicated by the presence of 20 completely overlapping SYCP3 and SYCP1 stretches, which can be visualized by using chromatin spread preparations. Synapsis is completed upon entry into the pachytene substage, whereby mature crossovers that are destined to form chiasmata between homologs are decorated with mutL homolog (MLH1/3) dimers to promote their accurate processing(Baker et al., 1996, Lipkin et al., 2002, Kolas et al., 2005). The structural maintenance of chromosomes (SMC) complexes, including cohesin, condensin, and the SMC5/6 complex, are important for the regulation of chromosome dynamics and structure throughout meiosis(Rankin, 2015a, Lee, 2013, Verver et al., 2016a, Hopkins et al., 2014b, Hwang et al., 2017). Collectively, these events ensure proper bi-orientation of homologous chromosomes to opposing spindle poles following disassembly of the SC.

The meiotic cell cycle is a powerful model to examine the roles of various proteins in genome maintenance due to the programmed induction and subsequent repair of DNA DSBs. Furthermore, mammalian meiosis is also a relevant model for the study of

epigenetic modifications and imprinting(Kota and Feil, 2010). However, it is technically difficult to assess these events during female meiosis, which takes place in fetal and neonatal ovaries in mammals **(Fig. 2.1)**. Prophase I can be divided into 5 substages: leptonema, zygonema, pachynema, diplonema and dictyate. Herein, we describe how to isolate and distinguish between fetal and neonatal ovaries and testes **(Fig. 2.2)**. Adapted from previously described methods, section 1 of this manuscript outlines a protocol with video demonstration for preparation of female meiotic prophase I chromatin spreads(Taketo, 2012, Sun and Cohen, 2013, Kim et al., 2013, Susiarjo et al., 2009b). When coupled with immunolabelling as described in sections 6-7, this protocol enables detailed microscopic analysis of prophase I events in oocytes.

Oogenesis is error-prone, and chromosome missegregation events during the first meiotic division represent the most common source of genetic disease in progeny(Hassold and Hunt, 2001b, Hassold et al., 2007). In section 2 of this manuscript, we describe a protocol in which mature GV-staged oocytes are extracted from primed ovaries of adult female mice. Under supportive conditions, fully-grown oocytes undergo luteinizing hormone-independent resumption of meiosis following isolation and culture(Pincus and Enzmann, 1935a). Following meiotic resumption, oocytes progress through meiosis I, then arrest at metaphase II. Oocytes remain arrested at metaphase II, unless fertilized. In sections 2-5, we adapt previously reported protocols with video demonstration to describe how to collect, culture and prepare MI and MII oocytes for chromatin spread preparations(Chambon et al., 2013). This chromatin spreading technique allows for clear immunolabelling of proteins associated with chromosomes. Furthermore, this protocol can also be used to distinguish between bivalent and univalent

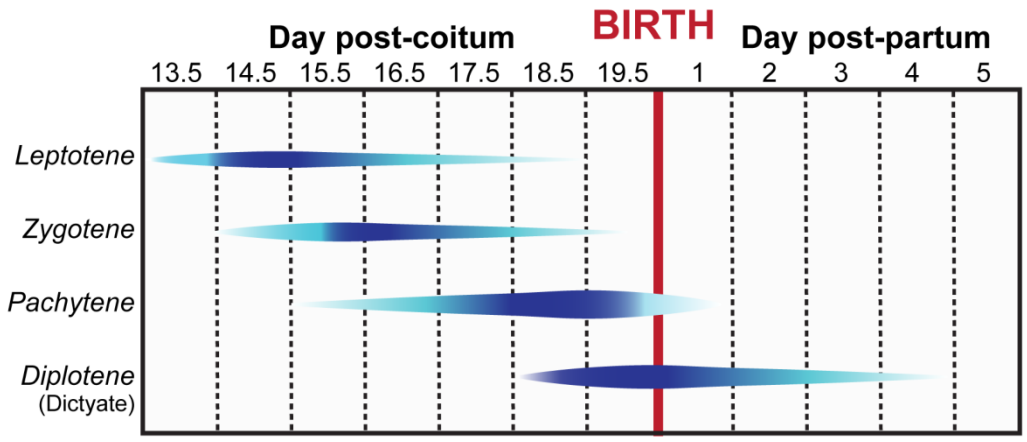

Figure 2.1. Meiotic prophase timeline during female embryonic and neonatal development. Blue contours indicate populations of specific prophase sub-stage germ cells (leptotene, zygotene, pachytene, and diplotene/dictyate stages) observed during embryonic and neonatal development. Increasing dark blue color indicates the timing at which the specific prophase sub-stage becomes more abundant. This figure was adapted from Keeney et al, 2015.

Figure 2.2. Ovary extraction from embryos and neonatal female pups. (A, B) The first cut (1) is made above the forelimbs to decapitate the embryo at the head/neck junction immediately upon retrieval from the maternal uterine horn. The second cut (2) is made along the ventral midline of the posterior half of the embryo, followed by incisions along the anterior half below the forelimbs (3). A final cut is made for removal the hind limbs and tail (4). **(A)** Frontal view schematic of dissection cuts for isolation of ovaries from female pups. **(B)** Side view schematic of dissection cuts for isolation of ovaries with relative positions of internal organs. Regions shown in light red include the liver and intestines, which are removed during dissection. The dorsal wall and associated organs are shown in light blue. This region includes the ovaries, which are attached to the inferior poles of the kidneys at the top of the uterine horn. **(C)** Frontal schematic view of dorsal wall of embryo following removal of the liver and intestines. **(D)** Schematic representation of morphological differences between male and female gonads at approximately 15-18 dpc.

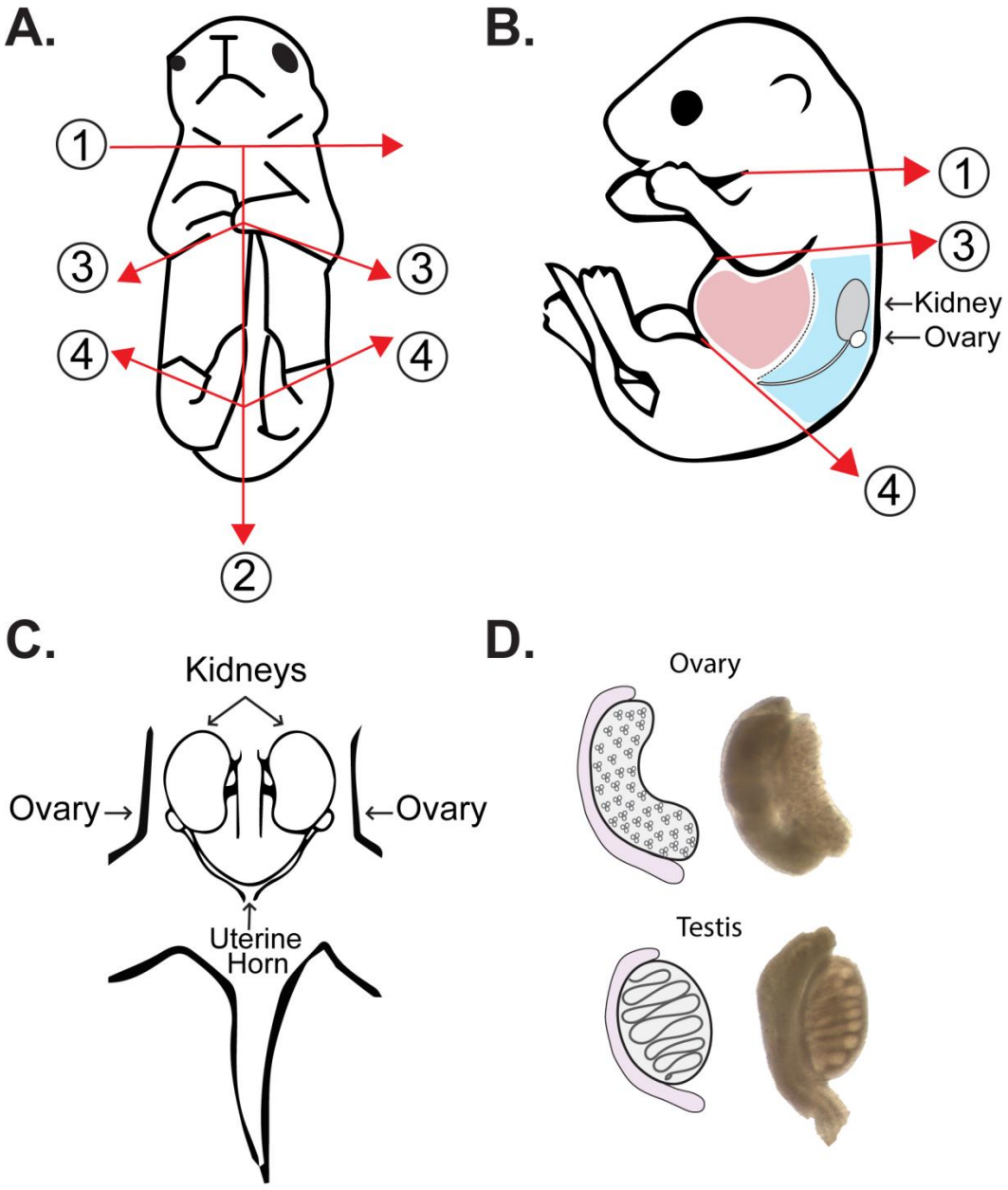
A.
1
3
3
4
4
2
B.
1
3
←Kidney
←Ovary
4
C.
Kidneys
Ovary→
←Ovary
Uterine
Horn
D.
Ovary
Testis

chromosomes, and can further resolve single sister chromatids to facilitate assessment of oocyte ploidy. Therefore, in addition to revealing localization patterns of meiotic proteins, this protocol can also serve as an invaluable tool for elucidating potential causes of chromosome missegregation during MI and MII.

Protocol

All methods described here have been approved by the Institutional Animal Care and Use Committee (IACUC) of Johns Hopkins University. Experiments were performed on wild-type C57BL/6J mice.

1. Harvesting fetal or neonatal ovaries and preparation of prophase chromatin spreads

1.1. To extract embryos at 14.5-19.5 days post-coitum (dpc) sacrifice the pregnant females via cervical dislocation or CO_2 asphyxiation according to IACUC guidelines. **Note:** For postnatal day 1-5 ovaries skip to step 1.3. **Fig. 2.1** summarizes the meiotic prophase stages enriched at different embryonic and post-natal ages.

1.2. Open the abdominopelvic cavity using sterile scissors, making a V-shaped opening. Dissect out the maternal uterine horn, separate the embryos from the placenta, and transfer embryos into 35 mm petri dishes containing 3 ml of pre-warmed 1x phosphate buffer saline (PBS) at 37°C. **Note**: A fliptop incubator set at 37°C can be used to maintain temperature. In addition, a temperature regulated glass stage can also be used to maintain temperature during ovary manipulation.

1.3. With 3.5 inch surgical scissors, sacrifice embryos or pups via decapitation according to IACUC guidelines. Place decapitated embryos or pups in pre-warmed PBS prior to further dissection.

1.4. Dissect one embryo or pup at a time in a separate 35 mm petri dish containing 3 ml of pre-warmed PBS at 37°C. Proceed by cutting along the ventral midline of the posterior half of the embryo, along the anterior half below the forelimbs and directly above the hind-limbs and tail as outlined in **Fig. 2.2A-B**.

1.5. Open the abdomen using 3.5 inch surgical scissors. Using fine-tipped forceps displace or remove the liver and loops of bowel, exposing the ovaries in a new 35 mm petri dish containing 3 ml of pre-warmed PBS at 37°C **(see guide in Fig. 2.2B)**. The ovaries are located immediately below and behind the kidney towards the posterior wall of the peritoneal cavity **(Fig. 2.2B-C)**. A guide for differentiating between male and female gonads is provided in **Fig. 2.2D**. **Note**: For optimal conditions, rapidly dissect out the ovaries after pregnant female is sacrificed.

1.6. Remove both ovaries from each female fetus using a pair of fine-tipped forceps under a dissection scope and place in a watch glasses or separate wells of a multi-well plate containing 0.5 to 1.0 ml of pre-warmed PBS and maintain at 37°C.

1.7. Place each pair of ovaries in 0.5 ml hypo-extraction buffer (17 mM trisodium citrate dihydrate, 50 mM sucrose, 5 mM EDTA, 0.5 mM DTT, 30 mM Tris-HCl, protease inhibitor, pH 8.2) in a clean watch glass or a small well of a 9-well plate, making sure to immerse the ovaries completely. Incubate for at least 15 min, but no more than 30 min. **Note**: Make hypo-extraction buffer fresh and use within 2 h of DTT addition.

1.8. During incubation, using a hydrophobic barrier PAP pen, draw two 22x22 mm squares on a clean glass 25x75 mm, 1 mm thick microscope slide as shown in **Fig. 2.3A. Note**: Slides can be prepared ahead of time.

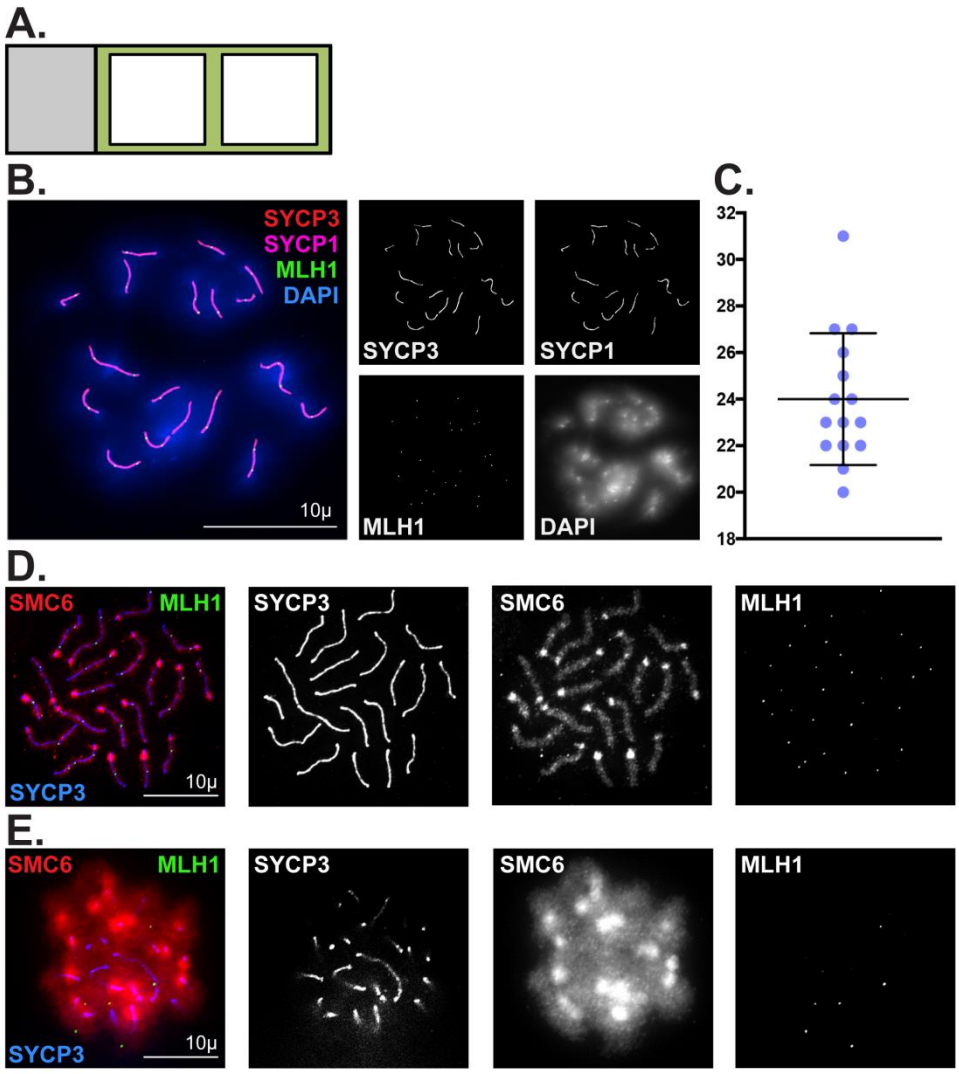

Figure 2.3. Representative prophase chromatin spread preparations. (A) Glass slide schematic for prophase chromatin spread preparations. Black square outlines represent liquid blocker pen outlines. **(B, C)** Representative images and quantification of crossover formation in wild-type pachytene stage oocytes using prophase chromatin spread preparation methods described in step 1. **(B)** Chromatin spreads were performed using ovaries from C57BL/6J mouse embryos isolated at 18.5 dpc. Chromatin spreads were immunolabeled with antibodies against the SC lateral element protein SYCP3 (red), and the SC central element protein SYCP1 (magenta), MLH1 (green, crossover event marker), and DAPI (blue, DNA). Scale bar: 10 μm. **(C)** Dot plot of MLH1 foci counts obtained from 15 pachytene stage chromatin spread preparations. Error bars represent standard deviation. **(D, E)** Comparison of optimal **(D)** and sub-optimal (**E**) prophase spread preparations, respectively. Chromatin spreads were immunolabeled with antibodies against SMC6 (red), MLH1 (green), and SYCP3 (blue). Scale bar: 10 μm.

1.9. Pipette 45–50 μL of 100 mM sucrose onto a clean slide and transfer one pair of ovaries to the drop.

1.10. Using the sharp ends of two 27-gauge needles, tease the ovaries apart to release cells into the sucrose solution. With forceps, remove large pieces of ovary and carefully pipette sucrose solution to disperse cells.

1.11. Place 40 μL of fixative solution (1% paraformaldehyde (PFA), 0.2% Triton X-100, pH 9.2) into each square of the prepared slide. With a 200 μl pipette tip, spread the fixative solution evenly over the slide surface.

1.12. Pipette 20 μL of the sucrose mix onto the each square of the slide containing the fixative. **Note**: This equates to using one pair of ovaries per slide.

1.13. Incubate the slides in a closed humid chamber overnight at room temperature. **Note**: The overnight incubation can range around (12-15 hrs) at room temperature.

1.14. Open the chamber lid and allow the slides to air-dry completely.

1.15. Wash slides in a Coplin jar containing 50 ml of 0.4% Photo-Flo PBS solution for 2 min, air dry, and proceed to immunolabelling protocol (Step 6). **Note**: It may be possible to store the slides at –80°C for later use, but this varies depending on the protein of interest. For optimal results proceed immediately to the immunolabelling protocol (Step 6).

2. Metaphase I oocyte collection

2.1. To maximize the number of antral follicles isolated from each mouse, intraperitoneally inject sexually mature virgin female mice with 5 IU of pregnant mare's serum gonadotropin (PMSG, also known as equine chorionic gonadotropin

(eCG)). **Note**: For optimal oocyte yield, mice should be 1 to 3 months of age as the number of oocytes harvested will decrease with age. To prepare PMSG, dissolve bottle of 5000 IU in 100 mL of sterile PBS (5 U/0.1 mL) Store in single-use aliquots of 600 μL at -20°C.

2.2. After 44-48 h, prepare collection medium, minimum essential medium alpha (MEMα) medium supplemented with 5% fetal bovine serum (FBS) and 3 mg/mL bovine serum albumin (BSA; MEMα/BSA/FBS). Sterilize media through a 0.2 μm pore filter. Decant 2.5 mL of MEMα/BSA/FBS medium into one glass dish per mouse and warm to 37°C in a 5% CO_2 incubator. **Note**: Other collection and culture media that are commercially available (M2 and M16) are also commonly used. **Caution:** We recommend removing culture dishes from the 5% CO_2 incubator one at a time for limited duration to minimize ambient air exposure during manipulation steps.

2.3. Sacrifice the mice via cervical dislocation or CO_2 asphyxiation according to IACUC guidelines.

2.4. Open the abdominopelvic cavity using sterile scissors, making a large V-shaped opening. Using forceps, displace intestines towards the head of the mouse. Locate each uterine horn, the ovaries are present proximal to the rib cage. Hold the oviduct with fine forceps and cut the fat superior to the ovary using dissection scissors (**Fig 2.4**). Continue to hold the oviduct, and with another set of fine forceps release the ovary from the bursa and place into collection dish containing MEMα/BSA/FBS medium. **Note**: It is imperative to keep the ovaries at 37°C, and maintain at 5% CO_2. A fliptop incubator hooked up to 5% CO_2 mix can be used to allow for optimal

maintenance of temperature and CO_2 levels. In addition, a temperature regulated glass stage should also be used to maintain temperature during oocyte manipulation.

2.5. Using a 1 ml syringe with a 27-gauge needle (or similar size), release cumulus oocyte complexes by manually puncturing the large antral follicles.

2.6. While observing through a dissection microscope, collect GV-staged oocytes using a mouth-operated glass pipette or capillary, or a hand-operated micrometer-syringe (**Fig. 2.5**). Only collect oocytes that are released from antral follicles. GV oocytes have a diameter of approximately 90 μm. GV oocytes may be surrounded by 2-3 layers of granulosa cells, and have a total diameter of around 200 μm.

2.7. Culture oocytes in a clean watch glass or a 9-well plate containing MEMα/BSA/FBS medium for 6 h to reach metaphase I at 37°C in a 5% CO_2 incubator.

2.8. Proceed to step 4.

3. Metaphase II (MII) oocyte collection

3.1. To maximize oocytes isolated from each mouse, intraperitoneally inject sexually mature virgin female mice with 5 IU of PMSG. After 44-48 h, intraperitoneally inject with 5 IU of human chorionic gonadotropin (hCG). **Note**: For optimal oocyte yield, mice should be 1 to 3 months of age as the number of oocytes harvested will decrease with age. To prepare hCG dissolve bottle of 10,000 U in 200 ml PBS (5 U/0.1 mL). Store in single-use aliquots of 600 μL at -20°C.

3.2. After 12-14 hrs, prepare MEMα/BSA/FBS collection medium, as described in step 2.2, above.

3.3. Sacrifice the mice via cervical dislocation or CO_2 asphyxiation according to IACUC guidelines.

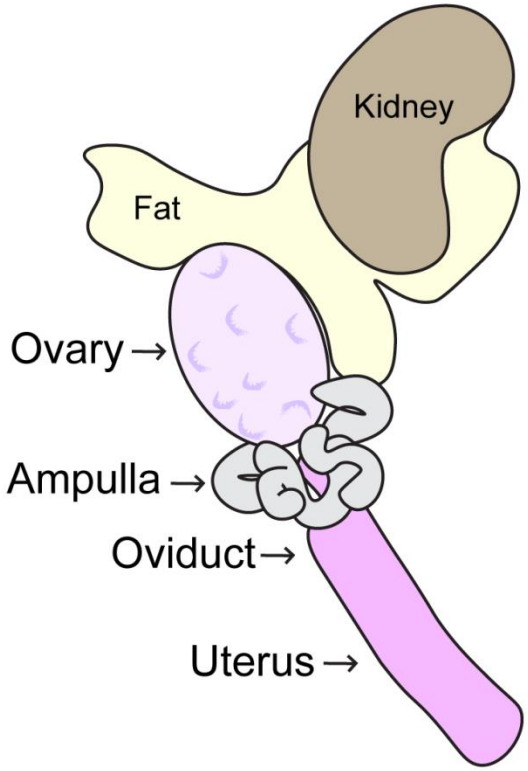

Figure 2.4: Schematic diagram of adult ovary. This diagram depicts the anatomy of the adult mouse ovary, oviduct, ampulla and uterus. Mouse ovaries should be removed by careful incision of ligaments connecting the ovaries to the inferior poles of the kidneys, and the posterior wall of the abdomen.

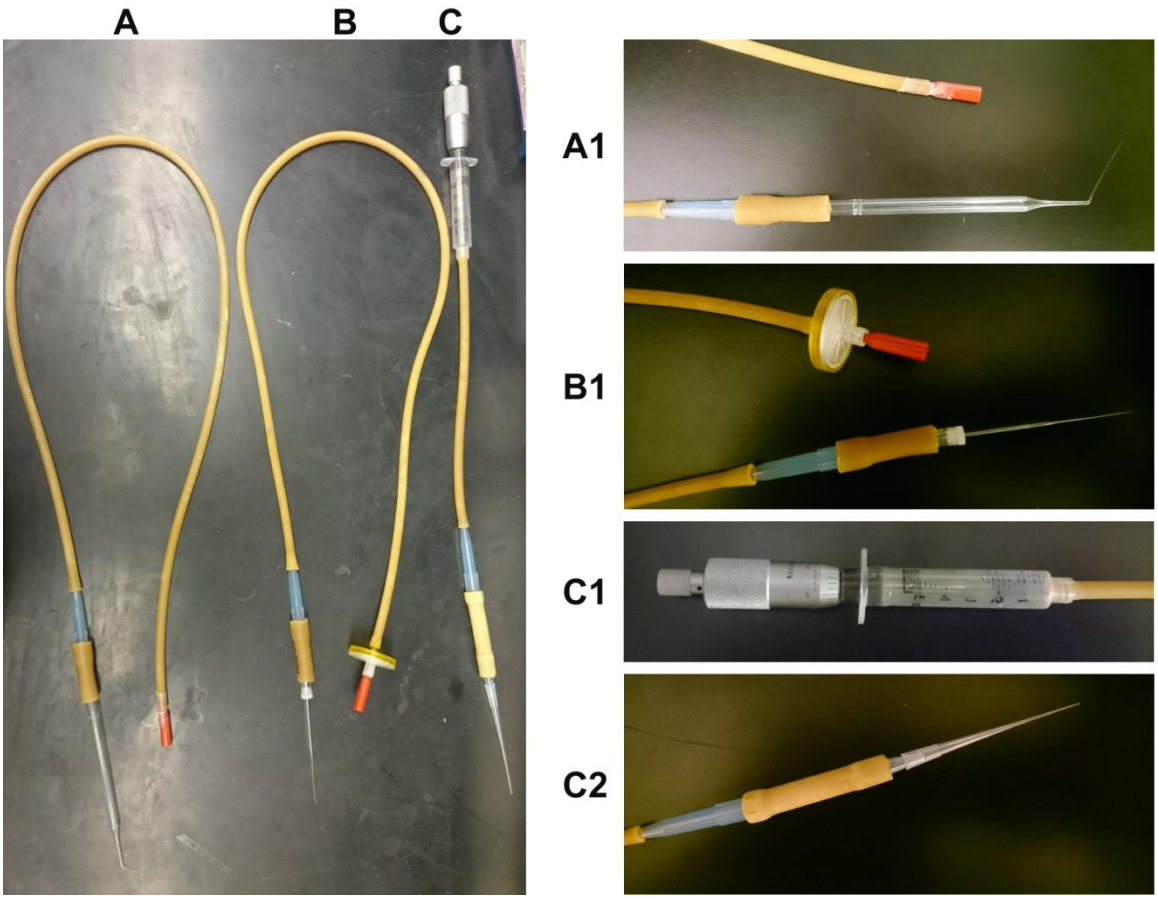

Figure 2.5. Images of mouth-operated glass pipette, glass capillary and hand-operated micrometer-syringe used for oocyte manipulation. (A) The glass pipette oocyte manipulator is composed of the following components in sequence: mouth piece, latex tubing (3.2 mm inner diameter (ID) x 6.4 mm outer diameter (OD)), 1 ml pipette tip, latex tubing (6.4 mm ID x 11.1 mm OD) and glass Pasteur pipette. The end of the glass Pasteur pipette has been heated over a flame and the end pulled to create a fine-tipped end (see zoom **Fig. 5A1**). **(B)** The glass capillary oocyte manipulator is composed of the following components in sequence: mouth piece, 0.45 µm filter (optional), latex tubing (3.2 mm ID x 6.4 mm OD), 1 ml pipette tip, latex tubing (6.4 mm ID x 11.1 mm OD) and 70 µl glass capillary. The glass capillary tubes are heated over a flame at the center and pulled in opposite directions to create two capillaries with fine tipped ends (see zoom **Fig. 5B1**). **(C)** The hand-operated micrometer-syringe is composed of the following components in sequence: Mitutoyo 150-208 micrometer head (middle size, 0-1" range, 0.001" graduation), 5 ml syringe, latex tubing (3.2 mm ID x 6.4 mm OD), 1 ml pipette tip, latex tubing (6.4 mm ID x 11.1 mm OD), 1 ml pipette tip and a 83 x 0.5 mm gel loading tip. The Mitutoyo 150-208 micrometer head is firmly inserted into the 5 ml syringe (**Fig. 5C1**). To ensure the gel loading tip is fastened securely, the connecting 1 ml pipette tip is cut (**Fig. 5C2**).

3.4. Open the abdominopelvic cavity using sterile scissors, making a large V-shaped opening. Using forceps, displace intestines towards the head of the mouse. Locate each uterine horn, the ovaries are present proximal to the rib cage. Hold the oviduct with fine forceps and cut the fat superior to the ovary using dissection scissors (**Fig. 4**). Then remove the ovary and oviduct and place into collection dish containing MEMα/BSA/FBS medium. **Note**: It is imperative to keep the ovaries at 37°C, and maintain at 5% CO_2. A fliptop incubator hooked up to 5% CO_2 mix can be used to allow for optimal maintenance of temperature and CO_2 levels. In addition, a temperature regulated glass stage should also be used to maintain temperature during oocyte manipulation.

3.5. Using a 1 ml syringe with a 27-gauge (or similar size) or sharp forceps, tear a hole in the ampulla of the oviduct to release the MII oocytes. **Note**: Be careful not to damage the oocytes in the ampulla. The ampulla will appear swollen and translucent such that the oocytes are visible (**Fig. 2.4**).

3.6. Harvest MII oocytes from the ampulla of the oviduct into a new dish with collection medium using a mouth-operated glass pipette or capillary, or a hand-operated micrometer-syringe (**Fig. 2.5**).

3.7. Proceed to Step 4.

4. Oocyte denuding and zona pellucida removal

4.1. Prepare 300 IU/mL of hyaluronidase in MEMα medium supplemented with 3 mg/ml BSA to denude oocytes of surrounding cumulus cells (2.5 mL/mouse) in a watch glass and keep at 37°C, 5% CO_2. **Note**: Hyaluronidase efficacy sharply decreases

after 1 h of preparation. For MII oocytes, hyaluronidase treatment is not required.

4.2. Expose oocyte-cumulus cell complexes to 300 IU/mL of hyaluronidase in MEMα/BSA for 3 min to denude oocytes of surrounding cumulus cells. **Caution:** Do not exceed 3 min exposure to hyaluronidase, as it will damage the oocytes.

4.3. To wash the oocytes, transfer oocytes to a fresh warmed MEMα/BSA medium dish. Using a small mouth-operated glass pipette or capillary (slightly larger than the diameter of the oocyte, which is approximately 90 μm), pipette the complexes up and down to completely detach the cumulus cells. Allow the oocytes to recover in the incubator while preparing for the next step.

4.4. Warm acidic Tyrode's solution, MEMα/BSA, and Waymouth's media to 37°C (500 μL/mouse). Into small 9-well glass plates, load 300 μL of each media and solution in separate wells..

4.5. To remove the zona pellucida (ZP) transfer 5-10 oocytes into Tyrode's solution. Expose the oocytes for only 30-45 s to the solution. **Note**: Too little exposure to the solution will not remove the ZP completely, which will prevent the oocytes from bursting and chromosomes from spreading. Too much exposure will damage and kill the oocyte. Watching the ZP dissolve under the dissection microscope can aid in optimizing exposure time. **Caution**: Using fresh Tyrode's solution is critical, as its function declines with age. Use a fresh well of Tyrode's solution for each group of oocytes treated to ensure uniform digestion of the ZP.

4.6. Immediately after ZP removal, wash the oocytes by transferring into warmed MEMα/BSA/FBS medium. Repeat this wash step. **Note**: Be careful when transferring as oocytes will easily stick together and to the glass pipette or capillary

following removal of the ZP. Pre-wetting the glass pipette or capillary in Waymouth's medium will minimize oocytes sticking together.

4.7. Transfer and allow the oocytes to recover for 30 minutes in Waymouth's medium at 37°C in a 5% CO_2 incubator.

4.8. Proceed to step 5.

5. MI and MII oocyte chromatin spreads

5.1. Using a PAP pen, draw a 11x44 mm rectangle on the glass slide as shown in **Fig. 2.6A**.

5.2. Coat the slide with a thin layer of fixative (1% paraformaldehyde, 0.2% Triton-X 100 in H_2O, pH 9.2) by pipetting 100 μL of fixative onto the slide and rocking the slide back and forth. Tap the slide to get rid of excess fixative.

5.3. Pick up between 5-10 oocytes with a mouth operated glass pipette or capillary with as little media as possible and drag the glass pipette or capillary in a line across the fixative-coated slide while depositing the oocytes from 1 cm above the slide into the fixative solution. Perform this step using a dissection microscope to ensure that the oocytes have been deposited and that they have burst. **Note**: The oocytes should burst immediately on the slide. The height at which the oocytes are deposited impact the degree of chromatin spreading. See representative results in **Fig. 2.6** for further details.

5.4. Incubate slides at room temperature in a closed humidified chamber overnight to allow the chromatin to adhere.

Figure 2.6. Representative metaphase I and II oocyte chromatin spread preparations. (A) Slide schematic for metaphase I and II oocyte chromatin spread preparations. Oocytes (circles) released via mouth-operated glass pipette or capillary in a straight line (following the arrow). Black rectangle outline represents liquid blocker pen outline. **(B, C)** Optimal metaphase I chromatin spread preparation. Metaphase I chromosomes were stained with DAPI (blue, DNA), and immunolabeled for CEN (green, kinetochore/centromere marker). Scale bars: 10 μm. **(B)** Antibodies against Histone H4 (di methyl K20, tri methyl K20) were used to label pericentromeric heterochromatin (PCH). **(C)** Antibodies against Topoisomerase IIα (TOPOII) were used to label the PCH and chromosome axes. **(D)** Optimal metaphase II chromatin spread preparation. Metaphase II chromosomes were stained with DAPI (blue, DNA), and immunolabeled for CEN (green), and Histone H4 (di-methyl K20, tri-methyl K20) to label the PCH. Scale bar: 10μm. **(E, F)** Poor metaphase I chromatin spread preparations. Chromosomes were stained with DAPI (blue, DNA), and immunolabeled for CEN (green) and the meiotic cohesin component, REC8. Scale bars: 10 μm **(E)** An oocyte that did not burst upon release onto PFA-coated slide. **(F)** Chromosomes that were spread too far apart.

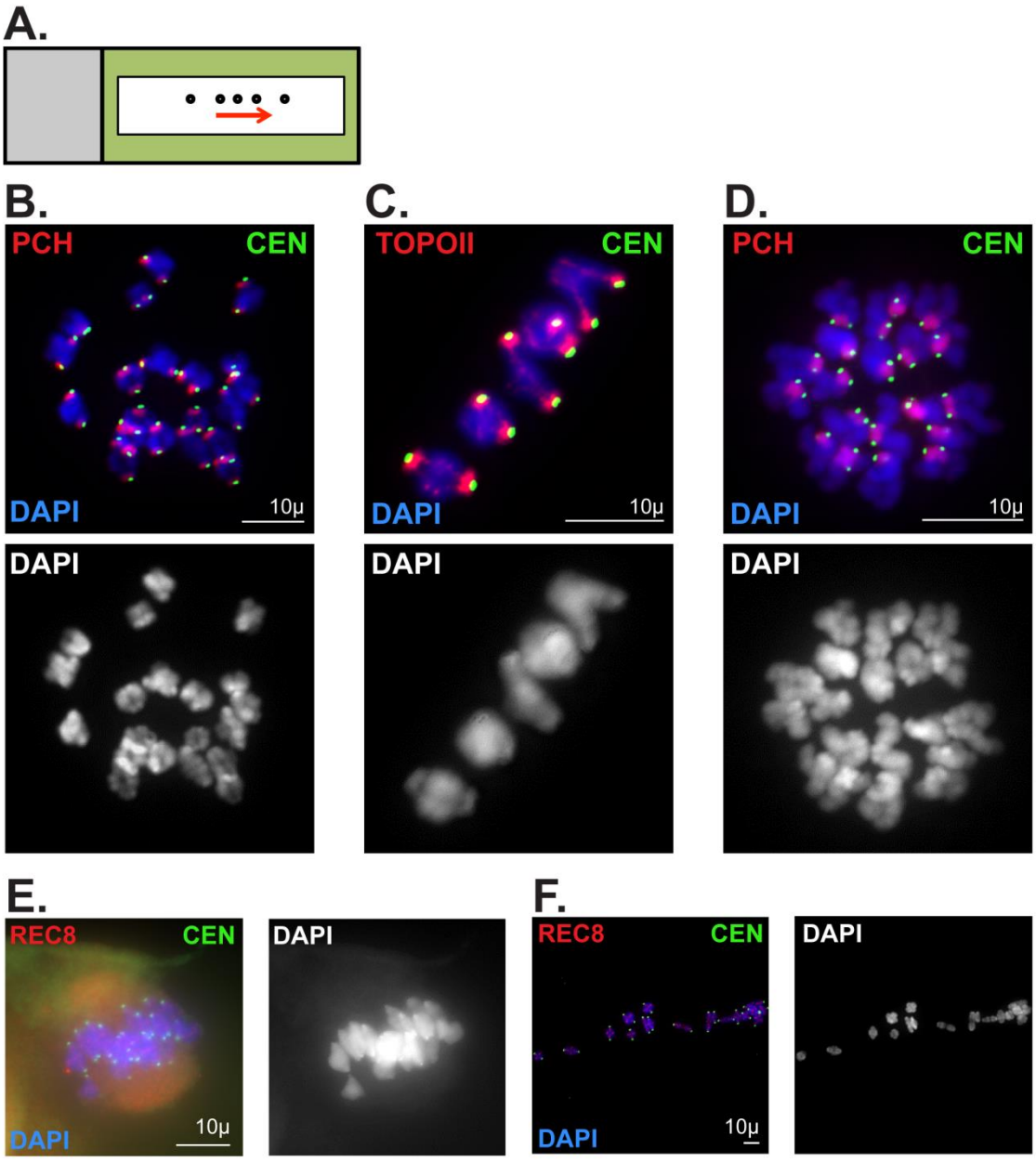
A.
B.
PCH
CEN
DAPI
10μ
DAPI
C.
TOPOII
CEN
DAPI
10μ
DAPI
D.
PCH
CEN
DAPI
10μ
DAPI
E.
REC8
CEN
DAPI
10μ
DAPI
F.
REC8
CEN
DAPI
10μ
DAPI

5.5. Allow the slides to air-dry completely and rinse slides in a Coplin jar containing 50 ml of 0.4% Photoflo-H_2O, pH 8.0.

5.6. Proceed to step 6.

6. Immunolabelling

6.1. Prepare the antibody dilution buffer (ADB) (1x PBS, 3% BSA, 10% Horse Serum, 10% detergent in PBS). Note: Store ADB at 4 °C or freeze stocks at -20 °C if making larger quantities. ADB can become contaminated, so make sure good aseptic techniques are used and assess the solution for contamination prior to each use. Smaller aliquots of ADB can also be prepared to minimize contamination.

6.2. Prepare two Coplin jars containing 50 mL of wash buffer (WB) solution (10% ADB diluted in PBS), and one Coplin jar containing 50 mL WB + 0.05% Triton X-100 solution (e.g. add 250 μL of 10% Triton X-100 to 50 mL WB).

6.3. Wash the slides that were prepared in section 1 and 5 of this protocol for 10 min in one Coplin jar containing 50 mL of WB. **Caution:** Do not let the slides dry at any point during immunolabelling.

6.4. Wash the slides for 10 min in the Coplin jar containing 50 mL WB + 0.05% Triton X-100 solution.

6.5. Wash the slides in the remaining Coplin jar containing 50 mL of WB solution for 10 min.

6.6. Tap off excess liquid and cover slide with 100 μL of selected primary antibodies diluted in ADB. Incubate at 4°C overnight in a closed humid chamber. **Note**: Incubation can be shortened to 2 to 3 hrs at 37°C. Use smaller volumes of antibody

(*e.g.* 50 µL) by covering the slide with a coverslip or parafilm.

6.7. Rinse slides in a Coplin jar containing 50 ml of 0.2% Photoflo-PBS solution, pH 8.0.

6.8. Repeat steps 6.2 to 6.5.

6.9. Tap off excess liquid and cover slide with 100 µL of selected secondary antibodies diluted in ADB. Incubate slides 1 to 2 hrs at 37°C in a closed humid chamber.

6.10. Wash slides 2 times for 10 minutes in Coplin jars containing 50 ml of 0.2% Photoflo-PBS solution, pH 8.0.

6.11. Wash slides 2 times for 5 minutes in Coplin jars containing 50 ml of 0.2% Photofo-H_2O solution, pH 8.0.

7. Mounting slides

7.1. For prophase chromatin spreads prepared in step 2, add 100 µL of mounting medium containing 4', 6-diamidino-2-phenylindole (DAPI, 1.5µg/ml). For MI and MII chromatin spreads prepared in step 5, add 50 µL of mounting medium containing DAPI (1.5µg/ml). Gently blot away excess liquid.

7.2. Place a 22 mm x 60 mm coverslip on top and seal with clear nail polish. Store in a slide box at 4°C or -20°C until assessment via fluorescence microscopy. **Note**: Tap lightly on cover slip to rid of excess mounting medium before sealing with nail polish.

Representative Results

We have described two techniques for visualizing and assessing meiotic chromosomes in oocytes. The first technique is catered toward assessing prophase progression in embryonic and neonatal ovaries. Prophase chromatin spread preparations are incredibly valuable for visualizing numerous dynamic processes during meiosis, including chromosome pairing, synapsis and desynapsis, homologous recombination, and epigenetic chromosome remodeling. Here, we have demonstrated the utility of this method for robust visualization and quantitative analysis of crossover formation in oocytes harvested from C57BL/6J embryos **(Fig. 2.3B and C)**. To enrich for cells in the pachytene substage, mouse embryos were retrieved at 18.5 dpc (**Fig. 2.1**). Two major hallmarks of the pachytene substage of prophase I are the completion of synapsis between homologs, and the formation of at least one MLH1/3-positive crossover per homolog pair. Complete synapsis between homologs is manifested by the presence of 20 overlapping SYCP3 and SYCP1 stretches. To characterize crossover formation in wild-type oocytes we immunolabeled prophase chromatin spread preparations using antibodies that detect SYCP3, SYCP1 and MLH1, and stained DNA using DAPI. **Fig. 3B** depicts a representative image of a pachytene stage oocyte, which is evidenced by the presence of 27 MLH1 foci distributed along 20 fully assembled SC structures. The average number of MLH1-positive crossovers detected in wild-type oocytes was 24±3 (**Fig. 2.3C**, N=15 oocytes). **Fig. 2.3D** shows SMC6 enriched at the pericentromeric heterochromatin (PCH) region and along the chromosome arms, and MLH1 foci distributed along the SC at the pachytene stage. **Fig. 2.3E** depicts a pachytene staged oocyte where the chromosome spread preparation was sub-optimal and individual chromosomes are indistinguishable,

preventing accurate assessment of SYCP3, SMC6 and MLH1. Sub-optimal chromosome spreads can be observed when incubation of ovaries in hypo-extraction buffer is for too long or not for long enough.

The second technique described can be used to assess chromatin morphology in oocytes following meiotic resumption (**Fig. 2.6B-D**). Protein localization, as well as ploidy can easily be assessed, exposing potential causes of chromosome segregation errors. **Fig. 2.6B** depicts a MI oocyte showing 20 chromosomes and clear centromere and pericentromeric heterochromatin staining. **Fig. 2.6C** is a zoomed image where topoisomerase IIα (TOPOII) can be seen along the chromosome arms and the PCH. **Fig. 2.6D** depicts a MII oocyte where paired sister chromatids can be distinguished by chromosome and centromere morphology. Common errors seen when attempting this technique include oocytes not bursting when released onto the PFA-coated slide, as well as chromosomes spreading too far apart (**Fig. 2.6E and F**). If the ZP is not removed completely, the chromosomes will remain associated to the spindle as shown in **Fig. 2.6E**. If the oocytes were dropped too high from the PFA-coated slide, the chromosomes can be spread too far apart as depicted in **Fig. 2.6F**.

Discussion

Chromatin spread preparations allow researchers to chronologically study female mammalian meiosis and the dynamic localization of proteins involved. The embryonic and neonatal chromatin spreads allow for close analysis of events throughout meiotic prophase. Metaphase I and metaphase II chromatin spreads can be used to distinguish single sister chromatids from paired sisters and paired homologous chromosomes, as well

as assess ploidy. By comparison, the protocol described here can be advantageous compared to whole oocyte immunolabelling, which frequently produces high levels of background signal that decreases the resolution of chromatin-bound proteins. Furthermore, chromatin spread techniques represent an attractive alternative to live-cell imaging, which requires a large investment of time and specialized equipment.

Embryonic and neonatal ovaries can be difficult to locate and extract. We recommend carefully extracting all other organs and material besides the kidneys in a separate dish containing PBS before searching for the ovaries, and using a fresh dish of PBS for each embryo/pup **(Fig. 2.2B)**. If the embryo/pup is male, the testis will be distinguishable by the tubule formation as well as the location of the gonads **(Fig. 2.2D)**. As male embryos develop, the testes will descend towards the penis, becoming larger and oval-shaped.

The oocyte chromatin spread technique requires mastery of oocyte collection and manipulation using mouth-operated glass pipette or capillary. We recommend practicing controlling the mouth pipette before performing this protocol. Pulling the proper size glass pipette/capillary for collection and denuding oocytes will increase chances of success and efficiency by minimizing time oocytes are outside of the incubator as well as in the Tyrode's solution. Correct timing for ZP removal is extremely important for the success of this method. If the oocytes are incubated in Tyrode's solution for an insufficient amount of time, the ZP will not be completely removed. This prevents the oocytes from bursting efficiently on the slide, as can be seen in **Fig. 2.6E**. However, if the oocytes are incubated in Tyrode's solution for too long, oocyte quality and downstream immunofluorescence staining will be severely compromised. We

recommend watching the oocytes under a microscope to determine the exact time the ZP dissolves in Tyrode's solution. Adding only 5-10 oocytes at a time to Tyrode's solution will minimize excessive exposure. If the oocytes are released too high above the PFA-coated slide, the chromosomes can be spread too far apart (**Fig. 2.6F**). Optimal results are found when oocytes are released 1 cm above the slide. Other factors that can hinder results include prolonged exposure to decreased CO_2 levels in ambient air during oocyte manipulation steps. This causes pH fluctuations in the media that are detrimental to oocyte quality, and is apparent by progressive color change of the media from orange-red to pink. The buffering capacity of the media also decreases over time; therefore, we do not recommend using media that has been stored (4°C) for longer than 1 week. M2 medium, which does not require CO_2 to be buffered, is commonly used as an alternative.

A limitation to chromatin spread preparations is the lack of visualization of the chromatin within the native context of the cell. Cellular material outside of the nucleus cannot be visualized and spindle formation cannot be assessed. Therefore, other methods can be used to assess oogenesis in addition to chromatin spreads, such as whole oocyte immunolabelling after monastrol treatment, which collapses the bi-polar spindle into a mono-polar spindle(Stein and Schindler, 2011a). This allows sister chromatids to be assessed within the context of the cell. Collectively, the chromatin spread methods described here can easily be applied to assess chromatin morphology and chromosome ploidy throughout oogenesis in novel transgenic and mutant mouse models.

Materials

All materials, including antibodies, needed are shown in **Table 2.1, Table 2.2**. and **Table 2.3**. Microscopes used were SteREO Discovery.V8 (Zeiss 495015-0001-000) and Observer Z1 (Zeiss).

Acknowledgements

This work was supported by NIGMS (R01GM11755) to P.W.J and by a training grant fellowship from the National Cancer Institute (NIH) (CA009110) to G.H. and J.H.

Table 2.1. Materials used for oocyte chromatin spread preparations

Name of Material/ Equipment	Company	Catalog Number	Comments/Description
10X Phosphate buffered saline (PBS) pH 7.4	Quality Biological	119-069-161	
60 mm x 15 mm petri dishes	Denville	T1106	
35mm x 12mm petri dishes	Denville	T1103	
Fine forceps	VWR	300-050	
Micro dissection scissors	Ted Pella	1340	
Dissecting scissors, sharp tip, 41/2"	VWR	82027-578	
	Carolina Biological Supply		
Watch glass square 1 5/8	Company	742300	Autoclave before each use
Sucrose	Sigma	S8501	
Trisodium Citrate Dihydrate	Sigma	S1804	
EDTA	Sigma	E6758	
Trizma Base	Sigma	T1503	
1,4-Dithiothreitol (DTT)	Sigma	646563	Add to hypotonic buffer immediately before use
50x Protease Inhibitor	Roche	11873580001	Add to hypotonic buffer immediately before use
Turberculin syringe with needle (1cc, 27 G x 1/2 in)	Becton, Dickinson (BD)	309623	
Gold seal ultra frost glass slides (25X75mm, 1mm thick)	Thermo	3063-002	
Super PAP pen, large (liquid blocker)	Electron Microscopy Sciences (EMS)	71310	
16% Paraformaldehyde aqueous	Electron Microscopy Sciences (EMS)	15710	
TritonX-100	Sigma	T8787	
Immuno stain moisture chamber	Evergreen	240-9020-Z10	
Coplin jars	Fisher	08-815	
Photo-flo 200	Electron Microscopy Sciences (EMS)	74257	
Pregnant mare serum gonadotropin (PMSG)	Sigma	G4877	Store aliquots at -20C
Human chorionic gonadotropin (HCG)	Sigma	C0434	Store aliquots at -20C
PYREX™ Spot Plates with nine concave cavities	Fisher	13-748B	Autoclave before each use
α-MEM	Invitrogen	11415049	
Waymouth's media	Life Technologies	11220035	
Fetal bovine serum	Fisher	A3160602	
Bovine serum albumin (BSA)	Sigma	A3311	For oocyte culture media
500ml filter units 0.22um	Denville	F5227	
Hyaluronidase	Sigma	H3506	
Tyrode's solution	Sigma	T1788	Store aliquots at -20C
Horse serum	Sigma	H-1270	For ADB/wash buffer
Bovine serum albumin (BSA)	Sigma	A1470	For ADB/wash buffer
VECTASHIELD antifade mounting medium with DAPI	Vector Labs	H-1200	
Microscope cover slides (22mmx60mm)	Fisher	12-544-G	
Clear nail polish	Amazon	N/A	

Table 2.2. Materials for making mouth operated glass pipette or capillary

Name of Material/ Equipment	Company	Catalog Number
Glass capillary	Fisher	22260943
Brand Parafilm M	Sigma	BR701501
Latex rubber tubing (3.2 mm inner diameter x 6.4 mm outer diameter)	Fisher	14-178-5B
Latex rubber tubing (6.4 mm inner diameter x 11.1 mm outer diameter)	Fisher	14-178-5D
Flexible silicone rubber nosepiece, hard plastic mouthpiece and 15 inches of latex tubing	Sigma	A5177-5EA
Mitutoyo micrometer head	Mituoyo	150-208
Syringe 5 mL	BD Biosciences	309646
Syringe filter 0.45 μm filter	Corning	431220
Glass Pasteur Pipette 5 3/4"	Fisher	13-678-6A
83 x 0.5 mm pipette tip	Denville	P3080

Table 2.3. Antibodies

Antibody	Company	Catalog Number	Dilution Factor
Primary Antibodies			
Mouse anti-MLH1	Life Technologies	MA5-15431	1:100
Rabbit anti-SYCP1	Life Technologies	PA1-16763	1:1000
Goat anti-SCP3	Santa Cruz	sc-20845	1:50
Human anti-centromere protein	Antibodies Incorporated	15-235	1:100
Rabbit anti- TOPOII	Abcam	ab109524	1:100
Mouse anti-Histone H4 (di methyl K20, tri methyl K20)	Abcam	ab78517	1:500
Rabbit anti-Rec8	Courtesy of Dr. Karen Schindler	N/A	1:10,000
Secondary Antibodies			
Donkey anti-goat IgG (H+L) Alexa Fluor 568 conjugate	Thermo-Fisher Scientific	A-11057	1:500
Donkey anti-mouse IgG (H+L) Alexa Fluor 488 conjugate	Thermo-Fisher Scientific	A-21202	1:500
Donkey anti-rabbit IgG (H+L) Alexa Fluor 647 conjugate	Thermo-Fisher Scientific	A-31573	1:500
Goat anti-mouse IgG (H+L) Alexa Fluor 568 conjugate	Thermo-Fisher Scientific	A-11004	1:500
Goat anti-Human IgG (H+L) Cross-Adsorbed Secondary Antibody, Alexa Fluor 488	Thermo-Fisher Scientific	A-11013	1:500
Goat anti-rabbit IgG (H+L) Alexa Fluor 568 conjugate	Thermo-Fisher Scientific	A-11011	1:500

CHAPTER III

SMC5/6 IS REQUIRED FOR THE FORMATION OF SEGREGATION-COMPETENT BIVALENT CHROMOSOMES DURING MEIOSIS I IN MOUSE OOCYTES

This chapter appeared in Development [Hwang, GH, Fengyun, S, O'Brien, M, Eppig, J, Handel MA, and Jordan, PW. (2017) Development. 144 (9), 1648-1660, doi:10.1242/dev.145607] and is reproduced here with minor edits.

Introduction

Meiosis is a specialized cell division required for the formation of haploid gametes. Following pre-meiotic DNA replication, homologous chromosomes pair and recombine. DNA recombination occurs within the context of a proteinaceous scaffold known as the synaptonemal complex (SC), which ensures close juxtaposition of homologs (Handel and Schimenti, 2010). After desynapsis, homologous chromosomes remain linked via chiasmata, which are a visible manifestation of crossover recombination. Chiasmata are biologically essential as they ensure that homologous chromosomes bi-orient and thus segregate from each other during the first meiotic division (meiosis I). Subsequently, sister chromatids segregate during meiosis II, resulting in the formation of haploid gametes.

Regulation of meiosis is sexually dimorphic in mammals. Research using the mouse as a model has helped to delineate the dimorphic features that are also observed in humans. In most male mammals, meiosis is initiated postnatally, with continual production of spermatocytes undergoing meiosis throughout life. In female mice, meiosis is initiated during fetal development but arrests in a prolonged diplotene, or dictyate, stage of prophase I. Cohorts of dictyate stage oocytes begin growth shortly after birth and meiosis does not resume in vivo until after the preovulatory surge of luteinizing hormone

(LH) in post-pubescent mice. However, fully-grown oocytes undergo spontaneous, LH-independent, resumption of meiosis after isolation and culture under supportive conditions (Pincus and Enzmann, 1935b). Meiosis, whether occurring in vivo or in vitro, becomes arrested again after progression to metaphase II and is completed only after fertilization or parthenogenic activation.

Cohorts of oocytes resume meiosis throughout the reproductive life span and therefore can reflect aging effects. As women age, their oocytes become more susceptible to chromosome missegregation, which can lead to infertility and developmental abnormalities (Hassold and Hunt, 2001a). Therefore, it is important to determine molecular pathways that are prone to error in oocytes, especially the proteins required for monitoring and facilitating chromosome segregation (MacLennan et al., 2015).
The structural maintenance of chromosomes (SMC) complexes are important regulators of chromosome dynamics and structure during mitosis and meiosis. Each member of the SMC family, which includes cohesin, condensin, and SMC5/6, is comprised of a V-shaped SMC protein heterodimer. The SMC proteins each have a hinge domain that is flanked by long coiled-coil domains, which allows the proteins to fold back on themselves. The C and N globular heads interact with each other, forming an ATP-binding and ATP hydrolysis site. The ATPase domains are bridged together by non-SMC elements (Nasmyth and Haering, 2005).

Cohesin is a SMC1/3 heterodimer that is linked by an α-kleisin and a stromal antigen protein. During mitosis, cohesin is required to maintain sister chromatid cohesion before the metaphase-to-anaphase transition (Remeseiro and Losada, 2013). However, to ensure that sister chromatids segregate together during meiosis I, centromeric cohesin is

maintained until meiosis II (Petronczki et al., 2003a). In addition, cohesin complexes are required for accurate recombination and synapsis between homologous chromosomes (Rankin, 2015b). Meiosis-specific cohesin components, including SMC1β, two α-kleisins (REC8 and RAD21L) and a stromal antigen protein (STAG3), are important for these additional requirements of cohesins during meiosis (Hopkins et al., 2014a, Fukuda et al., 2014, Winters et al., 2014, Llano et al., 2014, Xu et al., 2005, Revenkova et al., 2004, Herran et al., 2011, Bannister et al., 2004). Mutation of meiosis-specific cohesin components in female mice results in an increased frequency of oocyte aneuploidy and premature ovarian failure (Hodges et al., 2005, Murdoch et al., 2013, Herran et al., 2011).

The two condensin complexes (I and II) are composed of the SMC2 and SMC4 heterodimers, but their kleisin subunit, and pair of HEAT repeat elements are unique (Hirano, 2015). Condensins localize to the longitudinal axes of bivalents following meiotic resumption in mouse oocytes, and both complexes are required for chromosome compaction before meiosis I (Houlard et al., 2015b, Lee et al., 2011). However, only condensin II is essential for disentanglement of chromosomes prior to their segregation.

SMC5/6 heterodimers are linked by NSMCE4, a kleisin subunit (Verver et al., 2015). Two additional subunits, NSMCE1 and NSMCE3, interact with one another and with NSMCE4 (Pebernard et al., 2008b, Palecek et al., 2006a). NSMCE1 contains a RING-finger domain, common to E3 ubiquitin ligases, and NSMCE3 contains a MAGE (meleanoma-associated antigen gene) domain. NSMCE3 enhances the E3 ubiquitin ligase activity of NSMCE1 (Doyle et al., 2010b). NSMCE2, which contains an SP-RING domain, binds to the coiled-coil region of SMC5 and can function as an E3 SUMO ligase (Andrews et al., 2005b, Zhao and Blobel, 2005b, Potts and Yu, 2007a).

Studies assessing the SMC5/6 complex in mammalian germ cells have been limited to analyses of its localization pattern during mammalian spermatogenesis (Verver et al., 2014b, Gómez et al., 2013, Verver et al., 2013a). Because the regulation of meiosis is sexually dimorphic, there may be temporal and functional differences in the roles of SMC5/6 in females versus males. This study demonstrates that the SMC5/6 complex is enriched at the pericentromeric regions and is also detected along chromosome arms during female meiosis. To determine the function of the SMC5/6 complex following meiotic resumption in mouse oocytes, an oocyte-specific conditional knockout (cKO) mouse was created, deleting a floxed *Smc5* allele using the *Zp3-Cre* transgene, which is expressed in growing oocytes before meiotic resumption (Lan et al., 2004, Lewandoski et al., 1997). Analysis of the female *Smc5* cKO mutants led to two major findings: 1) Maternal expression of SMC5 before meiotic resumption is essential for embryogenesis; and 2) absence of SMC5/6 during meiotic resumption results in oocyte aneuploidy due to an inability to resolve chromosomes during meiosis I. Furthermore, protein levels of SMC5/6 components in oocytes decline as wild-type females age, implicating the SMC5/6 complex as a potential contributor to oocyte aneuploidy and infertility in aging females.

Results

SMC5/6 is enriched at oocyte pericentromeric heterochromatin during meiosis

Chromatin spreads were prepared to assess the localization of the SMC5/6 complex during female meiosis via immunofluorescence microscopy with antibodies raised against SMC5, SMC6 and NSMCE1 (**Fig. 3.1**; **Fig. S3.1**). Meiotic prophase sub-stages were determined by assessing chromosome axis morphology (synaptonemal

complex protein, SYCP3) and centromere pairing (anti-centromere autoantibody, CEN; also known as ACA and CREST). During leptonema SMC6 localized throughout the spread chromatin (**Fig. 3.1A**). By early zygonema, SMC6 was enriched at pericentromeric heterochromatin. At pachynema, SMC6 remained enriched at pericentromeric heterochromatin, and was also evident at lower intensity along the arms of chromosomes. These localization patterns were partially resistant to DNase treatment (**Fig. S3.2**). Additionally, SMC6 was observed as foci along chromosome axes and chromosome ends (**Fig. 3.1B**). SMC6 foci were not always evident on pachytene stage chromatin spreads, and did not overlap with MLH1 foci (**Fig. S3.3**), suggesting that they may be transient and stage-specific. At early diplonema, SMC6 remained enriched at the pericentromeric heterochromatin, however this enrichment was decreased by late diplonema. Analysis of SMC5, NSMCE1 and an additional antibody raised against SMC6 resulted in similar localization patterns (**Fig. S3.1**). Differences in localization patterns are likely due to epitope accessibility, as is the case with mouse prophase spermatocytes (Gómez et al., 2013), SMC6 localization to the pericentromeric heterochromatin in oocytes overlaps with that observed for TOP2A (**Fig. 3.1C**).

Following meiotic resumption, SMC6 was enriched at the pericentromeric heterochromatin during meiosis I and remained present at metaphase II (MII), when oocytes arrest (**Fig. 3.1D**). Chromosome spread preparations of metaphase I (MI) oocytes demonstrated that there was also some SMC6 protein along chromosome arms (**Fig. 3.1E**).

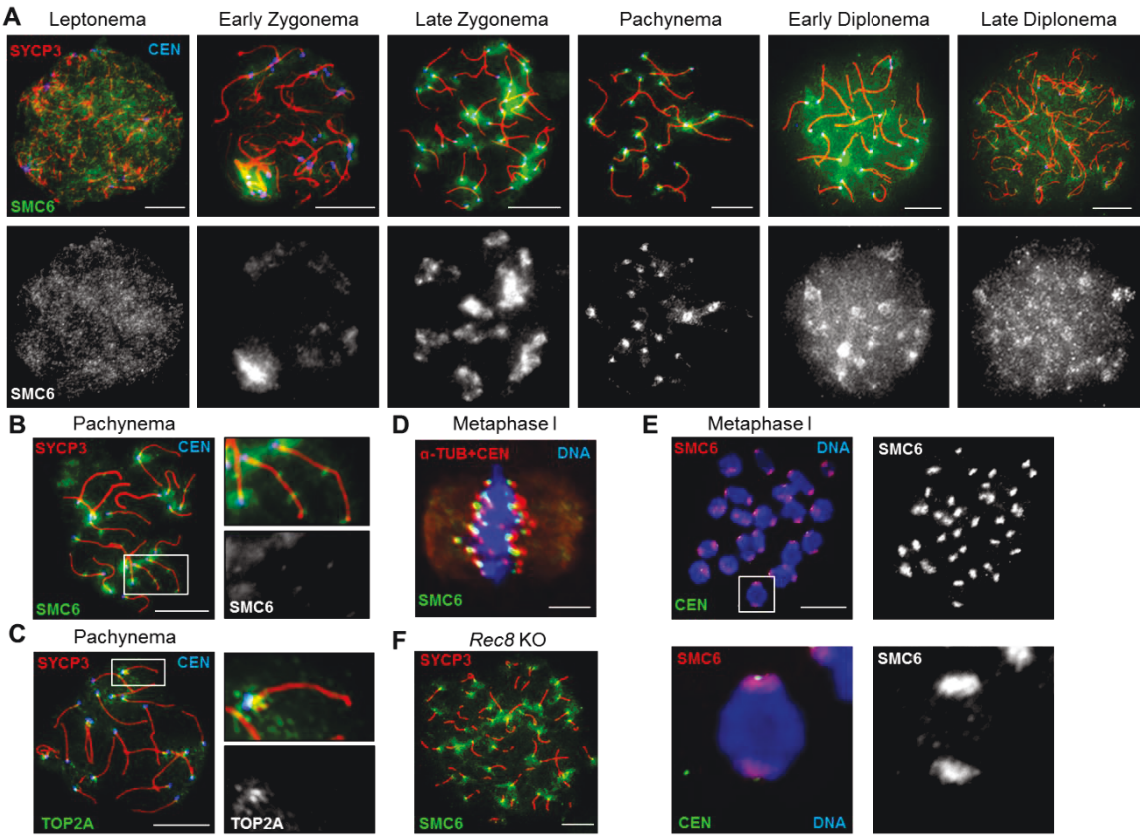

Figure 3.1. SMC5/6 localization during female meiosis. (**A-C**) Chromatin spread preparations of wild-type ovarian germ cells at different stages of meiotic prophase I. (**A-B**) Immunolabeled with antibodies against CEN (blue, kinetochore/centromere marker), the SC lateral element protein SYCP3 (red), and SMC6 (green, ab18039). (**B**) SMC6 localization on the pericentromeric heterochromatin, along chromosome arms and foci on chromosome axes during pachynema. (**C**) TOP2A (green) localization at pachynema. (**D**) Wild-type metaphase I whole oocyte preparation, DAPI (DNA, blue), SMC6 (green, ab18039), α-tubulin (red) and CEN (red). (**E**) Wild-type metaphase I chromatin spread, DAPI (blue), SMC6 (red, ab18039) and CEN (green). (F) Chromatin spread of an embryonic ovarian germ cell from a *Rec8* mutant, SYCP3 (red) and SMC6 (green, ab18039). Boxed regions are magnified 3x. Complementary data using additional SMC5/6 antibodies in Figure S1. Scale bar: 10μm

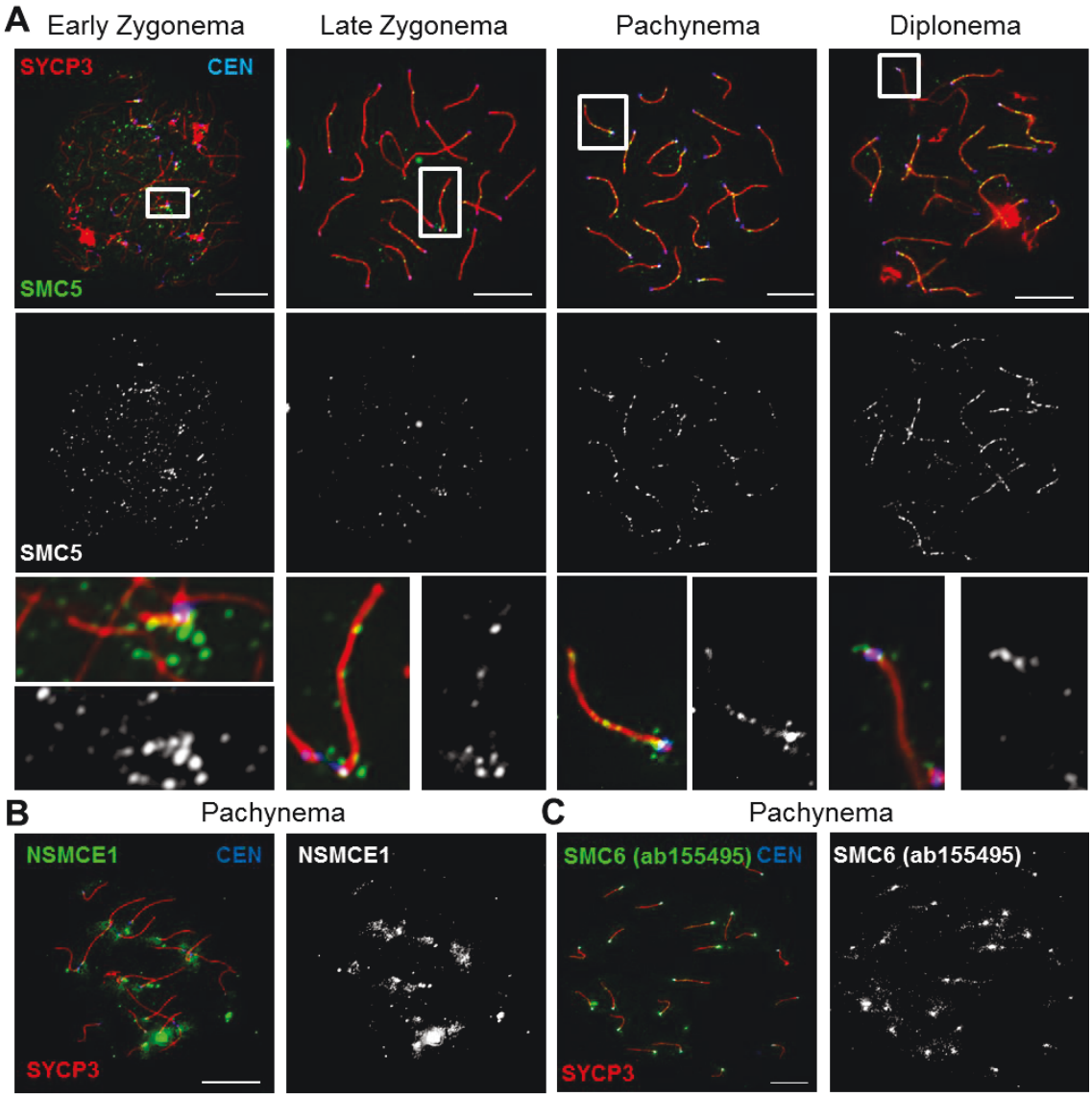

Supplemental Figure 3.1. SMC5/6 is enriched on pericentromeric heterochromatin during meiosis I. (**A-C**) Chromatin spread preparations of embryonic ovarian germ cells of 15.5 and 17.5 days post-coitum and 0.5 days post-partum from wild-type mice at different stages of meiotic prophase I. Chromatin spreads were immunolabeled with antibodies against CEN (blue, kinetochore/centromere marker), the SC lateral element protein SYCP3 (red), and an SMC5/6 (green) component. (**A**) Localization of SMC5 during zygotene, pachytene and diplotene stages of meiosis. The lower panels display SMC5 immunostaining as a greyscale image. The boxed regions are magnified 3× below the whole chromatin spread image to demonstrate the enrichment at the pericentromeric heterochromatin and along chromosome arms. (**B**) A pachytene stage oocyte spread showing NSMCE1 localization on the pericentromeric heterochromatin. (**C**) A pachytene stage oocyte spread showing SMC6 localization on the pericentromeric heterochromatin and along chromosome arms using an additional antibody raised against SMC6 (ab155495). Scale bar: 10μm

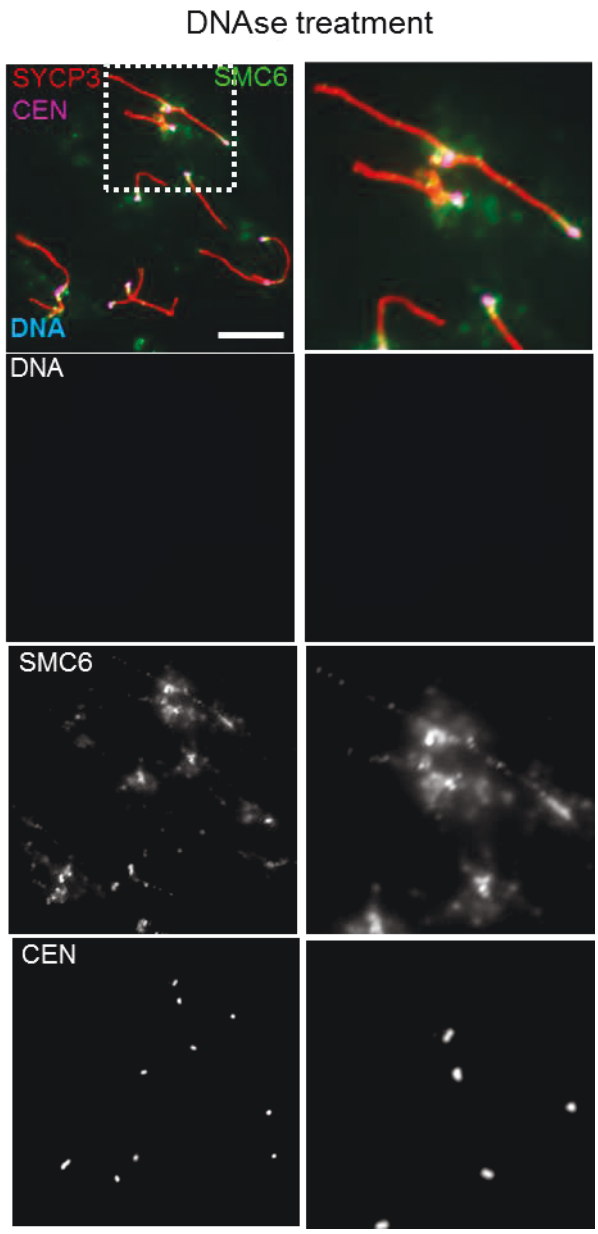

Supplemental Figure 3.2. SMC5/6 association to chromosome axes is resistant to DNase I treatment. Representative chromatin spread preparation of embryonic ovarian germ cells of 18.5 days post-coitum. Chromatin spreads were treated with DNase I and immunolabeled with antibodies against CEN (purple, kinetochore/centromere marker), the SC lateral element protein SYCP3 (red), and SMC6 (ab18039, green). Negative DAPI staining for DNA confirms successful DNase I treatment. Scale bar: 10µm

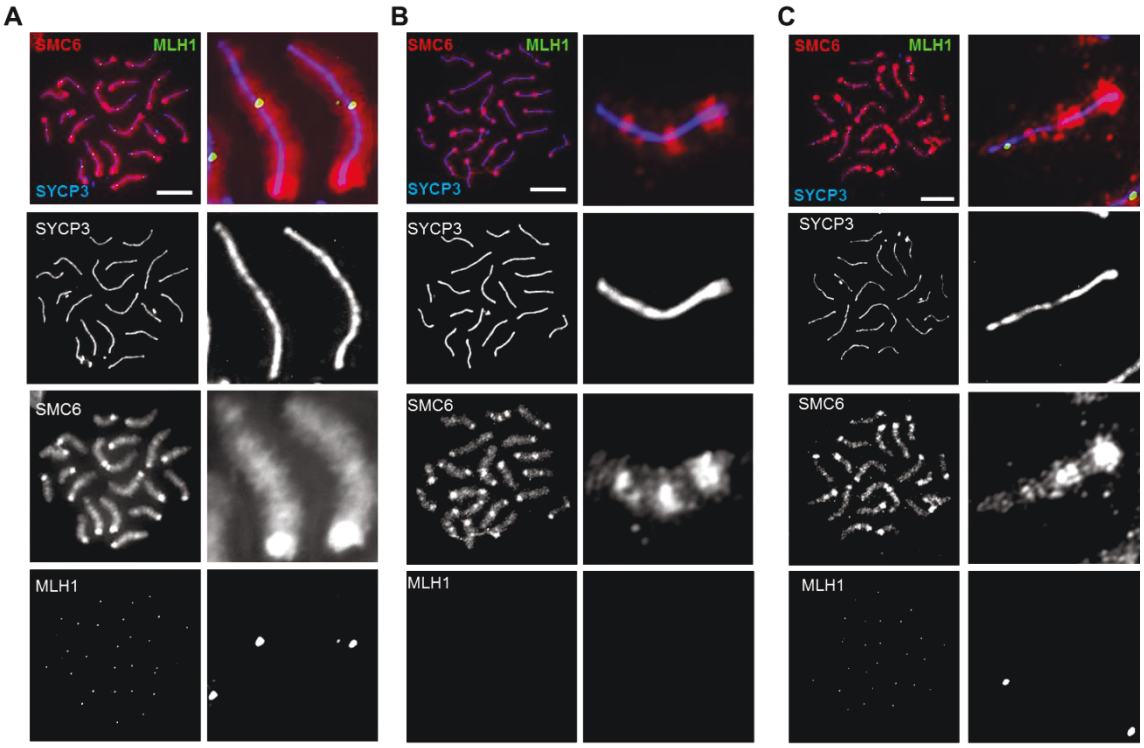

D

Embryos	Total Pachytene Spreads	% with SMC6 foci on the arms	% with MLH1	% with SMC6 +MLH1
3	56	17.86	64.29	13.89

Supplemental Figure 3.3. SMC6 foci do not colocalize with MLH1 foci. (**A-C**) Chromatin spread preparations of embryonic ovarian germ cells of 18.5 days post-coitum. Assessment of MLH1 (green), SYCP3 (blue) and SMC6 (ab18039, red) localization during pachynema. (**D**) Table summary of MLH1 and SMC6 foci observations. Scale bar: 10µm

Contrasting data have been reported on whether mutation of cohesin component, *REC8*, affects Smc5/6 axis loading during meiosis in budding yeast (Copsey et al., 2013b, Lilienthal et al., 2013b). Localization of SMC6 was assessed using a *Rec8* mouse mutant (Bannister et al., 2004). The enrichment of SMC6 to the pericentromeric heterochromatin and localization to chromosome arms was not affected in *Rec8* mutants (**Fig. 3.1F**), demonstrating that REC8 was not required for SMC6 localization. This finding is supported by observations made using mouse spermatocytes, where mutation of *Smc1β* did not affect SMC5/6 localization (Gómez et al., 2013).

Oocyte-specific conditional mutation of Smc5 results in infertility

Mice that harbored a conditional knockout (cKO) allele of *Smc5* were used to assess the requirement of the SMC5/6 complex for the meiotic divisions and formation of blastocysts (**Fig. 3.2A,B**, see Materials and Methods). Exon 4 of *Smc5* was flanked by loxP Cre recombinase target sequences and this allele was termed *Smc5 flox* (**Fig. 3.2A**). Breeding heterozygous *Smc5 flox* mice to mice expressing the Cre recombinase transgene generated a KO allele termed *Smc5 del*. The heterozygous *Smc5 del* mice exhibited no gross morphological abnormalities during development and adult life. No offspring homozygous for the *Smc5 del* mice allele were produced, indicating that homozygosity for the deletion allele is lethal. Therefore, to determine if *Smc5* is essential for oogenic meiotic divisions, a hemizygous Cre recombinase transgene under the control of the promoter for the zona-pelucida protein 3 gene (*Zp3-Cre tg/0*) was used. This transgene is expressed exclusively in growing dictyate oocytes before resumption of the first meiotic

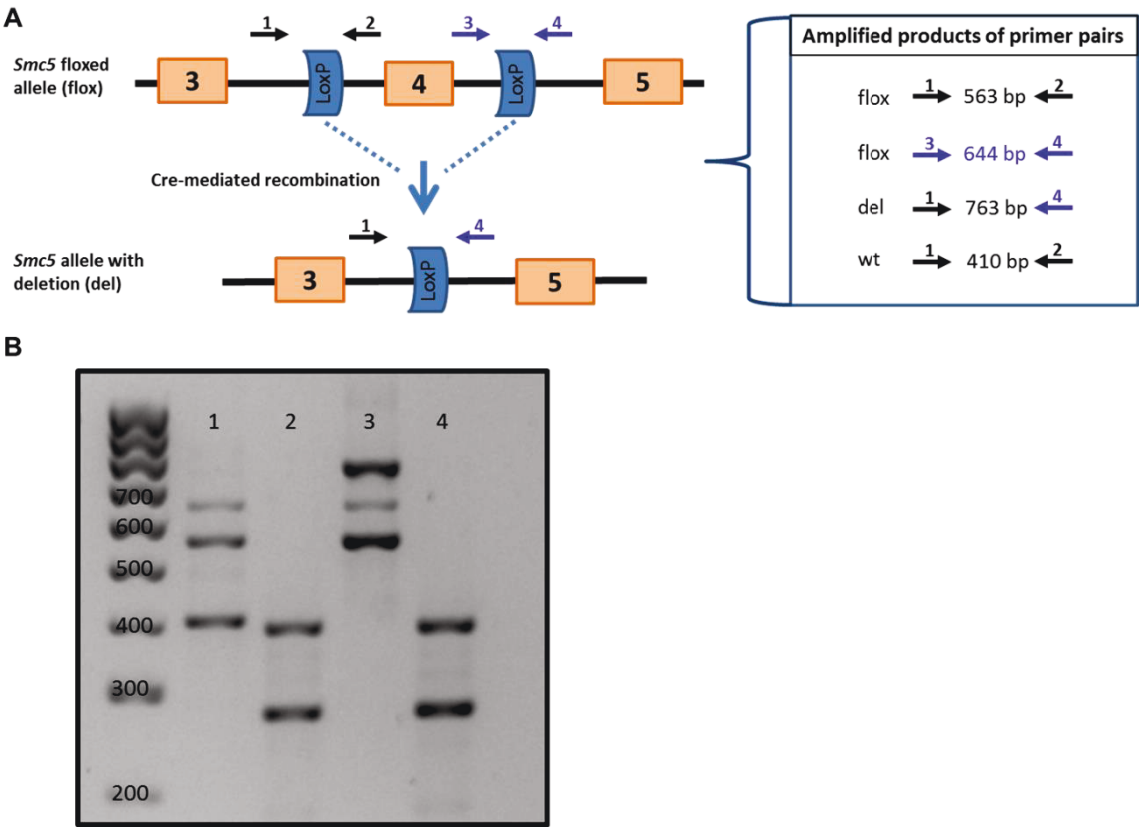

Figure 3.2. Conditional mutation of *Smc5* using the Zp3-Cre recombinase results in female infertility. (**A**) Schematic of mouse *Smc5* floxed allele containing loxP sites, flanking exon 4, and the resulting *Smc5* deleted allele after excision of exon 4 by Cre recombinase. Arrows represent primers for PCR genotyping of mice. (**B**) DNA agarose gel image of PCR products for genotyping. Lane 1 and 2 represent a control genotype (*Smc5 +/flox, Zp3-cre tg/0*). Lane 1 (*Smc5 +/flox*): 410bp wt allele, 563bp and 644bp *flox* allele. Lane 2 (*Zp3-cre tg/0*): 420bp internal control and 281bp *Zp3-Cre* transgene. Lane 3 and 4 represent *Smc5* cKO (*Smc5 flox/del, Zp3-cre tg/0*). Lane 3: (*Smc5 flox/del*): 563 bp and 644 bp *flox* allele, and 763 bp *del* allele. Lane 4 (*Zp3-cre tg/0*): Same as Lane 2.

Table 3.1. Fertility tests and offspring genotyping results for *Smc5* mutant and control mice

	Offspring			
Strain	***Smc5*+/+**	***Smc5+/flox***	***Smc5 +/del***	**Total**
♂ ***Smc5flox/del x*** ♀ ***wild-type (n=10)***	0 (0 pups)	51% (90 pups)	49% (87 pups)	177 pups (7.4/litter)
♂ ***Smc5flox/del, Zp3-Crex*** **x** ♀ ***wild-type (n=5)***	0 (0 pups)	55% (39 pups)	45% (32 pups)	71 pups (7.1/litter)
♀ ***Smc5 +/flox*** **x** ♂ ***wild-type (n=5)***	48% (31 pups)	52% (33 pups)	0 (0 pups)	64 pups (6.4/litter)
♀ ***Smc5 +/flox, Zp3-Cre*** **x** ♂ ***wild-type (n=5)***	47% (32 pups)	0 (0 pups)	53% (36 pups)	68 pups (6.8/litter)
♀ ***Smc5flox/del*** **x** ♂ ***wild-type (n=8)***	0 (0 pups)	47% (58 pups)	53% (66 pups)	124 pups (6.9/litter)
♀ ***Smc5flox/del, Zp3-Cre*** **x** ♂ ***wild-type (n=5)***	0 (0 pups)	0 (0 pups)	0 (0 pups)	0 (0 pups)

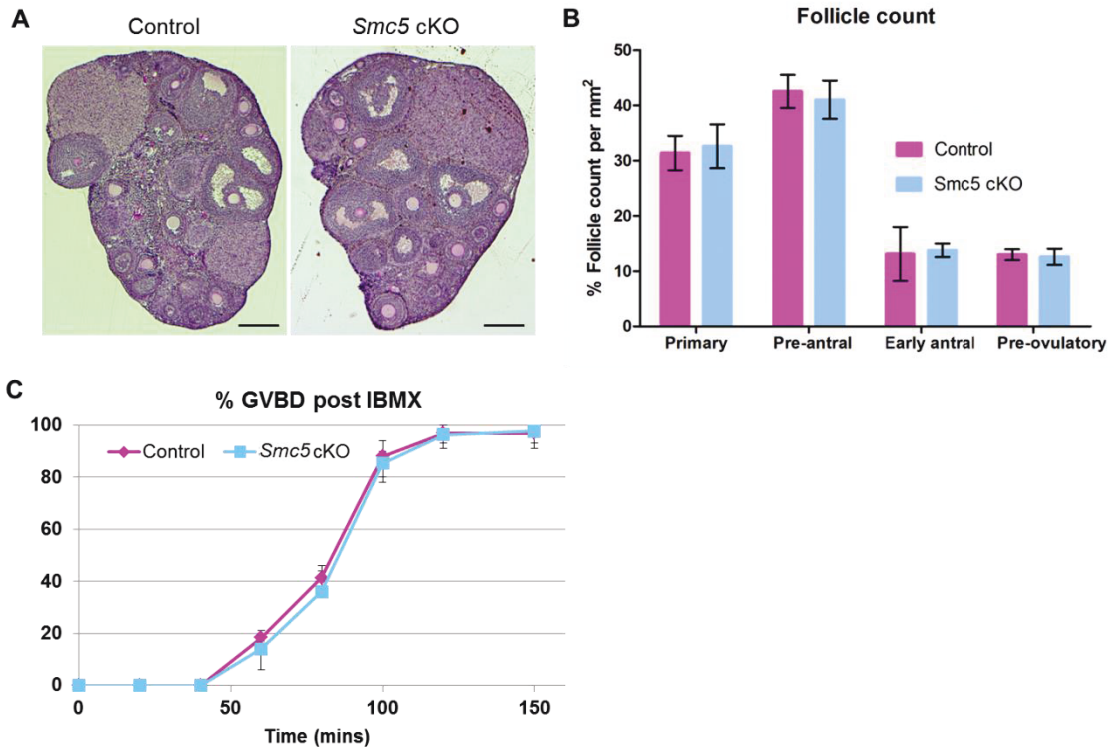

Supplemental Figure 3.4. *Smc5* cKO ovaries do not display any defects in primary or secondary oocyte number and oocytes do not have a delay in GVBD.
(**A**) Periodic acid-Schiff staining of 5 micron cross sections of control and *Smc5* cKO ovaries. Scale bar = 200 microns. (**B**) Proportion of primary, pre-antral, early antral and pre-ovulatory oocyte counts per mm^2 for control and *Smc5* cKO ovaries, 3 mice were used for each genotype, 12 weeks of age. Mean and standard deviation of the columns of each graph are represented by the black bars. No significant difference between the control and *Smc5* cKO was observed according to two-way ANOVA test. (**C**) GVBD kinetics of control and *Smc5* cKO oocytes isolated from mice 12 weeks of age. GV oocytes were harvested and cultured in MEMα/BSA + 5% FBS supplemented with IBMX (3-isobutyl-l-methyl-xanthine) to inhibit germinal vesicle breakdown (GVBD). The oocytes were then washed in MEMα/BSA + 5% FBS to remove the IBMX and assessed every 20 minutes for GVBD. The experiment was performed using three mice for the control and *Smc5* cKO groups. The error bars represent the variation between three independent experiments. The total number of oocytes used for control, N = 86 and *Smc5* cKO, N = 79.

division (Lan et al., 2004, Lewandoski et al., 1997). Breeding *Smc5 +/flox, Zp3-Cre tg/0* (control) females to wild-type males showed that mutation of the *Smc5 flox* allele mediated by Zp3-Cre was 100% efficient (**Table 1**). The *Smc5 flox/del*, *Zp3-Cre tg/0* (*Smc5* cKO) females failed to produce litters (N=5), despite having normal ovarian morphology and equivalent oocyte numbers (**Fig. S3.4A,B**).

Smc5 cKO oocytes are incapable of mature blastocyst formation following IVF

In vitro oocyte maturation (IVM) and fertilization (IVF) was used to determine whether blastocysts could be obtained from *Smc5* cKO oocytes. Fully-grown germinal vesicle (GV) oocytes were isolated from the large antral follicles of *Smc5* cKO (*Smc5 flox/del*, *Zp3-Cre tg/0*) and control (*Smc5 +/flox, Zp3-Cre tg/0*) female ovaries aged between 4 and 12 weeks, and cultured in media that supported meiotic resumption in vitro (IVM). There was no observable delay in GV break down (GVBD), indicative of meiotic resumption (**Fig. S3.4C**), and likewise no reduction in frequency of oocytes that underwent polar body extrusion (PBE) and metaphase II (MII) arrest (**Fig 3.3A,B**). However, following IVF using sperm from a wild-type mouse, fertilized oocytes from *Smc5* cKO females failed to form mature blastocysts, with many embryos arresting at the 4 to 16 cell stages (**Fig 3.3A-C**). Intriguingly, there was a difference in IVF results between oocytes from mice that were 4 weeks of age (considered as the "juvenile" cohort), and mice that were between 12 and 16 weeks of age (considered the "adult" cohort). In the "juvenile" cohort, fertilized oocytes progressed to the 2-cell stage at levels comparable to their littermate controls (**Fig. 3.3A**). In contrast, the cohort of "adult"

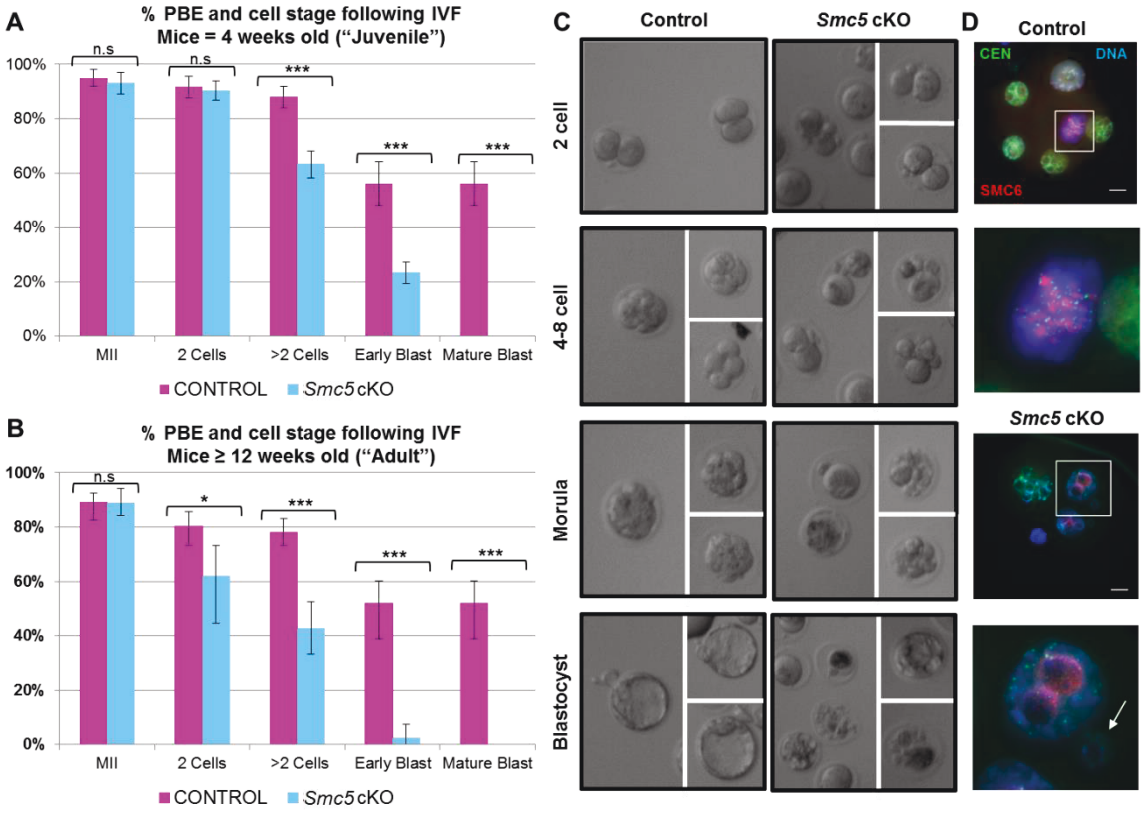

Figure 3.3. *Smc5* cKO oocytes fail to form mature blastocysts. (**A-C**) Assessment of PBE and blastocyst formation following IVF. (A) PBE and IVF data obtained for "juvenile" (4 weeks of age) control (*Smc5 +/flox, Zp3-Cre tg/0*) and *Smc5* cKO (*Smc5 flox/del*, *Zp3-Cre tg/0*). Oocytes used for control, N=123 and *Smc5* cKO, N=150. The P values (one-tailed paired t-test) for the indicated comparisons are P=0.0771 (n.s.), P=0.1085 (n.s.), P=0.0003 (***), P<0.0002 (***) and P<0.0001 (***) for MII, 2 cells, >2 cells, early blastocysts and mature blastocysts, respectively. (**B**). PBE and IVF data obtained for the "adult" (≥ 12 weeks of age) control and *Smc5* cKO. The total number of oocytes used for control, N=105 and *Smc5* cKO, N=134. The error bars represent the variation between three independent experiments. The P values (one-tailed paired t-test) for the indicated comparisons are P=0.4287 (n.s.), P=0.0282 (*), P=0.0004 (***), P<0.0001 (***) and P<0.0001 (***) for MII, 2 cells, >2 cells early blastocysts and mature blastocysts, respectively. (**C and D**) Example images of cell morphology following IVF for control and *Smc5* cKO. (**D**) Embryos stained with DAPI (blue, DNA), SMC6 (red) and CEN (green). Boxed regions are magnified 3x. Arrow points to a nucleus with irregular size. Collectively, IVF was performed six times using a total of 10 mice for each control and *Smc5* cKO cohort. Scale bar: 10µm

fertilized oocytes displayed a significant decrease in 2-cell stage embryos following IVF (**Fig. 3.3B**). In addition, although there was a significant decrease in embryos progressing beyond the 2-cell stage compared to the littermate control, the "juvenile" cohort of embryos collectively progressed further than the "adult" cohort (**Fig. 3.3A,B**). Embryos from the "juvenile" cohort were assessed via light and immunofluorescence microscopy. Cells and nuclei from the control embryos displayed similar shape and size, and the nuclei harbored an SMC6 signal (**Fig. 3.3C,D**; **Fig. S3.5**). In contrast, embryos from the *Smc5* cKO embryos contained low or undetectable levels of SMC6 protein, and nuclei were irregular in size, which is consistent with defects during mitosis and imbalanced chromosome segregation during cell division.

Only the "adult" Smc5 cKO oocytes display aneuploidy at metaphase II

To determine whether the observed failure to form blastocysts was due to defects in chromosome segregation during meiosis, the number and morphology of chromosomes in oocytes arrested at MII were assessed. Due to the age-related differences observed in the IVF studies, MII oocytes from "juvenile" and "adult" mice were assessed separately. MII chromosome spread preparations of the "juvenile" *Smc5* cKO oocytes did not exhibit significant increases of aneuploidy or chromosome abnormalities (**Fig. 3.4A, Table 2**). By contrast, chromosome spread preparations from the "adult" *Smc5* cKO females displayed abnormal chromosome number and morphology, and separated sister chromatids were observed (**Fig. 3.4A, Table 2**). Chromosome number and morphology was also assessed within the confines of the cell by treating the oocytes with monastrol.

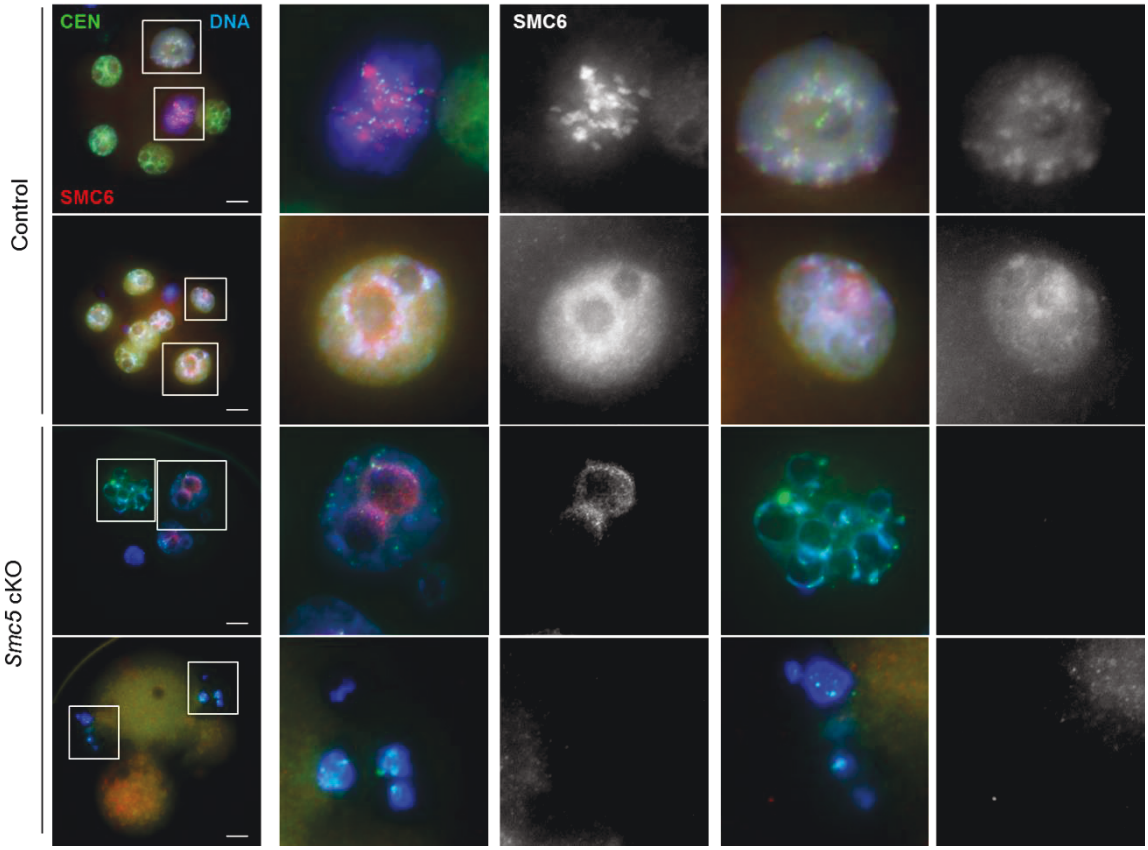

Supplemental Figure 3.5. *Smc5* cKO oocytes fail to form mature blastocysts. Oocytes from control and *Smc5* cKO "juvenile" mice were fertilized with C57BL6/J wild-type sperm and resultant embryos were fixed and stained for DAPI (blue, DNA), SMC6 (red), and CEN (green). The boxed regions are magnified 3x to the right of the whole embryo images. Scale bar: 10µm

Figure 3.4. Metaphase II oocytes from "adult" *Smc5* cKO have aneuploidy and abnormal chromosome morphology. Control (*Smc5 +/flox, Zp3-Cre tg/0*) and *Smc5* cKO (*Smc5 flox/del*, *Zp3-Cre tg/0*) oocytes arrested at MII were assessed for chromosome number, centromere number and chromosome morphology using two separate age groups ("juvenile" = 4 weeks old, and "adult" ≥ 12 weeks old). (**A**) Examples of chromosome spreads of control and *Smc5* cKO MII oocytes. Red arrows point to single chromatids and yellow arrow shows an example of abnormal chromosome morphology. (**B**) MII oocytes treated with monastrol, DAPI (blue, DNA), SMC6 (red), and CEN (green). (**C**) Scatter dot-plot graph of centromere counts from monastrol treated MII oocytes obtained from "juvenile" cohorts of control (average = 39.6, N = 50) and *Smc5* cKO mice (average=39.4, N=50) and "adult" cohorts of control (average = 39.1, N = 50) and *Smc5* cKO mice (average=36.7, N=25). Mean and standard deviation of the columns of each graph are represented by the black bars and P values are given for indicated comparisons (Mann-Whitney, two-tailed). (**D**) Bar graph of percentage of oocytes with abnormal chromosome morphology from "juvenile" cohorts of control (average=4.84%, N=62) and *Smc5* cKO mice (average=17.24%, N=50), and "adult" cohorts of control (average=13.25%, N=83) and *Smc5* cKO mice (average=53.49%, N=86). Mean and standard error measurement of the columns of each graph are represented by the black bars and P values are given for indicated comparisons (chi-square test). Collectively, at least 10 mice for each group were used to obtain the data. Scale bar: 10μm

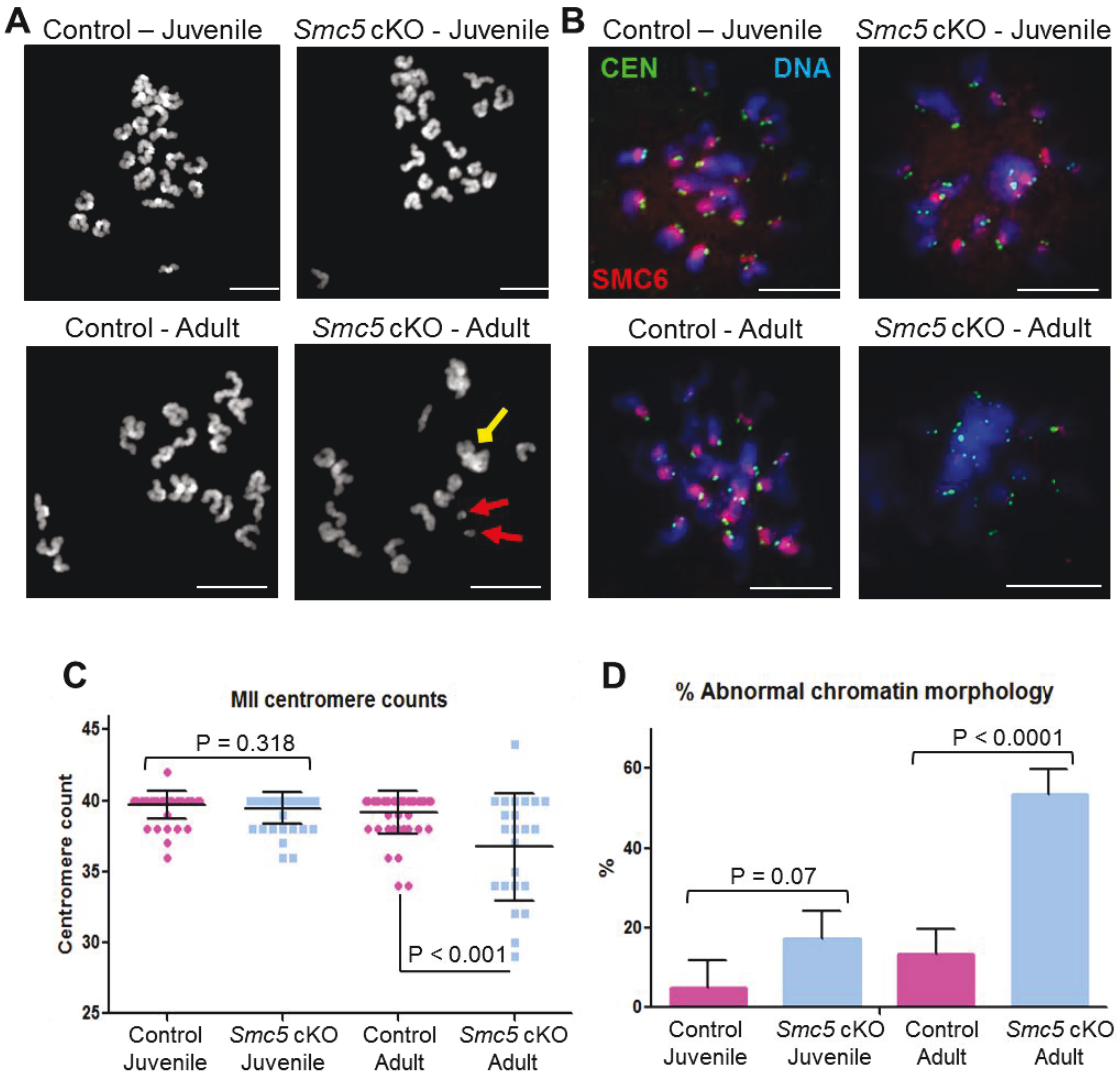
A
Control – Juvenile
Smc5 cKO - Juvenile
Control - Adult
Smc5 cKO - Adult
B
Control – Juvenile
Smc5 cKO - Juvenile
CEN
DNA
SMC6
Control - Adult
Smc5 cKO - Adult
C
MII centromere counts
Centromere count
45
40
35
30
25
P = 0.318
P < 0.001
Control Juvenile
Smc5 cKO Juvenile
Control Adult
Smc5 cKO Adult
D
% Abnormal chromatin morphology
%
60
40
20
0
P = 0.07
P < 0.0001
Control Juvenile
Smc5 cKO Juvenile
Control Adult
Smc5 cKO Adult

Table 3.2. Chromosome count data from chromosome spreads

		MII chromosome counts			
GROUP	**n**	**< 20 (%)**	**20 (%)**	**> 20 (%)**	**Single chromatid**
Control (4 weeks old)	83	15 (18.1)	68 (81.9)	0 (0.0)	0 (0.0)
Smc5 cKO (4 weeks old)	90	17 (18.9)	71 (78.9)	1 (1.1)	1 (1.1)
Control (≥ 12 weeks old)	76	14 (18.4)	62 (82.5)	0 (0.0)	0 (0.0)
Smc5 cKO (≥ 12 weeks old)	80	30 (37.5)	40 (50.0)	6 (7.5)	4 (5.0)

Monastrol binds to and disrupts the function of kinesin protein, KIF11, resulting in monopolar spindles making it easier to distinguish each sister chromatid pair (Stein and Schindler, 2011b). Centromere number was counted using an anti-centromere autoantibody (CEN). In addition, the presence of the SMC5/6 complex was determined using an SMC6 antibody. Complementary to the chromosome spread preparations (**Fig. 3.4A, Table 2**), the monastrol treated MII oocytes from the "juvenile" *Smc5* cKO cohort did not exhibit significant differences compared to the control oocytes with respect to centromere counts or chromatin morphology (**Fig. 3.4B-D**). Furthermore, most (83%) of the oocytes from the "juvenile" *Smc5* cKO harbored SMC6 protein signal. In contrast, the majority (61%) of monastrol treated oocytes from the "adult" *Smc5* cKO cohort lacked SMC6 signal, and presented significant differences with regards to centromere counts compared to littermate controls (**Fig. 3.4B,C**; **Fig. S3.6A**). Additionally, it was not possible to obtain centromere counts from more than 50% of the monastrol treated *Smc5* cKO oocytes from the "adult" mice, because the chromatin was grossly abnormal, demonstrating stretched morphology, and indistinguishable sister chromatid pairs (**Fig. 3.4B-D**; **Fig. S3.6A**). Furthermore, 5% of *Smc5* cKO MII oocytes displayed abnormal morphology indicative of oocyte degeneration (**Fig. S3.6B,C**).

Oocyte SMC5/6 protein levels decrease in aging females

Excision of the floxed 4th exon of *Smc5* driven by the *Zp3-Cre* transgene was shown to be 100% efficient based on mating tests, PCR analysis and the IVF data (**Fig. 3.2B,C**; **Fig. 3.3A**). However, data from monastrol treated MII oocytes demonstrated that

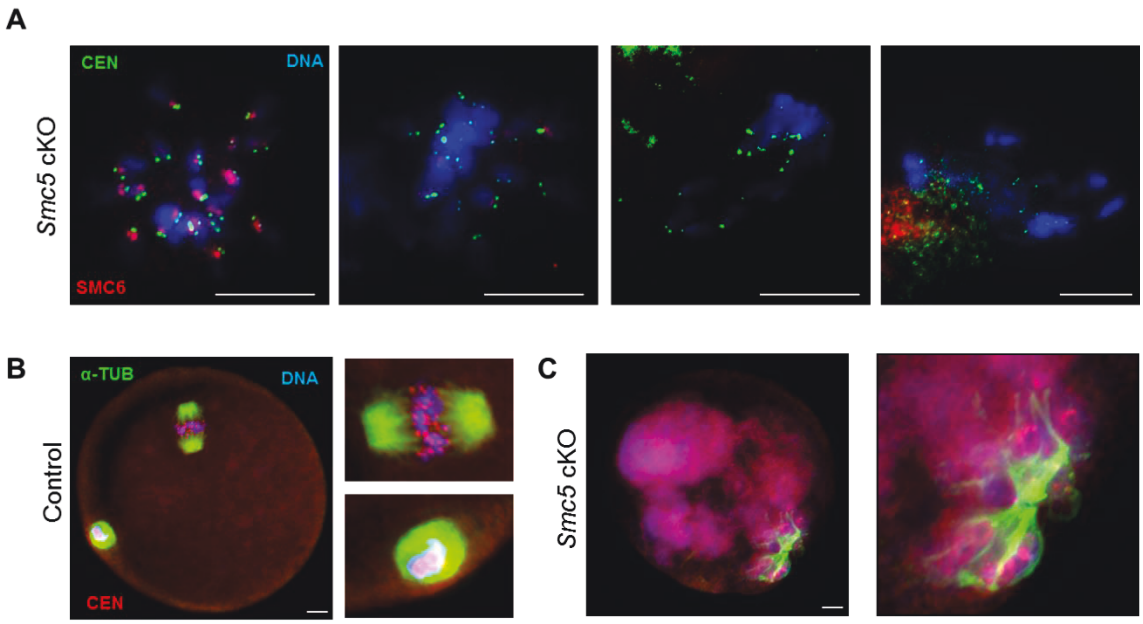

Supplemental Figure 3.6. *Smc5* cKO oocytes at MII. (**A**) MII oocytes from "adult" *Smc5* cKO mice treated with monastrol, DAPI (blue, DNA), SMC6 (red), and CEN (green). The purpose of each panel is to demonstrate the differences in chromatin morphology, centromere/kinetochore signal and SMC6 signal observed in these experiments. (**B and C**) Immunofluorescence images of oocytes from control and *Smc5* cKO mice. Oocytes were stained with DAPI (blue, DNA) and immunolabeled with antibodies against α-TUB (green) and CEN (red). (**B**) Example of an oocyte from the control mice that has reached MII arrest. The MII spindle and polar body are magnified 3x to the right of the whole oocyte image. (**C**) Example of an oocyte from the *Smc5* cKO mice that demonstrate degeneration. The abnormal spindle is magnified 3x to the right of the whole oocyte image. 5% of oocytes from the "adult" cohort of *Smc5* cKO mice harbored this defective morphology (N = 11/220). Scale bar: 10μm

the SMC6 protein was still present in most oocytes of the "juvenile" *Smc5* cKO cohort (**Fig. 3.4C**). These data suggest that SMC5/6 protein levels present before Cre-mediated deletion of *Smc5* are sufficient to support proficient meiosis, but not embryogenesis. Furthermore, the majority of oocytes from the "adult" cohort do not harbor residual SMC6 protein, and fail to form chromosomally normal MII oocytes (**Fig. 3.4**, **Table 2**). As fertility and genome integrity are negatively correlated with age, it can be postulated that SMC5/6 levels within GV oocytes of wild-type mice may decrease with age. To test this hypothesis oocyte protein extracts from three groups of C57BL6/J wild-type mice aged 4, 12 and 24 weeks were assessed for SMC5, SMC6, NSMCE1 and NSMCE2 protein levels (**Fig. 3.5A,B**). From this analysis it was determined that protein levels for all four SMC5/6 components decreased significantly in oocytes isolated from older mice.

Smc5 is a maternal-effect gene

As there were residual levels of SMC6 detected in the oocytes isolated from "juvenile" *Smc5* cKO mice, it was hypothesized that SMC5/6 levels were adequate to facilitate chromosome segregation during meiosis, but was insufficient for sustaining proper mitotic segregation during the early embryogenesis. To further assess the relationship between *Smc5* mutation and the capacity to form mature blastocysts, wild-type, heterozygous *Smc5 del* male and female mice were used for IVF to test effects of paternal versus maternal inheritance of the mutant allele. The oocytes used in these assays were from 4 week old mice, and therefore equivalent to the designated "juvenile" age group. In addition, *Smc5* cKO male mice (*Smc5 flox/del*, *Hspa2-Cre tg/0*), which are

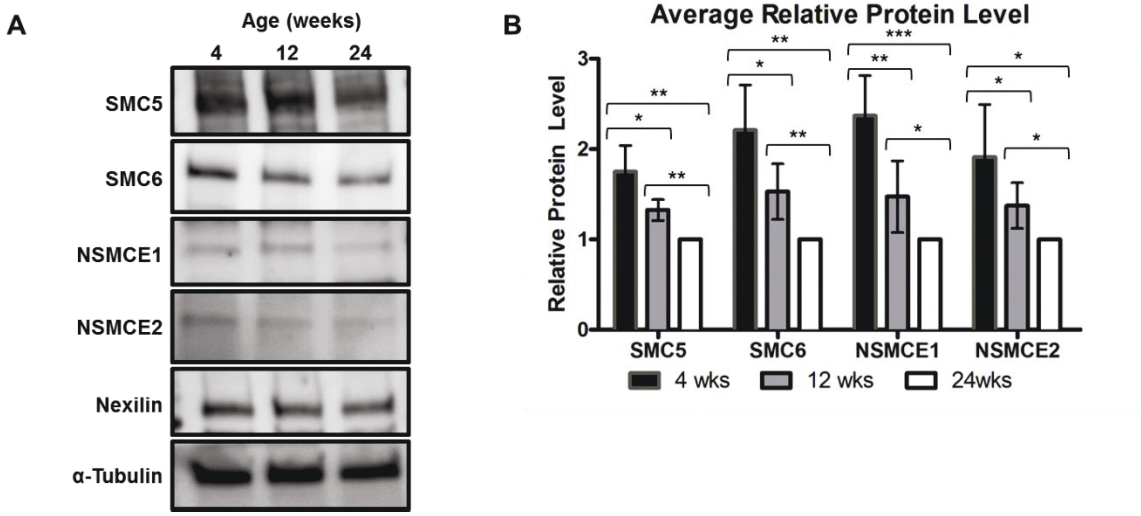

Figure 3.5. SMC5/6 protein levels decrease in oocytes as mice age and *Smc5* is essential for embryogenesis. (**A and B**) Protein was extracted from oocytes of wild-type C57BL6/J mice that were 4, 12 and 24 weeks of age. (**A**) Protein extracts from 150 oocytes from wild-type C57BL/6J mice were loaded onto each lane of a 4-15% SDS PAGE gradient gel and assessed for SMC5, SMC6, NSMCE1 and NSMCE2 protein levels. Nexilin and α-Tubulin were loading controls. (**B**) Bar graph of the average relative protein levels for each SMC5/6 complex component. Protein band signal intensities were normalized against the Nexilin loading control. Error bars represent standard deviation. Two-tailed paired t-tests were performed to compare each group and P values were defined as $P < 0.05$ (*), $P < 0.005$ (**) and $P < 0.0005$ (***). The data is based on five sets of 150 oocytes isolated from three separate rounds of oocyte harvest.

Table 3.3. Mating test and genotyping data for *Smc5 flox/del* (control) and *Smc5 flox/del, Hspa2-Cre* cKO males mated to C57BL6/J females

	Offspring		
Strain	***Smc5+/flox***	***Smc5+/del***	**Total**
♂ ***Smc5flox/del*** **x ♀ wild-type**	49% (51 pups)	51% (53 pups)	104 pups (6.9/litter)
♂ ***Smc5flox/del, Hspa2-Cre*** **x ♀ wild-type**	2% (1 pup)	98% (64 pups)	65 pups (7.2/litter)

n=5 males tested, three liters

Table 3.4. Mature blastocyst counts following IVF of MII oocytes

Cross	Blastocyst % (fraction) [number of repeats]
♂ wild type x ♀ wild-type	52% (34/66) [3]
♂ *Smc5 flox/del* x ♀ wild-type	48% (19/38) [2]
♂ *wild-type* x ♀ *Smc5 flox/del*	55% (41/75) [4]
♂ *Smc5flox/del*, *Hspa2-Cre* x ♀ wild-type	50% (39/77) [3]
♂ *Smc5 flox/del*, *Hspa2-Cre* x ♀ *Smc5 flox/del*	23% (10/43) [2]
♂ wild-type x ♀ *Smc5 flox/del, Zp3-Cre*	< 0.02% (0/79) [4]

fertile and produce sperm that almost exclusively carry the *Smc5 del* allele, were used for IVF. Based on mating tests with C57BL6/J wild-type females, 98% of progeny from the *Smc5 flox/del*, *Hspa2-Cre* males carry the *Smc5 del* allele (**Table 3**). When sperm from the heterozygous *Smc5 del* and *Smc5 flox/del*, *Hspa2-Cre* males were combined with wild-type oocytes the levels of mature blastocysts obtained were equivalent to the wild-type IVF (**Table 4**), showing that presence of the paternally inherited *Smc5 del* allele does not affect early embryogenesis. When female heterozygous *Smc5 del* oocytes were fertilized with wild-type sperm, levels of mature blastocysts were equivalent to the wild-type IVF results, suggesting that the expression of *Smc5* during oocyte growth is essential for supporting early stages of embryogenesis. When the heterozygous *Smc5 del* oocytes were fertilized with sperm from the *Smc5 flox/del*, *Hspa2-Cre* males, the level of blastocysts obtained reduced by approximately half, which supports the fact that early stages of embryonic development are affected in embryos homozygous for mutation of *Smc5*. Homozygous mutation of other components of the SMC5/6 complex, *Smc6* and *Nsmce2*, have also been shown to cause embryonic lethality (Jacome et al., 2015a, Ju et al., 2013). Taken together with the IVF and MII data obtained for the "juvenile" *Smc5* cKO females (**Fig. 3.3**, **Fig. 3.4**, **and Table 2**; **Fig. S3.5**), these results suggest that *Smc5* expression during oocyte growth, before meiotic resumption, is critical for embryogenesis, and therefore, *Smc5* is a maternal-effect gene.

Oocyte-specific cKO of Smc5 causes chromosome stretching during meiosis I

Because abnormal chromosome morphology was observed in oocytes from the "adult" *Smc5* cKO group at metaphase II arrest, it is possible that chromosome

morphology and segregation earlier, during meiosis I, was perturbed. The localization of SMC5/6 components in the *Smc5* cKO and control oocytes during meiosis I was assessed. SMC5/6 components SMC5, SMC6 and NSMCE1 were enriched at the pericentromeric heterochromatin during the metaphase to anaphase I transition in control oocytes, but were absent in the *Smc5* cKO oocytes (**Fig. 3.6A**). Oocytes were assessed during the metaphase to anaphase I transition (**Fig. 3.6B-D**). In the majority (95%, N = 144) of the control oocytes proficient segregation of homologous chromosomes was observed. In sharp contrast, the majority (62%, N = 220) of *Smc5* cKO experimental oocytes displayed chromosome stretching and lagging chromosomes. The severe chromatin stretching observed between homologous chromosomes (**Fig. 3.6C**) suggests that deletion of *Smc5* prevented decatenation of homologous chromosomes.

Given the meiotic abnormalities described above, the spindle assembly checkpoint (SAC) was assessed in the *Smc5* cKO oocytes. SAC satisfaction during the metaphase to anaphase I transition was indirectly determined by assessing the SAC protein MAD2, which normally localizes to kinetochores during prometaphase, and remains there until ubiquitous bipolar microtubule-kinetochore attachment satisfies the SAC (Lara-Gonzalez et al., 2012). MAD2 staining was present at the kinetochores at prometaphase in both control and *Smc5* cKO oocytes (**Fig. 3.6F**). MAD2 signal at the kinetochore was absent in both control and *Smc5* cKO oocytes undergoing the metaphase to anaphase I transition (**Fig. 3.6G**). These observations suggest that mutation of *Smc5* does not affect the temporal pattern of MAD2 localization, and therefore may not affect SAC function, consistent with the lack of MI oocyte arrest. Additionally, cell cycle kinase, PLK1, localized to kinetochores in control and *Smc5* cKO oocytes (**Fig. S3.7**).

Figure 3.6. *Smc5* cKO oocytes display lagging and stretched chromosomes during meiosis I. (**A**) Metaphase I oocytes from control (*Smc5 +/flox, Zp3-Cre tg/0*) and *Smc5* cKO (*Smc5 flox/del*, *Zp3-Cre tg/0*) mice, DAPI (blue, DNA), α-tubulin (green, α-TUB), CEN (green), and a subunit of the SMC5/6 complex (SMC5, SMC6, NSMCE1, red). (**B**) Oocytes transitioning from metaphase I to anaphase I, DAPI (blue, DNA), α-TUB (green) and CEN (red). (**C**) *Smc5* cKO oocyte undergoing metaphase I to anaphase I transition displaying chromatin stretching, DAPI (purple, DNA) and CEN (green). Images with a 3x magnification of chromosome stretches on the right. (**D**) Bar graph of percentages of oocytes (*n*=104 for control and *n*=167 for *Smc5* cKO) showing even metaphase I to anaphase I chromosome segregation (MI to AI even), chromosome stretching (MI to AI stretch); and in anaphase I (*n*=40 for control and *n*=53 for *Smc5* cKO) showing no lagging chromosomes (AI no lagging) and lagging chromosomes (AI lagging).
The *P* values (one-tailed paired *t*-test) for the indicated comparisons are *P*=0.004 (MI to AI) and *P*=0.0078 (AI). (**E**) Pro-metaphase I and (**F**) metaphase I oocytes were stained with DAPI (blue, DNA), MAD2 (green) and CEN (purple). (**H**) Pro-metaphase oocyte stained with DAPI (blue, DNA), Histone H4 dimetyl K20, trimetyl K20 (red, H4K20), and CEN (green). Collectively, at least 10 mice for each group were used to obtain the data. Scale bars: 10 μm.

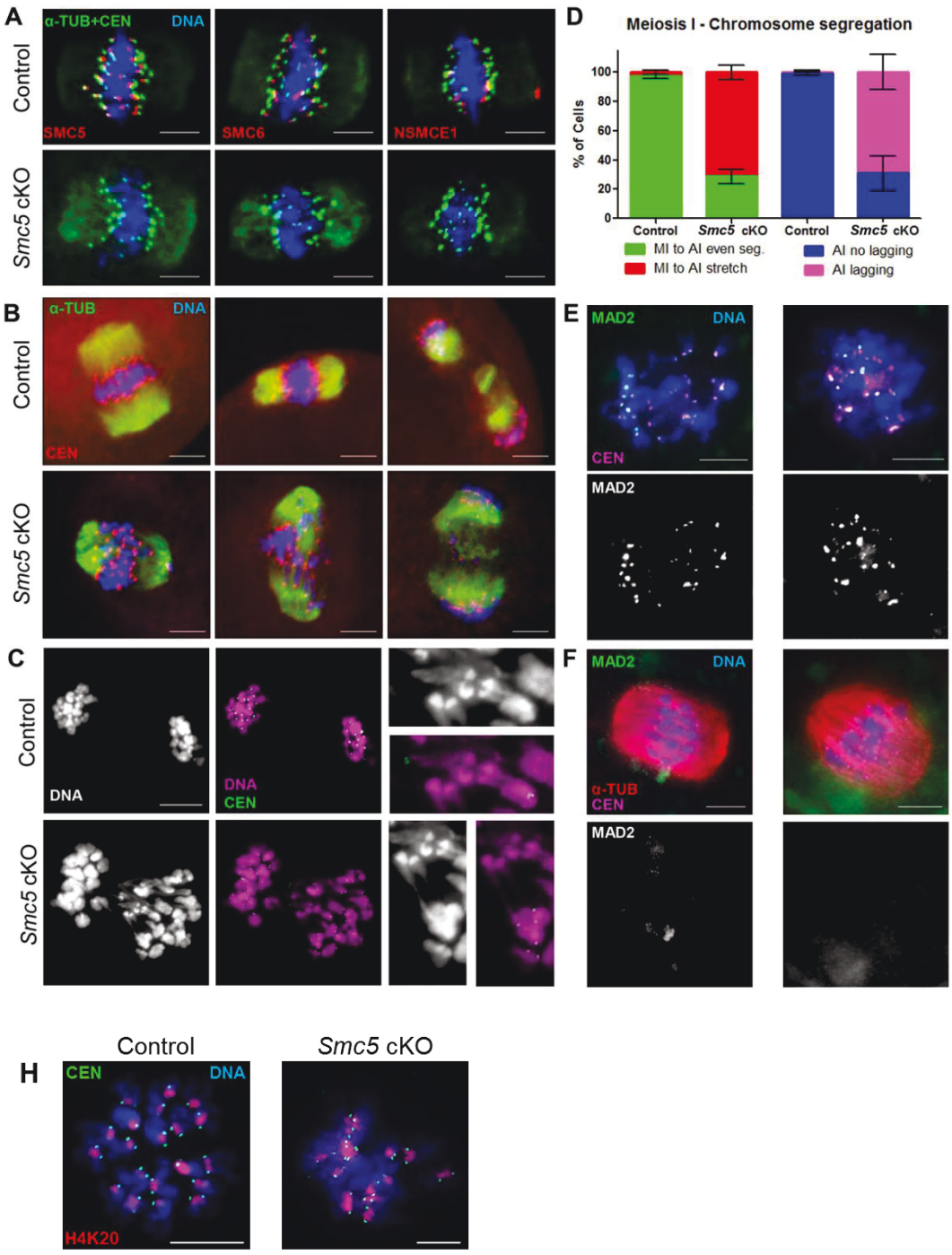
A
α-TUB+CEN
DNA
Control
SMC5
SMC6
NSMCE1
Smc5 cKO
B
α-TUB
DNA
CEN
C
DNA
DNA
CEN
D
Meiosis I - Chromosome segregation
% of Cells
100
80
60
40
20
0
Control
Smc5 cKO
Control
Smc5 cKO
MI to AI even seg.
MI to AI stretch
AI no lagging
AI lagging
E
MAD2
DNA
CEN
MAD2
F
MAD2
DNA
α-TUB
CEN
MAD2
H
Control
Smc5 cKO
CEN
DNA
H4K20

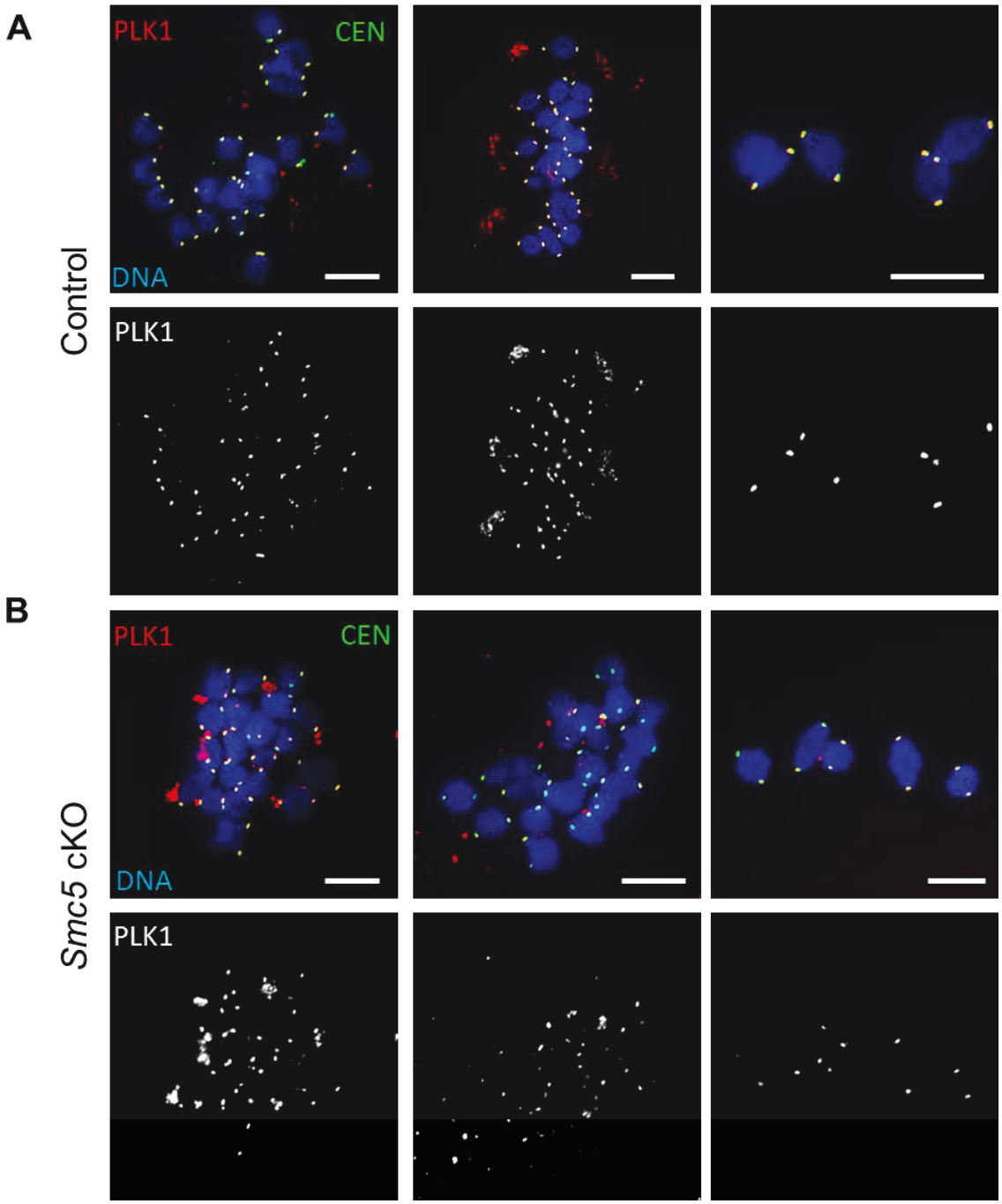

Supplemental Figure 3.7. Localization of PLK1 in control and *Smc5* cKO MI oocytes. (**A**) Chromatin spread preparations of MI-stage oocytes from "adult" control and *Smc5* cKO, DAPI (blue, DNA), PLK1 (red), CEN (green). (**B**) Whole oocyte preparations of MI-stage oocytes from "adult" control and *Smc5* cKO, DAPI (blue, DNA), Aurora B (red), CEN (green). Scale bar: 10μm

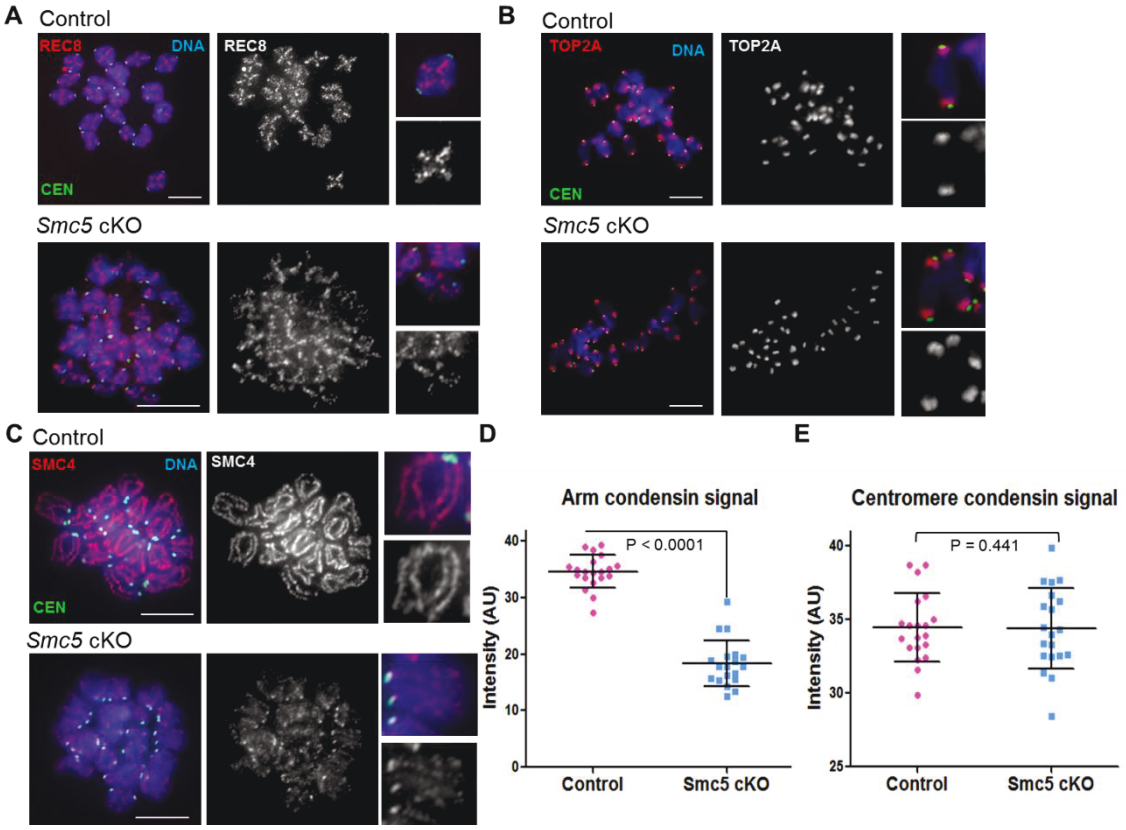

Figure 3.7. Condensin signal is reduced along chromosome arms in *Smc5* cKO oocytes during meiosis I. Chromatin spreads of metaphase I oocytes from control (*Smc5 +/flox, Zp3-Cre tg/0*) and *Smc5* cKO (*Smc5 flox/del*, *Zp3-Cre tg/0*) mice. Metaphase I chromosomes were stained with DAPI (blue, DNA), CEN (green) and either (A) cohesin component, REC8, (B) Topoisomerase IIα (TOP2A), or (C) condensin component, SMC4, in red. Representative chromosomes with a 3x magnification are present to the right of each chromosome spread. (D) Quantification of signal intensity of condensin (SMC4) signal along chromosome arms and associated with the centromere (overlapping with CEN). P values are given for indicated comparisons (Mann-Whitney, one-tailed) (N =20). Scale bar: 10μm

Absence of the SMC5/6 complex causes aberrant localization of condensin

Premature depletion of REC8 before the meiosis I division in oocytes is associated with chromosome missegregation (Tachibana-Konwalski et al., 2010b, Chiang et al., 2010). Therefore, localization of REC8 was assessed using metaphase I chromosome spreads. REC8 was present along the axes of the bivalents in control and *Smc5* cKO oocytes from "adult" mice, with no apparent difference between them (Fig. 7A). These results suggest that mutation of *Smc5* before meiotic resumption does not significantly affect localization of REC8-containing cohesins.

SMC5/6 colocalizes with TOP2A in mouse oocytes (**Fig. 3.1C**), and similar to the *Smc5* cKO oocytes from the "adult" cohort, inhibition of TOP2A function results in severe defects in chromosome condensation and homologous chromosome separation (Li et al., 2013). Therefore, the effect of *Smc5* cKO on the localization of TOP2A during meiosis I was determined using "adult" mice. TOP2A was enriched at the pericentromeric regions in control oocytes, and was also detected along chromosome arms (**Fig. 3.7B**). No detectable change in TOP2A localization was observed in the *Smc5* cKO oocytes (**Fig. 3.7B**).

Condensins are required to ensure chromosome segregation during meiosis I in mouse oocytes (Houlard et al., 2015b). Similar to the results presented here for *Smc5* cKO oocytes, conditional mutation of a condensin II component, *Ncaph2*, resulted in chromosome stretching during meiosis I due to an inability to disentangle chromosomes. To determine whether condensin localization is affected in the absence of the SMC5/6 complex, localization of the condensin I and II subunit SMC4 was assessed using "adult" cohorts of mice. In control metaphase I chromosome spread preparations, SMC4 was

present along the longitudinal axes of each bivalent (**Fig. 3.7C**). In contrast, in chromosome spread preparations from *Smc5* cKO metaphase I oocytes, there was a significant reduction in SMC4 signal along chromosome arms (**Fig. 3.7C,D**). In addition, the SMC4 signal on chromosome arms was discontinuous and the normal linear pattern along chromosomes axes was difficult to distinguish. However, there was no apparent reduction in condensin signal that colocalized with the kinetochore/centromeric regions in *Smc5* cKO metaphase I chromosome spread preparations compared to control (**Fig. 3.7E**).

Discussion

This study of a genetic model for oocyte depletion of SMC5 has demonstrated that the SMC5/6 complex is essential for ensuring accurate chromosome segregation following meiotic resumption and during early embryogenesis. Furthermore, the data suggest that SMC5/6 complex protein levels diminish as mice age, and *Smc5* is a maternal-effect gene.

Smc5/6 localization pattern implicates multiple-functions during meiosis

SMC5/6 is enriched at the pericentromeric heterochromatin regions throughout meiosis in mouse oocytes, which is consistent with what was found in mouse spermatocytes (Gomez et al., 2013, Verver et al., 2013). The pericentromeric heterochromatin region consists of densely packed repetitive sequences and is at high risk of aberrant recombination events when double-strand breaks within these regions are repaired via homologous recombination (HR) (Goodarzi and Jeggo, 2012). SMC5/6

prevents HR within repetitive sequences such as rDNA in yeast, and heterochromatin in *Drosophila* mitotic cells (Torres-Rosell et al., 2007, Chiolo et al., 2011). Taken together, studies using mouse spermatocytes and oocytes suggest that SMC5/6 performs a similar function at the pericentromeric heterochromatin during meiosis (Gomez et al., 2013; Verver et al., 2013).

Although lower in signal intensity, SMC5/6 also localized throughout the chromatin during meiosis. This is consistent to what has been reported for mouse spermatocytes (Gomez et al., 2013; Verver et al., 2013). SMC5/6 was also visible along chromosome axes at pachynema in oocytes, which was also detected in mouse spermatocytes (Gomez et al., 2013). In addition, transient foci of SMC6 were detected along the chromosome arms in female germ cells during pachynema, suggesting a role during meiotic recombination, which has previously been reported using budding yeast and *Caenorhabditis elegans* (Bickel et al., 2010, Hong et al., 2016, Checchi et al., 2014, Copsey et al., 2013a, Lilienthal et al., 2013a, Xaver et al., 2013).. In mammals, every chromosome pair obtains many recombination sites but generally yields only one to two crossover sites (Kauppi et al., 2004). Designations of which recombination sites become crossovers involve antagonistic roles between ubiquitin E3 ligase HEI10 and SUMO E3 ligase RNF212 (Reynolds et al., 2013, Qiao et al., 2014, Rao et al., 2017, Ahuja et al., 2017). It is possible that the SMC5/6 complex is a substrate of HEI10 and RNF212. Therefore, these SMC6 foci could indicate that SMC5/6 plays a role in regulating recombination during mammalian meiosis.

Differences between the Smc5 cKO oocytes isolated from "juvenile" and "adult" mice

SMC6 protein was detected in the majority of oocytes in the "juvenile" *Smc5* cKO cohort. However, SMC6 was not detected in the majority of "adult" *Smc5* cKO oocytes. As a consequence of this difference, oocytes from "juvenile" *Smc5* cKO mice progress to MII without aberrant chromosome configurations (**Fig. 3.4**, **Table 2**), whereas oocytes from "adult" *Smc5* cKO mice fail to accurately segregate chromosomes during meiosis I (**Fig.3.6**). Despite evidence for proficient meiosis from analysis of MII ploidy and chromosome morphology in oocytes from the "juvenile" *Smc5* cKO cohort, these oocytes failed to form mature blastocysts when fertilized with sperm bearing a wild-type *Smc5* gene. This failure to form mature blastocysts is attributed to aberrant chromosome segregation during mitosis (**Fig. 3.3**; **Fig. S3.5**). This phenotype is reminiscent to the mitotic catastrophe observed in *Smc5* cKO mouse embryonic stem cells (Pryzhkova and Jordan, 2016b).

The phenotypes observed and differences between "juvenile" and "adult" *Smc5* cKO mice implies the following hypotheses. Firstly, SMC5/6 protein levels before oocyte growth are important for proficient chromosome segregation during meiotic resumption (**Fig.3.4, Tables 2; Fig. 3.6**). Secondly, SMC5/6 protein levels present in oocytes diminish as mice age (**Fig. 3.5**, **Tables 3**, **Table 4**). Thirdly, there is a critical level of SMC5 protein that is required for proficient chromosome segregation during oocyte meiosis (**Fig. 3.4**, **Table 2**). Fourthly, expression of *Smc5* during the oocyte growth phase is critical during early embryogenesis (**Fig. 3.3**, **Fig.3.4**, **Table 2**).

SMC5/6 protein levels are diminished in aging oocytes

Frequency of meiotic segregation errors increases as women age, especially after the age of ~35, resulting in dramatically increased incidence of miscarriage and birth defects (Hassold and Hunt, 2001a). During the long prophase arrest that precedes meiosis I in female mammals, cohesin declines gradually and in aged oocytes the reduction of cohesin causes destabilization of chiasmata and separation of sister centromeres, which can result in chromosome missegregation during meiosis I (Tsutsumi et al., 2014, Tachibana-Konwalski et al., 2010b, Lister et al., 2010). This current study determined that SMC5/6 protein levels decrease in oocytes isolated from older mice, and by correlation of phenotypes, this could also contribute to age-related aneuploidy and infertility (**Fig.3.8**). Using an inducible transgene of *Rec8*, it was recently shown that cohesin is established in fetal oocytes during DNA replication, and there is no detectable turnover of cohesin in arrested oocytes, or during meiotic resumption (Burkhardt et al., 2016). Development of inducible, tagged version of an SMC5/6 component could be used to determine whether the SMC5/6 complex is replenished during meiotic resumption, or it remains stably associated with the chromatin for months following meiotic arrest.

Heterozygous mutants of cohesin components lead to age-related increases in oocyte aneuploidy (Murdoch et al., 2013). Therefore, it is possible that a heterozygous mutation of a SMC5/6 component could lead to age-related errors during oogenesis too. Supporting this notion, it has been shown that heterozygous mutation of *Nscme2* results in increased incidences of micronuclei and polynucleation in MEFs (Jacome et al., 2015a).

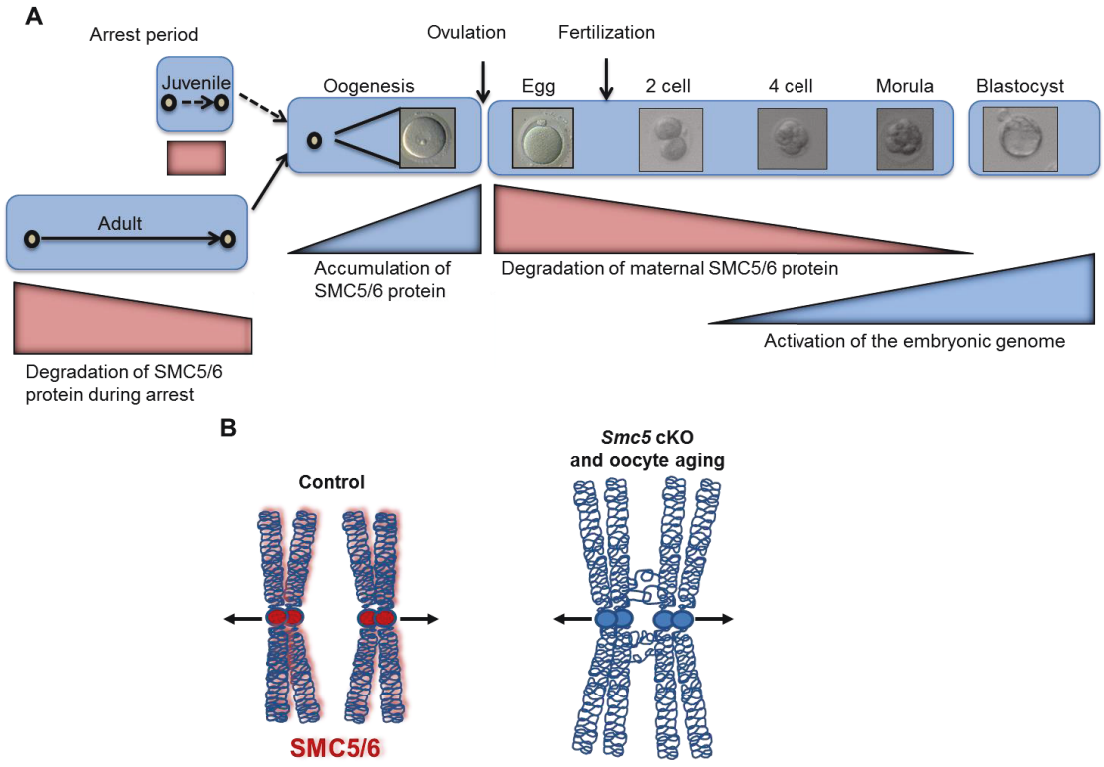

Figure 3.8. *Smc5* is a maternal-effect gene, and SMC5/6 is required for the formation of bivalent chromosomes capable of segregation during meiosis I in mouse oocytes. (A) SMC5/6 levels diminish in oocytes as mice age (red bars), leading to increased incidence of chromosome missegregation during meiosis. Regardless of age, maternal expression of SMC5 during oocyte maturation and early embryogenesis (blue bars), prior to activation of the embryonic genome (green bar), is essential for the formation of a functional blastocyst. (B) The SMC5/6 complex ensures that homologous chromosomes are accurately resolved and segregated during female meiosis I. Depletion of the SMC5/6 in aging oocytes may be a source of chromosome segregation error.

Smc5 is a maternal-effect gene

Early stages of embryogenesis are almost entirely dependent on the oocyte for subcellular organelles and proteins before the robust activation of the embryonic genome at cleavage-stage development (**Fig. 8A**). These maternal proteins are encoded by maternal-effect genes (Li et al., 2010). Approximately, 45-50 maternal-effect genes have been identified in mammals, and many of these are involved in chromatin structure, modification and genome integrity (Zhang and Smith, 2015). Reduced levels of maternal-effect genes have been associated with reduced oocyte developmental competence characteristic of ovarian aging (Guglielmino et al., 2011, Pan et al., 2008, Hamatani et al., 2004, Zhang and Smith, 2015). The IVF experiments presented in this study showed that embryogenesis was aberrant only when *Smc5* was mutated during the oocyte growth phase, and provision of a functional *Smc5* gene from sperm was insufficient to facilitate embryogenesis. These data suggest that *Smc5* is a maternal-effect gene in mouse. Recently, it was reported that *smc5* and *smc6* of *Drosophila melanogaster* are also maternal-effect genes (Tran et al., 2016), suggesting that this feature is conserved in many sexually reproducing organisms.

SMC5/6 may be required to assist condensin functions and TOP2A-dependent decatenation

Inhibition of TOP2A function in mouse oocytes and RNAi-mediated depletion in fly oocytes during meiosis I cause similar chromosome segregation defects observed in the *Smc5* conditional knockout mouse oocytes (Hughes and Hawley, 2014, Li et al., 2013). Components of the SMC5/6 complex colocalize with TOP2A during prophase and

following meiotic resumption in mouse oocytes. This is supported by previous observations made using mouse spermatocytes (Gómez et al., 2013). RNAi knockdown of *SMC5* and *SMC6* in human RPE-1 cells alters chromosomal localization properties of TOP2A (Gallego-Paez et al., 2013). Therefore, it was hypothesized that mutation of *Smc5* would affect TOP2A localization in mouse oocytes. However, no defects in TOP2A localization were observed, which aligns with what was reported for *Smc5* cKO in mouse embryonic stem cells (Pryzhkova and Jordan, 2016b). Studies of yeast SMC5/6 have shown that the complex is linked with TopoII-dependent catenation/decatenation functions (Kanno et al., 2015, Jeppsson et al., 2014c, Kegel et al., 2011b). Furthermore, meiotic depletion of Top2 in budding yeast affects Smc5 localization (Copsey et al., 2013b). While TOP2A localization is unaffected by mutation of *Smc5* in mouse oocytes, the functionality of TOP2A may still be affected.

Analysis of metaphase I chromosome spreads revealed that SMC5/6 is required for normal localization of condensin along chromosome arms. The phenotypes observed here for the *Smc5* cKO mutant are reminiscent of the *Ncaph2* condensin II cKO mutant (Houlard et al., 2015b), as both display abnormal chromosome morphology, similar stretching of chromosomes and chromosome segregation defects during meiosis I. There is mounting evidence for a functional link between SMC5/6 and condensin. RNAi depletion of SMC5 and SMC6 in human RPE-1 cells resulted in defective axial localization of condensin (Gallego-Paez et al., 2013). Abnormal condensin localization was also observed using *Smc5* cKO mouse embryonic stem cells (Pryzhkova and Jordan, 2016b). Furthermore, mutation of *smc-5* in *C. elegans* leads to abnormal distribution of condensin along bivalents during meiosis I (Hong et al., 2016). However, previous

studies were not able to determine whether the defects in condensin localization were specific to the prophase to metaphase transition. Utilizing the *Zp3-Cre* transgene to mutate *Smc5* suggests that there is a functional relationship between condensin and SMC5/6 that is specific to meiotic resumption.

It has been shown that condensin and TOP2A activities are coordinated to ensure efficient chromosome condensation, sister chromatid decatenation and subsequent segregation in budding yeast (Leonard et al., 2015, Charbin et al., 2014). Based on the collective observations made using human and mouse systems it is proposed that the aberrant localization of condensin observed in *Smc5* mutant oocytes results in the loss of coordination between condensin and TOP2A, leading to an inhibition of chromosome resolution during meiosis (Fig. 8B).

Conclusion

The data demonstrate that SMC5/6 levels diminish in oocytes as mice age, leading to increased incidence of chromosome missegregation during meiosis (**Fig. 3.8A**). Furthermore, *Smc5* is a maternal-effect gene and its expression during oocyte maturation is critical for early stages of embryogenesis (**Fig. 3.8A**). The SMC5/6 complex ensures that chromosomes are accurately resolved and segregated during female meiosis (**Fig. 3.8B**), and influences the localization of condensin, and based on published work this likely affects the function of TOP2A. Like cohesin and condensin, the SMC5/6 complex is critical to chromosome integrity in oocytes following their long arrested state. Protein levels of SMC5/6 components in oocytes are diminished in aging mice, suggesting that SMC5/6 levels are correlated with age-related oocyte and embryo

chromosomal abnormalities. These data present the possibility that genetic and expression variations of SMC5/6 components are linked with fertility differences between individuals and defects may cause premature ovarian failure.

Materials and methods

All mice were bred at The Jackson Laboratory (JAX, Bar Harbor, ME) and Johns Hopkins University (JHU, Baltimore, MD) in accordance with the National Institutes of Health and U.S. Department of Agriculture criteria and protocols for their care and use were approved by the Institutional Animal Care and Use Committees (IACUC) of JAX and JHU.

Mice

Mice harboring *Smc5* with a floxed exon 4 (designated $Smc5^{flox}$) and deleted exon 4 (designated $Smc5^{del}$) were previously described (Pryzhkova and Jordan, 2016b). Heterozygous $Smc5^{del}$ mice were bred to mice harboring the *Zp3-Cre* transgene (C57BL/6-Tg(Zp3-cre)93Knw/J), which resulted in progeny heterozygous for the $Smc5^{del}$ allele and hemizygous for the *Zp3-Cre* transgene ($Smc5^{+/del}$, *Zp3-Cre tg/0*). Male $Smc5^{+/del}$, *Zp3-Cre tg/0* mice were bred to homozygous $Smc5^{flox}$ female mice to derive *Smc5* cKO ($Smc5^{flox/del}$, *Zp3-Cre tg/0*) and control ($Smc5^{+/flox}$, *Zp3-Cre tg/0*) genotypes. The $Smc5^{flox/del}$ genotype was used as an additional control. The same mating strategy was employed to create the male $Smc5^{flox/del}$, *Hspa2-Cre tg/0* cKO mice, using mice harboring the *Hspa2-Cre* transgene (C57BL/6-Tg(Hspa2-cre)1Eddy/J).

PCR genotyping

Primers used are described in Figure 2 and Table S1. PCR conditions: 90°C for 2 min; 30 cycles of 90°C for 20 sec, 58°C for annealing, 72°C for 1 min.

Oocyte harvesting, culture and IVF

Female mice were injected intraperitoneally with 5 IU of equine chorionic (eCG; Sigma) to stimulate ovarian follicle development. GV-staged oocytes were harvested from ovaries 44 to 48 hrs later. Oocytes were cultured in MEMα medium supplemented with 5% fetal bovine serum (FBS; Gibco), and 3 mg/ml bovine serum albumin (BSA; Sigma-Aldrich). To harvest oocytes at metaphase II (MII) stage, mice were injected intraperitoneally with 5 IU of eCG (Sigma) and then with human chorionic gonadotropin (hCG; Sigma) 44-48 hrs later. After 15-16 hrs, MII oocytes were harvested from the ampulla of the oviduct. Ovulated oocyte-cumulus cell complexes were exposed to 300 IU/mL of hyaluronidase (Sigma) in MEMα medium supplemented with 3 mg/ml BSA to denude oocytes of surrounding cumulus cells.

For GVBD analysis, oocytes were harvested into MEMα medium supplemented with 5% FBS, 3 mg/ml BSA and 200 μM IBMX (Sigma-Aldrich). The oocytes were then washed and cultured in MEMα medium supplemented with 5% FBS, 3 mg/ml BSA and assessed for GVBD.

For IVF studies, eCG primed oocytes were first cultured in MEMα medium supplemented with 5% FBS, 3 mg/ml BSA and 2.5 μl EGF (10ng/ml; Epidermal Growth Factor) overnight. Following hyaluronidase treatment (Sigma), oocytes with a polar body indicative of progression to MII were counted. Oocytes were washed and cultured in

MEMα medium supplemented with 3 mg/ml BSA and 10 µl of sperm extracted from an adult male mouse epididymis. Following IVF oocytes were washed and cultured in KSOM media and observed each day to assess embryogenesis.

For monastrol treatment MII oocytes were incubated in 10 mM monastrol (Sigma-Aldrich) in MEMα medium for 1.5 hrs at 37°C. Oocytes were washed in MEMα medium prior to fixation.

All cultures were incubated at 37°C in a 5% CO_2, 5% O_2 and 90% N_2 atmosphere.

Microscopy

Prophase-stage oocyte chromatin spreads, whole-oocyte and embryo mounts, MII chromosome spreads for chromosome number counts, as well as MI and MII chromosome spreads for immunofluorescence microscopy analyses were performed using techniques previously described (Susiarjo et al., 2009a). Primary antibodies used and dilutions are listed in Table S2. Secondary antibodies against mouse, rabbit, and human IgG and conjugated to Alexa 488, 568 or 633 (Life Technologies) were used at 1:500 dilution. Oocytes were then mounted with Vectashield + DAPI medium (Vector Laboratories) or Clearmount (Invitrogen). DNase I treatment, chromatin spreads were treated with 100 U/ml of DNase I in DNaseI buffer (1% BSA, 10 mM $MnCl_2$, 1 mM $CaCl_2$, 50 mM Tris pH 7.5) for 1 hour at 37^{o}C prior to staining.

Images were captured using a Zeiss Cell Observer Z1 linked to an ORCA-Flash 4.0 CMOS camera (Hamamatsu) and analyzed with the Zeiss ZEN 2012 blue edition image software. Photoshop (Adobe) was used to prepare figure images.

Supplemental Table 3.1. Primers used in this study

Gene	Forward primers (5'-.....-3')	Reverse primers (5'-.....-3')
Smc5	GAGATGGCGCAACGCAATTAAT	GAGATGGCGCAACGCAATTAAT
Smc5	ACTCAGTCTCACACGGCAAG	ATCCTTCCCACCTTGGAAAC
Zp3-Cre	CCATCTGCCACCAGCCAG	TCGCCATCTTCCAGCAGG
Cpxm1	ACTGGGATCTTCGAACTCTTTGGAC	GATGTTGGGGCACTGCTCATTCACC

Supplemental Table S3.2. Antibodies used in this study

Primary Antibodies	Host	Source	Cat. Number	IF Dilution	WB Dilution
CREST (CEN)	Human	Antibodies Incorporated	15-235	1:50	
Histone H4 dimethyl K20, trimethyl K20 (H4K20)	Mouse	Abcam	ab78517	1:500	
MAD2	Rabbit	BioLegend	PRB-452C-200	1:250	
MLH1	Mouse	Thermo Fisher	MA5-15431	1:100	
Nexilin	Mouse	Sigma	SAB4200124		1:2000
NSMCE1	Rabbit	Abcam	ab66956	1:100	
NSMCE1	Mouse	Abcam	ab168578		1:1000
NSMCE2	Mouse	Novus Biologicals	H00286053-B01		1:500
PLK1	Rabbit	GeneTex	GTX104302	1:100	
REC8	Rabbit	Karen Schindler		1:1000	
SMC4	Rabbit	Novus Biologicals	NBP1-86635	1:50	
SMC5	Rabbit	GeneTex	GTX115669	1:50	
SMC5	Rabbit	Novus Biologicals	NB100-469		1:400
SMC6	Rabbit	Abcam	ab18039	1:200 to 1:500	1:20,000
SMC6	Rabbit	Abcam	ab155495	1:500	
SYCP3	Mouse	Santa Cruz	sc-74569	1:50	
Topoisomerase II α (TOPOII)	Rabbit	Abcam	ab109524	1:100	
α tubulin (TUB)	Mouse	Sigma	T9026	1:1000	1:10,000

Western blot analyses

Protein lysate from eCG primed oocytes were isolated from C57BL6/J mice using methods previously described (Marangos, 2016). Protein extracts containing 150 oocytes were run on 4-15% gradient SDS PAGE gels (Bio-Rad) and transferred to PVDF membranes. Primary antibodies and dilutions used are presented in Table S2. At a 1:10,000 dilution, goat anti-mouse and goat anti-rabbit horseradish peroxidase-conjugated antibodies (Invitrogen) were used as secondary antibodies. Antibody signal was detected via treatment with Bio-Rad ECL western blotting substrate and captured using Syngene XR5 system. Protein levels were assessed using Image J (NIH).

Acknowledgments

We thank John Schimenti for providing the *Rec8* mutant mouse, Karen Schindler for the REC8 antibody and Tatsuya Hirano for the NCAPH1 and 2 antibodies. We thank Marina Pryzhkova technical assistance.

Author Contributions:

G.H, J.J.E, M-A.H and P.W.J. conceived the project and wrote the manuscript. Experiments performed by G.H., F.S., M.O-B and P.W.J.

CHAPTER IV

DEPLETION OF SMC5/6 SENSITIZES MALE GERM CELLS TO DNA DAMAGE

This chapter has been submitted to PLOS Genetics, [Hwang G., Gaddipati H., Pryzhkova M.P., Verver D.E. , Handel M.A., Hamer G., and Jordan P.W.(under review)] and is reproduced here with minor edits. Hima Gaddipati and Dr. Marina Pryzhkova generated the MEF results, and histological analysis was done in collaboration with Dr. Dideke Emma Verver and Dr. Geert Hamer at the University of Amsterdam. I performed all other experiments.

Introduction

Mammalian spermatogenesis encompasses all events that lead to transformation of spermatogonia into elongated spermatids. During mammalian spermatogenesis, spermatogonial stem cells self-renew or differentiate into cells that are able to enter meiosis. During meiotic entry, replicated chromosomal DNA is subjected to SPO11-induced double-strand breaks (DSBs). These DSBs are primarily repaired via recombination between homologues within the context of a proteinaceous complex known as the synaptonemal complex (SC). When recombination is complete the SC is disassembled and homologues segregate during meiosis I. Sister chromatids remain associated until meiosis II, and the resulting haploid spermatids undergo differentiation to ultimately form motile sperm. Male meiosis is uniquely characterized by the presence of the heteromorphic X and Y chromosomes that lack homology to one another with the exception of a short 0.7Mb stretch of DNA called the pseudo-autosomal region (PAR) (Kauppi et al., 2013). During mid-prophase, when the autosomes are fully synapsed, only the PAR of the X-Y chromosome synapses and the X-Y chromatin is remodeled into a transcriptionally silenced heterochromatin domain known as the sex body(Handel, 2004, Turner, 2007).

Structural maintenance of chromosome complexes (SMC) are conserved multiprotein complexes expressed in mitotic and meiotic cells and are involved in ensuring genome integrity. There are three classes of SMC complexes expressed in mammals, cohesin, condensin and the SMC5/6 complex. Each SMC complex is comprised of two SMC proteins that interact with one another at their central hinge domains, and each protein folds back on itself via large coiled coil domains emanating from the hinge (Murray and Carr, 2008). The juxtaposed N and C termini of each SMC protein form ATPase domains. The ATPase domains of the SMC5 and SMC6 heterodimer are bridged by a kleisin protein, NSMCE4, together with the E3 ubiquitin ligase NSMCE1 and the MAGE domain containing protein, NSMCE3(Doyle et al., 2010a). Additionally, NSMCE2 is an SUMO E3 ligase component of the SMC5/6 complex, which interacts with the coiled-coil region of SMC5 (Doyle et al., 2010a, Potts and Yu, 2007b, Zhao and Blobel, 2005a).

The functions of cohesin and condensin during meiosis have been studied using various model organisms, including budding yeast, fission yeast, worms and mouse. Cohesin is required to ensure repair of SPO11-induced DSBs, SC formation between homologues and maintenance of sister chromatid cohesion (Klein et al., 1999, Severson and Meyer, 2014, Hopkins et al., 2014a, Ward et al., 2016, Revenkova et al., 2004, Hodges et al., 2005, Herran et al., 2011, Bannister et al., 2004, Xu et al., 2005, Caburet et al., 2014, Llano et al., 2014, Winters et al., 2014, Biswas et al., 2016, Watanabe and Nurse, 1999, Sakuno and Watanabe, 2009, Phadnis et al., 2015). It has been demonstrated that condensin is required for DSB formation and repair, normal chromosome compaction, and biorientation of sister chromatids during meiosis (Mets and Meyer,

2009, Houlard et al., 2015a, Brito et al., 2010, Lee et al., 2011). Researchers have used budding yeast, fission yeast and worms to assess the requirements of the SMC5/6 complex during meiosis (Verver et al., 2016a). The studies using yeast demonstrated that the SMC5/6 complex facilitates the resolution of joint molecules between homologous chromosomes prior to meiosis I (Wehrkamp-Richter et al., 2012a, Copsey et al., 2013a, Xaver et al., 2013, Lilienthal et al., 2013a). Chromosome fragmentation was observed during meiosis in worm mutants of the SMC5/6 complex (Bickel et al., 2010, Hong et al., 2016). Localization of the SMC5/6 complex during mouse spermatogonial differentiation and meiosis has been reported (Gomez et al., 2013, Verver et al., 2013b). Based on these studies, the SMC5/6 complex was implicated to have roles at the pericentromeric heterochromatin, the SC and the sex body. However, using primary spermatogonia in culture, it was found that SMC5/6 subunit NSMCE2 is dispensable for spermatogonial differentiation (Zheng et al., 2017).

To further assess the roles of the SMC5/6 complex during spermatogenesis, we created a *Smc5* conditional knockout (cKO) mouse model. We conditionally mutated the *Smc5* gene using three germ cell specific Cre recombinase transgenes, *Stra8-Cre*, *Spo11-Cre* and *Hspa2-Cre*, which mutated *Smc5* prior to meiotic entry, during early meiotic stages and during mid-meiotic stages, respectively (Sadate-Ngatchou et al., 2008, Lyndaker et al., 2013, Inselman et al., 2010). Despite efficient mutation of the *Smc5* cKO allele and corresponding protein depletion of SMC5/6 components, *Smc5* cKO mutant mice were fertile. Additionally, the *Smc5* cKO mutant mice did not display recombination defects or an inability to segregate chromosomes during meiosis. We observed a decrease in pre-leptotene spermatocyte number in the *Smc5*, *Stra8-Cre* cKO

mice; however, we did not observe any testicular abnormalities in the *Smc5*, *Spo11-Cre* and *Smc5*, *Hspa2-Cre* cKO mice. To determine the impact of *Smc5* cKO in the face of DNA damage, we introduced two different forms of exogenous DNA damage; ionizing radiation and etoposide. Both exposures caused an increase in enlarged round spermatids, which commonly harbored two acrosomes and displayed evidence of supernumerary chromosome content, indicative of aberrant meiotic divisions. From our observations, we propose that low levels of the SMC5/6 complex are sufficient to allow normal meiotic progression in the mouse. However, higher levels of the SMC5/6 complex are required when meiotic DNA processing events are perturbed by exogenous sources of DSBs.

Results

Conditional mutation of Smc5 via germ cell-specific Cre recombinase expression

We produced mice with a conditional knockout (cKO) allele for *Smc5* (*Smc5 flox*), in which the 4th exon is flanked by Cre-recombinase target loxP sites (**Fig. 4.1A**, see Materials and Methods). Cre-mediated deletion of the 4th exon results in a null allele of *Smc5* (*Smc5 del*). Mice with this allele were obtained only as heterozygotes, demonstrating that *Smc5* is essential for life. Mice heterozygous for the *Smc5 del* allele showed no visible morphological abnormalities during development and adult life. Therefore, we used *Smc5 flox/del* mice as controls and *Smc5 flox/del* mice that also harbored a germ cell-specific Cre transgene as our cKO animals (**Fig. 4.1B**). As an additional control, we assessed mice with a single floxed *Smc5* allele (*Smc5 +/flox*) and the germ-cell specific Cre transgene. *Stra8-Cre*, *Spo11-Cre* and *Hspa2-Cre* transgenes were used in this study. *Stra8-Cre* is first expressed at 3 days post-partum, in spermatogonia through to pre-leptotene stage spermatocytes (Sadate-Ngatchou et al.,

2008). *Spo11-Cre* is expressed as early as 10 days post-partum which corresponds to early prophase, pre-leptotene/leptotene stage, spermatocytes (Lyndaker et al., 2013). *Hspa2-Cre* is expressed by 14 days post-partum, corresponding to mid-prophase, zygotene/pachytene stage, spermatocytes (Inselman et al., 2010).

We assessed the fertility, litter size and Cre recombination efficiency of our cKO and control male mice by mating to wild-type C57BL6/J female mice (**Table 4.1**). The *Smc5 flox/del* control resulted in an average litter size of 7.6 pups, and the expected distribution of the *flox* and *del* alleles. The *Smc5 flox/del*, *Stra8-Cre* cKO mice were fertile, and produced litter sizes equivalent to the control. Almost all pups obtained from the *Smc5 flox/del*, *Stra8-Cre* cKO males harbored the *Smc5 del* allele. However, the *Smc5 flox* allele was observed in 6% of the progeny (N = 94 pups). The *Smc5 flox/del*, *Spo11-Cre* cKO and *Smc5 flox/del*, *Hspa2-Cre* cKO males were also fertile, with 15% and 2% of their pups harboring the *Smc5 flox* allele, respectively (N = 40 pups for *Spo11-Cre*, and N = 65 pups for *Hspa2-Cre*).

Conditional mutation of Smc5 results in destabilization of the SMC5/6 complex

Although the recombination efficiency of the *Smc5 flox* allele mediated by *Stra8-Cre*, *Spo11-Cre* and *Hspa2-Cre* expression was not 100%, we observed a pronounced decrease in SMC5 protein levels when assessing crude germ cell extracts via western blot (**Fig. 4.1C**; **Fig. S4.1A**). Moreover, the drop in SMC5 protein levels was accompanied by a drop in protein levels for other SMC5/6 components. This demonstrates that SMC5 is essential for the stability of the SMC5/6 complex. Interestingly, we observed a decrease in SMC6 and NSMCE2 levels that was equivalent to the decrease detected for SMC5.

Table 4.1: Analysis of fertility, litter size, and Cre excision efficiency

	Offspring		
Strain	***Smc5+/flox***	***Smc5+/del***	**Total**
♂ ***Smc5flox/del*** **x** ♀ ***wild-type***	51% (97 pups)	49% (94 pups)	191 pups
♂ ***Smc5flox/del, Stra8-Cre*** **x** ♀ ***wild-type***	6% (6 pups)	94% (88 pups)	94 pups
♂ ***Smc5flox/del*** **x** ♀ ***wild-type***	50% (26 pups)	50% (26 pups)	52 pups
♂ ***Smc5flox/del, Spo11-Cre*** **x** ♀ ***wild-type***	15% (6 pups)	85% (34 pups)	40 pups
♂ ***Smc5flox/del*** **x** ♀ ***wild-type***	49% (51 pups)	51% (53 pups)	104 pups
♂ ***Smc5flox/del, Hspa2-Cre*** **x** ♀ ***wild-type***	2% (1 pups)	98% (64 pups)	65 pups

The levels of the NSMCE1 and NSMCE4 proteins were reduced, but not to the same extent as the other SMC5/6 components. This difference could be attributed to their stabilization within the NSMCE1, 3, 4 trimer sub-complex, and there is evidence to suggest that these proteins have functions independent to the SMC5/6 complex (Kozakova et al., 2015, Hudson et al., 2011, Palecek et al., 2006a). Alternatively, this observation may be due to differences in individual protein turnover rates.

We observed the most robust depletion of SMC5/6 components using the *Stra8-Cre* transgene (**Fig. 1C**; **Fig. S1A**). To further confirm this depletion, we isolated early prophase (leptotene/zygotene stage), mid to late prophase (pachytene/diplotene stage) spermatocytes, and round spermatids using the STA-PUT density gradient germ cell purification method (La Salle et al., 2009). The Cre recombination efficiency of the *Smc5 flox* allele was assessed via PCR (**Fig 4.1D**). Protein levels of each SMC5/6 component was substantially decreased in *Smc5 flox/del*, *Stra8-Cre* germ cells, complementing the results obtained from the whole germ cell extracts (**Fig. 4.1E**; **Fig. S4.1B**). Finally, using immunofluorescence microscopy, we assessed the localization of SMC5/6 subunits on chromatin spread preparations (**Fig. 4.2, Table 4.2**). From these analyses, we found that most antibodies raised against SMC5/6 components detected a signal at the sex body during pachynema. A subset of SMC5/6 antibodies (SMC6, NSMCE1, NSMCE4) detected signal at the pericentromeric heterochromatin, and one SMC6 antibody detected signal along the SC. Analysis of pachytene stage chromatin spreads from the *Smc5 flox/del*, *Stra8-Cre* cKO mice, revealed that the localization of SMC5/6 components was diminished at the sex body. However, the localization to the pericentromeric heterochromatin and SC was still detected (**Fig. 4.2, Table 4.2**).

Figure 4.1. Conditional mutation of *Smc5* via germ cell-specific Cre recombinase expression does not affect fertility but causes destabilization of the SMC5/6 complex. (**A**) Schematic of mouse *Smc5* floxed allele containing loxP sites (yellow triangle), flanking exon 4 (dark green box), and the resulting *Smc5* deletion allele after excision of exon 4 by Cre recombinase. The purple round-sided rectangle represents the remaining Frt site following FLP-mediated recombination of the original conditional ready tm1a allele [58]. (**B**) Germ-cell specific Cre recombinase expression timeline. Black lines indicate when the corresponding Cre is first expressed. (**C**) Protein extracts from crude germ cell isolates from control, *Smc5* cKO (*Stra8-Cre*), *Smc5* cKO (*Spo11-Cre*), and *Smc5* cKO (*Hspa2-Cre*) were loaded on a 4-15% SDS PAGE gradient gel and assessed for SMC5, SMC6, NSMCE1, NSMCE2, and NSMCE4 protein levels. α-Tubulin was used as the loading control. Protein levels of SMC5/6 components are reduced in all *Smc5* cKO extracts compared to controls. (**D,E**) Spermatocytes were purified via STA-PUT into specified prophase substages: leptotene/zygotene (L/Z), pachytene (P), and round spermatid (RS). Spermatocytes were isolated from *Smc5 flox/del* (control) and *Smc5 flox/del, Stra8-cre*$^{tg/0}$ (*Smc5* cKO). (**D**) DNA agarose gel image of PCR products for genotyping, showing efficient deletion of the *Smc5* floxed exon 4 via Cre recombination. Lane 1 and 2 represent *Smc5 flox/del,* without Cre recombinase: 763 bp del allele, 563bp and 644bp flox allele. Lane 3 and 4 represent *Smc5 flox/del* with Cre recombinase: 763 bp del allele. Mouse embryonic stem cells were used as a control (mESC). (**E**) Protein extracts isolated from STA-PUT purified spermatocyte and round spermatids were loaded on a 4-15% SDS PAGE gradient gel and assessed for SMC5, SMC6, and NSMCE2. α-Tubulin was used as the loading control. Protein levels of SMC5 SMC6 and NSMCE2 are reduced in all *Smc5* cKO extracts compared to controls.

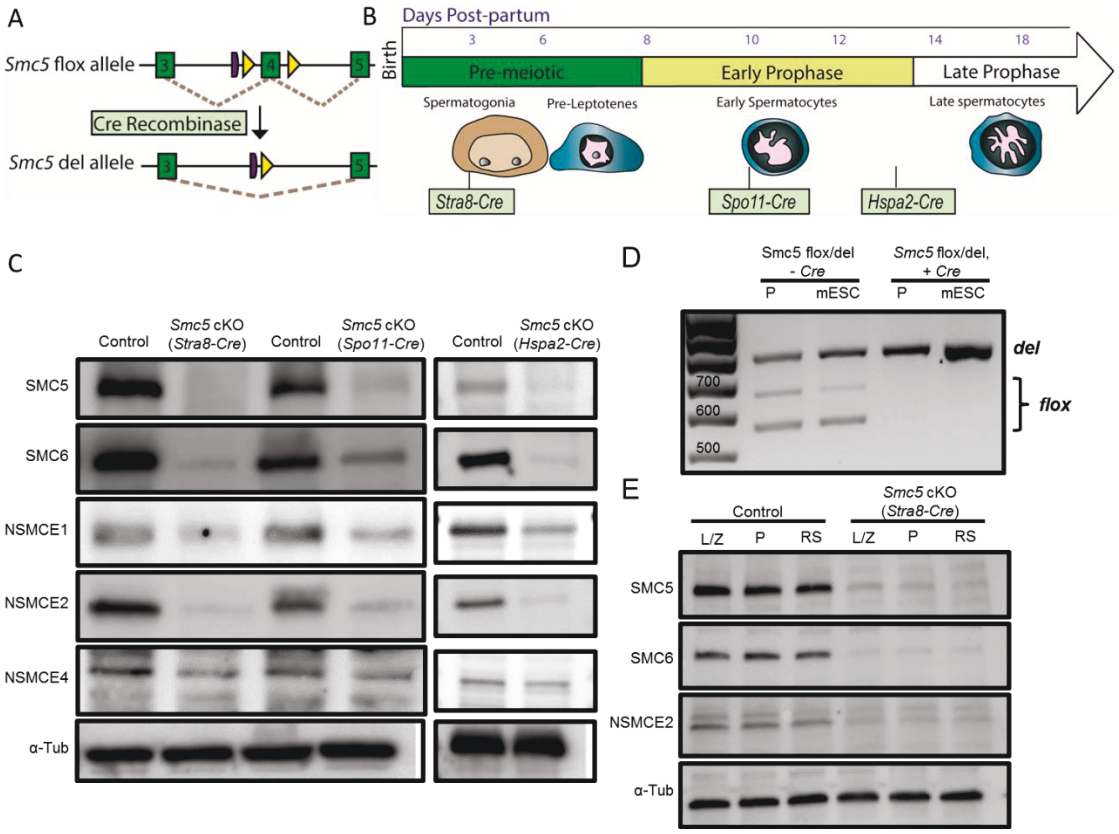
A
Smc5 flox allele
3
4
5
Cre Recombinase
Smc5 del allele
3
5
B
Days Post-partum
Birth
3
6
8
10
12
14
18
Pre-meiotic
Early Prophase
Late Prophase
Spermatogonia
Pre-Leptotenes
Early Spermatocytes
Late spermatocytes
Stra8-Cre
Spo11-Cre
Hspa2-Cre
C
Control
Smc5 cKO (Stra8-Cre)
Control
Smc5 cKO (Spo11-Cre)
Control
Smc5 cKO (Hspa2-Cre)
SMC5
SMC6
NSMCE1
NSMCE2
NSMCE4
α-Tub
D
Smc5 flox/del - Cre
Smc5 flox/del, + Cre
P
mESC
P
mESC
700
600
500
del
flox
E
Control
Smc5 cKO (Stra8-Cre)
L/Z
P
RS
L/Z
P
RS
SMC5
SMC6
NSMCE2
α-Tub

A

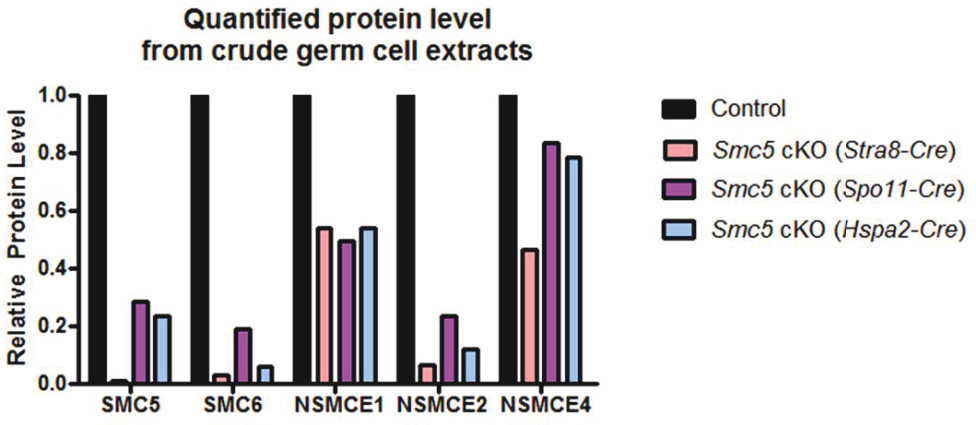

B

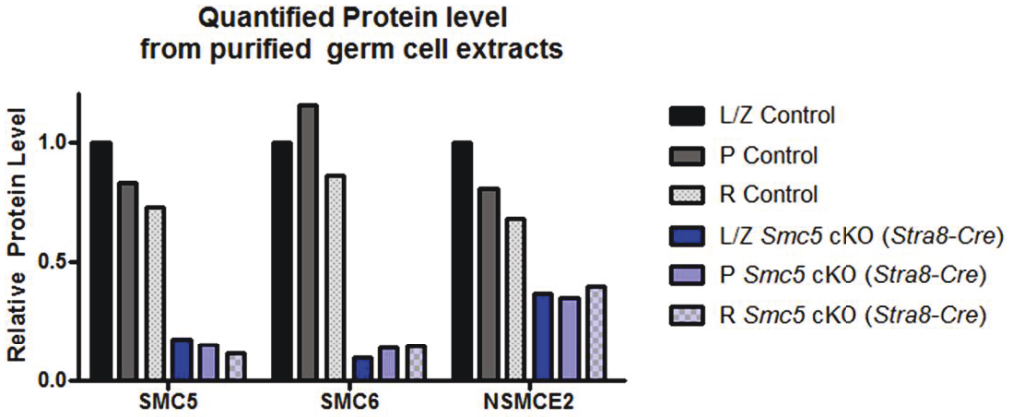

Supplemental Figure 4.1: Conditional mutation of *Smc5* via germ cell-specific Cre recombinases causes decreased protein levels of SMC5/6 complex components. (**A**) Bar graph of relative protein levels for each tested SMC5/6 complex component from crude germ cell isolates from control, *Smc5* cKO (*Stra8-Cre*), Smc5 cKO (*Spo11-Cre*), and *Smc5* cKO (*Hspa2-Cre*) loaded on 4-15% SDS PAGE gradient gels shown in Figure 1C. Protein band signal intensities were normalized against α-Tubulin loading control. Protein levels of SMC5/6 components are reduced in all *Smc5* cKO extracts compared to controls. (**B**) Bar graph of relative protein levels for each tested SMC5/6 complex component from STA-PUT purified germ cell isolates from control and *Smc5* cKO (*Stra8-Cre*) loaded on 4-15% SDS PAGE gradient gels shown in Figure 1E. Spermatocytes were purified via STA-PUT into specified prophase substages: leptotene/zygotene (L/Z), pachytene (P), and round spermatid (RS). Spermatocytes were isolated from *Smc5 flox/del* (control) and *Smc5 flox/del, Stra8-cre*$^{tg/0}$ (*Smc5* cKO). Protein levels of SMC5 SMC6 and NSMCE2 are reduced in all *Smc5* cKO extracts compared to controls.

Conditional mutation of Smc5 by Stra8-Cre results in depletion of pre-leptotene spermatocytes

To determine phenotypes of the cKO mice, the testis weight and tubule morphology were assessed. The *Smc5 flox/del*, *Stra8-Cre* cKO mice had a 15% reduction in testis weight compared to controls (**Fig. 4.3A, B**). The *Smc5 flox/del*, *Spo11-Cre* or *Smc5 flox/del*, *Hspa2-Cre* cKO mice did not show a difference in testis weight compared to controls (**Fig. S4.2A-B and D-E**), and furthermore, tubule cross sections from these mice showed no evidence of germ cell abnormalities (**Fig. S4.2C, F**). In contrast, tubule cross sections of adult *Smc5 flox/del*, *Stra8-Cre* cKO mice showed that many tubules were deficient for one or more germ cell-subtypes (**Fig. 4.3C, D**). Close analysis of PAS stained cross sections revealed that the depletion of germ cells occurred at the pre-leptotene stage of spermatogenesis (**Fig 4.3E, F**). A- and B-type spermatogonia were not affected in these cKO mice. Moreover, there were clear signs of spermatogenesis recovery within the tubule sections, indicating the presence of functional spermatogonial stem cells, and undifferentiated spermatogonia that were detected by LIN28 expression (**Fig. 4.3F**). To support our analysis, we assessed PCNA signal to determine the number cells actively undergoing DNA replication per tubule (**Fig. 4.3G**). We observed a significant decrease in PCNA positive cells per tubule in the *Smc5 flox/del*, *Stra8-Cre* cKO, which supports our initial observation that disappearance of germ cells occurred during the pre-meiotic S-phase (pre-leptotene) (**Fig. 4.3H**). In addition, TUNEL staining demonstrated an increase in apoptosis in the *Smc5 flox/del*, *Stra8-Cre* cKO mice (**Fig. 4.3I**). We also assessed DAZL and SYCP3 chromosome axes signal to further distinguish

Table 4.2. Summary of localization pattern observed using antibodies for different SMC5/6 components during pachynema

Antibody Information			Localization Pattern			
Antibody	**Company**	**ID**	**Pericentromeric heterochromatin**	**Sex Body**	**SC Axes**	**Difference in the *Smc5* cKO compared to control?**
SMC5 Antibodies						
rab α SMC5	Novus	100-469	no	yes	no	no sex body staining
rab α SMC5	Abcam	ab18038	no	yes	no	no sex body staining
rab α SMC5	Santa Cruz	sc-134544	no	yes	no	no sex body staining
rat α SMC5	Neobiolab	AP6962B	no	yes	no	no sex body staining
rab α SMC5	Thermo	PA5-30460	Did not show specific staining pattern			NA
rab α SMC5	Novus	NBP2-20419	Did not show specific staining pattern			NA
rab α SMC5	GeneTex	GTX115669	Did not show specific staining pattern			NA
SMC6 Antibodies						
rab α SMC6	Abcam	ab18039	yes	yes	no	less sex body staining (only on PCH)
rab α SMC6	Abcam	ab155495	no	yes	no	no sex body staining
gp α SMC6	Geert Hamer Lab	GH	no	yes	no	no sex body staining
rab α SMC6	Alan R. Lehmann Lab	ARL	no	yes	yes	no sex body staining
NSE Antibodies						
rab α NSE1	Abcam	ab66956	yes	yes	no	less sex body staining
mouse α NSE1	Abcam	ab168578	no	yes	no	less sex body staining
rab α NSE2	Protein Tech	13627-1-AP	no	yes	no	no sex body staining
rab α NSE4a	Abcam	ab178898	yes	no	no	no difference
rat α NSE4a	NeoBiolab	AP6962A	Did not show specific staining pattern			NA

Figure 4.2. Conditional mutation of *Smc5* via Stra8-Cre causes depletion of SMC5/6 subunits at the sex body. (**A-C**) Pachytene stage chromatin spread preparations immunolabeled with antibodies against CEN (blue, kinetochore/centromere marker), the SC lateral element protein SYCP3 (red), and corresponding SMC5/6 subunits (green). SMC5/6 subunits are depleted at the sex body (circle) in the *Smc5* cKO (*Stra8-Cre*) chromatin spreads. Scale Bar: 10 μm. (**A**) Chromatin spread preparations immunolabled with four different antibodies against SMC5 (Novus 100-469, sc-134544, ab18038, and AP6962B). (**B**) Chromatin spread preparations immunolabled with four different antibodies against SMC6 (Alan Lehmann, Geert Hamer, ab18039, and ab155495). (**C**) Chromatin spread preparations immunolabled with two different antibodies against NSMCE1 (ab66956, ab168578), or one antibody against NSMCE2 (13627-1-AP), or NSMCE4 (ab178898).

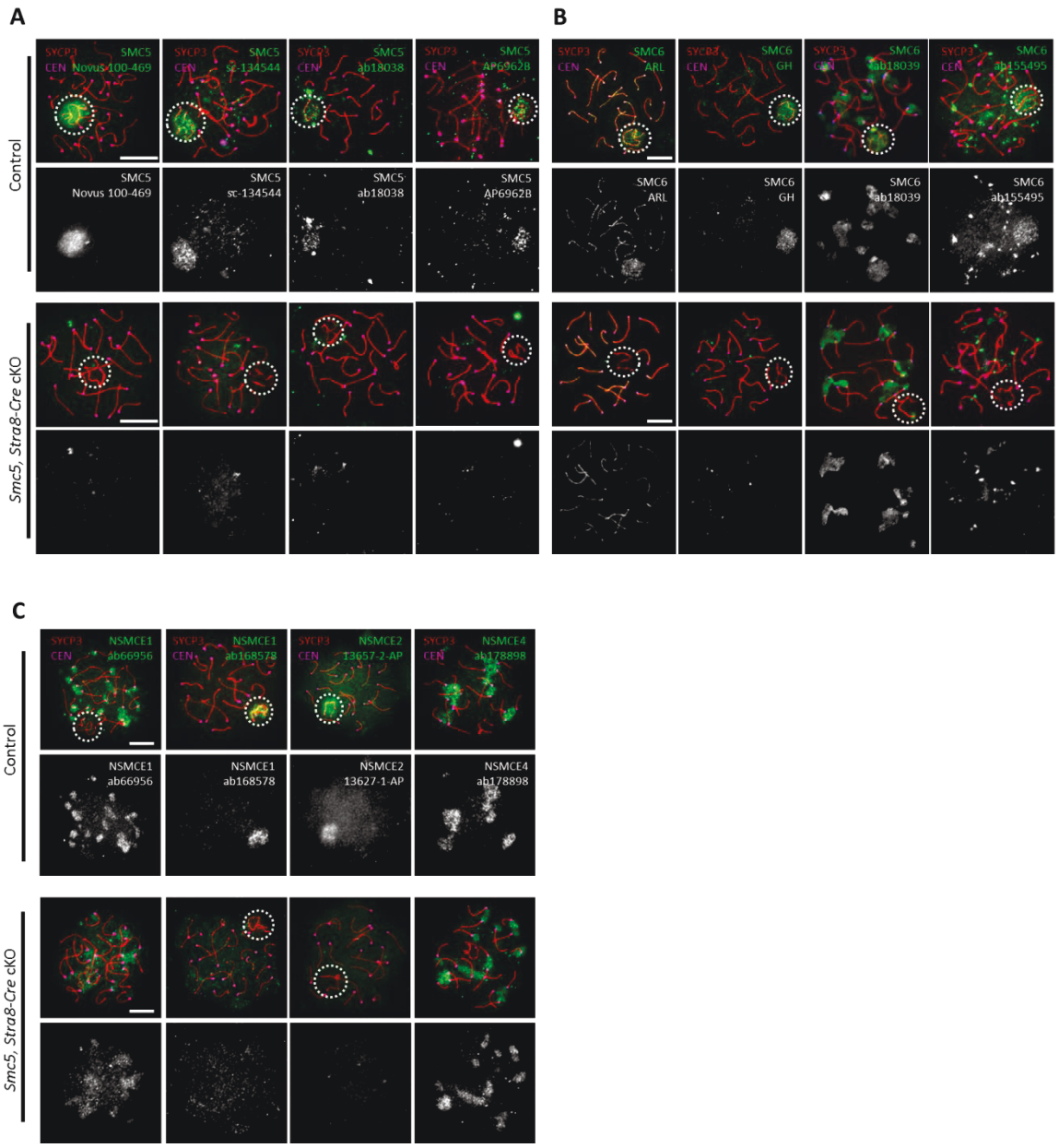
A
B
C
Control
Smc5, Stra8-Cre cKO
SYCP3
CEN
SMC5
Novus 100-469
sc-134544
ab18038
AP6962B
SMC6
ARL
GH
ab18039
ab155495
NSMCE1
ab66956
ab168578
NSMCE2
13627-1-AP
NSMCE4
ab178898

Supplemental Figure 4.2: *Smc5 flox/del, Spo11-Cre* or *Smc5 flox/del, Hspa2-Cre* cKO mice did not show a difference in testis weight compared to controls. (**A**) Testis of adult control (*Smc5 +/flox, Spo11-cre*$^{tg/0}$) and *Smc5* cKO (*Smc5 flox/del, Spo11-cre*$^{tg/0}$) mice. (**B**) Assessment of testis to body rate ratio (mg/mg) of adult control (n=4, mean= 0.39) and *Smc5* cKO (*Spo11-Cre*) (n=4, mean= 0.40) mice. Bars indicate average and standard error. The *P* value (Mann-Whitney, two-tailed) for the indicated comparison is not significant (n.s.). (**C**) Examples of tubule cross sections of testes from adult control and *Smc5* cKO (*Spo11-Cre*) mice stained with hematoxylin and eosin. *Smc5* cKO (*Spo11-Cre*) tubules are indistinguishable from controls. Scale bar: 500 μm. (**D**) Testis of adult control (*Smc5 +/flox, Hspa2-cre*$^{tg/0}$) and *Smc5* cKO (*Smc5 flox/del, Hspa2-cre*$^{tg/0}$) mice. (**E**) Assessment of testis to body rate ratio (mg/mg) of adult control (n= 8, average= 0.35) and *Smc5* cKO (*Hspa2-Cre*) (n=6, average= 0.33) mice. Bars indicate average and standard error. The *P* value (Mann-Whitney, two-tailed) for the indicated comparison is not significant (n.s.). (**F**) Examples of tubule cross sections of testes from adult control and *Smc5* cKO (*Hspa2-Cre*) mice stained with hematoxylin and eosin. *Smc5* cKO (*Hspa2-Cre*) tubules are indistinguishable from controls. Scale bar: 500 μm.

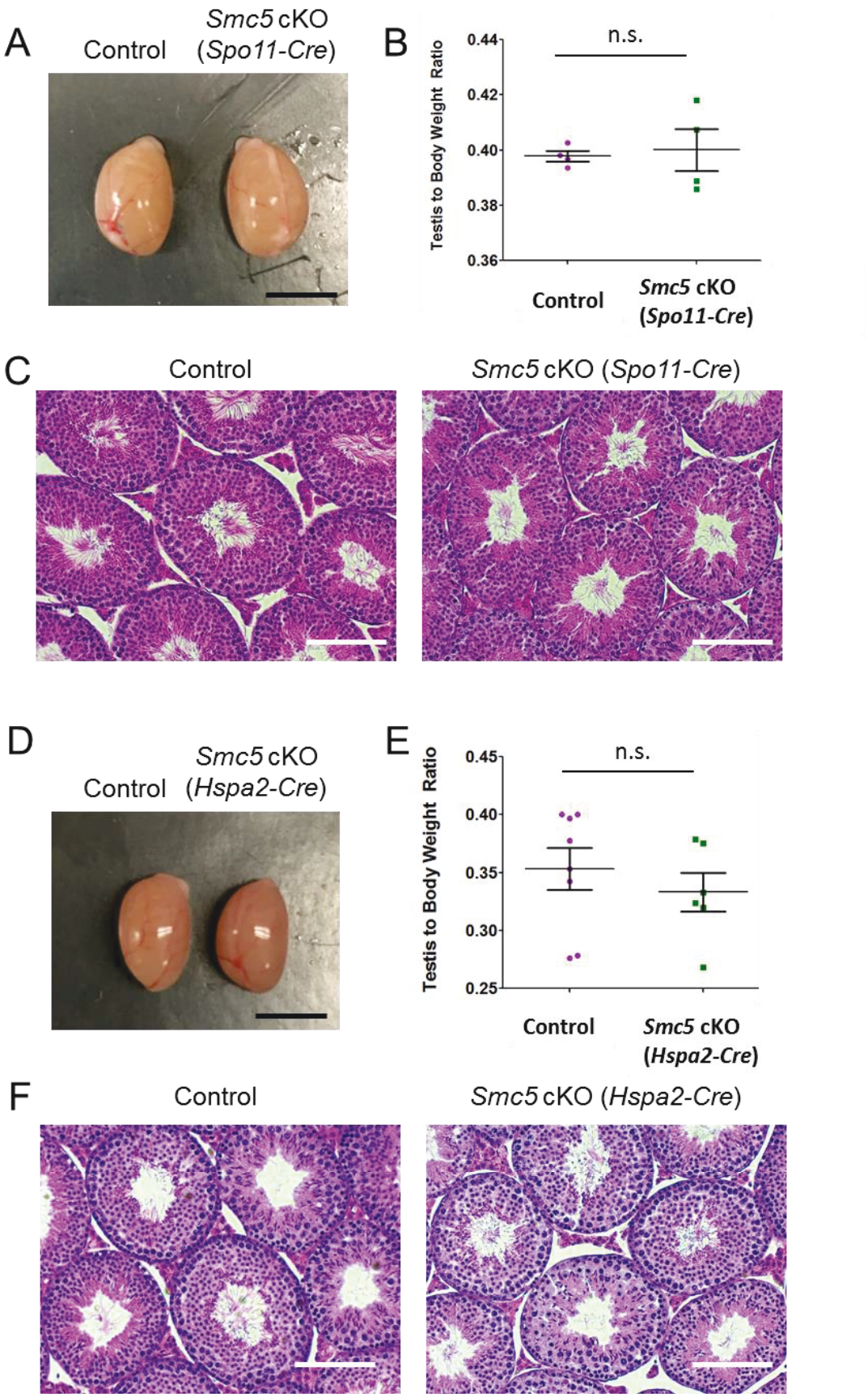
A
Control
Smc5 cKO
(Spo11-Cre)
B
n.s.
Testis to Body Weight Ratio
0.44
0.42
0.40
0.38
0.36
Control
Smc5 cKO
(Spo11-Cre)
C
Control
Smc5 cKO (Spo11-Cre)
D
Control
Smc5 cKO
(Hspa2-Cre)
E
n.s.
Testis to Body Weight Ratio
0.45
0.40
0.35
0.30
0.25
Control
Smc5 cKO
(Hspa2-Cre)
F
Control
Smc5 cKO (Hspa2-Cre)

Figure 4.3. Conditional mutation of *Smc5* via Stra8-Cre results in depletion of pre-leptotene spermatocytes. (**A**) Testis of adult control and *Smc5* cKO (*Stra8-Cre*) mice. (B) Assessment of adult testis to body weight ratio (mg/mg), whereby *Smc5* cKO (*Stra8-Cre*) (n=7, mean=0.31) ratios are decreased compared to control (n=11, mean= 0.36). Bars indicate mean and standard error. The *P* value (Mann-Whitney, two-tailed) for the indicated comparison is significant, $P<0.05$ (*). (**C**) Bar graph assessing average tubule diameter found in control (205.8 μm) and *Smc5* cKO (179.1 μm) testes with bars indicating standard error. The *P* value (Mann-Whitney, two-tailed) for the indicated comparison is significant, $P<0.0001$ (***). (**D**) Tubule cross sections of testes from adult control and *Smc5* cKO mice stained with hematoxylin and eosin. The three cross sections displayed for *Smc5* cKO demonstrate the varied tubule morphology observed. Scale bar: 50 μm. (**E**) Periodic acid-Schiff staining of tubule cross sections from control and *Smc5* cKO testes. Black arrows mark pre-leptotene spermatocytes that are missing in *Smc5* cKO mice. Scale bar: 50 μm. (**F**) Periodic acid-Schiff staining of tubule cross sections from control and *Smc5* cKO testes. Undifferentiated spermatogonia (brown) were detected using an antibody against LIN28. Scale bar: 50 μm. (**G**) Hematoxylin and eosin staining of tubule cross sections from adult control and *Smc5* cKO mice testes. Actively replicating, pre-meiotic cells are marked with PCNA (brown). Scale bar: 50 μm. (**H**) Scatter dot-plot graph showing the reduction of PCNA positive cells per tubule cross section in adult *Smc5* cKO (n=78, mean= 32.9) compared to control (n=66, mean= 48) testes. Bars indicate mean and standard error. The *P* value (Mann-Whitney, two-tailed) for the indicated comparison is significant, $P<0.0001$ (***). (**I**) Graph showing increased counts of TUNEL positive (apoptotic) cells per tubule in adult *Smc5* cKO testes compared to control. The *P* value (Mann-Whitney, two-tailed) for the indicated comparison is significant, $P<0.0001$ (***).

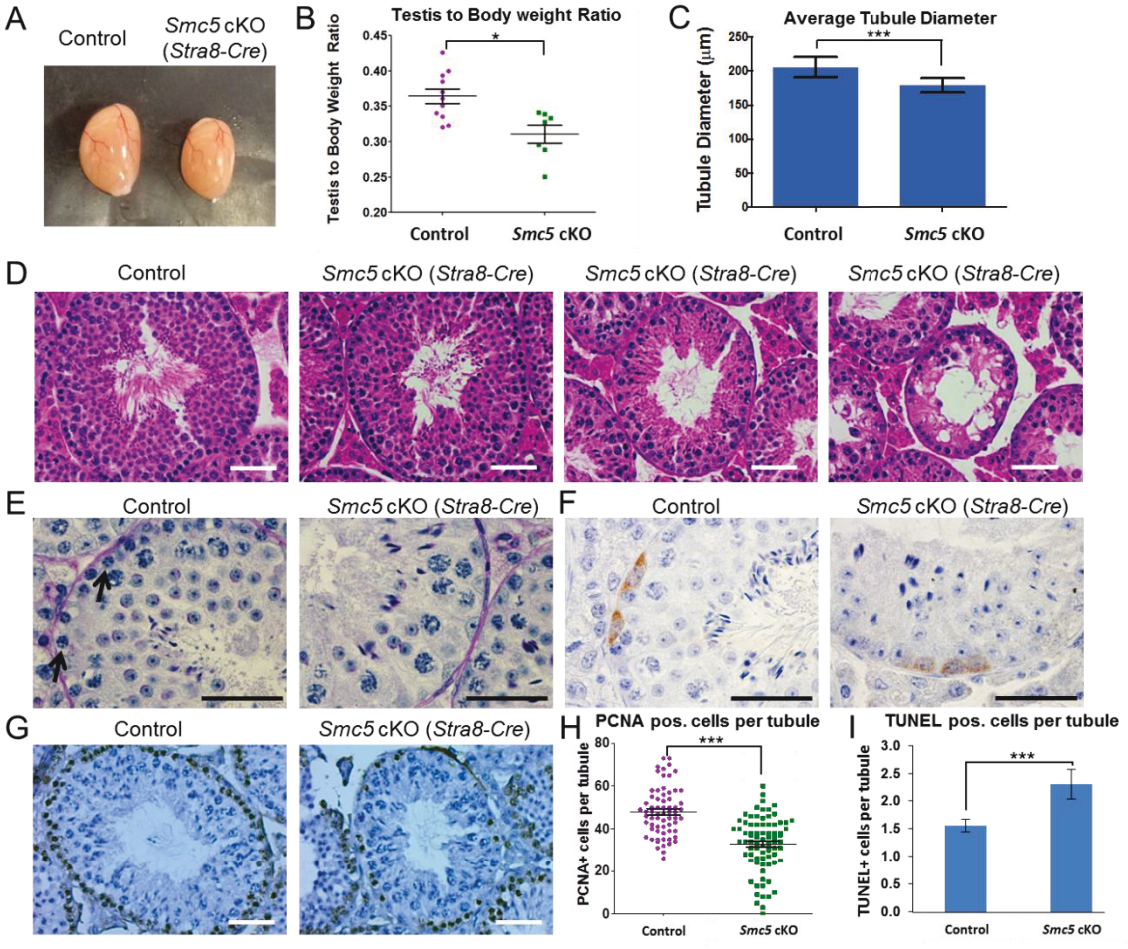
A
Control
Smc5 cKO (Stra8-Cre)
B
Testis to Body weight Ratio
Testis to Body Weight Ratio
0.45
0.40
0.35
0.30
0.25
0.20
*
Control
Smc5 cKO
C
Average Tubule Diameter
Tubule Diameter (μm)
250
200
150
100
50
0
***
Control
Smc5 cKO
D
Control
Smc5 cKO (Stra8-Cre)
Smc5 cKO (Stra8-Cre)
Smc5 cKO (Stra8-Cre)
E
Control
Smc5 cKO (Stra8-Cre)
F
Control
Smc5 cKO (Stra8-Cre)
G
Control
Smc5 cKO (Stra8-Cre)
H
PCNA pos. cells per tubule
PCNA+ cells per tubule
80
60
40
20
0
***
Control
Smc5 cKO
I
TUNEL pos. cells per tubule
TUNEL+ cells per tubule
3.0
2.5
2.0
1.5
1.0
0.5
0.0
***
Control
Smc5 cKO

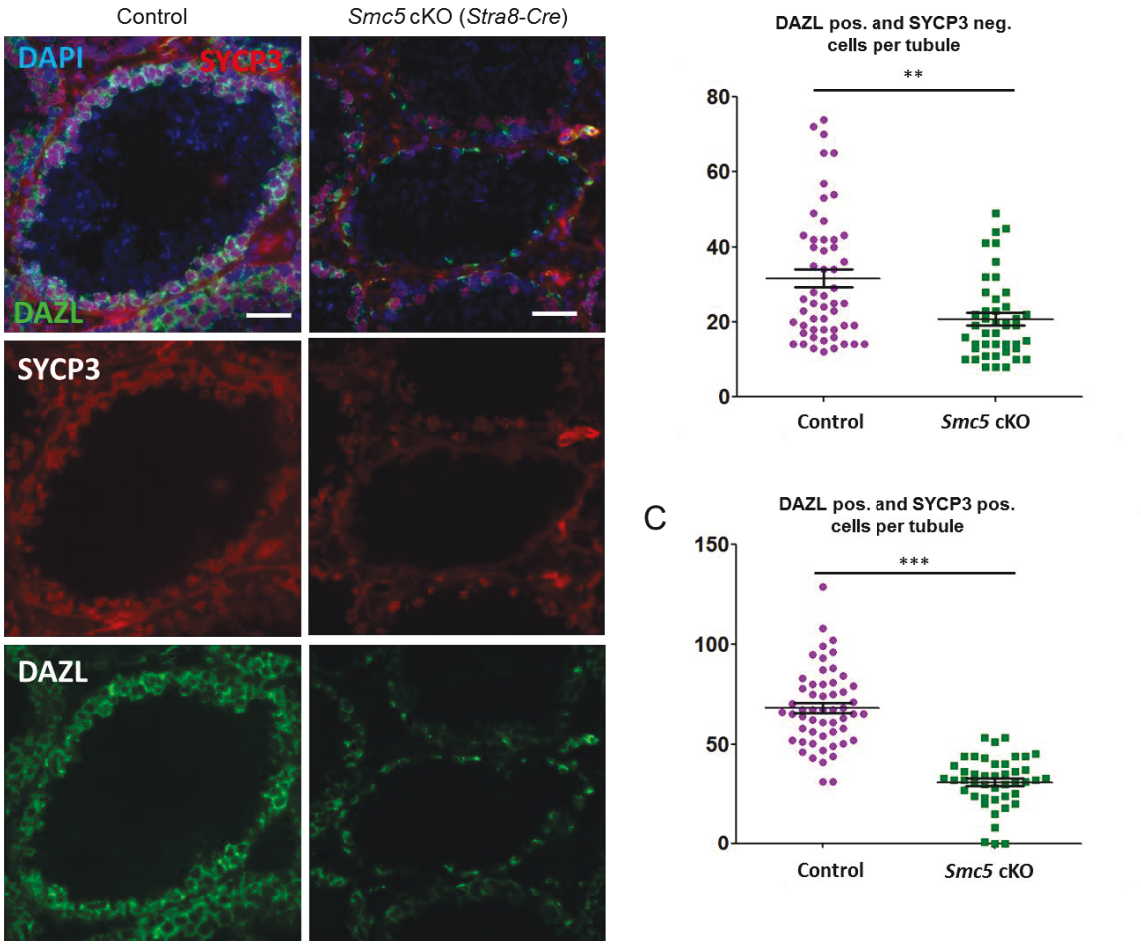

Supplemental Figure 4.3: *Smc5 flox/del*, *Stra8-Cre*$^{tg/0}$ mutants display decrease in pre-leptotene spermatocytes compared to the control. (**A**) Examples of tubule cross sections of testes from adult control and *Smc5* cKO (*Stra8-Cre*) mice immunolabeled with antibodies against the SC lateral element protein SYCP3 (red), and DAZL (nucleus of spermatogonia, green) and counterstained with DAPI (DNA, blue). Scale bar: 50 μm. (**B**) Scatter dot-plot graph showing decreased DAZL positive and SYCP3 negative cells per tubule in adult *Smc5* cKO (n=46, mean= 20.50) compared to control (n=53, mean= 31.62). Bars indicate mean and standard error. The *P* value (Mann-Whitney, two-tailed) for the indicated comparison is significant, $P<0.0005$ (**). (**C**) Scatter dot-plot graph showing decreased DAZL positive and SYCP3 positive cells per tubule in adult *Smc5* cKO (n=44, mean= 30.84). compared to control (n=54, mean= 68.15). Bars indicate mean and standard error. The *P* value (Mann-Whitney, two-tailed) for the indicated comparison is significant, $P<0.0001$ (***).

spermatogonia and pre-leptotene spermatocytes from prophase I stages of spermatogenesis. The *Smc5 flox/del*, *Stra8-Cre* cKO displayed a decrease in DAZL positive, SYCP3 negative cells and, consequently, this decrease appeared even greater in the DAZL and SYCP3 positive prophase I cells (**Fig. S4.3**). To complement these data, we also assessed tubule cross sections of juvenile mice undergoing the first wave of spermatogenesis. These analyses showed depletion of germ cells, increased apoptosis (via TUNEL staining), and decreased PCNA positive cells per tubule in *Smc5 flox/del*, *Stra8-Cre* cKO mice (**Fig. 4.4A-C**).

We hypothesized that the subset of pre-leptotene stage spermatocytes are undergoing apoptosis due to spontaneous errors during pre-meiotic DNA replication. However, pre-lepotene stage spermatocytes are difficult to isolate for culture to enable assessment of DNA replication errors. Therefore, we decided to complement our observations using immortalized mouse embryonic fibroblasts (MEFs), which allow for 4-OH tamoxifen-induced conditional mutation of *Smc5* (**Fig. 4.5A,B**). We reasoned that if SMC5/6 is required for DNA replication fork stability, then cells depleted for SMC5/6 would be sensitive to replication perturbation. We treated cultured MEFs in the presence of hydroxyurea, which impedes DNA synthesis by depleting dNTPs via inhibition of ribonucleotide reductase (Yarbro, 1992). We determined that hydroxyurea treatment, following the depletion of SMC5/6, results in increased numbers of micronuclei, DNA bridges and lagging chromosomes (**Fig. 4.5 C-E**). In yeast, it has been shown that absence of the SMC5/6 complex can lead to replication fork instability, inefficient replication restart and formation of aberrant recombination intermediates (Murray and Carr, 2008). Therefore, we counted RAD51 foci to indicate the number of recombination

events per cell. Depletion of SMC5/6 was correlated to increased RAD51 foci, suggesting that replication fork collapse and recombination intermediates occurred more predominantly in the *Smc5* cKO MEFs compared to controls (**Fig. 4.5F and G**).

Conditional mutation of Smc5 does not result in abnormal meiotic progression in mouse

Although we see loss of a subset of pre-leptotene stage primary spermatocytes in *Smc5 flox/del*, *Stra8-Cre* cKO mice, there are elongated spermatids in the testes, and the mice are fertile, producing in viable progeny (**Fig. 4.3, Table 4.1**). Because meiotic recombination and chromosome segregation defects have been reported for SMC5/6 mutant yeast and worms, we assessed meiotic progression in our *Smc5* cKO mutants (Wehrkamp-Richter et al., 2012a, Copsey et al., 2013a, Xaver et al., 2013, Bickel et al., 2010, Hong et al., 2016). The distribution of meiotic prophase stages analyzed was not different between the *Smc5 flox/del*, *Stra8-Cre* cKO and control (**Fig. 4.6A,B**). SC morphology and SC disassembly, together with sex body formation in the *Smc5 flox/del*, *Stra8-Cre* cKO were equivalent to the control (**Fig. 4.6A, Fig. S4.4**). We did not observe any defects with respect to DNA repair as assessed by yH2AX staining (**Fig. 4.6A**). We analyzed RAD51/DMC1 foci at pachytene stage and determined that the numbers were comparable between the control and cKO mice, including on the X-Y chromosome axes (**Fig. 4.6C-F**). Assessment of MLH1 foci indicated that there was no alteration in CO frequency (**Fig. 4.6G, H**). Additionally, there was no morphological differences between metaphase I chromosomes from *Smc5 flox/del*, *Stra8-Cre* cKO or control spermatocytes (**Fig. 4.6I**). The SMC5/6 complex colocalizes with TOP2A at the pericentromeric heterochromatin and centromere during prophase I and the meiotic divisions, respectively

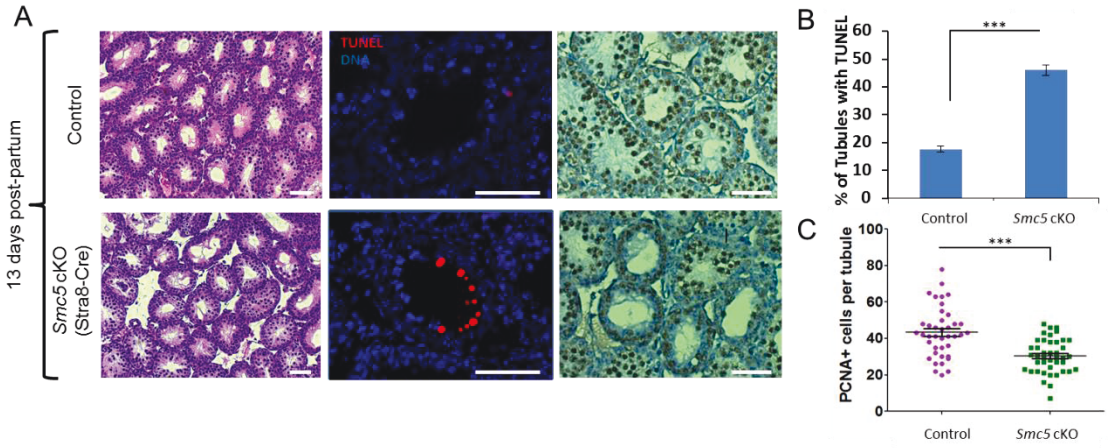

Figure 4.4. *Smc5* cKO juvenile mice, undergoing the first wave of spermatogenesis, show pre-meiotic cell defects. (**A-C**) Histological analysis of juvenile (13 days post-partum) control and *Smc5* cKO (*Stra8-Cre*) testes. (**A**) Tubule cross sections stained with hematoxylin and eosin (first panel), TUNEL and DAPI (second panel, red and blue, respectively), and hematoxylin and eosin with PCNA (third panel, blue and brown, respectively). Scale bar: 50 μm. (**B**) Bar graph showing increase percentage of TUNEL positive (apoptotic) tubules in juvenile *Smc5* cKO testes compared to control. Bars standard error. The *P* value (Mann-Whitney, two-tailed) for the indicated comparison is significant, P<0.0001 (***). (**C**) Scatter-dot plot graph showing decreased PCNA positive cells per tubule in juvenile *Smc5* cKO (n=42, mean=42) compared to control (n= 40, mean= 43.30) testes. Bars indicate mean and standard error. The *P* value (Mann-Whitney, two-tailed) for the indicated comparison is significant, *P*<0.0001 (***).

Figure 4.5. Conditional mutation of *Smc5* in MEFs results in hypersensitivity to hydroxyurea and etoposide. (**A**) PCR analysis of *Smc5* cKO (*Smc5 flox/del, Cre-ERT2*) and control (*Smc5 +/flox, Cre-ERT2*) immortalized MEFs showed efficient deletion of floxed DNA fragment. Shown are untreated cells (Unt) and MEFs after 3, 6 and 9 days of 4-OH TAM treatment. **(B**) Western blot analysis revealed efficient depletion of SMC5 and SMC6 in *Smc5* cKO MEFs after 3 days of 4-OH TAM treatment, but not in control MEFs. (**C**) Following 6 days of culture in the presence or absence of 4-OH TAM (TAM), *Smc5* cKO and control MEFs were treated with hydroxyurea for 24 hours. The *Smc5* cKO MEFs treated with 4-OH TAM and hydroxyurea displayed a significant increase of cells containing micronuclei (N = 100 nuclei per condition, repeated 3 times). Based on Chi-square test; P value < 0.0001 (***). (**D**) Examples of DNA morphology observed following hydroxyurea and etoposide treatment. DNA was stained with DAPI, and in one example the cell was also immunolabeled with antibodies for a kinetochore/centromere marker (CEN, red) and alpha-tubulin (α-Tub, green). (**E**) The *Smc5* cKO MEFs treated with 4-OH TAM and hydroxyurea displayed a significant increase of mitotic cells with lagging chromosomes and DNA bridges (N = 100 nuclei per condition, repeated 3 times). Based on paired, two-tailed t-tests, P values < 0.0001 (***) when comparing DNA bridges and lagging chromosomes observed for *Smc5* cKO in the presence of 4-OH TAM to the other three conditions. (**F**) The *Smc5* cKO MEFs treated with 4-OH TAM and hydroxyurea displayed a significant increase in RAD51 foci counts (N = 50 nuclei per condition). Based on Mann-Whitney, two-tailed t-test, P value < 0.0001 (***) when comparing RAD51 foci numbers for *Smc5* cKO in the presence of 4-OH TAM to the other three conditions. (**G**) Example images of RAD51 foci (red) observed following hydroxyurea treatment for *Smc5* cKO and control MEFs in the presence and absence of tamoxifen. DNA was stained with DAPI. (**H**) Following 6 days of culture in the presence or absence of 4-OH TAM (TAM), *Smc5* cKO and control MEFs were treated with etoposide for 12 hours (N = 100 nuclei per condition, repeated 3 times). The *Smc5* cKO MEFs treated with 4-OH TAM and etoposide displayed a significant increase of mitotic catastrophe and nuclear fragmentation. Based on paired, two-tailed t-tests, P values < 0.0001 (***) when comparing mitotic catastrophe and nuclear fragmentation observed for *Smc5* cKO in the presence of 4-OH TAM to the other three conditions.

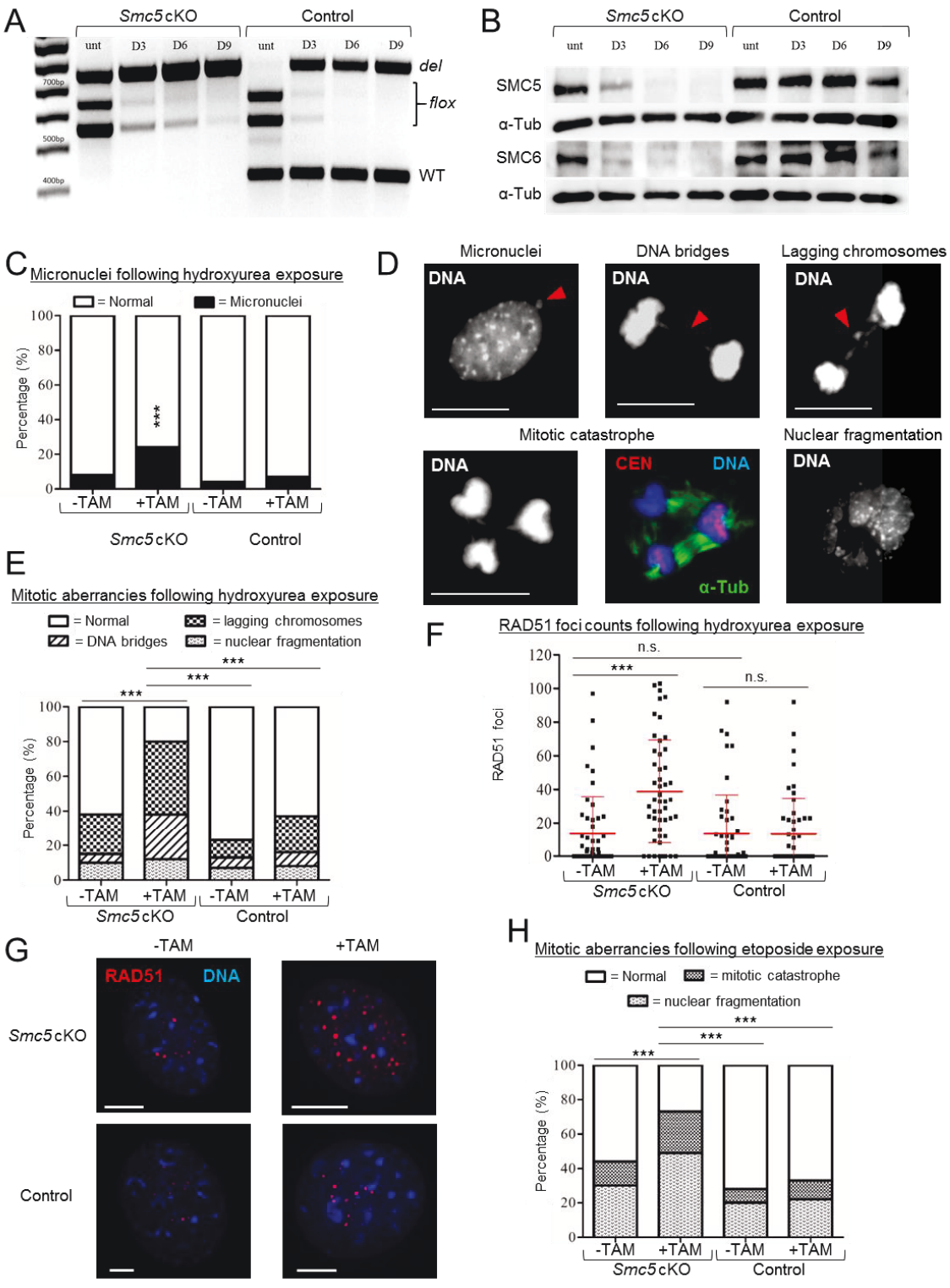
A
Smc5cKO
Control
unt
D3
D6
D9
del
flox
WT
700bp
500bp
400bp
B
SMC5
α-Tub
SMC6
α-Tub
C
Micronuclei following hydroxyurea exposure
= Normal
= Micronuclei
Percentage (%)
***
-TAM
+TAM
Smc5cKO
Control
D
Micronuclei
DNA bridges
Lagging chromosomes
Mitotic catastrophe
Nuclear fragmentation
DNA
CEN
α-Tub
E
Mitotic aberrancies following hydroxyurea exposure
= Normal
= lagging chromosomes
= DNA bridges
= nuclear fragmentation
F
RAD51 foci counts following hydroxyurea exposure
RAD51 foci
n.s.
G
-TAM
+TAM
RAD51
DNA
Smc5cKO
Control
H
Mitotic aberrancies following etoposide exposure
= Normal
= mitotic catastrophe
= nuclear fragmentation

Figure 4.6. Conditional mutation of *Smc5* does not result in abnormal meiotic progression in male mice. (**A-I**) No differences were observed when comparing chromatin spread preparations from juvenile control and *Smc5* cKO (*Stra8-Cre*) germ cells staged at prophase to metaphase I. Scale bar: 10 μm. (A) Chromatin spreads were immunolabeled with antibodies against γH2AX (blue), the SC lateral element protein SYCP3 (red), and the SC central element protein SYCP1 (green). Scale bar: 10 μm. (**B**) Bar graph showing comparable distributions of prophase stages in control and *Smc5* cKO testes. Black bars indicate standard error. The *P* values (Mann-Whitney, two-tailed) for the indicated comparisons are not significant (n.s.). (**C,E,**) Chromatin spread preparations were immunolabeled with antibodies for the SC lateral element protein SYCP3 (red), CEN (kinetochore/centromere marker) and DNA repair proteins RAD51 or DMC1 (green). (**D**) Scatter dot-plot graph showing RAD51 foci counts per cell on the autosomal chromosomes or the XY chromosome of juvenile control mice (n=74, autosomal average=13.22, XY mean= 7.34) and *Smc5* cKO mice (n=75, autosomal mean=15.40, XY average=8.44). Bars indicate mean RAD51 foci number per cell with 95% confidence interval. The *P* values (Mann-Whitney two-tailed test) for the indicated comparisons are not significant (n.s.). (**F**) Scatter dot-plot graph showing DMC1 foci counts per cell on the autosomal chromosomes or the XY chromosome of juvenile control mice (n=18, autosomal mean=21.22, XY mean= 9.22) and *Smc5* cKO mice (n=18, autosomal mean=20.50, XY mean= 8.11). Bars indicate mean DMC1 foci number per cell with 95% confidence interval The *P* values (Mann-Whitney, two-tailed) for the indicated comparisons are not significant (n.s.). (**G**) Chromatin spreads were immunolabeled with antibodies, the SC lateral element protein SYCP3 (red), and the MLH1 (crossover protein, green). (**H**) Scatter dot-plot graph showing no significant difference in the mean number of MLH1 foci per chromosome axis when comparing control (n= 24, mean= 1.16) and *Smc5* cKO (n=25, mean= 1.14) chromosome spread preparations. Bars indicate the average with standard error. The *P* value (Mann-Whitney two-tailed test) for the indicated comparison is not significant (n.s.). (**I**) No differences were observed in chromatin spread preparations of control and *Smc5* cKO (*Stra8-Cre*) germ cells at metaphase I after treatment with okadaic acid. Chromatin spreads were immunolabeled with antibodies against the SC lateral element protein SYCP3 (red), and CEN (kinetochore/centromere marker, blue) and counterstained with DAPI (DNA, blue).

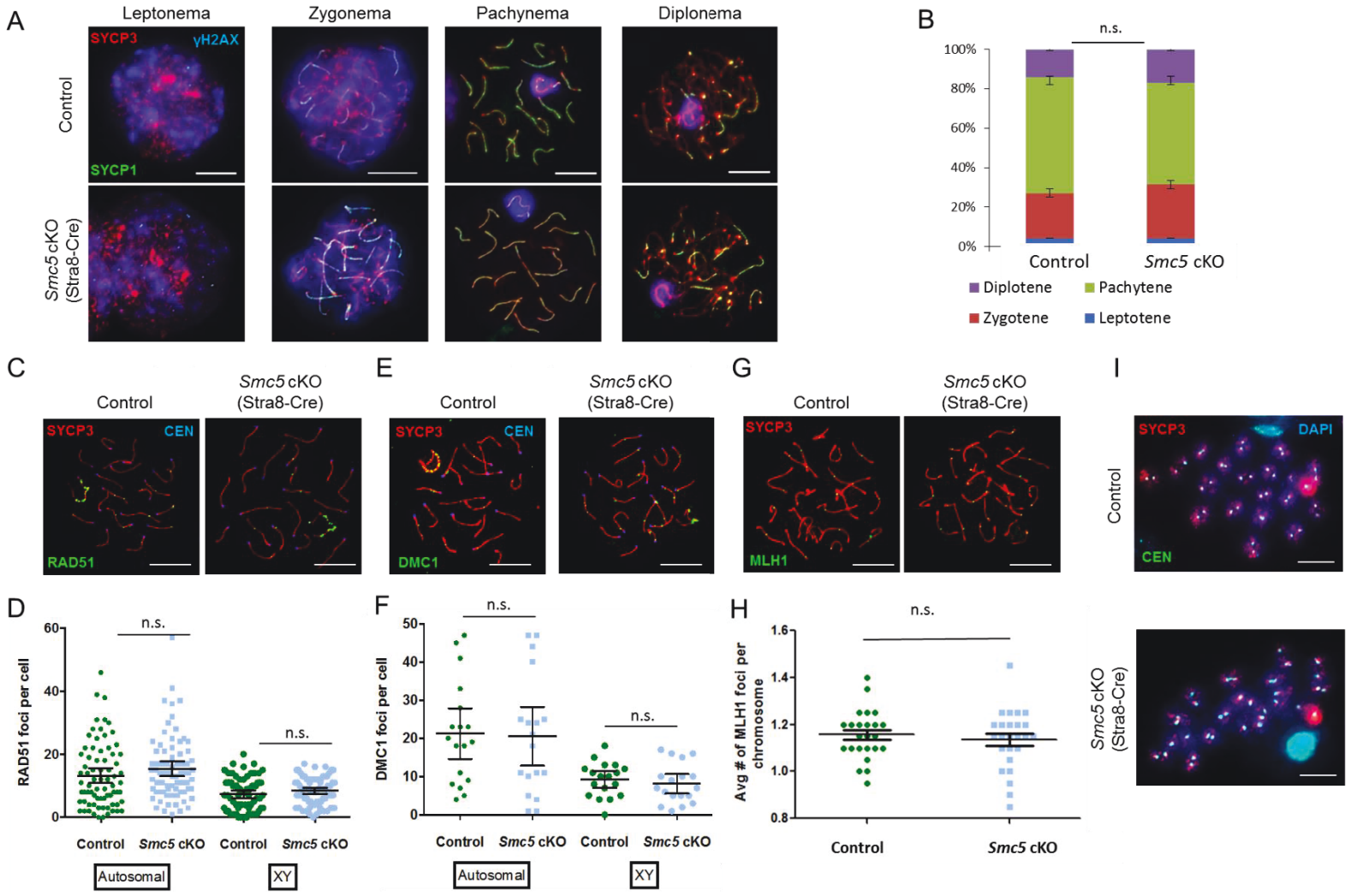
A
Leptonema
Zygonema
Pachynema
Diplonema
SYCP3
γH2AX
SYCP1
Control
Smc5 cKO (Stra8-Cre)
B
n.s.
100%
80%
60%
40%
20%
0%
Control
Smc5 cKO
Diplotene
Pachytene
Zygotene
Leptotene
C
Control
Smc5 cKO (Stra8-Cre)
SYCP3
CEN
RAD51
D
RAD51 foci per cell
n.s.
Control
Smc5 cKO
Autosomal
XY
E
DMC1
F
DMC1 foci per cell
G
MLH1
H
Avg # of MLH1 foci per chromosome
I
DAPI
CEN

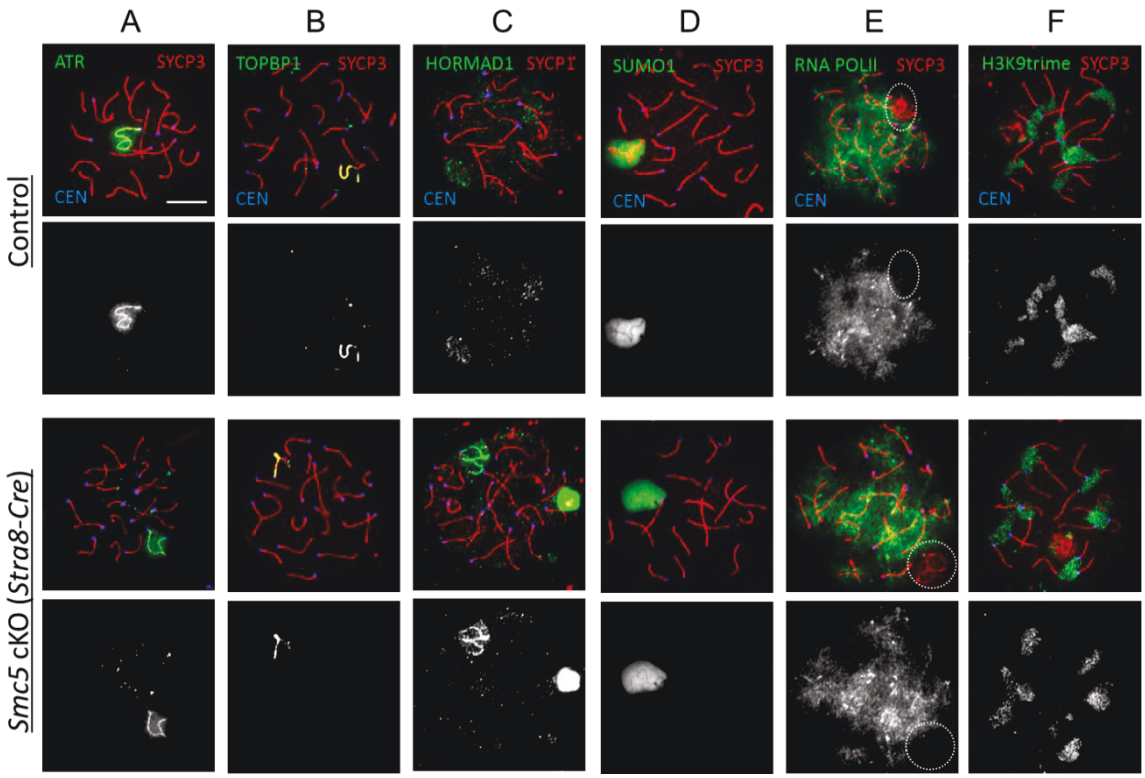

Supplemental Figure 4.4. *Smc5 flox/del*, *Stra8-Cre*$^{tg/0}$ mutants do not have aberrant localization of proteins related to sex body formation and transcriptional silencing. Pachytene stage chromatin spread preparations from control and *Smc5* cKO (*Stra8*-Cre) mice immunolabeled with antibodies against CEN (blue, kinetochore/centromere marker), the SC lateral element protein SYCP3 (red) and proteins required for sex body formation (green) including (**A**) ATR, (**B**) TOPBP1, (**C**) HORMAD1, (**D**) SUMO1, (**E**) RNA polymerase II (RNA POLII), and Histone H3 tri-methyl K9 (H3K9trime). (D) Sex body is circled to show lack of RNA polymerase II signal. All proteins assessed did not show an abnormal localization pattern in *Smc5* cKO chromatin spreads compared to the control. Scale bar: 10 μm.

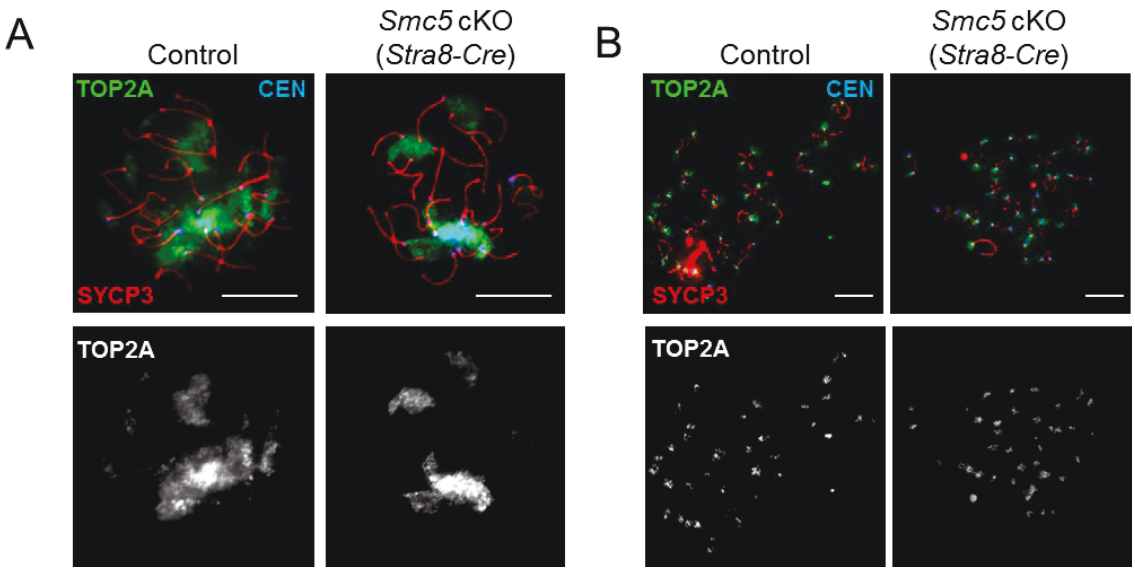

Supplemental Figure 4.5. Conditional mutation of *Smc5* does not perturb topoisomerase IIα localization at the pericentromeric heterochromatin region during meiosis. (**A**) Pachytene stage and (**B**) metaphase I chromatin spread preparations from control and *Smc5* cKO (*Stra8*-Cre) mice immunolabeled with antibodies against CEN (blue, kinetochore/centromere marker), the SC lateral element protein SYCP3 (red), and topoisomerase IIα (TOPOII, green). Scale bar: 10 μm.

(Gomez et al., 2013), reflecting the interaction between TOP2A and SMC5 and SMC6 recently reported (Verver et al., 2016b). We did not observe loss or aberrant TOP2A localization at these regions during meiotic prophase or metaphase in *Smc5 flox/del*, *Stra8-Cre* cKO spermatocytes (**Fig. S4.5**). We also assessed the meiotic prophase and metaphase stages in the *Smc5 flox/del*, *Spo11-Cre* and *Smc5 flox/del*, *Hspa2-Cre* cKO and control and did not observe any defects (data not shown).

Mutation of Smc5 results in increased sensitivity to exogenous DNA damage

Results of siRNA-mediated knockdown and mutation studies using human cell lines reveal that depletion of the SMC5/6 complex leads to increased sensitivity to exogenous DNA damage, such as irradiation and etoposide exposures (Verver et al., 2016b, Payne et al., 2014b, Wu et al., 2012). Therefore, we assessed whether *Smc5* cKO germ cells had elevated abnormalities when exposed to gamma irradiation and etoposide. Ionizing radiation induces a variety of DNA lesions, with DSBs being the most harmful (Dexheimer, 2013). Etoposide binds to the topoisomerase II-DNA complex, which induces the formation of DSBs (Heisig, 2009).

Adult *Smc5 flox/del*, *Stra8-Cre*, *Smc5 flox/del*, *Spo11-Cre* and *Smc5 flox/del*, *Hspa2-Cre* cKO and control mice were irradiated and assessed for defects at 5, 8 and 10 days post-irradiation (**Fig. S4.6**). 5 days post-irradiation, germ cells that were in early pachytene stage (tubule stages I to III) at the time of irradiation will have progressed to late pachytene and diplotene stages, and late pachytene stage germ cells (tubule stages X to XII) will have developed into to round spermatids (Kent and Griswold, 2014, Ventela et al., 2012). At this time point, we did not observe a difference between mutant and

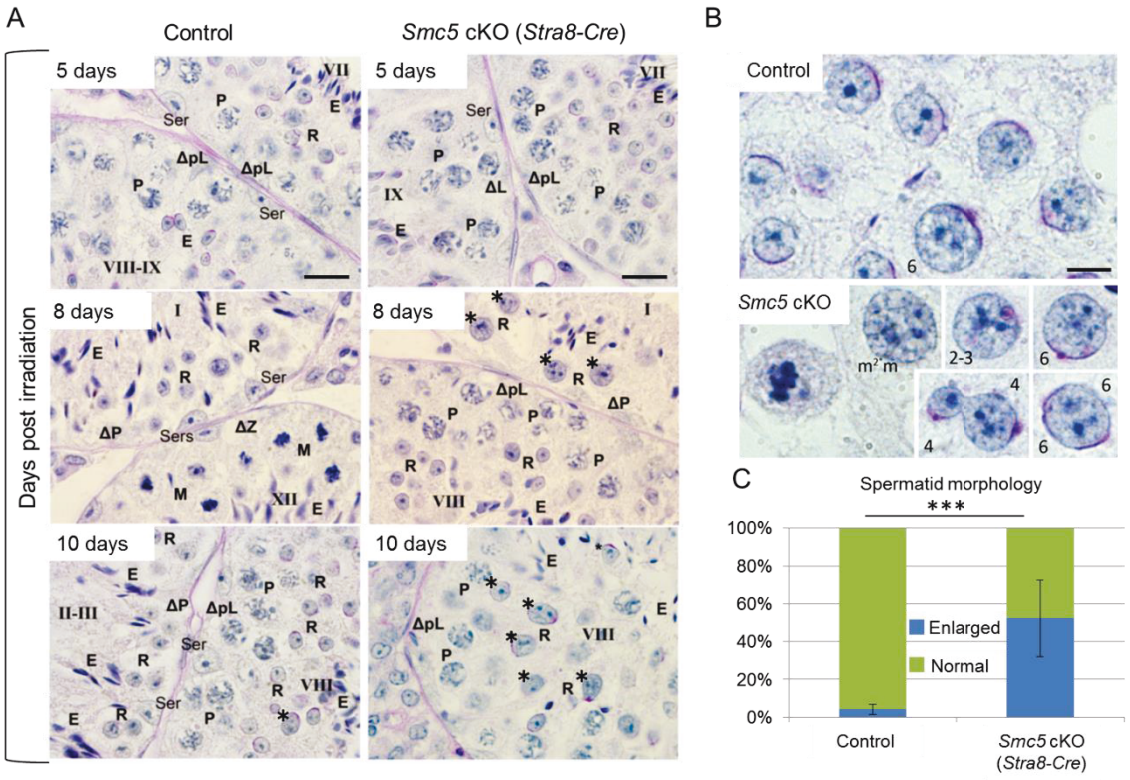

Figure 4.7. Conditional mutation of *Smc5* results in increased sensitivity to exogenous DNA damage, producing abnormal round spermatids. (**A**) Tubule cross sections of adult control and *Smc5* cKO (*Stra8-Cre*) mice testes with periodic acid-schiff staining extracted at 5, 8 or 10 days post-irradiation with 5 gy. Markers: (*) abnormal enlarged spermatids, (P) pachytene stage, (R) round spermatid, (ΔpL) pre-leptotene stage, (ΔL) leptotene stage, (Ser) sertoli cell, (E) elongated spermatids. Roman numerals correspond to the seminiferous tubule stage. *Smc5* cKO cross sections display increased numbers of abnormal enlarged spermatids compared to the controls at 8 and 10 days post-irradiation. Scale bar: 20 μm. (**B**) Magnified images of tubule cross sections for control and *Smc5* cKO testes with Periodic acid-Schiff staining, showing examples of normal and abnormal round spermatids. Round spermatids in *Smc5* cKO testes display an array of abnormalities, such as increase in size, atypical cell shape, and multiple acrosomes. Acrosomes on round spermatids are stained in purple. Numbers indicate stage of round spermatid development. Scale bar: 5 μm (**C**) Bar graph showing significantly increased percentage of spermatids with enlarged morphology in *Smc5* cKO testes (n = 513) compared to the control (n = 2291) 10 days post-irradiation. Bars indicate the average with standard deviation. The *P* value (Mann-Whitney, two-tailed) for the indicated comparison is significant, P<0.0001 (***).

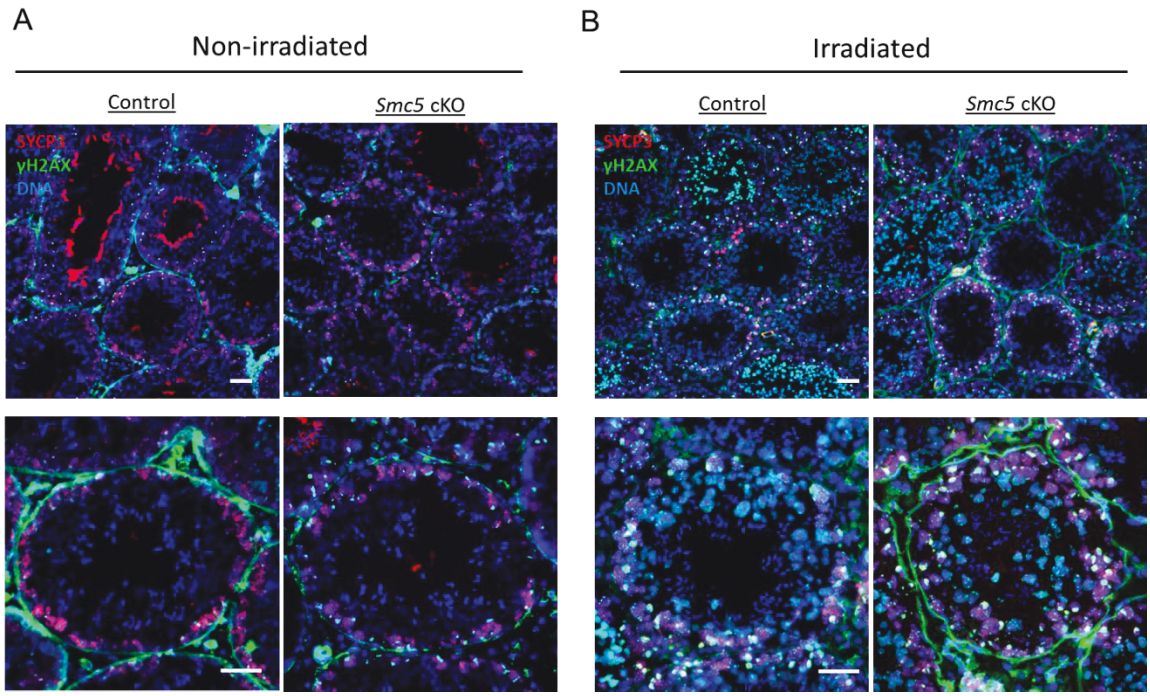

Supplemental Figure 4.6. Whole body γ-irradiation causes DNA damage in control and *Smc5* cKO (*Stra8-Cre*) testes. (**A,B**) Tubule cross sections in testes from control and *Smc5* cKO (*Stra8-Cre*) adult mice that were not irradiated (**A**) and from testes 6 days post whole body γ-irradiation (**B**). Cross sections immunolabeled with antibodies against the SC lateral element protein, SYCP3 (red), γH2AX (green), and counterstaining of chromatin with DAPI (blue, DNA). Magnified images of single tubule in the bottom row. γH2AX, a marker for DNA damage, signal is not exclusive to the sex body in pachytene stage spermatocytes after whole body γ-irradiation in both the control and *Smc5* cKO (*Stra8-Cre*) testes, indicating γ-irradiation caused exogenous DNA damage to tubules. Scale bar: 50 μm.

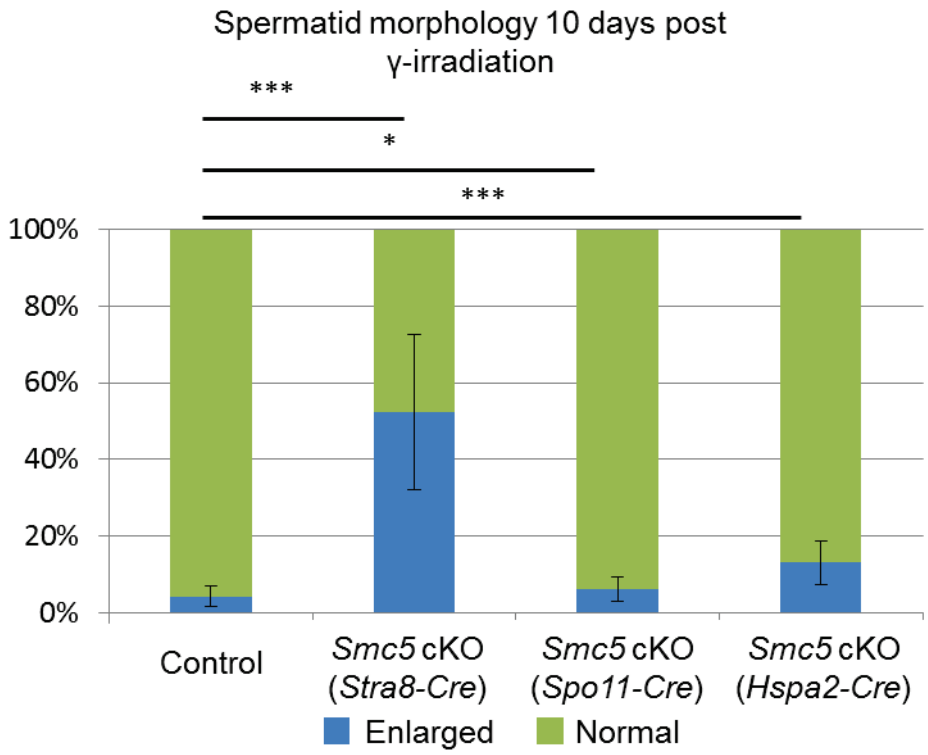

Supplemental Figure 4.7. Conditional mutations of *Smc5* via germ cell specific-Cre recombinases causes increased sensitivity to γ-irradiation resulting in increased spermatids abnormal morphology in tubules compared to control mice. Bar graph assessing the percentage of spermatids with enlarged and normal morphology in control (n=2,291), *Smc5* cKO (*Stra8-Cre*, n=513), Smc5 cKO (*Spo11-Cre*, n=2,408), and *Smc5* cKO (*Hspa2-Cre*, n=1,252) testes 10 days post-irradiation. While all *Smc5* cKO mutants have increased percentages of enlarged spermatids to the controls, *Smc5* cKO (*Stra8-Cre*) mice have the highest percentage, which is likely due to *Stra8-Cre* recombinase being expressed earlier that *Spo11-Cre* and *Hspa2-Cre*. Bars indicate standard error. The *P* values (Mann Whitney two-tailed t test) for the indicated comparisons are significant, $P<0.0001$ (***) and $P<0.05$ (*).

control mice (**Fig. 4.7A**). However, at 10 days post-irradiation, when germ cells that were in early pachytene stage at the time of irradiation have become round spermatids, we observed a marked difference between the *Smc5 flox/del*, *Stra8-Cre* cKO and control. In PAS stained tubule sections we observed more than a 12-fold increase in the number of enlarged round spermatids, commonly with two acrosome structures, a defect indicative of failure to segregate chromosomes during meiosis or cytokinesis failure (**Fig. 4.7, Fig. S4.7**). From analysis of tubule sections from 5, 8 and 10 days post-irradiation, we delineated the stages of spermatocyte development affected by irradiation.

We determined that spermatocytes irradiated at early or mid-pachynema (Stages I to VII) developed into enlarged round spermatids, whereas those irradiated at late pachynema (Stage VIII and beyond) formed normal sized spermatids. We also observed a 2 to 3-fold increase in enlarged spermatids in the *Smc5 flox/del*, *Spo11-Cre* and *Smc5 flox/del*, *Hspa2-Cre* compared to their littermate controls (**Fig. S4.7B**). The reduced effect observed in both of these cKO models is likely due to the timing of *Smc5* mutation, and in the case of the *Spo11-Cre*, reduced excision efficiency (**Table 4.1**).

Most round spermatids from control and *Smc5 flox/del*, *Stra8-Cre* cKO had γH2AX foci colocalizing with DNA 10 days post-irradiation, which indicates that DNA damage remains following meiotic chromosome segregation (**Fig. 4.8A**). However, round spermatids from the control often had a single γH2AX focus (average = 0.92 per nucleus, range = 0-2 foci, N = 61), whereas almost half of the *Smc5 flox/del*, *Stra8-Cre* cKO round spermatids had more than one γH2AX focus (average = 1.7 per nucleus, range = 1-5 foci, N = 52). These observations suggest that DNA damage response and/or repair may be

Figure 4.8. *Smc5* mutants show increased numbers of enlarged round spermatids with supernumerary centromeres after irradiation. (**A**) Tubule cross sections of adult control and *Smc5* cKO (*Stra8-Cre*) testes 10 days post-irradiation, immunolabeled with antibodies against the SC lateral element protein, SYCP3 (red), γH2AX (green), and counterstaining DNA with DAPI (blue, DNA). Scale bar: 50 μm. (**B**) Magnified images of corresponding numbered round spermatids (white squares) from A displaying DNA (DAPI, white) or γH2AX (white) immunostaining. Round spermatids 3 to 6 are enlarged, and spermatids 4-6 display increased γH2AX foci. Scale Bar: 50 μm. (**C**) Example of round spermatids from control and *Smc5* cKO observed 10 days post-irradiation. Spermatids were immunolabeled with an antibody for CEN (kinetochore/centromere marker, red) and stained with Lectin PNA-AF488 conjugate to mark the acrosome (green) and DAPI to detect the DNA (blue). Spermatid DNA is bordered with white dash lines. *Smc5* cKO round spermatid has two groups centromere bodies within one chromatin body and a supernumerary centromere count. Scale bar: 5 μm (**D**) Graph showing counts of CEN (kinetochore/centromere marker) in control and *Smc5* cKO testes 10 days post-irradiation. *Smc5* cKO mice have increased incidences of round spermatids with supernumerary centromere counts. The P value (Mann-Whitney, two-tailed) for the indicated comparisons are significant, $P<0.0001$ (***).

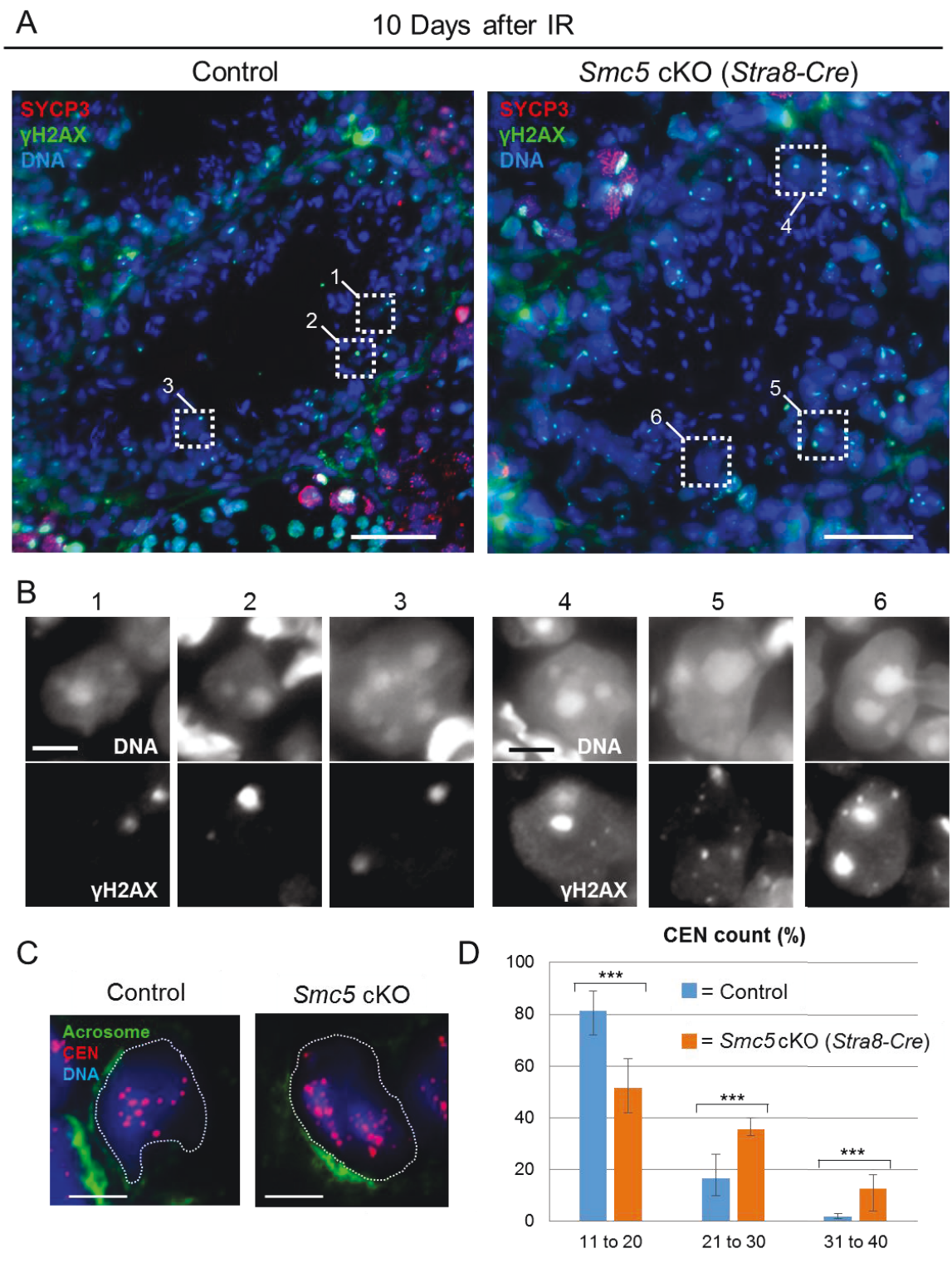
A
10 Days after IR
Control
Smc5 cKO (Stra8-Cre)
SYCP3
γH2AX
DNA
1
2
3
4
5
6
B
DNA
γH2AX
C
Control
Smc5 cKO
Acrosome
CEN
DNA
D
CEN count (%)
100
80
60
40
20
0
= Control
= Smc5 cKO (Stra8-Cre)
***
11 to 20
21 to 30
31 to 40

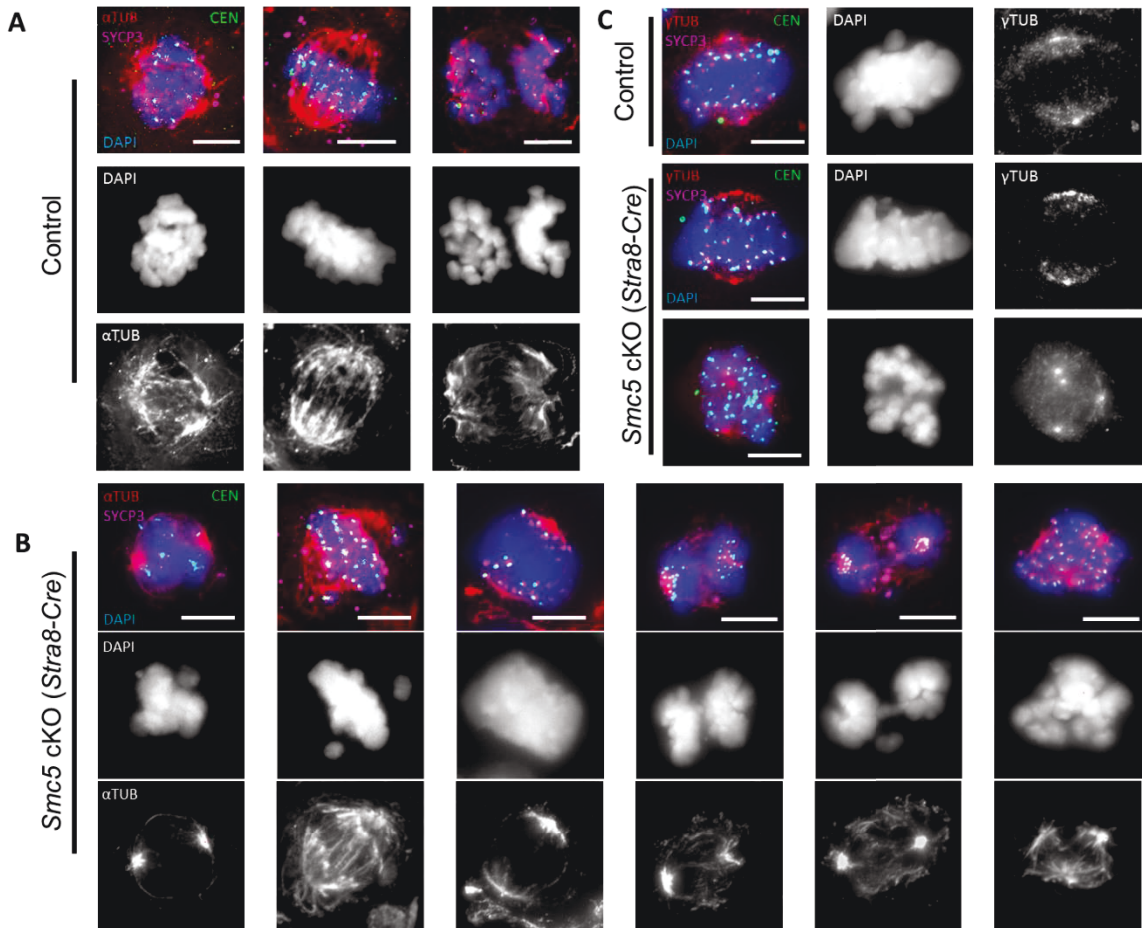

Figure 4.9. Conditional mutation of *Smc5* results abnormal spindle formation and chromosome segregation errors after irradiation. (**A-C**) Immunostaining on tubule squash preparations of primary spermatocytes from control and *Smc5* cKO (*Stra8-Cre*) mice undergoing meiotic chromosome segregation following irradiation. Scale Bar: 10 μm. (**A,B**) Triple-immunolabeling of primary spermatocytes with antibodies against CEN (green, kinetochore/centromere marker), the SC lateral element protein SYCP3 (pink), and α-tubulin (red, α-TUB) and counterstaining of chromatin with DAPI (blue) of germ cells. (**A**). Representative meiotic cells from control mice at metaphase I or undergoing anaphase I. (**B**) Representative meiotic cells from *Smc5* cKO mice at metaphase I or undergoing anaphase I. *Smc5* cKO spermatocytes show a range of chromosome condensation and segregation errors, including lagging chromosomes, tri-polar spindles, and chromosome bridging. (**C**) Triple-immunolabeling of primary spermatocytes with antibodies against CEN (green, kinetochore/centromere marker), the SC lateral element protein SYCP3 (pink), and γ-tubulin (red, γ-TUB) and counterstaining of chromatin with DAPI (blue) of germ cells from control and *Smc5* cKO mice. Majority of *Smc5* cKO spermatocytes show normal bi-polar spindles; however, there are incidences of four spindle poles, indicative of chromosome segregation failure.

aberrant or not as efficient in *Smc5 flox/del*, *Stra8-Cre* cKO spermatocytes compared to the controls.

The *Smc5 flox/del*, *Stra8-Cre* cKO had a significant increase of spermatids with supernumerary chromosome number as assessed by centromere signals (**Fig. 4.8B, C**). To determine whether irradiation of the *Smc5 flox/del*, *Stra8-Cre* cKO results in failure to segregate chromosomes during meiosis or cytokinesis failure, we assessed irradiated juvenile mice that were undergoing the first wave of spermatogenesis. We observed cells from the *Smc5 flox/del*, *Stra8-Cre* cKO with lagging chromosomes, chromosome bridges, tri- or tetra-polar spindles, and abnormal chromosome condensation (**Fig. 4.9A-C**). This suggests that the enlarged spermatids observed in the *Smc5 flox/del*, *Stra8-Cre* cKO following irradiation are due to an inability to segregate their chromosomes during meiosis.

Previous reports have shown that mutation of SMC5/6 components causes sensitivity to etoposide, and SMC5/6 colocalizes and interacts with topoisomerase Iiα (Gomez et al., 2013, Verver et al., 2016b). To determine whether the mutant germ cells were also susceptible to etoposide adult *Smc5 flox/del*, *Stra8-Cre* cKO and control mice were injected with etoposide and assessed for defects 3, 5, 8, and 10 days post-injection (**Fig. 4.10**). Etoposide exposure caused a similar phenotype as irradiation. Following 8 days of exposure an increase in enlarged spermatids, often had two acrosomes, were observed. This was complemented by our observations using the *Smc5* cKO MEFs. We observed an enhanced sensitivity to etoposide when comparing the *Smc5* cKO MEFs to controls, which resulted in increased mitotic catastrophe and nuclear fragmentation (**Fig. 4.5H**).

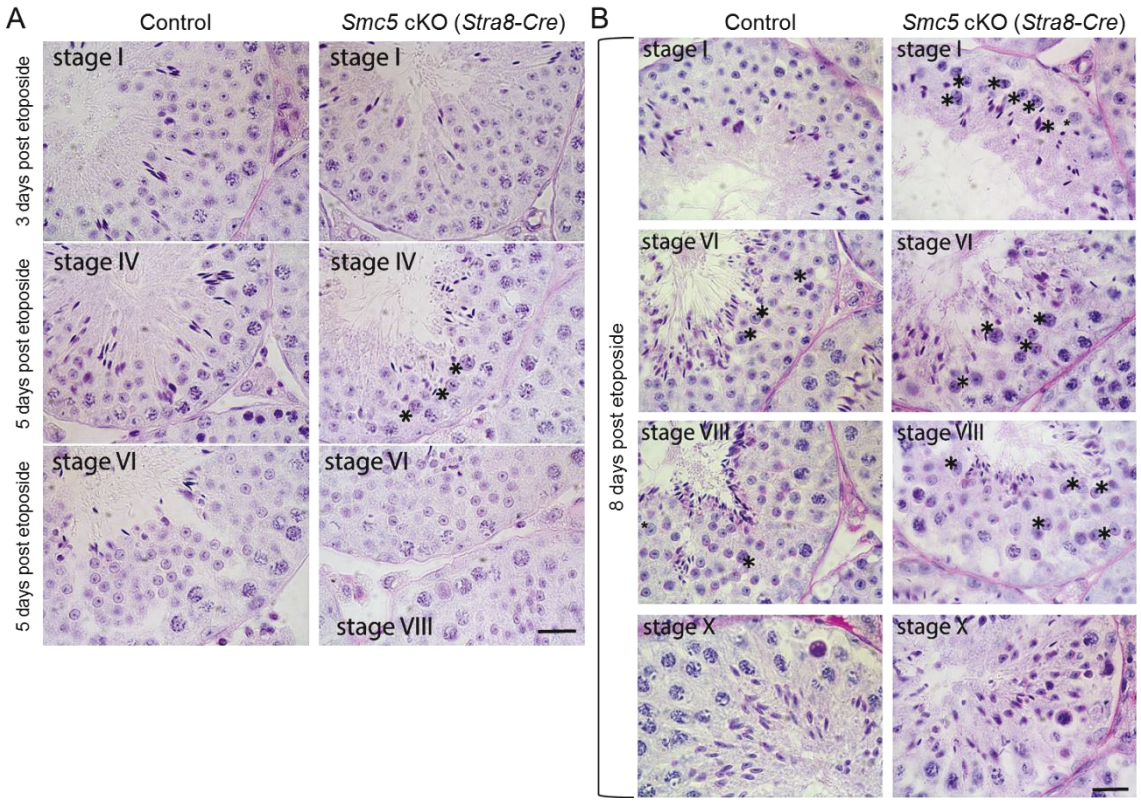

Figure 4.10. Conditional mutation of *Smc5* results in increased sensitivity to etoposide, producing similar phenotype as irradiation. (A-B) Periodic acid-Schiff stained tubule cross sections of adult control and *Smc5* cKO (*Stra8-Cre*) testes extracted at 3, 5, or 8 days post-exposure to etoposide. Smc5 cKO testes have increased numbers of abnormal enlarged round spermatids (*). Roman numerals correspond to the seminiferous tubule stage. Scale bar 20 μm.

Discussion

SMC5/6 – role in pre-meiotic DNA replication

Based on our analysis of the *Smc5 flox/del*, *Stra8-Cre* cKO, we observe germ cell loss at the pre-leptotene stage. These cells are undergoing pre-meiotic DNA replication, and we propose that the SMC5/6 complex is required to ensure genomic integrity during this process. Depletion of the SMC5/6 complex has been shown to hinder DNA replication progression in human RPE-1 cells (Gallego-Paez et al., 2014, Bermudez-Lopez et al., 2010). Upon siRNA-mediated knockdown of Smc5 or Smc6, DNA replication in RPE-1 cells progresses at a much slower rate, with a concomitant generation of replication-related DNA damage. As only a subset of pre-leptotene stage spermatocytes are affected in the *Smc5 flox/del*, *Stra8-Cre* cKO, we predict that the SMC5/6 complex is particularly important when DNA replication processes are hindered in some way, such as a replication fork collapse. This hypothesis is supported by our analysis of *Smc5* cKO MEFs (**Fig. 4.5A-G**), and research using mutant yeast and human cell lines (Payne et al., 2014b, Bermudez-Lopez et al., 2010, Branzei et al., 2006, Ampatzidou et al., 2006).

SMC5/6 – is not essential for meiosis during mammalian spermatogenesis

Previous studies using yeast and worms implicate the SMC5/6 complex as important for mediating meiotic recombination events (Wehrkamp-Richter et al., 2012a, Copsey et al., 2013a, Xaver et al., 2013, Lilienthal et al., 2013a, Bickel et al., 2010, Hong et al., 2016). Therefore, it was unexpected to find no evidence that the SMC5/6 complex is required for mouse spermatogenesis and male fertility. Although one concern could be

that mutation of the floxed *Smc5* allele was not efficient, genotyping data indicated that both *Stra8-Cre* and *Hspa2-Cre* were close to 100% efficiency in excision. The *Spo11-Cre* was less efficient, but even so a mosaic meiotic phenotype would be expected. Furthermore, in purified primary spermatocytes and round spermatids, we confirmed the efficiency of *Smc5* excision via PCR, as well as observed almost complete depletion of the SMC5 protein, and substantial loss of other SMC5/6 components. Despite the efficiency of the *Stra8-Cre*, we do not observe defects in meiotic prophase I events including DNA damage repair, SC formation, crossover levels, sex body formation or chiasmata morphology. We cannot exclude that the residual levels of the SMC5/6 complex that remain following Cre mediated mutation of *Smc5* are sufficient to allow proficient progression of spermatogenesis. This is supported by still observing SMC5/6 components localizing on the chromatin of pachytene stage spermatocytes in the the *Smc5 flox/del*, *Stra8-Cre* cKO. In these experiments we observe the loss of SMC5/6 components on the sex body, but signal remains enriched on the pericentromeric heterochromatin. SMC5/6 is already present on the pericentromeric heterochromatin in differentiating spermatogonia, and it is possible that the SMC5/6 complex in these regions remains stable throughout spermatogenesis (Verver et al., 2013b). For example, it has been shown that the SMC5/6 and cohesin complexes remain stably associated with chromatin for months following their loading during oogenesis (Hwang et al., 2017, Burkhardt et al., 2016). Despite the loss of SMC5/6 components at the sex body, following mutation of *Smc5*, we do not observe impairment of meiotic sex chromosome inactivation or any other meiotic defects. Therefore, we can conclude that following cKO

of *Smc5* via Stra8-Cre mediated excision, *Smc5* expression during spermatogenesis is not essential for fertility in male mice.

SMC5/6 – is important for maintaining spermatocyte genome integrity following exogenous DNA damage

As we did not observe a defect in the progression of meiosis in our *Smc5* cKO models, we proposed that the SMC5/6 complex is not required for meiosis during spermatogenesis, unless DNA processing events are perturbed. To test this hypothesis, we used gamma irradiation and etoposide as a source to sensitize cells with DNA damage. Interestingly, we determined that spermatocytes staged at early and mid pachynema at the time of treatment were affected by irradiation and etoposide exposure, causing the formation of enlarged round spermatids, which had two acrosomes and supernumerary chromosome content. In contrast, the late pachytene stage spermatocytes were not affected by irradiation, and formed normal spermatids. This distinction between the earlier and later stages of pachynema could be explained by differing DNA template preference during DNA repair. At early to mid-pachytene stage, there is a mechanism that biases towards inter-homolog recombination over inter-sister recombination (Wojtasz et al., 2009, Lao and Hunter, 2010). However, this bias is lost during late pachynema, thus facilitating repair of DSBs via inter-sister recombination (Moens et al., 1997, Kauppi et al., 2011). Endogenous DNA damage induced during the earlier stages of pachytene could result in the formation of complex joint molecules, involving multiple chromatids, which cannot be resolved prior to meiotic divisions. Repair of the endogenous DNA damage might be facilitated primarily by inter-sister repair during later

stages of pachytene when homolog bias is relaxed, and this would be more likely to be resolved. In budding yeast, the Smc5/6 complex was demonstrated to be required to inhibit the formation of complex joint molecules, which involve recombination intermediates between sisters and homologs (Copsey et al., 2013a, Xaver et al., 2013). Furthermore, the yeast Smc5/6 complex is required for appropriate loading of the Mus81-Mms4/Eme1 resolvase complex to chromatin, and subsequent resolution of inter-sister and multiple chromatid joint molecules (Wehrkamp-Richter et al., 2012a, Copsey et al., 2013a, Xaver et al., 2013). In mouse, the MUS81-EME1 complex is required for the resolution of approximately 5-10% of crossovers, which cannot be processed as noncrossovers by the BLM helicase (Holloway et al., 2008, Holloway et al., 2011). We attempted to determine whether the localization of the MUS81-EME1 complex in our spermatocytes was affected, however immunostaining was not successful.

We demonstrate that *Smc5* conditional mutants are sensitive to gamma irradiation and etoposide exposure. It has been suggested that the SMC5/6 complex regulates TOP2A-mediated decatenation of intertwined DNA complexes. The SMC5/6 complex colocalizes with TOP2A at the pericentromeric heterochromatin and centromeric regions during pachynema and meiotic divisions, respectively (Gomez et al., 2013). Furthermore, upon treatment with etoposide, SMC5/6 colocalizes with TOP2A on lagging chromosomes during meiosis I (Gomez et al., 2013). It was recently demonstrated that SMC5 physically interacts with TOP2A, using U2OS cells (Verver et al., 2016b). siRNA-mediated depletion of SMC5 and SMC6 in human RPE-1 cells caused mislocalization of TOP2A away from the pericentormeric regions to the chromosome arms (Gallego-Paez et al., 2014). However, similar to the observations of this study, mouse TOP2A loading on

chromosomes during meiosis and mitosis is not dependent on SMC5/6, suggesting a slightly different mechanism (Hwang et al., 2017, Pryzhkova and Jordan, 2016b). Regardless, future work is needed to determine how the SMC5/6 influences TOP2A function.

Conclusion

We have determined that the depletion of the SMC5/6 complex does not lead to meiotic failure during mouse spermatogenesis. However, we do observe a partial loss of pre-meiotic germ cells, suggesting a role in proficient pre-meiotic DNA replication. We also demonstrate that the SMC5/6 complex is important for proficient repair of exogenous DNA damage in primary germ cells. From our data, we propose that the SMC5/6 complex acts as a DNA damage response surveillance complex. When genomic integrity is compromised, the SMC5/6 complex ensures that DNA repair processes are controlled to avoid complex recombination intermediates that would otherwise cause errors during chromosome segregation, and thus, infertility.

Materials and Methods

Animal use and care

Mice were bred by the investigators at The Jackson Laboratory (JAX, Bar Harbor, ME) and Johns Hopkins University (JHU, Baltimore, MD) in accordance with criteria of the National Institutes of Health and U.S. Department of Agriculture. All animal

procedures were conducted with approval from the Institutional Animal Care and Use Committees (IACUC) of The Jackson Laboratory and Johns Hopkins University.

Mice and Husbandry

Creation of mice with the *Smc5 flox* and *Smc5 del* alleles was previously described (Hwang et al., 2017). Heterozygous *Smc5 del* mice were bred to mice with germ cell-specific Cre recombinase transgenes, *Stra8-Cre* (B6.FVB-Tg(Stra8-icre)1Reb/LguJ, Stock No. 017490, JAX), *Spo11-Cre* (Lyndaker et al., 2013) and *Hspa2-Cre* (C57BL/6-Tg(Hspa2-cre)1Eddy/J, Stock No. 008870, JAX), which resulted in progeny heterozygous for the *Smc5 del* allele and hemizygous for the germ cell-specific transgenes. These mice were bred to homozygous *Smc5 flox* mice to derive cKO (*Smc5 flox/del, Germ cell-specific Cre*) and controls (*Smc5 flox/del* and *Smc5 +/flox, Germ cell-specific Cre*) genotypes.

For fertility testing, 8- to 12-week old cKO and control males were singly housed with wild-type C57BL6/J females. Pregnant females were monitored daily, and viable pups were counted on the first day of life. Subsequently, genotyping samples were taken from each pup to determine the efficiency of Cre-mediated excision of the floxed 4th exon of the *Smc5* allele.

MEF derivation and treatments

Heterozygous *Smc5 del* mice were bred to mice harboring the conditional *Cre-ERT2* (B6.129-*Gt(ROSA)26Sortm1(cre/ERT2)Tyj*/J, JAX), which resulted in progeny heterozygous for the *Smc5 del* allele and hemizygous for the *Cre-ERT2* genotype. These

mice were bred to homozygous *Smc5 flox* mice to derive *Smc5* cKO (*Smc5 flox/del, Cre-ERT2*) and control (*Smc5 +/flox, Cre-ERT2*) genotypes. Primary MEFs were obtained from embryos at 13.5 days post-coitum. MEF culture medium consisted of 89% DMEM (Invitrogen), 10% FBS (Hyclone), 1% penicillin/streptomycin (100U/100μg). Standard NIH 3T3 protocol was used for establishing immortal MEF cell lines (Todaro and Green, 1963). The deletion in *Smc5* gene was induced by treating experimental cells with 0.2μM 4-OH tamoxifen (Sigma H7904) (4-OH TAM). 4-OH TAM in cell culture medium was replenished every 2 days. Hydroxyurea and etoposide treatments were performed following 6 days of 4-OH TAM treatment. Replication fork stalling was induced by treating cells with 2mM hydroxyurea (H8627, Sigma) for 24 hours. Cells were treated with 15mM etoposide (E1383, Sigma) for 12 hours, then allowed to recover in MEF culture medium for 12 hours prior to assessment.

Induction of DNA damage via irradiation

Adult mice were irradiated with a single sub-lethal dose (5 Gy) using a 137Cs source (Forand et al., 2004). The mice were monitored daily before their euthanasia 5, 8, and 10 days following irradiation. Juvenile mice at 16 days post-partum were irradiated with a single sub-lethal dose (1.3 Gy) using a 137Cs source (Forand et al., 2004, Hamer et al., 2003). After irradiation, the mice were monitored daily before their euthanasia at 23 days post-partum. Testes were extracted for spermatocyte squash preparation.

Induction of DNA damage via etoposide

For etoposide assessment, adult mice were injected intraperitoneally with a single dose of etoposide (80 mg/kg body weight, Sigma) (Marchetti et al., 2006, Lee et al., 1995). After injection, the mice were monitored daily before their euthanasia at 3, 5, or 8 days after treatment.

Histological analysis and TdT-mediated dUTP nick end labelling (TUNEL) assay

Testes were either fixed in Bouins fixative or cryo-preserved using Tissue-Tek® optimal cutting temperature compound (O.C.T., Sakura Finetek). Fixed tissues were embedded in paraffin and serial sections of 5-micron thickness were placed onto slides and stained with hematoxylin and eosin or Periodic acid-Schiff. For the TUNEL assay, sections were deparaffinized and apoptotic cells were detected using the in situ BrdU-Red DNA fragmentation (TUNEL) assay kit (Abcam) and counterstained with DAPI. Cyropreserved testes were sectioned at a 5-micron thickness in series using a Cryostat (Thermo Scientific CyroStar NX70). Cryopreserved testes were subsequently fixed (1% PFA 0.1% Triton-X in 1x PBS), and subjected to standard immunostaining procedures. Primary antibodies and dilution used are presented in Supplemental Table S1. Secondary antibodies against human, rabbit, rat, mouse and guinea pig IgG and conjugated to Alexa 350, 488, 568 or 633 (Life Technologies) were used at 1:500 dilution.

Mouse germ-cell isolation and culture

Isolation of mixed germ cells from testes was performed using techniques previously described (La Salle et al., 2009, Bellve, 1993). Leptotene/zygotene and pachytene/diplotene stage spermatocytes and round spermatids were enriched using a 2–4% BSA gradient generated in a STA-PUT sedimentation chamber (ProScience Inc.), as previously described (La Salle et al., 2009). Highly enriched pachytene stage spermatocytes (2.5 x 10^6 cells/ml) were cultured for 10 hours at 32°C in 5% CO2 in HEPES (25 mM)-buffered MEMa culture medium (Sigma) supplemented with 25 mM NaHCO3, 5% fetal bovine serum (Atlanta Biologicals), 10 mM sodium lactate, 59 mg/ml penicillin, and 100 mg/ml streptomycin. To initiate the G2/MI transition, cultured pachytene stage spermatocytes were treated with 5 mM okadaic acid (OA; Sigma).

Protein analyses

For protein level analyses, proteins were extracted from germ cells using RIPA buffer (Santa Cruz) containing 1× protease inhibitor cocktail (Roche). Protein concentration was calculated using a BCA protein assay kit (Pierce). Lanes of 4–15% gradient SDS polyacrylamide gels (Bio-Rad) were loaded with 20 µl of 1 mg/ml protein extract. For STA-PUT, 20 µl of 0.1 mg/ml protein extracts from purified leptotene/zygotene and pachytene/diplotene stage spermatocytes and round spermatids were loaded per lane on SDS polyacrylamide gels. Following protein separation via standard SDS PAGE, proteins were transferred to PVDF membranes using the Trans-Blot® Turbo™ western transfer system (Bio-Rad). Primary antibodies and dilution used are presented in Supplemental Table S1. At a 1:5,000 dilution, goat anti-mouse (62-6520)

and goat anti-rabbit (A10533) horseradish peroxidase-conjugated antibodies (Invitrogen) were used as secondary antibodies. The presence of antibodies on the PVDF membranes was detected via treatment with Pierce ECL western blotting substrate (Thermo Scientific) and captured using the Syngene XR5 gel documentation system. Protein levels were assessed using Image J (NIH).

Chromatin spread analyses

Germ cell chromatin spreads were prepared as previously described (Jordan et al., 2012), or with some modifications. Briefly, germ cells were placed in 50% hypotonic buffer (30mM Tris, 50mM sucrose, 17mM trisodium citrate dihydrate, 5mM EDTA, 2.5mM DTT) for 8 minutes. The cells were then resuspended in a second hypotonic buffer (1:1 of PBS and 100μM sucrose). The cell suspension was fixed using 1% PFA on a glass slide for 1 hour in a humid chamber. The slides were air dried for 1 hour, washed in 0.4% Photo-Flo (Kodak) in H_2O overnight, and dried again for 30 minutes. The slides were immunolabelled immediately afterwards. Primary antibodies and dilution used are presented in **Fig. S4.1**. Rat-anti-SMC5 (AP6962B) and rat-anti-NSE4a (AP6962A) antibodies were prepared using peptide sequences, cys-PHMLEPNRWNLKAF and ys-PKPRSDRPRQPRMIE, respectively (Neobiolabs). Secondary antibodies against human, rabbit, rat, mouse and guinea pig IgG and conjugated to Alexa 350, 488, 568 or 633 (Life Technologies) were used at a dilution of 1:500.

Spermatocyte squash preparation

Spermatocyte squashes were performed as previously described (Wellard SR, 2017). Briefly, minced seminiferous tubules from 23 day old male mice were fixed in freshly prepared 2% formaldehyde in 1× PBS containing 0.1% Triton X-100. After 5 min, several seminiferous tubule fragments were placed on a slide and squashed, and the coverslip removed after freezing in liquid nitrogen. Slides were washed with 1× PBS and immunostained immediately afterwards.

Microscopy

Images from chromatin spread, tubule squash and testis cryosection preparations were captured using a Zeiss CellObserver Z1 microscope linked to an ORCA-Flash 4.0 CMOS camera (Hamamatsu). Testis sections stained with hematoxylin and eosin or Periodic Acid and Schiff staining were captured using a Zeiss AxioImager A2 microscope linked to an AxioCam ERc5s camera. Images were analyzed with Zeiss ZEN 2012 blue edition image software including foci and length measurement capabilities. Photoshop (Adobe) was used to prepare figure images.

Acknowledgements

We thank Sakshi Khurana for technical support. We are grateful to Dr. Alan R. Lehmann for an SMC6 antibody, and to Paula Cohen and Mitch Eddy for mice harboring the *Spo11-Cre* mice and *Hspa2-Cre* transgenes, respectively.

Supplemental Table 4.1. Primary antibodies used in this study

Primary Antibodies					
Antibodies	**Host**	**Source**	**Cat. Number**	**IHC Dilution**	**WB Dilution**
ATR	Goat	Santa Cruz	sc-18887	1:50	
CREST (CEN)	Human	Antibodies Incorporated	15-235	1:50	
Histone H3 tri-methyl K9 (H3K9trime)	Mouse	Abcam	ab6001	1:100	
HORMAD1	Rabbit	Abcam	ab155176	1:100	
Lectin PNA-AF488 conjugate	NA	Molecular Probes	L21409	1:700	
LIN28	Rabbit	Abcam	ab46020	1:5000	
MLH1	Mouse	Thermo-Fisher	MA51531	1:100	
NSE1	Rabbit	Abcam	ab66956	1:100	
NSE1	Mouse	Abcam	ab168578	1:50	1:1000
NSE2	Mouse	Novus Biologicals	H00286053-B01		1:500
NSE2	Rabbit	Protein Tech	13627-1-AP	1:50	
NSE4a	Rabbit	Abcam	ab178898	1:100	
NSE4a	Rabbit	NeoBiolab	AP6962A	1:10	
NSE4a	Rabbit	Sigma	HPA037459		1:100
RAD51	Rabbit	Thermo	PA527195	1:100	
RNA Polymerase II (RNA POLII)	Mouse	Millipore	05-623	1:400	
SMC5	Rabbit	GeneTex	GTX115669	1:50	
SMC5	Rabbit	Novus Biologicals	NB100-469	1:100	1:400
SMC5	Rabbit	Abcam	ab18038	1:50	
SMC5	Rabbit	Santa Cruz	sc-134544	1:50	
SMC5	Rat	Neobiolab	AP6962B	1:10	
SMC6	Rabbit	Abcam	ab18039	1:200	
SMC6	Rabbit	Abcam	ab155495	1:100	1:500
SMC6	Guinea pig	Geert Hamer	GH	1:100	
SMC6	Rabbit	Alan R. Lehmann	ARL	1:100	
SUMO1	Mouse	Michael Matunis	21C7	1:200	
SYCP3	Mouse	Santa Cruz	sc-74569	1:50	
SYCP3	Goat	Santa Cruz	sc-20845	1:50	
SYCP3	Goat	Novus Biologicals	af3750	1:100	
TOPBP1	Rabbit	Abcam	ab2402	1:100	
Topoisomerase II α (TOP2A)	Rabbit	Abcam	ab109524	1:100	
α tubulin (αTUB)	Mouse	Sigma	T9026	1:1000	1:10000
γH2AX	Mouse	Thermo	MA1-2022	1:500	
γ tubulin (TUB)	Mouse	Sigma	T6557	1:1000	

Funding

This work was supported by a UK-US Fulbright Distinguished Scholar Award to P.W.J, the National Institutes of Health (NIH) K99/R00 HD069458 to P.W.J, NIH R01 HD33816 to M.A.H, NIH R01 GM117155 to P.W.J, an institutional NIH Cancer Center award CA34196 to The Jackson Laboratory, and training grant CA009110 fellowship to G.H.

Addendum

The platinum core of cisplatin binds primarily to purine residues and adducts on adjacent bases can form intrastrand crosslinks, which block DNA replication and transcription (Cheung-Ong et al., 2013, Tanida et al., 2012). Irradiation and etoposide treatment caused an increase in enlarged spermatids, which commonly harbored two acrosomes and displayed evidence of supernumerary chromosome content. However, spermatogenesis defects observed following cisplatin treatment were not discernable between *Smc5* CKO and control mice (**Figure S4.8**). From our observations, we propose higher levels of the SMC5/6 complex are required when meiotic DNA processing events are perturbed by exogenous sources of DSBs, but not intrastrand links.

Induction of DNA damage via etoposide and cisplatin

For cisplatin assessments, adult mice were injected intraperitoneally with a single dose of cisplatin (3 mg/ kg body weight, Sigma) (Bhattacharyya et al., 2000, Sawhney et al., 2005). After injection, the mice were monitored daily before their euthanasia at taken 8 days after treatment.

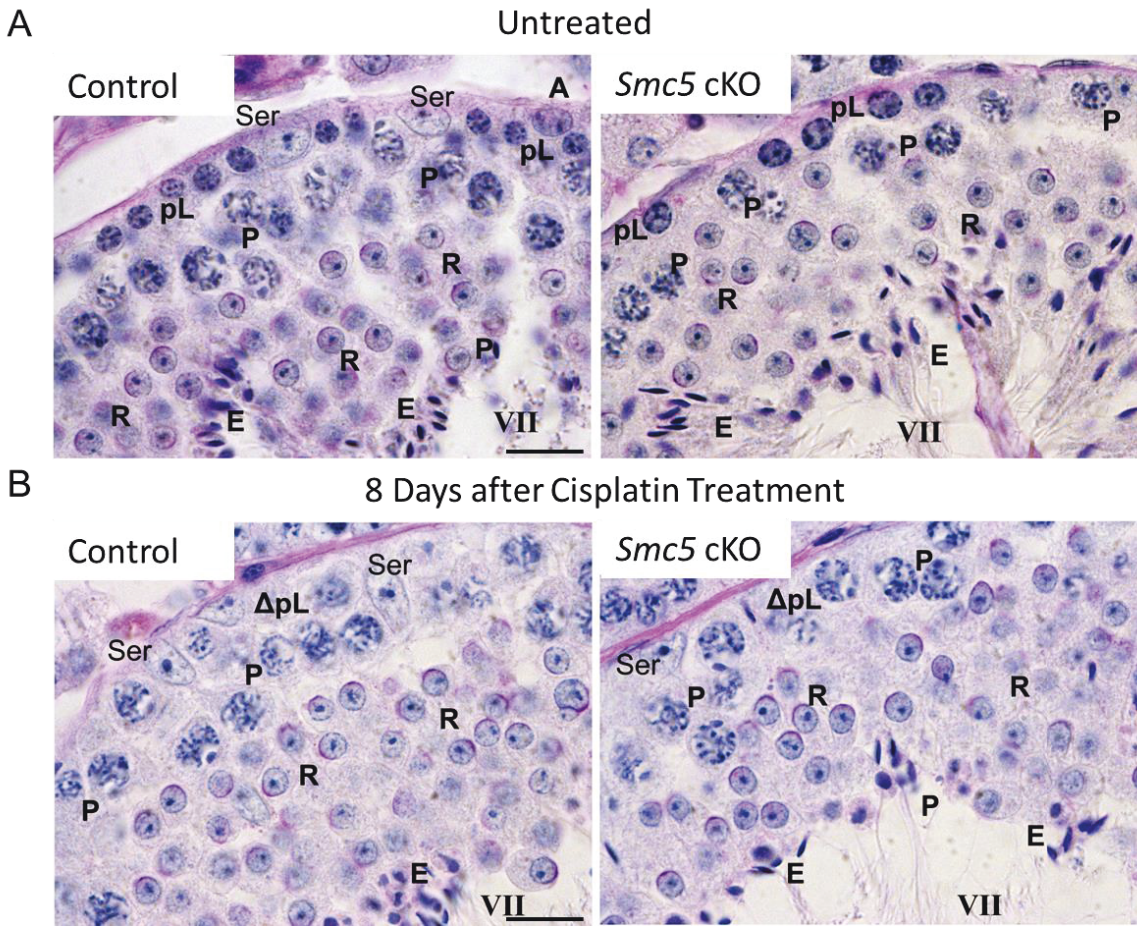

Supplemental Figure 4.8. Conditional mutation of *Smc5* does not result in increased sensitivity to cisplatin (**A,B**) Tubule cross sections of adult control and *Smc5* cKO (*Stra8-Cre*) mice testes with periodic acid-schiff staining extracted after no treatment (**A**) or 8 or post-induction of cisplatin (**B**). No discernable differences were seen between the control and *Smc5* cKO after cisplatin treatment. Markers: (*) abnormal enlarged spermatids, (P) pachytene stage, (R) round spermatid, (ΔpL) pre-leptotene stage, (ΔL) leptotene stage, (Ser) sertoli cell, (E) elongated spermatids. Roman numerals correspond to the seminiferous tubule stage. *Smc5* cKO cross sections display increased numbers of abnormal enlarged spermatids compared to the controls at 8 and 10 days post-irradiation. Acrosomes on round spermatids are stained in purple. Numbers indicate stage of round spermatid development. Scale bar: 20 μm.

CHAPTER V

DISCUSSION AND FUTURE DIRECTIONS

SMC complexes are essential for regulating chromosome organization and dynamics across organisms and biological processes. As majority of studies on SMC complexes have been focused on cohesin and condensin, the SMC5/6 complex is the least understood of the SMC complexes, especially in the context of mammals. The focus of this thesis is to shed light on the functional roles of the SMC5/6 complex in both female and male mammalian processes, specifically in meiosis. Does SMC5/6 have diverse roles in maintaining genome maintenance in mammalian germ cells? At the onset of this project, it was known that SMC5/6 localizes to the pericentromeric heterochromatin regions in rodent spermatocytes (Gomez et al., 2013, Verver et al., 2013b) and SC of synapsed homologous chromosomes in human spermatocytes (Verver et al., 2014c), suggesting that SMC5/6 plays a critical role in spermatogenesis (Chapter I). There were no studies on the localization of SMC5/6 during oogenesis, and the complete molecular and functional understanding of SMC5/6 was still lacking. Using conditional *Smc5* mutant mice, this thesis work has substantially contributed to this subject and became the first study to see functional differences for SMC5/6 complex between sexes. I show that while in females, SMC5/6 is required for fertility and for accurate and efficient germ cell chromosome segregation (Chapter III), the complex is only required for maintaining genome integrity in the event of exogenous DNA damage in male germ cells (Chapter IV). Thus, this work represents a major step in understanding the functional capabilities and the sexual dimorphic nature of the SMC5/6 complex.

In this final chapter, I extend the discussion in previous chapters on potential future directions as well as public health relevance of this work.

SMC5/6 and interacting partners

The interacting partners of SMC5/6 are still largely unknown. Recently, it has been found that TOP2A physically interacts with SMC5/6 (Verver et al., 2016b), and NSE2 has been shown to SUMOlayte telomere associated proteins, TRF1 and TRF2 (Potts and Yu, 2007b). Dr. Andras Horvath in our lab has determined that that NSMCE4A, a subunit of SMC5/6, interacts with CNS1 (also known as GPS1) via yeast two-hybrid (Y2H) and Co-immunoprecipitation (Co-IP). CSN1 is part of the COP9 signalosome—which is a protein complex involved in protein degradation—specifically denneddlyation. In previous studies, it has been shown that the recruitment of cullin 4A, a subunit of the COP9 signalosome, to sites of laser-induced DNA damage is CSN- and neddylation-dependent (Meir et al., 2015, Fuzesi-Levi et al., 2014). SMC5/6 has also been shown to localize to double-strand breaks induced by laser as well (Wu et al., 2012). Dr. Andras Horvath and our collaborator Dr. Gergely Rona at NYU are looking to further to further assess this DNA repair response interaction in detail. The COP9 signalosome has also been shown to be involved meiotic processes such as synaptonemal complex assembly and regulating degradation of Cyclin B1 and Securin via APC/C (Kim et al., 2011). This can be assessed in more detail, specifically in relation to SMC5/6 roles in meiosis.

In order to discover other SMC5/6 interaction partners, proteins can also be extracted specifically from purified germ cells from testis. Synchronized cultured cells

and cells treated with DNA damaging agents can also be used. Following protein extraction, interactions between SMC5/6 complex components and other proteins will be determined using Co-IP and subsequent mass spectrometry analysis and Y2H. It is clear to expand the functional capabilities of SMC5/6, its interacting partners need to be explored.

Infertility

In Chapter III, I demonstrate that SMC5/6 may be contributing to infertility correlated with the increase in maternal age. The results show that as maternal age increases protein expression levels of SMC5/6 components in mouse oocytes decrease, leading to chromosome missegregation during meiosis and failure in embryogenesis. Future studies should determine if this phenotype can be rescued in aging oocytes and *Smc5* cKO oocytes by microinjection of *Smc5* RNA. Because SMC5/6 is not the only factor that is contributing to the age-related aneuploidy, I hypothesize that the microinjection of *Smc5* transcript will not rescue the phenotype completely in aging oocytes. For example, it is known that the decrease of cohesin protein expression levels, thus sister chromatid cohesion with maternal age, leads to precocious chromosome segregation as well in mice and humans (Lister et al., Tachibana-Konwalski et al., 2010a, Tsutsumi et al., 2014). In addition to decrease in cohesin levels, there are other factors correlated to aging such as increased oxidative stress which leads to dysfunctional mitochondria, and improper epigenetic changes in oocytes due to internal or external elements (Ge et al., 2015, Igarashi et al., 2015). Thus, as even the control adult mice have fewer mature oocytes and increased incidences of chromosome segregation errors

compared to juvenile mice, I predict that only microinjection of *Smc5* will not rescue age-related infertility. It is clear that aging affects many processes involved in fertility.

While it is clear that the depletion of SMC5/6 does not affect fertility in male mice, the complex is essential to maintain germ cell genome integrity after exposure to exogenous DNA damaging agents such as irradiation and etoposide (Chapter IV). Irradiation and etoposide, are common cancer therapy agents, and it has been shown that both can cause temporary or permanent infertility, especially combined with other treatments (Howell and Shalet, 2005, Ahmad and Agarwal, 2017). Human testis has also been shown to be more sensitive to irradiation and recovery in spermatogenesis is more delayed than in rodents (Meistrich and Samuels, 1985). Mutations in SMC5/6 have also been linked to cancer (as discussed in the following section). Therefore, especially with prolonged exposure to these agents, Smc5/6 may be a contributing factor in the mechanism in which these agents affect fertility in humans. Expression levels of SMC5/6 may be a predicative factor for patients whose fertility that will be affected by chemotherapy agents or irradiation. Additionally, our studies suggest that expression levels of SMC5/6 may be a predictive factor for infertility in general for men and especially for women.

Cancer and developmental diseases

The SMC5/6 complex and its subunits has been linked to cancer and several other diseases. For example, NSE2 has been implicated in the SUMOlaytion of proteins involved in the alternative lengthening of telomeres (ALT) pathway in human cells (Potts

and Yu, 2007b). The depletion of NSE2 by RNAi inhibits telomere homologous recombination, resulting telomere shortening and senescence in ALT cells (Potts and Yu, 2007b). One of the hallmarks of cancer is the activation of telomere maintenance for replicative continuity, and ~5-15% of cancers use the ALT pathway, which usually results in poor prognosis (Dilley and Greenberg, 2015). However, these studies still need to be verified as off target effects were confirmed using NSE2 (Wu et al., 2012). Yet recently, it has been shown that shortened telomere length, *TP53* mutations, and chromothripsis, is correlated with the loss of *Smc5* in high risk chronic lymphocytic leukeumia (Steinbrecher et al., 2017). Future studies should be completed aiming to understanding the molecular mechanism in which SMC5/6 could be regulating telomere length. Furthermore, different cancers and even subsets of specific cancers have vast variances in expression profiles, leading to different prognosis. According to the Human Protein Atlas, colorectal cancer patients with high RNA expression levels of *Smc5* have a higher 5-year survival rate than those with low RNA expression level; while the opposite is the case for prostate cancer. Therefore, simply linking the depletion of SMC5/6 expression levels to cancer development and prognosis is an overgeneralization. It is apparent that roles of SMC5/6 plays in cancer development and etiology should be delineated in a mechanistic manner to explain the trends seen.

The deletion of *Nse2* causes premature aging in mice, and NSE2 was shown to be a tumor suppressor independently of SUMO by limiting recombination and facilitating chromosome segregation in B lymphocytes (Jacome et al., 2015b). In addition, human patients with reduced levels of NSE2 have been discovered and presented dwarfism, gonadal failure, altered pigmentation, and increased micronuclei (Payne et al., 2014b).

The patients had compound heterozygous frameshift mutations, hypomorphic mutations, in NSE2, which resulted in reduced levels of SMC5 and SMC6 (Payne et al., 2014b). Recently, it was found that children with severe lung disease to have biallelic missense mutations in NSE3, which destabilized the SMC5/6 complex (van der Crabben et al., 2016). These patients also showed chromosome rearrangements, micronuclei, inaccurate HR in addition to sensitivity to replication stress and DNA damage in T and B cells (van der Crabben et al., 2016). Taken together with this thesis work and previous studies (Chapter I), a consistent role of SMC5/6 across different cell types is that it facilitates chromosome segregation and suppresses gross rearrangements, preventing catastrophe and disease development.

Hepatitis B

There have been several recent studies on SMC5/6 and its role in inhibiting the production of hepatitis B virus gene expression. Hbx protein promotes the transcription of the viral genome, which exists as an extrachromosomal DNA circle in infected human cells, by regulating E3 ubiquitin ligase DDB1-CUL4-ROC1 to target SMC5/6 for degradation (Decorsière et al., 2016, Murphy et al., 2016). Cohesin and condensin are not targeted by HBx (Murphy et al., 2016). SMC5/6 has a novel role as a transcription restriction factor that selectively blocks extrachromosomal DNA replication, limiting viral infection. Chronic hepatitis B virus infection can cause cirrhosis and liver cancer (Seeger and Mason, 2000, Ganem and Prince, 2004). Also, the fact that SMC5/6 influences transcription in this context could mean that it also regulates transcription for the cell in general. Cohesin (Borrie et al., 2017, Busslinger et al., 2017) and condensin

(Sutani et al., 2015) both influence gene transcription—why not SMC5/6? Future assessments should be completed in order to see if SMC5/6 coordinates transcription in other contexts—which would make the complex a novel target for therapy.

Final Thoughts

SMC5/6 is an integral factor in genome maintenance across cell types and organisms. The complex has been implicated to be part of numerous DNA replicative and repair processes. Therefore, it is no surprise that the complex is linked to various diseases, aging and cancer. Continued studies focusing on the functions of SMC5/6 will most likely show links to additional genetic diseases. Yet, there is still a dearth of the biochemical, molecular, and functional understanding of SMC5/6 in mammals, especially in humans. Our studies show that SMC5/6 has sexual dimorphic roles in meiosis. This may be because meiosis is in nature sexually dimorphic. Could other proteins involved in genome maintenance also have different functions in meiosis? For example, mutations in Aurora C, a cell cycle kinase critical for proper chromosome segregation, causes infertility in men, but no effect have yet to seen in women (Dieterich et al., 2007, Ben Khelifa et al., 2011, 2012 Could these functional differences lead to differences in susceptibility and prognosis for diseases? Studies have found sex differences in expression profiles and tumor etiology, as well as cancer susceptibility (Dorak and Karpuzoglu, 2012). This would suggest that different treatment options should be considered between sexes. Taken together, we hope that our work and the work of others on SMC5/6 will ultimately contribute in finding novel treatments for developmental and genetic diseases.

REFERENCES

AGOSTINHO, A., MEIER, B., SONNEVILLE, R., JAGUT, M., WOGLAR, A., BLOW, J., JANTSCH, V. & GARTNER, A. 2013. Combinatorial regulation of meiotic holliday junction resolution in C. elegans by HIM-6 (BLM) helicase, SLX-4, and the SLX-1, MUS-81 and XPF-1 nucleases. *PLoS Genet,* 9**,** e1003591.

AHMAD, G. & AGARWAL, A. 2017. Ionizing Radiation and Male Fertility. *In:* GUNASEKARAN, K. & PANDIYAN, N. (eds.) *Male Infertility: A Clinical Approach.* New Delhi: Springer India.

AHUJA, J. S., SANDHU, R., MAINPAL, R., LAWSON, C., HENLEY, H., HUNT, P. A., YANOWITZ, J. L. & BORNER, G. V. 2017. Control of meiotic pairing and recombination by chromosomally tethered 26S proteasome. *Science,* 355**,** 408-411.

AMPATZIDOU, E., IRMISCH, A., O'CONNELL, M. J. & MURRAY, J. M. 2006. Smc5/6 is required for repair at collapsed replication forks. *Mol Cell Biol,* 26**,** 9387-401.

ANDREWS, E. A., PALECEK, J., SERGEANT, J., TAYLOR, E., LEHMANN, A. R. & WATTS, F. Z. 2005a. Nse2, a component of the Smc5-6 complex, is a SUMO ligase required for the response to DNA damage. *Mol Cell Biol,* 25**,** 185-96.

ANDREWS, E. A., PALECEK, J., SERGEANT, J., TAYLOR, E., LEHMANN, A. R. & WATTS, F. Z. 2005b. Nse2, a Component of the Smc5-6 Complex, Is a SUMO Ligase Required for the Response to DNA Damage. *Molecular and Cellular Biology,* 25**,** 185-196.

BAKER, S. M., PLUG, A. W., PROLLA, T. A., BRONNER, C. E., HARRIS, A. C., YAO, X., CHRISTIE, D. M., MONELL, C., ARNHEIM, N., BRADLEY, A., ASHLEY, T. & LISKAY, R. M. 1996. Involvement of mouse Mlh1 in DNA mismatch repair and meiotic crossing over. *Nat Genet,* 13**,** 336-42.

BANNISTER, L. A., REINHOLDT, L. G., MUNROE, R. J. & SCHIMENTI, J. C. 2004. Positional cloning and characterization of mouse mei8, a disrupted allele of the meiotic cohesin Rec8. *genesis,* 40**,** 184-194.

BARLOW, J. H., FARYABI, R. B., CALLEN, E., WONG, N., MALHOWSKI, A., CHEN, H. T., GUTIERREZ-CRUZ, G., SUN, H. W., MCKINNON, P., WRIGHT, G., CASELLAS, R., ROBBIANI, D. F., STAUDT, L., FERNANDEZ-

CAPETILLO, O. & NUSSENZWEIG, A. 2013. Identification of early replicating fragile sites that contribute to genome instability. *Cell,* 152**,** 620-32.

BELLVE, A. R. 1993. Purification, culture, and fractionation of spermatogenic cells. *Methods Enzymol,* 225**,** 84-113.

BENNETT, R. J., SHARP, J. A. & WANG, J. C. 1998. Purification and characterization of the Sgs1 DNA helicase activity of Saccharomyces cerevisiae. *J Biol Chem,* 273**,** 9644-50.

BERCHOWITZ, L. E., FRANCIS, K. E., BEY, A. L. & COPENHAVER, G. P. 2007. The role of AtMUS81 in interference-insensitive crossovers in A. thaliana. *PLoS Genet,* 3**,** e132.

BERMUDEZ-LOPEZ, M., CESCHIA, A., DE PICCOLI, G., COLOMINA, N., PASERO, P., ARAGON, L. & TORRES-ROSELL, J. 2010. The Smc5/6 complex is required for dissolution of DNA-mediated sister chromatid linkages. *Nucleic Acids Res,* 38**,** 6502-12.

BERMUDEZ-LOPEZ, M., POCINO-MERINO, I., SANCHEZ, H., BUENO, A., GUASCH, C., ALMEDAWAR, S., BRU-VIRGILI, S., GARI, E., WYMAN, C., REVERTER, D., COLOMINA, N. & TORRES-ROSELL, J. 2015. ATPase-Dependent Control of the Mms21 SUMO Ligase during DNA Repair. *PLoS Biol,* 13**,** e1002089.

BHATTACHARYYA, A., EAR, U. S., KOLLER, B. H., WEICHSELBAUM, R. R. & BISHOP, D. K. 2000. The breast cancer susceptibility gene BRCA1 is required for subnuclear assembly of Rad51 and survival following treatment with the DNA cross-linking agent cisplatin. *J Biol Chem,* 275**,** 23899-903.

BICKEL, J. S., CHEN, L., HAYWARD, J., YEAP, S. L., ALKERS, A. E. & CHAN, R. C. 2010. Structural maintenance of chromosomes (SMC) proteins promote homolog-independent recombination repair in meiosis crucial for germ cell genomic stability. *PLoS Genet,* 6**,** e1001028.

BISWAS, U., HEMPEL, K., LLANO, E., PENDAS, A. & JESSBERGER, R. 2016. Distinct Roles of Meiosis-Specific Cohesin Complexes in Mammalian Spermatogenesis. *PLoS Genet,* 12**,** e1006389.

BODDY, M. N., GAILLARD, P. H., MCDONALD, W. H., SHANAHAN, P., YATES, J. R., 3RD & RUSSELL, P. 2001. Mus81-Eme1 are essential components of a Holliday junction resolvase. *Cell,* 107**,** 537-48.

BOLCUN-FILAS, E., COSTA, Y., SPEED, R., TAGGART, M., BENAVENTE, R., DE ROOIJ, D. G. & COOKE, H. J. 2007. SYCE2 is required for synaptonemal complex assembly, double strand break repair, and homologous recombination. *J Cell Biol,* 176**,** 741-7.

BOLCUN-FILAS, E., HALL, E., SPEED, R., TAGGART, M., GREY, C., DE MASSY, B., BENAVENTE, R. & COOKE, H. J. 2009. Mutation of the mouse Syce1 gene disrupts synapsis and suggests a link between synaptonemal complex structural components and DNA repair. *PLoS Genet,* 5**,** e1000393.

BORNER, G. V., KLECKNER, N. & HUNTER, N. 2004. Crossover/noncrossover differentiation, synaptonemal complex formation, and regulatory surveillance at the leptotene/zygotene transition of meiosis. *Cell,* 117**,** 29-45.

BORRIE, M. S., CAMPOR, J. S., JOSHI, H. & GARTENBERG, M. R. 2017. Binding, sliding, and function of cohesin during transcriptional activation. *Proc Natl Acad Sci U S A,* 114**,** E1062-e1071.

BRANZEI, D., SOLLIER, J., LIBERI, G., ZHAO, X., MAEDA, D., SEKI, M., ENOMOTO, T., OHTA, K. & FOIANI, M. 2006. Ubc9- and mms21-mediated sumoylation counteracts recombinogenic events at damaged replication forks. *Cell,* 127**,** 509-22.

BRITO, I. L., YU, H. G. & AMON, A. 2010. Condensins promote coorientation of sister chromatids during meiosis I in budding yeast. *Genetics,* 185**,** 55-64.

BURGOYNE, P. S., MAHADEVAIAH, S. K. & TURNER, J. M. 2009. The consequences of asynapsis for mammalian meiosis. *Nat Rev Genet,* 10**,** 207-16.

BURKHARDT, S., BORSOS, M., SZYDLOWSKA, A., GODWIN, J., WILLIAMS, SUZANNAH A., COHEN, PAULA E., HIROTA, T., SAITOU, M. & TACHIBANA-KONWALSKI, K. 2016. Chromosome Cohesion Established by Rec8-Cohesin in Fetal Oocytes Is Maintained without Detectable Turnover in Oocytes Arrested for Months in Mice. *Current Biology,* 26**,** 678-685.

BUSSLINGER, G. A., STOCSITS, R. R., VAN DER LELIJ, P., AXELSSON, E., TEDESCHI, A., GALJART, N. & PETERS, J.-M. 2017. Cohesin is positioned in mammalian genomes by transcription, CTCF and Wapl. *Nature,* 544**,** 503.

CABURET, S., ARBOLEDA, V. A., LLANO, E., OVERBEEK, P. A., BARBERO, J. L., OKA, K., HARRISON, W., VAIMAN, D., BEN-NERIAH, Z., GARCIA-TUNON, I., FELLOUS, M., PENDAS, A. M., VEITIA, R. A. & VILAIN, E. 2014. Mutant cohesin in premature ovarian failure. *N Engl J Med,* 370**,** 943-949.

CARTER, S. D. & SJOGREN, C. 2012. The SMC complexes, DNA and chromosome topology: right or knot? *Crit Rev Biochem Mol Biol,* 47**,** 1-16.

CHAMBON, J. P., HACHED, K. & WASSMANN, K. 2013. Chromosome spreads with centromere staining in mouse oocytes. *Methods Mol Biol,* 957**,** 203-12.

CHARBIN, A., BOUCHOUX, C. & UHLMANN, F. 2014. Condensin aids sister chromatid decatenation by topoisomerase II. *Nucleic Acids Research,* 42**,** 340-348.

CHECCHI, P. M., LAWRENCE, K. S., VAN, M. V., LARSON, B. J. & ENGEBRECHT, J. 2014. Pseudosynapsis and Decreased Stringency of Meiotic Repair Pathway Choice on the Hemizygous Sex Chromosome of Caenorhabditis elegans Males. *Genetics,* 197**,** 543-560.

CHEN, C., FARMER, A. D., LANGLEY, R. J., MUDGE, J., CROW, J. A., MAY, G. D., HUNTLEY, J., SMITH, A. G. & RETZEL, E. F. 2010. Meiosis-specific gene discovery in plants: RNA-Seq applied to isolated Arabidopsis male meiocytes. *BMC Plant Biol,* 10**,** 280.

CHEUNG-ONG, K., GIAEVER, G. & NISLOW, C. 2013. DNA-Damaging Agents in Cancer Chemotherapy: Serendipity and Chemical Biology. *Chemistry & Biology,* 20**,** 648-659.

CHIANG, T., DUNCAN, F. E., SCHINDLER, K., SCHULTZ, R. M. & LAMPSON, M. A. 2010. Evidence that Weakened Centromere Cohesion Is a Leading Cause of Age-Related Aneuploidy in Oocytes. *Current Biology,* 20**,** 1522-1528.

CHIOLO, I., MINODA, A., COLMENARES, S. U., POLYZOS, A., COSTES, S. V. & KARPEN, G. H. 2011. Double-strand breaks in heterochromatin move outside of a dynamic HP1a domain to complete recombinational repair. *Cell,* 144**,** 732-44.

COPSEY, A., TANG, S., JORDAN, P. W., BLITZBLAU, H. G., NEWCOMBE, S., CHAN, A. C., NEWNHAM, L., LI, Z., GRAY, S., HERBERT, A. D., ARUMUGAM, P., HOCHWAGEN, A., HUNTER, N. & HOFFMANN, E. 2013a. Smc5/6 coordinates formation and resolution of joint molecules with chromosome morphology to ensure meiotic divisions. *PLoS Genet,* 9**,** e1004071.

COPSEY, A., TANG, S., JORDAN, P. W., BLITZBLAU, H. G., NEWCOMBE, S., CHAN, A. C.-H., NEWNHAM, L., LI, Z., GRAY, S., HERBERT, A. D., ARUMUGAM, P., HOCHWAGEN, A., HUNTER, N. & HOFFMANN, E. 2013b. Smc5/6 Coordinates Formation and Resolution of Joint Molecules with Chromosome Morphology to Ensure Meiotic Divisions. *PLoS Genet,* 9**,** e1004071.

COST, G. J. & COZZARELLI, N. R. 2006. Smc5p promotes faithful chromosome transmission and DNA repair in Saccharomyces cerevisiae. *Genetics,* 172**,** 2185-200.

CROMIE, G. A., HYPPA, R. W., TAYLOR, A. F., ZAKHARYEVICH, K., HUNTER, N. & SMITH, G. R. 2006. Single Holliday junctions are intermediates of meiotic recombination. *Cell,* 127**,** 1167-78.

DAVIS, L. & SMITH, G. R. 2003. Nonrandom homolog segregation at meiosis I in Schizosaccharomyces pombe mutants lacking recombination. *Genetics,* 163**,** 857-74.

DE MUYT, A., JESSOP, L., KOLAR, E., SOURIRAJAN, A., CHEN, J., DAYANI, Y. & LICHTEN, M. 2012. BLM helicase ortholog Sgs1 is a central regulator of meiotic recombination intermediate metabolism. *Mol Cell,* 46**,** 43-53.

DE PICCOLI, G., CORTES-LEDESMA, F., IRA, G., TORRES-ROSELL, J., UHLE, S., FARMER, S., HWANG, J. Y., MACHIN, F., CESCHIA, A., MCALEENAN, A., CORDON-PRECIADO, V., CLEMENTE-BLANCO, A., VILELLA-MITJANA, F., ULLAL, P., JARMUZ, A., LEITAO, B., BRESSAN, D., DOTIWALA, F., PAPUSHA, A., ZHAO, X., MYUNG, K., HABER, J. E., AGUILERA, A. & ARAGON, L. 2006. Smc5-Smc6 mediate DNA double-strand-break repair by promoting sister-chromatid recombination. *Nat Cell Biol,* 8**,** 1032-4.

DE PICCOLI, G., TORRES-ROSELL, J. & ARAGON, L. 2009. The unnamed complex: what do we know about Smc5-Smc6? *Chromosome Res,* 17**,** 251-63.

DE VRIES, F. A., DE BOER, E., VAN DEN BOSCH, M., BAARENDS, W. M., OOMS, M., YUAN, L., LIU, J. G., VAN ZEELAND, A. A., HEYTING, C. & PASTINK, A. 2005. Mouse Sycp1 functions in synaptonemal complex assembly, meiotic recombination, and XY body formation. *Genes Dev,* 19**,** 1376-89.

DECORSIÈRE, A., MUELLER, H., VAN BREUGEL, P. C., ABDUL, F., GEROSSIER, L., BERAN, R. K., LIVINGSTON, C. M., NIU, C., FLETCHER, S. P., HANTZ, O. & STRUBIN, M. 2016. Hepatitis B virus X protein identifies the Smc5/6 complex as a host restriction factor. *Nature,* 531**,** 386.

DEXHEIMER, T. S. 2013. DNA Repair Pathways and Mechanisms. *In:* MATHEWS, L. A., CABARCAS, S. M. & HURT, E. M. (eds.) *DNA Repair of Cancer Stem Cells.* Dordrecht: Springer Netherlands.

DILLEY, R. L. & GREENBERG, R. A. 2015. ALTernative Telomere Maintenance and Cancer. *Trends in cancer,* 1**,** 145-156.

DORAK, M. T. & KARPUZOGLU, E. 2012. Gender Differences in Cancer Susceptibility: An Inadequately Addressed Issue. *Frontiers in Genetics,* 3**,** 268.

DOYLE, J. M., GAO, J., WANG, J., YANG, M. & POTTS, P. R. 2010a. MAGE-RING protein complexes comprise a family of E3 ubiquitin ligases. *Mol Cell,* 39**,** 963-74.

DOYLE, J. M., GAO, J., WANG, J., YANG, M. & POTTS, P. R. 2010b. MAGE-RING Protein Complexes Comprise a Family of E3 Ubiquitin Ligases. *Molecular Cell,* 39**,** 963-974.

DUAN, X., YANG, Y., CHEN, Y. H., ARENZ, J., RANGI, G. K., ZHAO, X. & YE, H. 2009. Architecture of the Smc5/6 Complex of Saccharomyces cerevisiae Reveals a Unique Interaction between the Nse5-6 Subcomplex and the Hinge Regions of Smc5 and Smc6. *J Biol Chem,* 284**,** 8507-15.

ECKERT-BOULET, N. & LISBY, M. 2009. Regulation of rDNA stability by sumoylation. *DNA Repair (Amst),* 8**,** 507-16.

FABRE, F., CHAN, A., HEYER, W. D. & GANGLOFF, S. 2002. Alternate pathways involving Sgs1/Top3, Mus81/ Mms4, and Srs2 prevent formation of toxic recombination intermediates from single-stranded gaps created by DNA replication. *Proc Natl Acad Sci U S A,* 99**,** 16887-92.

FARMER, S., SAN-SEGUNDO, P. A. & ARAGÓN, L. 2011. The smc5-smc6 complex is required to remove chromosome junctions in meiosis. *PLoS ONE,* 6**,** e20948.

FORAND, A., DUTRILLAUX, B. & BERNARDINO-SGHERRI, J. 2004. Gamma-H2AX expression pattern in non-irradiated neonatal mouse germ cells and after low-dose gamma-radiation: relationships between chromatid breaks and DNA double-strand breaks. *Biol Reprod,* 71**,** 643-9.

FUJIOKA, Y., KIMATA, Y., NOMAGUCHI, K., WATANABE, K. & KOHNO, K. 2002. Identification of a novel non-structural maintenance of chromosomes (SMC) component of the SMC5-SMC6 complex involved in DNA repair. *J Biol Chem,* 277**,** 21585-91.

FUKUDA, T., FUKUDA, N., AGOSTINHO, A., HERNÁNDEZ-HERNÁNDEZ, A., KOUZNETSOVA, A. & HÖÖG, C. 2014. STAG3-mediated stabilization of REC8 cohesin complexes promotes chromosome synapsis during meiosis. *EMBO Journal,* 33**,** 1243-1255.

FUZESI-LEVI, M. G., BEN-NISSAN, G., BIANCHI, E., ZHOU, H., DEERY, M. J., LILLEY, K. S., LEVIN, Y. & SHARON, M. 2014. Dynamic regulation of the COP9 signalosome in response to DNA damage. *Mol Cell Biol,* 34**,** 1066-76.

GALLEGO-PAEZ, L. M., TANAKA, H., BANDO, M., TAKAHASHI, M., NOZAKI, N., NAKATO, R., SHIRAHIGE, K. & HIROTA, T. 2013. Smc5/6-mediated regulation of replication progression contributes to chromosome assembly during mitosis in human cells. *Molecular Biology of the Cell,* 25**,** 302-317.

GALLEGO-PAEZ, L. M., TANAKA, H., BANDO, M., TAKAHASHI, M., NOZAKI, N., NAKATO, R., SHIRAHIGE, K. & HIROTA, T. 2014. Smc5/6-mediated regulation of replication progression contributes to chromosome assembly during mitosis in human cells. *Mol Biol Cell*.

GANEM, D. & PRINCE, A. M. 2004. Hepatitis B virus infection--natural history and clinical consequences. *N Engl J Med,* 350**,** 1118-29.

GE, Z.-J., SCHATTEN, H., ZHANG, C.-L. & SUN, Q.-Y. 2015. Oocyte ageing and epigenetics. *Reproduction,* 149**,** R103-R114.

GOMEZ, R., JORDAN, P. W., VIERA, A., ALSHEIMER, M., FUKUDA, T., JESSBERGER, R., LLANO, E., PENDAS, A. M., HANDEL, M. A. & SUJA, J.

A. 2013. Dynamic localization of SMC5/6 complex proteins during mammalian meiosis and mitosis suggests functions in distinct chromosome processes. *J Cell Sci,* 126**,** 4239-52.

GÓMEZ, R., JORDAN, P. W., VIERA, A., ALSHEIMER, M., FUKUDA, T., JESSBERGER, R., LLANO, E., PENDÁS, A. M., HANDEL, M. A. & SUJA, J. A. 2013. Dynamic localization of SMC5/6 complex proteins during mammalian meiosis and mitosis suggests functions in distinct chromosome processes. *Journal of Cell Science,* 126**,** 4239-4252.

GOODARZI, A. A. & JEGGO, P. A. 2012. The heterochromatic barrier to DNA double strand break repair: how to get the entry visa. *Int J Mol Sci,* 13**,** 11844-60.

GUGLIELMINO, M. R., SANTONOCITO, M., VENTO, M., RAGUSA, M., BARBAGALLO, D., BORZÌ, P., CASCIANO, I., BANELLI, B., BARBIERI, O., ASTIGIANO, S., SCOLLO, P., ROMANI, M., PURRELLO, M. & DI PIETRO, C. 2011. TAp73 is downregulated in oocytes from women of advanced reproductive age. *Cell Cycle,* 10**,** 3253-3256.

HAMATANI, T., FALCO, G., CARTER, M. G., AKUTSU, H., STAGG, C. A., SHAROV, A. A., DUDEKULA, D. B., VANBUREN, V. & KO, M. S. H. 2004. Age-associated alteration of gene expression patterns in mouse oocytes. *Human Molecular Genetics,* 13**,** 2263-2278.

HAMER, G., GELL, K., KOUZNETSOVA, A., NOVAK, I., BENAVENTE, R. & HÖÖG, C. 2006. Characterization of a novel meiosis-specific protein within the central element of the synaptonemal complex. *J Cell Sci,* 119**,** 4025-32.

HAMER, G., NOVAK, I., KOUZNETSOVA, A. & HOÖG, C. 2008. Disruption of pairing and synapsis of chromosomes causes stage-specific apoptosis of male meiotic cells. *Theriogenology,* 69**,** 333-9.

HAMER, G., ROEPERS-GAJADIEN, H. L., VAN DUYN-GOEDHART, A., GADEMAN, I. S., KAL, H. B., VAN BUUL, P. P. & DE ROOIJ, D. G. 2003. DNA double-strand breaks and gamma-H2AX signaling in the testis. *Biol Reprod,* 68**,** 628-34.

HANDEL, M. A. 2004. The XY body: a specialized meiotic chromatin domain. *Exp Cell Res,* 296**,** 57-63.

HANDEL, M. A. & SCHIMENTI, J. C. 2010. Genetics of mammalian meiosis: regulation, dynamics and impact on fertility. *Nat Rev Genet,* 11**,** 124-136.

HASSOLD, T., HALL, H. & HUNT, P. 2007. The origin of human aneuploidy: where we have been, where we are going. *Hum Mol Genet,* 16 Spec No. 2**,**, R203-8.

HASSOLD, T. & HUNT, P. 2001a. TO ERR (MEIOTICALLY) IS HUMAN: THE GENESIS OF HUMAN ANEUPLOIDY. *Nature Reviews Genetics,* 2**,** 280.

HASSOLD, T. & HUNT, P. 2001b. To err (meiotically) is human: the genesis of human aneuploidy. *Nat Rev Genet,* 2**,** 280-291.

HAZBUN, T. R., MALMSTROM, L., ANDERSON, S., GRACZYK, B. J., FOX, B., RIFFLE, M., SUNDIN, B. A., ARANDA, J. D., MCDONALD, W. H., CHIU, C. H., SNYDSMAN, B. E., BRADLEY, P., MULLER, E. G., FIELDS, S., BAKER, D., YATES, J. R., 3RD & DAVIS, T. N. 2003. Assigning function to yeast proteins by integration of technologies. *Mol Cell,* 12**,** 1353-65.

HEISIG, P. 2009. Type II topoisomerases--inhibitors, repair mechanisms and mutations. *Mutagenesis,* 24**,** 465-9.

HERRAN, Y., GUTIERREZ-CABALLERO, C., SANCHEZ-MARTIN, M., HERNANDEZ, T., VIERA, A., BARBERO, J. L., DE ALAVA, E., DE ROOIJ, D. G., SUJA, J. A., LLANO, E. & PENDAS, A. M. 2011. The cohesin subunit RAD21L functions in meiotic synapsis and exhibits sexual dimorphism in fertility. *EMBO J,* advance online publication.

HIGGINS, J. D., BUCKLING, E. F., FRANKLIN, F. C. & JONES, G. H. 2008. Expression and functional analysis of AtMUS81 in Arabidopsis meiosis reveals a role in the second pathway of crossing-over. *Plant J,* 54**,** 152-62.

HIRANO, T. 2015. Chromosome Dynamics during Mitosis. *Cold Spring Harbor Perspectives in Biology*.

HODGES, C. A., REVENKOVA, E., JESSBERGER, R., HASSOLD, T. J. & HUNT, P. A. 2005. SMC1[beta]-deficient female mice provide evidence that cohesins are a missing link in age-related nondisjunction. *Nat Genet,* 37**,** 1351-1355.

HOLLOWAY, J. K., BOOTH, J., EDELMANN, W., MCGOWAN, C. H. & COHEN, P. E. 2008. MUS81 generates a subset of MLH1-MLH3-independent crossovers in mammalian meiosis. *PLoS Genet,* 4**,** e1000186.

HOLLOWAY, J. K., MOHAN, S., BALMUS, G., SUN, X., MODZELEWSKI, A., BORST, P. L., FREIRE, R., WEISS, R. S. & COHEN, P. E. 2011. Mammalian BTBD12 (SLX4) protects against genomic instability during mammalian spermatogenesis. *PLoS Genet,* 7**,** e1002094.

HONG, Y., SONNEVILLE, R., AGOSTINHO, A., MEIER, B., WANG, B., BLOW, J. J. & GARTNER, A. 2016. The SMC-5/6 Complex and the HIM-6 (BLM) Helicase Synergistically Promote Meiotic Recombination Intermediate Processing and Chromosome Maturation during <italic>Caenorhabditis elegans</italic> Meiosis. *PLoS Genet,* 12**,** e1005872.

HOPKINS, J., HWANG, G., JACOB, J., SAPP, N., BEDIGIAN, R., OKA, K., OVERBEEK, P., MURRAY, S. & JORDAN, P. W. 2014a. Meiosis-Specific Cohesin Component, <italic>Stag3</italic> Is Essential for Maintaining Centromere Chromatid Cohesion, and Required for DNA Repair and Synapsis between Homologous Chromosomes. *PLoS Genet,* 10**,** e1004413.

HOPKINS, J., HWANG, G., JACOB, J., SAPP, N., BEDIGIAN, R., OKA, K., OVERBEEK, P., MURRAY, S. & JORDAN, P. W. 2014b. Meiosis-specific cohesin component, Stag3 is essential for maintaining centromere chromatid cohesion, and required for DNA repair and synapsis between homologous chromosomes. *PLoS Genet,* 10**,** e1004413.

HOULARD, M., GODWIN, J., METSON, J., LEE, J., HIRANO, T. & NASMYTH, K. 2015a. Condensin confers the longitudinal rigidity of chromosomes. *Nat Cell Biol,* 17**,** 771-781.

HOULARD, M., GODWIN, J., METSON, J., LEE, J., HIRANO, T. & NASMYTH, K. 2015b. Condensin confers the longitudinal rigidity of chromosomes. *Nat Cell Biol,* advance online publication.

HOWELL, S. J. & SHALET, S. M. 2005. Spermatogenesis After Cancer Treatment: Damage and Recovery. *JNCI Monographs,* 2005**,** 12-17.

HUDSON, J. J., BEDNAROVA, K., KOZAKOVA, L., LIAO, C., GUERINEAU, M., COLNAGHI, R., VIDOT, S., MAREK, J., BATHULA, S. R., LEHMANN, A. R. & PALECEK, J. 2011. Interactions between the Nse3 and Nse4 components of

the SMC5-6 complex identify evolutionarily conserved interactions between MAGE and EID Families. *PLoS One,* 6**,** e17270.

HUGHES, S. E. & HAWLEY, R. S. 2014. Topoisomerase II Is Required for the Proper Separation of Heterochromatic Regions during <italic>Drosophila melanogaster</italic> Female Meiosis. *PLoS Genet,* 10**,** e1004650.

HWANG, G., SUN, F., O'BRIEN, M., EPPIG, J. J., HANDEL, M. A. & JORDAN, P. W. 2017. SMC5/6 is required for the formation of segregation-competent bivalent chromosomes during meiosis I in mouse oocytes. *Development,* 144**,** 1648-1660.

HYPPA, R. W. & SMITH, G. R. 2010. Crossover invariance determined by partner choice for meiotic DNA break repair. *Cell,* 142**,** 243-55.

ICHIJIMA, Y., SIN, H. S. & NAMEKAWA, S. H. 2012. Sex chromosome inactivation in germ cells: emerging roles of DNA damage response pathways. *Cell Mol Life Sci,* 69**,** 2559-72.

IGARASHI, H., TAKAHASHI, T. & NAGASE, S. 2015. Oocyte aging underlies female reproductive aging: biological mechanisms and therapeutic strategies. *Reproductive Medicine and Biology,* 14**,** 159-169.

INSELMAN, A. L., NAKAMURA, N., BROWN, P. R., WILLIS, W. D., GOULDING, E. H. & EDDY, E. M. 2010. Heat shock protein 2 promoter drives Cre expression in spermatocytes of transgenic mice. *Genesis,* 48**,** 114-20.

IRMISCH, A., AMPATZIDOU, E., MIZUNO, K., O'CONNELL, M. J. & MURRAY, J. M. 2009. Smc5/6 maintains stalled replication forks in a recombination-competent conformation. *Embo J,* 28**,** 144-55.

JACOME, A., GUTIERREZ-MARTINEZ, P., SCHIAVONI, F., TENAGLIA, E., MARTINEZ, P., RODRÍGUEZ-ACEBES, S., LECONA, E., MURGA, M., MÉNDEZ, J., BLASCO, M. A. & FERNANDEZ-CAPETILLO, O. 2015a. NSMCE2 suppresses cancer and aging in mice independently of its SUMO ligase activity. *The EMBO Journal,* 34**,** 2504-2519.

JACOME, A., GUTIERREZ-MARTINEZ, P., SCHIAVONI, F., TENAGLIA, E., MARTINEZ, P., RODRÍGUEZ-ACEBES, S., LECONA, E., MURGA, M., MÉNDEZ, J., BLASCO, M. A. & FERNANDEZ-CAPETILLO, O. 2015b.

NSMCE2 suppresses cancer and aging in mice independently of its SUMO ligase activity. *The EMBO Journal,* 34**,** 2604-2619.

JEPPSSON, K., CARLBORG, K. K., NAKATO, R., BERTA, D. G., LILIENTHAL, I., KANNO, T., LINDQVIST, A., BRINK, M. C., DANTUMA, N. P., KATOU, Y., SHIRAHIGE, K. & SJOGREN, C. 2014a. The chromosomal association of the Smc5/6 complex depends on cohesion and predicts the level of sister chromatid entanglement. *PLoS Genet,* 10**,** e1004680.

JEPPSSON, K., KANNO, T., SHIRAHIGE, K. & SJOGREN, C. 2014b. The maintenance of chromosome structure: positioning and functioning of SMC complexes. *Nat Rev Mol Cell Biol,* 15**,** 601-14.

JEPPSSON, K., KANNO, T., SHIRAHIGE, K. & SJOGREN, C. 2014c. The maintenance of chromosome structure: positioning and functioning of SMC complexes. *Nat Rev Mol Cell Biol,* 15**,** 601-614.

JESSOP, L. & LICHTEN, M. 2008. Mus81/Mms4 endonuclease and Sgs1 helicase collaborate to ensure proper recombination intermediate metabolism during meiosis. *Mol Cell,* 31**,** 313-23.

JESSOP, L., ROCKMILL, B., ROEDER, G. S. & LICHTEN, M. 2006. Meiotic chromosome synapsis-promoting proteins antagonize the anti-crossover activity of sgs1. *PLoS Genet,* 2**,** e155.

JORDAN, P. W., KARPPINEN, J. & HANDEL, M. A. 2012. Polo-like kinase is required for synaptonemal complex disassembly and phosphorylation in mouse spermatocytes. *J Cell Sci,* 125**,** 5061-72.

JU, L., WING, J., TAYLOR, E., BRANDT, R., SLIJEPCEVIC, P., HORSCH, M., RATHKOLB, B., RÁCZ, I., BECKER, L., HANS, W., ADLER, T., BECKERS, J., ROZMAN, J., KLINGENSPOR, M., WOLF, E., ZIMMER, A., KLOPSTOCK, T., BUSCH, D. H., GAILUS-DURNER, V., FUCHS, H., ANGELIS, M. H. D., VAN DER HORST, G. & LEHMANN, A. R. 2013. SMC6 is an essential gene in mice, but a hypomorphic mutant in the ATPase domain has a mild phenotype with a range of subtle abnormalities. *DNA Repair,* 12**,** 356-366.

KANNO, T., BERTA, DAVIDE G. & SJÖGREN, C. 2015. The Smc5/6 Complex Is an ATP-Dependent Intermolecular DNA Linker. *Cell Reports,* 12**,** 1471-1482.

KAUPPI, L., BARCHI, M., BAUDAT, F., ROMANIENKO, P. J., KEENEY, S. & JASIN, M. 2011. Distinct properties of the XY pseudoautosomal region crucial for male meiosis. *Science,* 331**,** 916-20.

KAUPPI, L., BARCHI, M., LANGE, J., BAUDAT, F., JASIN, M. & KEENEY, S. 2013. Numerical constraints and feedback control of double-strand breaks in mouse meiosis. *Genes Dev,* 27**,** 873-86.

KEENEY, S. 2008. Spo11 and the Formation of DNA Double-Strand Breaks in Meiosis. *Genome Dyn Stab,* 2**,** 81-123.

KEENEY, S., GIROUX, C. N. & KLECKNER, N. 1997. Meiosis-specific DNA double-strand breaks are catalyzed by Spo11, a member of a widely conserved protein family. *Cell,* 88**,** 375-84.

KEENEY, S., LANGE, J. & MOHIBULLAH, N. 2014. Self-organization of meiotic recombination initiation: general principles and molecular pathways. *Annu Rev Genet,* 48**,** 187-214.

KEGEL, A., BETTS-LINDROOS, H., KANNO, T., JEPPSSON, K., STROM, L., KATOU, Y., ITOH, T., SHIRAHIGE, K. & SJOGREN, C. 2011a. Chromosome length influences replication-induced topological stress. *Nature,* 471**,** 392-6.

KEGEL, A., BETTS-LINDROOS, H., KANNO, T., JEPPSSON, K., STROM, L., KATOU, Y., ITOH, T., SHIRAHIGE, K. & SJOGREN, C. 2011b. Chromosome length influences replication-induced topological stress. *Nature,* 471**,** 392-396.

KENT, T. & GRISWOLD, M. 2014. Checking the Pulse of Vitamin A Metabolism and Signaling during Mammalian Spermatogenesis. *Journal of Developmental Biology,* 2**,** 34.

KIM, E., YOON, S.-J., KIM, E.-Y., KIM, Y., LEE, H.-S., KIM, K.-H. & LEE, K.-A. 2011. Function of COP9 Signalosome in Regulation of Mouse Oocytes Meiosis by Regulating MPF Activity and Securing Degradation. *PLoS ONE,* 6**,** e25870.

KIM, J. H., ISHIGURO, K., KUDO, N. & WATANABE, Y. 2013. Studying meiosis-specific cohesins in mouse embryonic oocytes. *Methods Mol Biol,* 957**,** 47-57.

KLEIN, F., MAHR, P., GALOVA, M., BUONOMO, S. B., MICHAELIS, C., NAIRZ, K. & NASMYTH, K. 1999. A central role for cohesins in sister chromatid cohesion, formation of axial elements, and recombination during yeast meiosis. *Cell,* 98**,** 91-103.

KOLAS, N. K., SVETLANOV, A., LENZI, M. L., MACALUSO, F. P., LIPKIN, S. M., LISKAY, R. M., GREALLY, J., EDELMANN, W. & COHEN, P. E. 2005. Localization of MMR proteins on meiotic chromosomes in mice indicates distinct functions during prophase I. *J Cell Biol,* 171**,** 447-58.

KOTA, S. K. & FEIL, R. 2010. Epigenetic transitions in germ cell development and meiosis. *Dev Cell,* 19**,** 675-86.

KOZAKOVA, L., VONDROVA, L., STEJSKAL, K., CHARALABOUS, P., KOLESAR, P., LEHMANN, A. R., ULDRIJAN, S., SANDERSON, C. M., ZDRAHAL, Z. & PALECEK, J. J. 2015. The melanoma-associated antigen 1 (MAGEA1) protein stimulates the E3 ubiquitin-ligase activity of TRIM31 within a TRIM31-MAGEA1-NSE4 complex. *Cell Cycle,* 14**,** 920-30.

LA SALLE, S., SUN, F. & HANDEL, M. A. 2009. Isolation and short-term culture of mouse spermatocytes for analysis of meiosis. *Methods Mol Biol,* 558**,** 279-97.

LAFLAMME, G., TREMBLAY-BOUDREAULT, T., ROY, M. A., ANDERSEN, P., BONNEIL, E., ATCHIA, K., THIBAULT, P., D'AMOURS, D. & KWOK, B. H. 2014. Structural maintenance of chromosome (SMC) proteins link microtubule stability to genome integrity. *J Biol Chem,* 289**,** 27418-31.

LAN, Z.-J., XU, X. & COONEY, A. J. 2004. Differential Oocyte-Specific Expression of Cre Recombinase Activity in GDF-9-iCre, Zp3cre, and Msx2Cre Transgenic Mice. *Biology of Reproduction,* 71**,** 1469-1474.

LAO, J. P. & HUNTER, N. 2010. Trying to avoid your sister. *PLoS Biol,* 8**,** e1000519.

LARA-GONZALEZ, P., WESTHORPE, FREDERICK G. & TAYLOR, STEPHEN S. 2012. The Spindle Assembly Checkpoint. *Current Biology,* 22**,** R966-R980.

LEE, J. 2013. Roles of Cohesin and Condensin in Chromosome Dynamics During Mammalian Meiosis. *The Journal of Reproduction and Development,* 59**,** 431-436.

LEE, J., OGUSHI, S., SAITOU, M. & HIRANO, T. 2011. Condensins I and II are essential for construction of bivalent chromosomes in mouse oocytes. *Molecular Biology of the Cell,* 22**,** 3465-3477.

LEE, J. S., TAKAHASHI, T., HAGIWARA, A., YONEYAMA, C., ITOH, M., SASABE, T., MURANISHI, S. & TASHIMA, S. 1995. Safety and efficacy of intraperitoneal injection of etoposide in oil suspension in mice with peritoneal carcinomatosis. *Cancer Chemother Pharmacol,* 36**,** 211-6.

LEE, K. M., NIZZA, S., HAYES, T., BASS, K. L., IRMISCH, A., MURRAY, J. M. & O'CONNELL, M. J. 2007. Brc1-mediated rescue of Smc5/6 deficiency: requirement for multiple nucleases and a novel Rad18 function. *Genetics,* 175**,** 1585-95.

LEHMANN, A. R., WALICKA, M., GRIFFITHS, D. J., MURRAY, J. M., WATTS, F. Z., MCCREADY, S. & CARR, A. M. 1995. The rad18 gene of Schizosaccharomyces pombe defines a new subgroup of the SMC superfamily involved in DNA repair. *Mol Cell Biol,* 15**,** 7067-80.

LEONARD, J., SEN, N., TORRES, R., SUTANI, T., JARMUZ, A., SHIRAHIGE, K. & ARAGÓN, L. 2015. Condensin Relocalization from Centromeres to Chromosome Arms Promotes Top2 Recruitment during Anaphase. *Cell Reports,* 13**,** 2336-2344.

LEWANDOSKI, M., WASSARMAN, K. M. & MARTIN, G. R. 1997. Zp3–cre, a transgenic mouse line for the activation or inactivation of loxP-flanked target genes specifically in the female germ line. *Current Biology,* 7**,** 148-151.

LI, L., ZHENG, P. & DEAN, J. 2010. Maternal control of early mouse development. *Development,* 137**,** 859-870.

LI, X.-M., YU, C., WANG, Z.-W., ZHANG, Y.-L., LIU, X.-M., ZHOU, D., SUN, Q.-Y. & FAN, H.-Y. 2013. DNA Topoisomerase II Is Dispensable for Oocyte Meiotic Resumption but Is Essential for Meiotic Chromosome Condensation and Separation in Mice. *Biology of Reproduction,* 89**,** 118, 1-11.

LILIENTHAL, I., KANNO, T. & SJOGREN, C. 2013a. Inhibition of the Smc5/6 complex during meiosis perturbs joint molecule formation and resolution without significantly changing crossover or non-crossover levels. *PLoS Genet,* 9**,** e1003898.

LILIENTHAL, I., KANNO, T. & SJÖGREN, C. 2013b. Inhibition of the Smc5/6 Complex during Meiosis Perturbs Joint Molecule Formation and Resolution without Significantly Changing Crossover or Non-crossover Levels. *PLoS Genet,* 9**,** e1003898.

LINDROOS, H. B., STROM, L., ITOH, T., KATOU, Y., SHIRAHIGE, K. & SJOGREN, C. 2006. Chromosomal association of the Smc5/6 complex reveals that it functions in differently regulated pathways. *Mol Cell,* 22**,** 755-67.

LIPKIN, S. M., MOENS, P. B., WANG, V., LENZI, M., SHANMUGARAJAH, D., GILGEOUS, A., THOMAS, J., CHENG, J., TOUCHMAN, J. W., GREEN, E. D., SCHWARTZBERG, P., COLLINS, F. S. & COHEN, P. E. 2002. Meiotic arrest and aneuploidy in MLH3-deficient mice. *Nat Genet,* 31**,** 385-90.

LISTER, L. M., KOUZNETSOVA, A., HYSLOP, L. A., KALLEAS, D., PACE, S. L., BAREL, J. C., NATHAN, A., FLOROS, V., ADELFALK, C., WATANABE, Y., JESSBERGER, R., KIRKWOOD, T. B., HÖÖG, C. & HERBERT, M. Age-Related Meiotic Segregation Errors in Mammalian Oocytes Are Preceded by Depletion of Cohesin and Sgo2. *Current Biology,* 20**,** 1511-1521.

LISTER, L. M., KOUZNETSOVA, A., HYSLOP, L. A., KALLEAS, D., PACE, S. L., BAREL, J. C., NATHAN, A., FLOROS, V., ADELFALK, C., WATANABE, Y., JESSBERGER, R., KIRKWOOD, T. B., HÖÖG, C. & HERBERT, M. 2010. Age-Related Meiotic Segregation Errors in Mammalian Oocytes Are Preceded by Depletion of Cohesin and Sgo2. *Current Biology,* 20**,** 1511-1521.

LLANO, E., GOMEZ-H, L., GARCÍA-TUÑÓN, I., SÁNCHEZ-MARTÍN, M., CABURET, S., BARBERO, J. L., SCHIMENTI, J. C., VEITIA, R. A. & PENDAS, A. M. 2014. STAG3 is a strong candidate gene for male infertility. *Human Molecular Genetics*.

LYNDAKER, A. M., LIM, P. X., MLECZKO, J. M., DIGGINS, C. E., HOLLOWAY, J. K., HOLMES, R. J., KAN, R., SCHLAFER, D. H., FREIRE, R., COHEN, P. E. & WEISS, R. S. 2013. Conditional inactivation of the DNA damage response gene Hus1 in mouse testis reveals separable roles for components of the RAD9-RAD1-HUS1 complex in meiotic chromosome maintenance. *PLoS Genet,* 9**,** e1003320.

LYNN, A., ASHLEY, T. & HASSOLD, T. 2004. Variation in human meiotic recombination. *Annu Rev Genomics Hum Genet,* 5**,** 317-49.

LYNN, A., SOUCEK, R. & BORNER, G. V. 2007. ZMM proteins during meiosis: crossover artists at work. *Chromosome Res,* 15**,** 591-605.

MACLENNAN, M., CRICHTON, J. H., PLAYFOOT, C. J. & ADAMS, I. R. 2015. Oocyte development, meiosis and aneuploidy. *Seminars in Cell & Developmental Biology,* 45**,** 68-76.

MARANGOS, P. 2016. Preparation of Cell Lysate from Mouse Oocytes for Western Blotting Analysis. *In:* NEZIS, P. I. (ed.) *Oogenesis: Methods and Protocols.* New York, NY: Springer New York.

MARCHETTI, F., PEARSON, F. S., BISHOP, J. B. & WYROBEK, A. J. 2006. Etoposide induces chromosomal abnormalities in mouse spermatocytes and stem cell spermatogonia. *Hum Reprod,* 21**,** 888-95.

MATOS, J., BLANCO, M. G., MASLEN, S., SKEHEL, J. M. & WEST, S. C. 2011. Regulatory control of the resolution of DNA recombination intermediates during meiosis and mitosis. *Cell,* 147**,** 158-72.

MCALEENAN, A., CORDON-PRECIADO, V., CLEMENTE-BLANCO, A., LIU, I. C., SEN, N., LEONARD, J., JARMUZ, A. & ARAGON, L. 2012. SUMOylation of the alpha-kleisin subunit of cohesin is required for DNA damage-induced cohesion. *Curr Biol,* 22**,** 1564-75.

MCDONALD, W. H., PAVLOVA, Y., YATES, J. R., 3RD & BODDY, M. N. 2003. Novel essential DNA repair proteins Nse1 and Nse2 are subunits of the fission yeast Smc5-Smc6 complex. *J Biol Chem,* 278**,** 45460-7.

MEIR, M., GALANTY, Y., KASHANI, L., BLANK, M., KHOSRAVI, R., FERNANDEZ-AVILA, M. J., CRUZ-GARCIA, A., STAR, A., SHOCHOT, L., THOMAS, Y., GARRETT, L. J., CHAMOVITZ, D. A., BODINE, D. M., KURZ, T., HUERTAS, P., ZIV, Y. & SHILOH, Y. 2015. The COP9 signalosome is vital for timely repair of DNA double-strand breaks. *Nucleic Acids Res,* 43**,** 4517-30.

MEISTRICH, M. L. & SAMUELS, R. C. 1985. Reduction in sperm levels after testicular irradiation of the mouse: a comparison with man. *Radiat Res,* 102**,** 138-47.

MENGISTE, T., REVENKOVA, E., BECHTOLD, N. & PASZKOWSKI, J. 1999. An SMC-like protein is required for efficient homologous recombination in Arabidopsis. *Embo J,* 18**,** 4505-12.

METS, D. G. & MEYER, B. J. 2009. Condensins regulate meiotic DNA break distribution, thus crossover frequency, by controlling chromosome structure. *Cell,* 139**,** 73-86.

MOENS, P. B., CHEN, D. J., SHEN, Z., KOLAS, N., TARSOUNAS, M., HENG, H. H. & SPYROPOULOS, B. 1997. Rad51 immunocytology in rat and mouse spermatocytes and oocytes. *Chromosoma,* 106**,** 207-15.

MORELLI, M. A. & COHEN, P. E. 2005. Not all germ cells are created equal: aspects of sexual dimorphism in mammalian meiosis. *Reproduction,* 130**,** 761-81.

MURDOCH, B., OWEN, N., STEVENSE, M., SMITH, H., NAGAOKA, S., HASSOLD, T., MCKAY, M., XU, H., FU, J., REVENKOVA, E., JESSBERGER, R. & HUNT, P. 2013. Altered Cohesin Gene Dosage Affects Mammalian Meiotic Chromosome Structure and Behavior. *PLoS Genet,* 9**,** e1003241.

MURPHY, C. M., XU, Y., LI, F., NIO, K., RESZKA-BLANCO, N., LI, X., WU, Y., YU, Y., XIONG, Y. & SU, L. 2016. Hepatitis B Virus X Protein Promotes Degradation of SMC5/6 to Enhance HBV Replication. *Cell Rep,* 16**,** 2846-2854.

MURRAY, J. M. & CARR, A. M. 2008. Smc5/6: a link between DNA repair and unidirectional replication? *Nat Rev Mol Cell Biol,* 9**,** 177-82.

NASMYTH, K. & HAERING, C. H. 2005. THE STRUCTURE AND FUNCTION OF SMC AND KLEISIN COMPLEXES. *Annual Review of Biochemistry,* 74**,** 595-648.

NITISS, J. L. 2009. DNA topoisomerase II and its growing repertoire of biological functions. *Nat Rev Cancer,* 9**,** 327-37.

O'NEIL, N. J., MARTIN, J. S., YOUDS, J. L., WARD, J. D., PETALCORIN, M. I., ROSE, A. M. & BOULTON, S. J. 2013. Joint molecule resolution requires the redundant activities of MUS-81 and XPF-1 during Caenorhabditis elegans meiosis. *PLoS Genet,* 9**,** e1003582.

OAKES, M. L., JOHZUKA, K., VU, L., ELIASON, K. & NOMURA, M. 2006. Expression of rRNA genes and nucleolus formation at ectopic chromosomal sites in the yeast Saccharomyces cerevisiae. *Mol Cell Biol,* 26**,** 6223-38.

OH, S. D., LAO, J. P., TAYLOR, A. F., SMITH, G. R. & HUNTER, N. 2008. RecQ helicase, Sgs1, and XPF family endonuclease, Mus81-Mms4, resolve aberrant joint molecules during meiotic recombination. *Mol Cell,* 31**,** 324-36.

OSMAN, F., DIXON, J., DOE, C. L. & WHITBY, M. C. 2003. Generating crossovers by resolution of nicked Holliday junctions: a role for Mus81-Eme1 in meiosis. *Mol Cell,* 12**,** 761-74.

OUTWIN, E. A., IRMISCH, A., MURRAY, J. M. & O'CONNELL, M. J. 2009. Smc5-Smc6-dependent removal of cohesin from mitotic chromosomes. *Mol Cell Biol,* 29**,** 4363-75.

PALECEK, J., VIDOT, S., FENG, M., DOHERTY, A. J. & LEHMANN, A. R. 2006a. The Smc5-Smc6 DNA Repair Complex. *Journal of Biological Chemistry,* 281**,** 36952-36959.

PALECEK, J., VIDOT, S., FENG, M., DOHERTY, A. J. & LEHMANN, A. R. 2006b. The Smc5-Smc6 DNA repair complex. bridging of the Smc5-Smc6 heads by the KLEISIN, Nse4, and non-Kleisin subunits. *J Biol Chem,* 281**,** 36952-9.

PAN, H., MA, P., ZHU, W. & SCHULTZ, R. M. 2008. Age-associated increase in aneuploidy and changes in gene expression in mouse eggs. *Developmental Biology,* 316**,** 397-407.

PAYNE, F., COLNAGHI, R., ROCHA, N., SETH, A., HARRIS, J., CARPENTER, G., BOTTOMLEY, W. E., WHEELER, E., WONG, S., SAUDEK, V., SAVAGE, D., O'RAHILLY, S., CAREL, J. C., BARROSO, I., O'DRISCOLL, M. & SEMPLE, R. 2014a. Hypomorphism in human NSMCE2 linked to primordial dwarfism and insulin resistance. *J Clin Invest,* 124**,** 4028-38.

PAYNE, F., COLNAGHI, R., ROCHA, N., SETH, A., HARRIS, J., CARPENTER, G., BOTTOMLEY, W. E., WHEELER, E., WONG, S., SAUDEK, V., SAVAGE, D., O'RAHILLY, S., CAREL, J.-C., BARROSO, I., O'DRISCOLL, M. & SEMPLE, R. 2014b. Hypomorphism in human NSMCE2 linked to primordial dwarfism and insulin resistance. *The Journal of Clinical Investigation,* 124**,** 4028-4038.

PEBERNARD, S., MCDONALD, W. H., PAVLOVA, Y., YATES, J. R. & BODDY, M. N. 2004. Nse1, Nse2, and a novel subunit of the Smc5-Smc6 complex, Nse3, play a crucial role in meiosis. *Molecular biology of the cell,* 15**,** 4866-4876.

PEBERNARD, S., PERRY, J. J., TAINER, J. A. & BODDY, M. N. 2008a. Nse1 RING-like domain supports functions of the Smc5-Smc6 holocomplex in genome stability. *Mol Biol Cell,* 19**,** 4099-109.

PEBERNARD, S., PERRY, J. J. P., TAINER, J. A. & BODDY, M. N. 2008b. Nse1 RING-like Domain Supports Functions of the Smc5-Smc6 Holocomplex in Genome Stability. *Molecular Biology of the Cell,* 19**,** 4099-4109.

PEBERNARD, S., WOHLSCHLEGEL, J., MCDONALD, W. H., YATES, J. R., 3RD & BODDY, M. N. 2006. The Nse5-Nse6 dimer mediates DNA repair roles of the Smc5-Smc6 complex. *Mol Cell Biol,* 26**,** 1617-30.

PETRONCZKI, M., SIOMOS, M. F. & NASMYTH, K. 2003a. Un Menage a Quatre: The Molecular Biology of Chromosome Segregation in Meiosis. *Current Biology,* 112**,** 423.

PETRONCZKI, M., SIOMOS, M. F. & NASMYTH, K. 2003b. Un ménage à quatre: the molecular biology of chromosome segregation in meiosis. *Cell,* 112**,** 423-40.

PHADNIS, N., CIPAK, L., POLAKOVA, S., HYPPA, R. W., CIPAKOVA, I., ANRATHER, D., KARVAIOVA, L., MECHTLER, K., SMITH, G. R. & GREGAN, J. 2015. Casein Kinase 1 and Phosphorylation of Cohesin Subunit Rec11 (SA3) Promote Meiotic Recombination through Linear Element Formation. *PLoS Genet,* 11**,** e1005225.

PINCUS, G. & ENZMANN, E. V. 1935a. The Comparative Behavior of Mammalian Eggs In vivo and In vitro: I. The Activation of Ovarian Eggs. *J Exp Med,* 62**,** 665-75.

PINCUS, G. & ENZMANN, E. V. 1935b. THE COMPARATIVE BEHAVIOR OF MAMMALIAN EGGS IN VIVO AND IN VITRO: I. THE ACTIVATION OF OVARIAN EGGS. *The Journal of Experimental Medicine,* 62**,** 665-675.

POTTS, P. R. 2009. The Yin and Yang of the MMS21-SMC5/6 SUMO ligase complex in homologous recombination. *DNA Repair (Amst),* 8**,** 499-506.

POTTS, P. R., PORTEUS, M. H. & YU, H. 2006. Human SMC5/6 complex promotes sister chromatid homologous recombination by recruiting the SMC1/3 cohesin complex to double-strand breaks. *Embo J,* 25**,** 3377-88.

POTTS, P. R. & YU, H. 2007a. The SMC5/6 complex maintains telomere length in ALT cancer cells through SUMOylation of telomere-binding proteins. *Nat Struct Mol Biol,* 14**,** 581-590.

POTTS, P. R. & YU, H. 2007b. The SMC5/6 complex maintains telomere length in ALT cancer cells through SUMOylation of telomere-binding proteins. *Nat Struct Mol Biol,* 14**,** 581-90.

PRYZHKOVA, M. V. & JORDAN, P. W. 2016a. Conditional mutation of Smc5 in mouse embryonic stem cells perturbs condensin localization and mitotic progression. *Journal of Cell Science,* 129**,** 1619-1634.

PRYZHKOVA, M. V. & JORDAN, P. W. 2016b. Conditional mutation of Smc5 in mouse embryonic stem cells perturbs condensin localization and mitotic progression. *Journal of Cell Science*.

QIAO, H., PRASADA RAO, H. B., YANG, Y., FONG, J. H., CLOUTIER, J. M., DEACON, D. C., NAGEL, K. E., SWARTZ, R. K., STRONG, E., HOLLOWAY, J. K., COHEN, P. E., SCHIMENTI, J., WARD, J. & HUNTER, N. 2014. Antagonistic roles of ubiquitin ligase HEI10 and SUMO ligase RNF212 regulate meiotic recombination. *Nat Genet,* 46**,** 194-9.

RANKIN, S. 2015a. Complex elaboration: making sense of meiotic cohesin dynamics. *FEBS Journal,* 282**,** 2426-2443.

RANKIN, S. 2015b. Complex elaboration: making sense of meiotic cohesin dynamics. *FEBS Journal***,** n/a-n/a.

RAO, H. B., QIAO, H., BHATT, S. K., BAILEY, L. R., TRAN, H. D., BOURNE, S. L., QIU, W., DESHPANDE, A., SHARMA, A. N., BEEBOUT, C. J., PEZZA, R. J. & HUNTER, N. 2017. A SUMO-ubiquitin relay recruits proteasomes to chromosome axes to regulate meiotic recombination. *Science,* 355**,** 403-407.

RÄSCHLE, M., SMEENK, G., HANSEN, R. K., TEMU, T., OKA, Y., HEIN, M. Y., NAGARAJ, N., LONG, D. T., WALTER, J. C., HOFMANN, K., STORCHOVA, Z., COX, J., BEKKER-JENSEN, S., MAILAND, N. & MANN, M. 2015. Proteomics reveals dynamic assembly of repair complexes during bypass of DNA cross-links. *Science,* 348.

REMESEIRO, S. & LOSADA, A. 2013. Cohesin, a chromatin engagement ring. *Current Opinion in Cell Biology,* 25**,** 63-71.

REVENKOVA, E., EIJPE, M., HEYTING, C., HODGES, C. A., HUNT, P. A., LIEBE, B., SCHERTHAN, H. & JESSBERGER, R. 2004. Cohesin SMC1[beta] is required for meiotic chromosome dynamics, sister chromatid cohesion and DNA recombination. *Nat Cell Biol,* 6**,** 555-562.

REYNOLDS, A., QIAO, H., YANG, Y., CHEN, J. K., JACKSON, N., BISWAS, K., HOLLOWAY, J. K., BAUDAT, F., DE MASSY, B., WANG, J., HÖÖG, C., COHEN, P. E. & HUNTER, N. 2013. RNF212 is a dosage-sensitive regulator of crossing-over during mammalian meiosis. *Nature genetics,* 45**,** 269-278.

ROY, M. A. & D'AMOURS, D. 2011. DNA-binding properties of Smc6, a core component of the Smc5-6 DNA repair complex. *Biochem Biophys Res Commun,* 416**,** 80-5.

ROY, M. A., SIDDIQUI, N. & D'AMOURS, D. 2011. Dynamic and selective DNA-binding activity of Smc5, a core component of the Smc5-Smc6 complex. *Cell Cycle,* 10**,** 690-700.

SADATE-NGATCHOU, P. I., PAYNE, C. J., DEARTH, A. T. & BRAUN, R. E. 2008. Cre recombinase activity specific to postnatal, premeiotic male germ cells in transgenic mice. *Genesis,* 46**,** 738-42.

SAKUNO, T. & WATANABE, Y. 2009. Studies of meiosis disclose distinct roles of cohesion in the core centromere and pericentromeric regions. *Chromosome Res,* 17**,** 239-49.

SAWHNEY, P., GIAMMONA, C. J., MEISTRICH, M. L. & RICHBURG, J. H. 2005. Cisplatin-Induced Long-term Failure of Spermatogenesis in Adult C57/Bl/6J Mice. *Journal of Andrology,* 26**,** 136-145.

SCHRAMM, S., FRAUNE, J., NAUMANN, R., HERNANDEZ-HERNANDEZ, A., HOOG, C., COOKE, H. J., ALSHEIMER, M. & BENAVENTE, R. 2011. A novel mouse synaptonemal complex protein is essential for loading of central element proteins, recombination, and fertility. *PLoS Genet,* 7**,** e1002088.

SEEGER, C. & MASON, W. S. 2000. Hepatitis B virus biology. *Microbiol Mol Biol Rev,* 64**,** 51-68.

SEVERSON, A. F. & MEYER, B. J. 2014. Divergent kleisin subunits of cohesin specify mechanisms to tether and release meiotic chromosomes. *Elife,* 3**,** e03467.

SHEEDY, D. M., DIMITROVA, D., RANKIN, J. K., BASS, K. L., LEE, K. M., TAPIA-ALVEAL, C., HARVEY, S. H., MURRAY, J. M. & O'CONNELL, M. J. 2005. Brc1-mediated DNA repair and damage tolerance. *Genetics,* 171**,** 457-68.

STEIN, P. & SCHINDLER, K. 2011a. Mouse oocyte microinjection, maturation and ploidy assessment. *J Vis Exp*.

STEIN, P. & SCHINDLER, K. 2011b. Mouse Oocyte Microinjection, Maturation and Ploidy Assessment. e2851.

STEINBRECHER, D., JEBARAJ, B. M. C., SCHNEIDER, C., EDELMANN, J., CYMBALISTA, F., LEBLOND, V., DELMER, A., IBACH, S., TAUSCH, E., SCHEFFOLD, A., BLOEHDORN, J., HALLEK, M., DREGER, P., DÖHNER, H. & STILGENBAUER, S. 2017. Telomere length in poor-risk chronic lymphocytic leukemia: associations with disease characteristics and outcome. *Leukemia & Lymphoma***,** 1-1.

STEPHAN, A. K., KLISZCZAK, M., DODSON, H., COOLEY, C. & MORRISON, C. G. 2011. Roles of vertebrate Smc5 in sister chromatid cohesion and homologous recombinational repair. *Molecular and cellular biology,* 31**,** 1369-1381.

STROM, L., LINDROOS, H. B., SHIRAHIGE, K. & SJOGREN, C. 2004. Postreplicative recruitment of cohesin to double-strand breaks is required for DNA repair. *Mol Cell,* 16**,** 1003-15.

SUGAWARA, N., GOLDFARB, T., STUDAMIRE, B., ALANI, E. & HABER, J. E. 2004. Heteroduplex rejection during single-strand annealing requires Sgs1 helicase and mismatch repair proteins Msh2 and Msh6 but not Pms1. *Proc Natl Acad Sci U S A,* 101**,** 9315-20.

SUN, X. & COHEN, P. E. 2013. Studying recombination in mouse oocytes. *Methods Mol Biol,* 957**,** 1-18.

SUSIARJO, M., RUBIO, C. & HUNT, P. 2009a. Analyzing Mammalian Female Meiosis. *In:* KEENEY, S. (ed.) *Meiosis.* Humana Press.

SUSIARJO, M., RUBIO, C. & HUNT, P. 2009b. Analyzing mammalian female meiosis. *Methods Mol Biol,* 558**,** 339-54.

SUTANI, T., SAKATA, T., NAKATO, R., MASUDA, K., ISHIBASHI, M., YAMASHITA, D., SUZUKI, Y., HIRANO, T., BANDO, M. & SHIRAHIGE, K. 2015. Condensin targets and reduces unwound DNA structures associated with transcription in mitotic chromosome condensation. *Nature Communications,* 6**,** 7815.

TACHIBANA-KONWALSKI, K., GODWIN, J., VAN DER WEYDEN, L., CHAMPION, L., KUDO, N. R., ADAMS, D. J. & NASMYTH, K. 2010a. Rec8-containing cohesin maintains bivalents without turnover during the growing phase of mouse oocytes. *Genes Dev,* 24**,** 2505-16.

TACHIBANA-KONWALSKI, K., GODWIN, J., VAN DER WEYDEN, L., CHAMPION, L., KUDO, N. R., ADAMS, D. J. & NASMYTH, K. 2010b. Rec8-containing cohesin maintains bivalents without turnover during the growing phase of mouse oocytes. *Genes & Development,* 24**,** 2505-2516.

TAKETO, T. 2012. Microspread ovarian cell preparations for the analysis of meiotic prophase progression in oocytes with improved recovery by cytospin centrifugation. *Methods Mol Biol,* 825**,** 173-81.

TANIDA, S., MIZOSHITA, T., OZEKI, K., TSUKAMOTO, H., KAMIYA, T., KATAOKA, H., SAKAMURO, D. & JOH, T. 2012. Mechanisms of Cisplatin-Induced Apoptosis and of Cisplatin Sensitivity: Potential of BIN1 to Act as a Potent Predictor of Cisplatin Sensitivity in Gastric Cancer Treatment. *Int J Surg Oncol,* 2012**,** 862879.

TAPIA-ALVEAL, C., OUTWIN, E. A., TREMPOLEC, N., DZIADKOWIEC, D., MURRAY, J. M. & O'CONNELL, M. J. 2010. SMC complexes and topoisomerase II work together so that sister chromatids can work apart. *Cell Cycle,* 9**,** 2065-70.

TAYLOR, E. M., COPSEY, A. C., HUDSON, J. J. R., VIDOT, S. & LEHMANN, A. R. 2008. Identification of the proteins, including MAGEG1, that make up the human SMC5-6 protein complex. *Molecular and cellular biology,* 28**,** 1197-1206.

TAYLOR, E. M., MOGHRABY, J. S., LEES, J. H., SMIT, B., MOENS, P. B. & LEHMANN, A. R. 2001. Characterization of a novel human SMC heterodimer

homologous to the Schizosaccharomyces pombe Rad18/Spr18 complex. *Molecular biology of the cell,* 12**,** 1583-1594.

TODARO, G. J. & GREEN, H. 1963. Quantitative studies of the growth of mouse embryo cells in culture and their development into established lines. *J Cell Biol,* 17**,** 299-313.

TORRES-ROSELL, J. & LOSADA, A. 2011. Smc5 flies solo. *Cell Cycle,* 10**,** 874-5.

TORRES-ROSELL, J., MACHIN, F. & ARAGON, L. 2005a. Smc5-Smc6 complex preserves nucleolar integrity in S. cerevisiae. *Cell Cycle,* 4**,** 868-72.

TORRES-ROSELL, J., MACHIN, F., FARMER, S., JARMUZ, A., EYDMANN, T., DALGAARD, J. Z. & ARAGON, L. 2005b. SMC5 and SMC6 genes are required for the segregation of repetitive chromosome regions. *Nat Cell Biol,* 7**,** 412-9.

TORRES-ROSELL, J., SUNJEVARIC, I., DE PICCOLI, G., SACHER, M., ECKERT-BOULET, N., REID, R., JENTSCH, S., ROTHSTEIN, R., ARAGON, L. & LISBY, M. 2007. The Smc5-Smc6 complex and SUMO modification of Rad52 regulates recombinational repair at the ribosomal gene locus. *Nat Cell Biol,* 9**,** 923-31.

TRAN, M., TSAROUHAS, V. & KEGEL, A. 2016. Early development of Drosophila embryos requires Smc5/6 function during oogenesis. *Biology Open*.

TSUTSUMI, M., FUJIWARA, R., NISHIZAWA, H., ITO, M., KOGO, H., INAGAKI, H., OHYE, T., KATO, T., FUJII, T. & KURAHASHI, H. 2014. Age-Related Decrease of Meiotic Cohesins in Human Oocytes. *PLOS ONE,* 9**,** e96710.

TURNER, J. M. 2007. Meiotic sex chromosome inactivation. *Development,* 134**,** 1823-31.

UNAL, E., ARBEL-EDEN, A., SATTLER, U., SHROFF, R., LICHTEN, M., HABER, J. E. & KOSHLAND, D. 2004. DNA damage response pathway uses histone modification to assemble a double-strand break-specific cohesin domain. *Mol Cell,* 16**,** 991-1002.

VAN DER CRABBEN, S. N., HENNUS, M. P., MCGREGOR, G. A., RITTER, D. I., NAGAMANI, S. C. S., WELLS, O. S., HARAKALOVA, M., CHINN, I. K.,

ALT, A., VONDROVA, L., HOCHSTENBACH, R., VAN MONTFRANS, J. M., TERHEGGEN-LAGRO, S. W., VAN LIESHOUT, S., VAN ROOSMALEN, M. J., RENKENS, I., DURAN, K., NIJMAN, I. J., KLOOSTERMAN, W. P., HENNEKAM, E., ORANGE, J. S., VAN HASSELT, P. M., WHEELER, D. A., PALECEK, J. J., LEHMANN, A. R., OLIVER, A. W., PEARL, L. H., PLON, S. E., MURRAY, J. M. & VAN HAAFTEN, G. 2016. Destabilized SMC5/6 complex leads to chromosome breakage syndrome with severe lung disease. *The Journal of Clinical Investigation,* 126**,** 2881-2892.

VENTELA, S., COME, C., MAKELA, J. A., HOBBS, R. M., MANNERMAA, L., KALLAJOKI, M., CHAN, E. K., PANDOLFI, P. P., TOPPARI, J. & WESTERMARCK, J. 2012. CIP2A promotes proliferation of spermatogonial progenitor cells and spermatogenesis in mice. *PLoS One,* 7**,** e33209.

VERKADE, H. M., BUGG, S. J., LINDSAY, H. D., CARR, A. M. & O'CONNELL, M. J. 1999. Rad18 is required for DNA repair and checkpoint responses in fission yeast. *Mol Biol Cell,* 10**,** 2905-18.

VERVER, D., HWANG, G., JORDAN, P. & HAMER, G. 2015. Resolving complex chromosome structures during meiosis: versatile deployment of Smc5/6. *Chromosoma***,** 1-13.

VERVER, D. E., HWANG, G. H., JORDAN, P. W. & HAMER, G. 2016a. Resolving complex chromosome structures during meiosis: versatile deployment of Smc5/6. *Chromosoma,* 125**,** 15-27.

VERVER, D. E., LANGEDIJK, N. S., JORDAN, P. W., REPPING, S. & HAMER, G. 2014a. The SMC5/6 complex is involved in crucial processes during human spermatogenesis. *Biol Reprod,* 91**,** 22.

VERVER, D. E., LANGEDIJK, N. S. M., JORDAN, P. W., REPPING, S. & HAMER, G. 2014b. The SMC5/6 Complex Is Involved in Crucial Processes During Human Spermatogenesis. *Biology of Reproduction,* 91**,** 22, 1-10.

VERVER, D. E., LANGEDIJK, N. S. M., JORDAN, P. W., REPPING, S. & HAMER, G. 2014c. The SMC5/6 Complex Is Involved in Crucial Processes During Human Spermatogenesis1. *Biology of Reproduction,* 91**,** 22, 1-10-22, 1-10.

VERVER, D. E., VAN PELT, A. M., REPPING, S. & HAMER, G. 2013a. Role for rodent Smc6 in pericentromeric heterochromatin domains during spermatogonial differentiation and meiosis. *Cell Death Dis,* 4**,** e749.

VERVER, D. E., VAN PELT, A. M., REPPING, S. & HAMER, G. 2013b. Role for rodent Smc6 in pericentromeric heterochromatin domains during spermatogonial differentiation and meiosis. *Cell Death &Amp; Disease,* 4**,** e749.

VERVER, D. E., ZHENG, Y., SPEIJER, D., HOEBE, R., DEKKER, H. L., REPPING, S., STAP, J. & HAMER, G. 2016b. Non-SMC Element 2 (NSMCE2) of the SMC5/6 Complex Helps to Resolve Topological Stress. *Int J Mol Sci,* 17.

VIGNARD, J., CHARBONNEL, C. & MASSON, J. Y. 2011. Partners apart: Smc6-independent DNA binding activity of Smc5 on single-strand DNA. *Cell Cycle,* 10**,** 1025-6.

WARD, A., HOPKINS, J., MCKAY, M., MURRAY, S. & JORDAN, P. W. 2016. Genetic Interactions Between the Meiosis-Specific Cohesin Components, STAG3, REC8, and RAD21L. *G3 (Bethesda),* 6**,** 1713-24.

WATANABE, K., PACHER, M., DUKOWIC, S., SCHUBERT, V., PUCHTA, H. & SCHUBERT, I. 2009. The STRUCTURAL MAINTENANCE OF CHROMOSOMES 5/6 complex promotes sister chromatid alignment and homologous recombination after DNA damage in Arabidopsis thaliana. *Plant Cell,* 21**,** 2688-99.

WATANABE, Y. & NURSE, P. 1999. Cohesin Rec8 is required for reductional chromosome segregation at meiosis. *Nature,* 400**,** 461-4.

WEHRKAMP-RICHTER, S., HYPPA, R. W., PRUDDEN, J., SMITH, G. R. & BODDY, M. N. 2012a. Meiotic DNA joint molecule resolution depends on Nse5-Nse6 of the Smc5-Smc6 holocomplex. *Nucleic Acids Res,* 40**,** 9633-46.

WEHRKAMP-RICHTER, S., HYPPA, R. W., PRUDDEN, J., SMITH, G. R. & BODDY, M. N. 2012b. Meiotic DNA joint molecule resolution depends on Nse5-Nse6 of the Smc5-Smc6 holocomplex. *Nucleic acids research,* 40**,** 9633-9646.

WELLARD SR, H. J., AND JORDAN PW 2017. A Seminiferous Tubule Squash Technique for the Cytological Analysis of Spermatogenesis Using the Mouse Model. *J Vis Exp.,* In Press.

WINTERS, T., MCNICOLL, F. & JESSBERGER, R. 2014. Meiotic cohesin STAG3 is required for chromosome axis formation and sister chromatid cohesion. *EMBO Journal,* 33**,** 1243-1255.

WOJTASZ, L., DANIEL, K., ROIG, I., BOLCUN-FILAS, E., XU, H., BOONSANAY, V., ECKMANN, C. R., COOKE, H. J., JASIN, M., KEENEY, S., MCKAY, M. J. & TOTH, A. 2009. Mouse HORMAD1 and HORMAD2, two conserved meiotic chromosomal proteins, are depleted from synapsed chromosome axes with the help of TRIP13 AAA-ATPase. *PLoS Genet,* 5**,** e1000702.

WU, N., KONG, X., JI, Z., ZENG, W., POTTS, P. R., YOKOMORI, K. & YU, H. 2012. Scc1 sumoylation by Mms21 promotes sister chromatid recombination through counteracting Wapl. *Genes Dev,* 26**,** 1473-85.

WU, N. & YU, H. 2012. The Smc complexes in DNA damage response. *Cell Biosci,* 2**,** 5.

XAVER, M., HUANG, L., CHEN, D. & KLEIN, F. 2013. Smc5/6-mms21 prevents and eliminates inappropriate recombination intermediates in meiosis. *PLoS Genet,* 9**,** e1004067.

XU, H., BEASLEY, M. D., WARREN, W. D., VAN DER HORST, G. T. & MCKAY, M. J. 2005. Absence of mouse REC8 cohesin promotes synapsis of sister chromatids in meiosis. *Dev. Cell,* 8**,** 949-961.

XUE, X., CHOI, K., BONNER, J., CHIBA, T., KWON, Y., XU, Y., SANCHEZ, H., WYMAN, C., NIU, H., ZHAO, X. & SUNG, P. 2014. Restriction of replication fork regression activities by a conserved SMC complex. *Mol Cell,* 56**,** 436-45.

YARBRO, J. W. 1992. Mechanism of action of hydroxyurea. *Semin Oncol,* 19**,** 1-10.

YONG-GONZALES, V., HANG, L. E., CASTELLUCCI, F., BRANZEI, D. & ZHAO, X. 2012. The Smc5-Smc6 complex regulates recombination at centromeric regions and affects kinetochore protein sumoylation during normal growth. *PLoS One,* 7**,** e51540.

YOUDS, J. L. & BOULTON, S. J. 2011. The choice in meiosis - defining the factors that influence crossover or non-crossover formation. *J Cell Sci,* 124**,** 501-13.

ZAKHARYEVICH, K., TANG, S., MA, Y. & HUNTER, N. 2012. Delineation of joint molecule resolution pathways in meiosis identifies a crossover-specific resolvase. *Cell,* 149**,** 334-47.

ZHANG, K. & SMITH, G. W. 2015. Maternal control of early embryogenesis in mammals. *Reproduction, fertility, and development,* 27**,** 880-896.

ZHAO, X. & BLOBEL, G. 2005a. A SUMO ligase is part of a nuclear multiprotein complex that affects DNA repair and chromosomal organization. *Proc Natl Acad Sci U S A,* 102**,** 4777-82.

ZHAO, X. & BLOBEL, G. N. 2005b. A SUMO ligase is part of a nuclear multiprotein complex that affects DNA repair and chromosomal organization. *Proceedings of the National Academy of Sciences of the United States of America,* 102**,** 4777-4782.

ZHENG, Y., JONGEJAN, A., MULDER, C. L., MASTENBROEK, S., REPPING, S., WANG, Y., LI, J. & HAMER, G. 2017. Trivial role for NSMCE2 during in vitro proliferation and differentiation of male germline stem cells. *Reproduction,* 154**,** 81-95.

ZICKLER, D. & KLECKNER, N. 2015. Recombination, Pairing, and Synapsis of Homologs during Meiosis. *Cold Spring Harb Perspect Biol,* 7.

CURRICULUM VITAE

Grace H. Hwang

615 North Wolfe Street, Baltimore, Maryland 21205
Phone: 410-502-7968, Email: ghwang2@jhu.com

Education

Doctor of Philosophy: Biochemistry and Molecular Biology (2012-2018)

- Johns Hopkins University Bloomberg School of Public Health, Baltimore, MD

Master of Science: Biochemistry and Molecular Biology (2010-2012)

- Johns Hopkins University Bloomberg School of Public Health, Baltimore, MD

Bachelor of Arts: Biochemistry and Cell Biology (2006-2010)

- Rice University, Houston, TX

Relevant Experience

Doctor of Philosophy (PhD) Graduate Student (2012-Present)

- Johns Hopkins University Bloomberg School of Public Health, Baltimore, MD
- Thesis project: *The Role of the SMC5/6 Complex in Genome Integrity in Mammals*
    - Principal Investigator: Philip Jordan, PhD

Masters of Science (ScM) Student (2010-2012)

- Johns Hopkins University Bloomberg School of Public Health, Baltimore, MD
- ScM Thesis project: *Investigating the Role of Hr39 in the Germline Stem Cell Lineage*
    - Principal Investigator: Daniela Drummond-Barbosa, PhD
- Masters of Health Science (MHS) Thesis: *Therapy-related Leukemia*. (2011)
    - Thesis submitted for Master of Health Science fulfillment

Clinical Research Assistant (2007-2010)

- The University of Texas M. D. Anderson Cancer Center, Houston, TX
- Research project: *Enhancing Knowledge on Cardiac Implantable Pulse Generators*
    - Principal Investigators: Maria E. Suarez-Almazor, MD, PhD; Marc Rozner, MD, PhD
- Research project: *Treatment Adherence with Compliance Prompting Packaging*
    - Principal Investigator: Maria E. Suarez-Almazor, MD, PhD

Publications

- **Hwang, GH,** Fengyun, S, O'Brien, M, Eppig, J, Handel MA, and Jordan, PW. *SMC5/6 is required for the formation of segregation-competent bivalent chromosomes during meiosis I in mouse oocytes.* (2017) Development. 144 (9), 1648-1660, doi:10.1242/dev.145607
- Verver, DE*, **Hwang, GH***, Jordan PW, and Hamer G. *Resolving complex chromosome structures during meiosis: versatile deployment of Smc5/6*. (2015) Chromosoma. doi: 10.1007/s00412-015-0518-9. * Co-first author
- **Hwang, GH**, Hopkins, J, and Jordan, PW. *Chromatin Spread Preparations for the Analysis of Mouse Oocyte Progression from Prophase to Metaphase II*. J. Vis. Exp. (Pending Publication), e56736, In-press (2018).
- Ables, ET, **Hwang, GH**, Finger, DS, Hinnant, TD, and Drummond-Barbosa, D. *A genetic mosaic screen for ecdysone-responsive genes regulating Drosophila oogenesis*. (2016) G3. doi: 10.1534/g3.116.028951.

- Hopkins, J, **Hwang, GH,** Jacobs, J, Sapp, N, Bedigian, R, Oka, K, Overbeek, P, Murray, S and Jordan, PW. *Meiosis-specific cohesin component, Stag3 is essential for mediating recombination and synapsis between homologous chromosomes and maintaining sister chromatid cohesion*. (2014) PLoS Genet 10(7): e1004413. doi:10.1371/journal.pgen.1004413

Manuscript in preparation:

- **Hwang, GH**, Gaddipati, H, Pryzhkova, MP, Verver, DE, Handel, MA, Hamer, G, and Jordan, PW. *Depletion of SMC5/6 sensitizes male germ cells to DNA damage.* (In Review)
- Zheng, Y, Jongejan, A, Mulder, CL, van Daalen, S, Mastenbroek, S, **Hwang, G**, Jordan, PW, Repping, S, and Hamer, G. *On the increasing sensitivity of differentiating spermatogonia to DNA damage*. (submitted)

Selected Presentations

- **Hwang, G**, Hamer, G, Verver, DE, Handel MA, and Jordan P.W. *SMC5/6 is essential for repair of exogenous DNA damage during spermatogenesis* (2017)
  - Poster presentation at Biochemistry and Molecular Biology Departmental Retreat
- **Hwang, GH**, Fengyun, S, O'Brien, M, Eppig, J, Handel MA, and Jordan, PW. *SMC5/6 is required for the formation of bivalent chromosomes capable of segregation during meiosis I in oocytes* (2016)
  - Oral presentation at The Allied Genetics Conference 2016 (TAGC16)
- **Hwang, GH**, Fengyun, S, O'Brien, M, Eppig, J, Handel MA, and Jordan, PW. *SMC5/6 is required for the formation of bivalent chromosomes capable of segregation during meiosis I in oocytes* (2016)
  - Oral presentation at Meiosis Supergroup Meeting at the NIH
- **Hwang, GH**, Fengyun, S, O'Brien, M, Eppig, J, Handel MA, and Jordan, PW. *SMC5/6 is required for the formation of bivalent chromosomes capable of segregation during meiosis I in oocytes* (2016)
  - Poster presentation at 2016 NCI Symposium on Chromosome Biology
- Pryzhkova, M.V., **Hwang G.H.,** and Jordan, P.W. *Structural Maintenance of Chromosomes in Stem Cells* (2016)
  - Poster presentation at the 8th Annual Maryland Stem Cell Research Symposium
- **Hwang, G**., O'Brien, M., Sun, F., Eppig, J., Handel, M., and Jordan, P. *Smc5/6 is required for chromosome segregation in mammalian meiosis* (2014)
  - Poster presentation at the Germ Cell Meeting at Cold Spring Harbor, New York
- **Hwang, G.,** Ables, E.T., and Drummond-Barbosa, D. *Investigating the Role of HR39 in the Germline Stem Cell Lineage* (2012)
  - Poster presentation at the 2012 Drosophila Genetics Research Conference in Chicago, Illinois
- Pollono, E. N., **Hwang, G**., Rodriguez, S., Looney, C., Kallen, M. and Rozner, M. A. *Most Common Problems Identified in a Pacemaker/Defibrillator Clinic*. (2010)
  - Poster presentation at Division of Internal Medicine Research Retreat at M.D. Anderson Cancer Center

Teaching Experiences

- Research Mentor
  - MHS student Zach Perdun (Sep 2015- Sep 2016)
  - MHS student Sakshi Khurana (Jan 2017- May 2017)
- Assistant for Diversity Summer Internship Program for Undergraduates at Johns Hopkins School of Public Health (Jun 2015- Sep 2016)

- Teacher Assistant
    - Fundamentals of Reproductive Biology at Johns Hopkins University Bloomberg School of Public Health (Sep 2015- Oct 2015)
    - Fundamentals of Reproductive Biology at Johns Hopkins University Bloomberg School of Public Health (Online) (Nov 2016- Dec 2016)
    - Genetics at the Johns Hopkins University School of Medicine (October 2016-Dec 2016)

Grants/Funding

National Cancer Institute Training Grant (NIH) (CA009110) (Aug 2013-Jun 2016)

Scholarships and Awards

The Allied Genetics Conference (TAGC16) GSA Travel Award (2016)
International Mammalian Genome Society Travel Award (2016)

Scientific Society Memberships

International Mammalian Genome Society (2016-Present)
Genetic Society of America (2015-Present)
Society for the Study of Reproduction (2014-Present)
American Association for the Advancement of Science (AAS) (2012-Present)